

NORTHWESTERN UNIVERSITY

User-Modulated Impedance Control

*Using Two-Site Proportional Myoelectric Signals*

A DISSERTATION

SUBMITTED TO THE GRADUATE SCHOOL

IN PARTIAL FULFILLMENT OF THE

REQUIREMENTS

for the degree

DOCTOR OF PHILOSOPHY

Field of Biomedical Engineering

By

Jonathon W. Sensinger

EVANSTON, ILLINOIS

June 2007

© Copyright by Jonathon W. Sensinger 2007

All Rights Reserved

## Abstract

User-Modulated Impedance Control *Using Two-Site Proportional Myoelectric Signals*

Jonathon W. Sensinger

Commercially available electrically powered prosthetic elbows are stiff and unyielding. Making these artificial limb replacements more closely mimic human elbows by increasing their compliance may be beneficial. In addition to having increased compliance compared with current electrically powered prosthetic elbows, humans modulate the overall impedance of their joints. The author proposes to create a user-modulated impedance controlled prosthesis and to see if persons using this prosthesis demonstrate improved movement performance using it compared with traditional motion control.

Specifically, the author proposes to:

- Quantify flexion/extension compliance modulation at the interface between the residual limb's humerus of a person with an above-elbow amputation and their socket.
- Create a compliant clinically applicable prosthetic elbow that controls motion and impedance.
- Compare user performance when using impedance control and traditional control of a prosthetic elbow in the presence of environmental perturbations and mental distraction.
- Determine if users modulate impedance of the prosthetic elbow when they interact with different environments.

These studies should lead to improvements in future prostheses and test the value of impedance control in prosthetic and robotic applications.

## Dedication

This thesis is dedicated to my Savior and Lord, Jesus Christ, for as in all that I do, it is to you that I owe my trials and my successes; my life and my work. This degree, in humbling me, has brought me closer to you, and I pray you may be pleased that it be ascribed to you.

*The Lord gives, The Lord takes away.  
Blessed be the Name of the Lord*

*~ Job 1:21 ~*

## Acknowledgements

I owe an enormous debt of gratitude to my advisor, *Richard Weir*. His breadth of knowledge and personal contacts have been an enormous help. His role in advising me – supportively allowing me to independently grow and learn has worked very well. His ability to quickly review the numerous iterations of my papers and thesis has allowed me to proceed with research unhindered. Finally, his demonstrable commitment to his own family, and his continuous willingness support me in my commitment to my own, has made him a role model on par with Joan Feynman (Hirshberg, 2002). I sincerely appreciate all of his help.

My committee has likewise been incredibly supportive, while allowing me freedom to grow. Each member of my committee has contributed in distinct ways, from the practical perspective of *Dr. Todd Kuiken*, to the help *Dr. Ed Colgate* has given me in debugging unexpected instabilities, to the help that *Dr. Zev Rymer* has given me in presenting my research. I am very proud to have each of them on my committee.

*Dr. Eric Perreault*, *Ed Grabn* and *Craig Heckathorn* have provided invaluable and consistent advise with the small details of design that cannot be learned from a textbook, but that are essential to good design of a robotic prosthesis. I am very grateful for the time they've spent with me, and for the many tips I've learned from them. *Dr. Dudley Childress*, the director emeritus of my laboratory, has been my largest critic, and I sincerely appreciate that. I have also enjoyed reading books that he has recommended on the philosophy of science, and hope that my results of my research, both in this thesis and in the future, hold up to his high standard of scientific methodology.

My partners in upper-limb prosthetic crime, *Todd Farrell* and *Bolu Ajiboye*, have also been great sources of help, exceptional lab mates, and good friends. I've sincerely enjoyed our many conversations about random topics, as well as their patience in being interrupted to answer silly questions. I think of all the things I will miss about leaving NUPRL, the greatest will be not sitting next to you guys. *Blair Lock* has also been a great source of help and fun, and I've enjoyed his MacGyver approach to life, disdain for PhD academia, and yet very intelligent solutions to an amazing array of problems.

Since I finished my Master's degree, *Dr. Andy Hansen* has been kind enough to let me win one game of racquetball. For that I acknowledge him, as well as for his help in conceptual and practical problems, his lighthearted nature, and his great perspective when my papers were rejected. Likewise I'm very grateful for the lighthearted nature and help that *BJ Johnson* has provided in the lab. I am very grateful for everyone in the lab – you have all been a very non-engineering bunch, social and happy, and you've been a great group to be around. Thanks to all of you for participating in my experiment.

The people in *NECAL* have been a tremendous source of support, especially *Dr. Laura Miller*, *Robert Lipschutz*, and *Kathy Stubblefield*, from giving advice to helping me adapt prostheses with very short notice, to supplying me with subjects and leads to find subjects. I doubt I would have completed half my thesis without their help, and I'm very grateful for

their enthusiastic willingness to help me. I'm especially proud of Kathy Stubblefield's proclamation that I'm "dumber than dirt."

*Delip Thakar* has machined a large quantity of parts required for my thesis to exacting precision. I'm grateful for the amount of time and care he spent making my parts, and for the many conversations we had. I'm also grateful to the office staff, specifically *Bonnie Collard* and *Elizabeth Schreiber*, for support over the years. Initially skeptical, I have slowly grown accustomed to your personalities, and in the process learned to thoroughly enjoy working with you. I think you do an excellent job, and *NUPRL* owes a great deal to the stability that you maintain in the lab. I would also like to acknowledge the efforts of *Angie Zhang*, who recently joined the office staff. I think she's done an amazing job in processing financial matters, allowing me to focus on research. *Lon*, from Northwestern Memorial Hospital, was a tremendous help in completing my fluoroscopy study.

I would also like to thank *Mrs. Mauch* for her generous support that allowed me to attend a Mechatronics conference in Beijing, China. I am very grateful for the chance to have attended and presented at that conference, and for Mrs. Mauch's scholarship, which allowed for the international travel. Many thanks to *Angie Thornton* and *Yorleni Sanchez* for translating my consent form into Spanish. I greatly appreciate the time you spent in helping me.

*Jim Limber*, my landlord and friend, has been a constant source of ideas and suggestions and fun throughout the course of my PhD. I'm very proud to have him as a landlord, very appreciative of the ideas he's had and time he's spent listening to me describe my research, and very grateful for his intentional support of research through allowing us to live in a beautiful apartment for a very low price. I am also grateful for the friendship of *Steve Reed*, who has kept me grounded and humble over the years, made sure I wasn't too caught up in research, and who broke my prosthetic elbow. I'm also grateful for the friendship of *Dan Krainak*, my roommate during my Master's degree, who has doggedly met with me throughout my PhD for lunch, exchanging ideas ranging from science and statistics to literary works and social obligations. I have greatly appreciated our different perspectives on life.

I owe a deep debt of gratitude to all four of my parents – both my mom and dad, and my wife's mom and dad, as well as to all of my family. My mom and dad have been a constant source of support for my education and exploration of knowledge, and I am deeply appreciative to the impact they have had in my life. Likewise, my wife's parents have been very supportive of my continued presence in school while married to their daughter, and have provided a great deal of support in helping me manage life, apart from which it would have taken years longer to finish my degree.

My daughter, *Adelaide Wren*, was born as I started my PhD, and to be honest, from an academic standpoint I worried her presence would be a great hindrance – the birth of a child during graduate school certainly seems to be a dreaded fear in academia. Her presence has indeed taxed my limited ability to transition between science and babble, but I love her immensely, and I'm very grateful for the opportunity she has provided to play, laugh, and smile, and to marvel afresh at this amazing world. I am very grateful that I've been able to



share my PhD with her, and I only regret that any other children we may have will not be afforded the same experience.

My wife, dearest *Valerie Cristin*, has been an enthusiastic source of support: interested in my research, willing to listen to me describe it almost every day, willing to joyfully resign herself to life with a man who's brain is always working on an engineering problem, willing to have the covers pulled off her multiple times a night when I would get up to jot down a new idea - in short, not merely resigned like Eeyore to the odd quirks that everyone must have, but embracing the quirky scientist she adoringly calls her husband. For that gift, I am extremely grateful. It is only matched by her refusal to let me think too highly of myself, no matter how much I may think of science, her zest and skip in life, and her humble adoration of God.

Finally, I would like to acknowledge my Father in heaven and Jesus Christ, my Savior, who I have never known more closely than through the ups and downs of this degree. Thank you for allowing me to fall and thank you for drawing me closer to you. May this work be pleasing in your sight, may the servant who did it be more like you, and may it bring you and you alone glory.

## Contents

List of Figures.....	13
List of Tables.....	16
List of Variables .....	17
1 Introduction .....	20
1.1 Specific Aims & Hypotheses .....	21
2 Background.....	24
2.1 Physiology .....	24
2.1.1 Summary of muscle properties .....	25
2.1.2 Differences in muscle properties of persons with an amputation .....	26
2.1.3 Mimicking muscle properties in prostheses .....	27
2.2 Control .....	31
2.2.1 Control of Prostheses.....	31
2.2.2 Impedance Control .....	33
2.2.3 Admittance Control.....	39
2.2.4 Choosing Between Impedance Control and Admittance Control.....	40
2.3 Technologies.....	42
2.3.1 Electromagnetic Motor Alternatives:.....	43
2.3.2 Inertia reduction .....	44
2.3.3 Passive impedance modulation.....	45
2.3.4 Joint Torque Control.....	46
2.3.5 Increased Compliance .....	47
3 Socket-Residual Limb Interface Rotational Stiffness .....	55
3.1 Modeling.....	57
3.1.1 Mathematical Modeling .....	58
3.1.2 Finite Element Modeling .....	63
3.2 Fluoroscopy.....	64
3.2.1 Subjects .....	65
3.2.2 Apparatus & Procedures .....	66
3.2.3 Data Analysis .....	67
3.3 Results.....	68
3.3.1 Mathematical model.....	68
3.3.2 Mathematical model compared with FEA model .....	69
3.3.3 Empirical Results .....	70
3.4 Discussion .....	73
3.4.1 Clinical Implications .....	74
3.5 Conclusion.....	75
4 Improvements to Series Elastic Actuators .....	76
4.1 Modeling Sensor Placement .....	76

4.2	Modeling Feedback control .....	78
4.3	Experiment Setup .....	82
4.4	Results: Sensor placement .....	83
4.5	Results: Inner control .....	85
4.6	Summary of results .....	87
4.7	Discussion .....	88
5	Design of the Prosthetic Elbow .....	89
5.1	Mechanical Design Principles .....	89
5.2	Mechanical Design .....	93
5.3	Controller Design .....	96
5.3.1	Signal Processing .....	97
5.3.2	Impedance Controller .....	99
5.3.3	Torque Controller .....	100
6	Impedance Modulation Evaluation .....	101
6.1	Plant modeling .....	101
6.2	2D projection of a multivariate root locus .....	104
6.3	Empirical Testing .....	108
6.4	Discussion .....	113
6.5	Conclusion .....	114
7	Critical Decisions required to Implement Impedance Control .....	115
7.1	Questions to Address .....	115
7.2	Experimental Apparatus .....	117
7.3	Results .....	124
7.3.1	Performance of Underlying Motion Paradigm .....	124
7.3.2	Impedance Baselines .....	125
7.4	Discussion .....	129
7.5	Conclusion .....	131
8	User Modulated Proportional Impedance Control by Able Bodied Subjects .....	132
8.1	Control Paradigms .....	132
8.2	Experimental Tasks .....	133
8.3	Results .....	137
8.3.1	Co-contraction .....	138
8.3.2	Performance .....	141
8.4	Discussion .....	143
8.5	Conclusion .....	145
9	User Modulated Proportional Impedance Control by Subjects with an Amputation	146
10	Conclusions .....	148
11	Future Work .....	151
	References .....	153
12	Appendices .....	162
12.1	Expanded Physiology Review .....	162

12.1.1	Muscle Physiology .....	162
12.1.2	Control of Movement.....	169
12.2	Fluoroscopy Notes .....	178
12.2.1	Verifying sampling frequency of Fluoroscopy machine .....	178
12.2.2	Measuring inertia of a body-powered prosthesis.....	181
12.2.3	Calculating the slope of data .....	181
12.3	Review of Metrics to Optimize Impedance Control .....	182
12.3.1	Exploration of Impedance Metrics.....	187
12.4	Internal Dynamics Compensation .....	193
12.5	Pilot Study notes.....	198
12.6	Co-contraction values for individual targets .....	205
12.7	Mechanical Design .....	212
12.8	Pilot Matlab Control .....	241
12.8.1	Controllers.....	242
12.8.2	Processing .....	249
12.9	Remaining Subject Matlab Control .....	258
12.9.1	Controllers.....	259
12.9.2	Processing .....	266
12.10	Matlab Code .....	274
12.10.1	Calibration.m.....	274
12.10.2	Fmain.m.....	278
12.10.3	Fitt.m .....	280
12.10.4	Tmain.m .....	285
12.10.5	Track.m.....	286
12.10.6	Setscreen.m .....	289
12.10.7	nid.m.....	290
12.10.8	mlt.m .....	290
12.11	Data sheets .....	291
Vita.....		303

## Figures

Figure 2.1: Impedance Control .....	35
Figure 2.2: Admittance Control.....	39
Figure 2.3: Different solutions to minimize high frequency impedance .....	45
Figure 2.4: Intentional Compliance in Robots .....	48
Figure 2.5: Series Elastic Actuator.....	49
Figure 2.6: Effect of Compliance on Torque Frequency Saturation. ....	53
Figure 3.1: Socket-residual limb interface compliance between socket and residual limb.....	56
Figure 3.2: Deformation of tissue when a load is applied to the socket. ....	59
Figure 3.3: A transverse plane depiction of tissue deformation.....	62
Figure 3.4: Finite Element Model.....	64
Figure 3.5: Graphical representation of subject residual limb. ....	65
Figure 3.6: Fluoroscopy images.....	66
Figure 3.7: Empirical rotational stiffness of socket-residual limb interface for subject A .....	70
Figure 3.8: Empirical rotational stiffness of socket-residual limb interface for subject B.....	71
Figure 3.9: Empirical rotational stiffness of socket-residual limb interface for subject C.....	71
Figure 3.10: Empirical rotational stiffness of socket-residual limb interface for subject C.....	72
Figure 4.1: Sensor placement.....	78
Figure 4.2: Internal feedback.....	79
Figure 4.3: Effect of inner control loop on system dynamics .....	81
Figure 4.4: Linear SEA with high levels of friction.....	83
Figure 4.5: Comparison of sensor placement .....	84
Figure 4.6: Force control of a linear SEA with no internal control .....	85
Figure 4.7: Internal Control loops. ....	86
Figure 5.1: Spandrel Cross section .....	90
Figure 5.2: Prosthetic Elbow .....	95
Figure 5.3: Expanded Impedance Control Diagram.....	97
Figure 5.4: Extraction of Motion and Impedance from MES RMS Signals.....	98
Figure 6.1: Bond graph of system prosthetic elbow .....	102
Figure 6.2: Control system.....	103
Figure 6.3: Scatter plot of poles for the random variation of 3 variables .....	105
Figure 6.4: The endpoints of 1 variable overlaid on a scatter plot of all variables.....	106
Figure 6.5: Scatter plot, showing the effect of three variables .....	107
Figure 6.6: Unconstrained Impedance Control.....	109
Figure 6.7: Unconstrained Impedance Control:.....	110
Figure 6.8: Bode plot of position response of the unconstrained actuator using impedance control.....	111

Figure 6.9: The modeled effect of output backlash on the system's ability to maintain a stiffness of 100 Nm/rad .....	112
Figure 7.1: Calibrating Signal thresholds.....	119
Figure 7.2: Experimental Apparatus.....	122
Figure 7.3: Boxplot comparison of motion paradigms.....	125
Figure 7.4: Co-contraction & Impedance Modulation Ranges for Proportional Position Control (PPC).....	126
Figure 7.5: Co-contraction & Impedance Modulation Ranges for Proportional Velocity Control (PVC).....	128
Figure 8.1. Experimental apparatus for pointing task. ....	134
Figure 8.2: A picture showing the tracking task.....	136
Figure 8.3: Experiment Sequence. ....	137
Figure 8.4: Impedance Modulation, compared by paradigm. ....	139
Figure 8.5: Impedance Modulation, compared by task. ....	140
Figure 8.6: Co-contraction across movement regions. ....	141
Figure 8.7: Impedance paradigm effect on performance.....	142
Figure 8.8: Impedance effect on performance. ....	143
Figure 9.1: Co-contraction levels for subjects with an amputation. ....	147
Figure 12.1: Force Length relationship .....	165
Figure 12.2: Illustration of Force vs. velocity.....	166
Figure 12.3: Stretch Reflex .....	168
Figure 12.4: Equilibrium Point Shift.....	171
Figure 12.5: Predicted Trajectories in the absence of proprioceptive feedback.....	172
Figure 12.6: Clock.....	180
Figure 12.7: Series Circuit - Maximum power transfer through $R_L$ .....	184
Figure 12.8 Parallel circuit - Maximum power transfer through $Z_E$ .....	186
Figure 12.9 Series Impedance Circuit - Maximum Average Power Transfer Through $Z_E$ .....	189
Figure 12.10 Parallel Impedance Circuit - Maximum Average Power Transfer Through $Z_E$ . 191	
Figure 12.11: Common Friction Models.....	195
Figure 12.12: Computationally simple friction model .....	196
Figure 12.13: Velocity Profile:.....	197
Figure 12.14: Placement of Internal Dynamics Compensation .....	198
Figure 12.15: Experiment B Setup.....	199
Figure 12.16: Trajectory & Accuracy Range due to Index of Difficulty Range .....	200
Figure 12.17: Index of Difficulty Range .....	201
Figure 12.18: Fitts Law applied to 4 subjects.....	203
Figure 12.19: Impedance for individual targets, for able bodied subjects .....	206
Figure 12.20 : Impedance for individual targets, for subjects with an amputation .....	207
Figure 12.21: Co-contraction across movement regions.....	208
Figure 12.22 Impedance for individual target <i>regions</i> , for able bodied subjects .....	209
Figure 12.23 Impedance for individual target <i>regions</i> , for subjects with an amputation.....	210

Figure 12.24: Co-contraction distinctions between paradigms for individual subjects.....211  
Figure 12.25: Repeated trials for 3 subjects who demonstrated initial co-contraction distinction  
between impedance paradigms .....211

## Tables

Table 2.1 Alternative Control Paradigms .....	35
Table 3.1 Subject Anthropomorphic data .....	65
Table 3.2 Results of Math & FEA analysis for a sample subject .....	69
Table 3.3 Modeled and Measured Socket-residual limb interface Rotational Stiffness for 4 subjects .....	72
Table 4.1 Comparison of different control schemes .....	87
Table 12.1 Measured Sampling frequency of fluoroscopy machine .....	180



## Variables

Symbol	Measure	Units
<i>A</i>	Area	$m^2$
<i>C</i>	Compliance	$\text{rad}/N \cdot m$
<i>D</i>	Derrivative gain	
<i>E</i>	Modulus of Elasticity	$N/m^2$
<i>F</i>	Force	N
<i>G</i>	Shear modulus	$N/m^2$
<i>I</i>	Current	Amp
<i>J</i>	Rotational inertia	$kg \cdot m^2$
<i>K</i>	Stiffness	$Nm/\text{rad}$
<i>L</i>	Inductance	Henry
<i>N</i>	Gear ratio	
<i>P</i>	Power	Watt
<i>R</i>	Resistance	$\Omega$
<i>S</i>	Socket length	m
<i>T</i>	Torque	$N \cdot m$
<i>U</i>	Strain energy	$N \cdot m$
<i>V</i>	Volume OR voltage	$m^3$ or volt
<i>X</i>	Position	m
<i>Z</i>	Impedance	

Symbol	Measure	Units
$b$	Rotational damping	$\text{N} \cdot \text{m} \cdot \text{s}$
$d$	Depth	$\text{m}$
$e$	Effort	$\text{N}$
$f$	Flow	$\text{m}/\text{s}$
$g$	Gravitational constant	$\text{m}/\text{s}^2$
$j$	$\sqrt{-1}$	
$l$	Length	$\text{m}$
$m$	Mass	$\text{kg}$
$n$	Number of subjects	
$p$	Frequentist probability	
$s$	$j\omega$	
$w$	width	$\text{m}$

Symbol	Measure	Units
$\alpha$	Angular acceleration	$\text{rad}/\text{s}^2$
$\varepsilon$	Strain	
$\gamma$	Strain angle	$\text{rad}$
$\nu$	Poisson's ratio	
$\theta$	Angular position	$\text{rad}$
$\sigma$	Standard deviation	
$\tau$	Sampling time	$\text{s}$
$\omega$	Angular speed	$\text{rad}/\text{s}$

*It requires some very sophisticated thinking to arrive at a simple solution.*

*It is much easier to work out a complicated and expensive solution. Indeed, whenever one encounters an expensive and complicated technology, one can take it that the basic issues have not been understood...*

*What we want is more, not less science in the developing world.*

*~ Dr. Pramod Karan Sethi*

# 1 Introduction

Commercially available electrically powered prosthetic elbows are stiff and unyielding. Making these artificial limb replacements more closely mimic human elbows by increasing their compliance (reducing stiffness) may be beneficial. Several other potential advantages of increasing the compliance of prosthetic elbows include:

- Creating elbows that are less likely to break in the event of a fall
- Improving movement fluidity and improving physical interaction with the environment.

In addition to having increased compliance compared with current electrically powered prosthetic elbows, humans modulate the compliance of their joints depending on the task. Different tasks require different levels of interaction with the environment. When writing, one does not wish the movement of a pencil to be hindered by minute fluctuations in the writing surface. In contrast, when moving an egg it is better to be knocked off course than to break the egg by staying on the initially intended trajectory. Impedance, defined as the relationship between exerted force and movement displacements (which includes compliance), expresses this tradeoff in mechanical terms. Able-bodied persons modulate the impedance of their limbs in accordance with the task by co-contracting their muscles. **The author has created a prosthetic elbow capable of user-modulated impedance control, and examined whether subjects are capable of modulating the impedance of the elbow and whether this**

user-modulated impedance control improves performance compared with current electrically powered prosthetic elbow technology.

### **1.1 Specific Aims & Hypotheses**

- Quantify flexion/extension compliance at the interface between the residual limb of a person with a trans-humeral (above elbow) amputation and their socket. The compliance of this interface has implications for the usefulness of modulating the impedance of the joint immediately distal to the interface. The author examined this stiffness by using fluoroscopy to measure deflection at the interface during loading of the artificial limb while measuring the load placed on the prosthesis with a load cell.
- Create a clinically viable compliant prosthetic elbow, where the motion and impedance of the prosthesis may be independently controlled.
- Compare user performance when using impedance control and traditional control of a prosthetic elbow in the presence of environmental perturbations and mental distraction. The author examined performance by examining two different tasks.
- Determine if users modulate impedance of the prosthetic elbow when they interact with different environments. The user-modulated impedance levels will be recorded for three phases of trajectory execution, both in the absence of perturbations and in the presence of two different perturbations.

**Chapter 2** presents motivation for user-modulated impedance control and background work in physiology and robotic control.

**Chapter 3** presents modeling and empirical results quantifying the interface between prostheses and users.

**Chapter 4** presents some improvements to series elastic actuators, the type of actuator used in this thesis.

**Chapter 5** presents the mechanical and control design proposed to implement user-modulated impedance control.

**Chapter 6** presents modeling of the design, and empirical results validating the actuator's ability to mimic several impedances.

**Chapter 7** presents a preliminary pilot study in which subjects modulate impedance. Several variables are examined, including the preferred motion paradigm, preferred impedance, and ability of subjects to co-contract their muscles to alter impedance while maintaining performance.

**Chapter 8** presents two impedance modulation tasks performed by 15 able-bodied subjects.

**Chapter 9** presents two impedance modulation tasks performed by three subjects with an amputation.

**Chapter 10** presents the conclusions of this thesis.

**Chapter 11** presents future work to be done in this area.

The **Appendices** include:

- Expansions on several topics, including muscle physiology, impedance optimization metrics, and internal dynamics compensation
- More detailed notes on the experiments
- The schematics for machined parts, the wiring diagram for the electronics circuit, Simulink model of control, and code to interface between the prosthetic elbow and the task.
- Data sheets for parts that were purchased

## **2 Background**

Weight, practicality, and modularity are cardinal factors in designing prostheses. These features take precedence over esoteric factors such as increased performance in the presence of perturbations, increased versatility, and reduced mental loading. Lack of these esoteric features is acceptable because the user can learn innovative ways to function without them. Inclusion of these features in a way that does not conflict with the cardinal factors, however, could improve the performance of persons using prostheses. To see if these features may be harmonized with practical prostheses, several topics are reviewed below, including the physiology of able-bodied persons and persons with amputations, potential control paradigms of prostheses, and methods to characterize and synthesize parameters needed to simply and accurately control prostheses.

### ***2.1 Physiology***

Humans satisfactorily complete a variety of tasks in daily life. They transition from unconstrained movement to interaction with constrained objects fluidly, and they seamlessly transition from tasks that require precise manipulation to tasks that require large amounts of power. It should be noted that muscles, the actuators of humans, are not intrinsically superior to engineered solutions for all tasks, as evidenced by robotic assembly lines and milling machines. Biomimetic solutions, although typically elegant in nature, are not necessarily better than other solutions. Regardless of whether a biomimetic solution is appropriate for a



particular task, understanding the interaction between humans and their environment is useful when creating a device that will interact with humans. Attempting to understand the physical structure of human muscles as well as any potential optimization features used by humans when interacting with their environment may shed light on the appropriate way to construct replacement limbs that will adapt appropriately to the environment.

### **2.1.1 Summary of muscle properties**

Models of underlying mechanisms of muscle contraction physiology and control of movement are detailed in Appendix 12.1. The modeled effects of muscle physiology and movement control may be summarized as follows: Human muscles in an agonist/antagonist relationship intrinsically resist perturbations with respect to position and even more so with respect to velocity. They further compensate using reflexive feedback loops and anticipate forces required using an adaptive knowledge of internal dynamics. The recruitment process of individual muscle fibers allows them to seamlessly transition between tasks that require precision and tasks that require power in an efficient manner. The antagonistic structure of the musculoskeletal system allows the impedance of joints to be modulated according to the task. Both the position of the limb segments, via spindle fibers, and the tension placed on muscles, via Golgi tendon organs, are fed back into the system at low and high levels of control.

### **2.1.2 Differences in muscle properties of persons with an amputation**

Although the majority of muscle physiology of persons with amputations is equivalent to that of able-bodied persons, there are several noteworthy distinctions. When an upper limb amputation occurs, two surgical procedures are suggested to connect muscle: myodesis, in which the deep muscles are tied to the bone, and myoplasty, in which muscles are tied to each other over the end of the residual limb (Smith, Michael & Bowker, 2004). These procedures preserve tension in muscle, allowing the preservation of muscle tone. Although these procedures are recommended, they are not often performed in surgery. As a result, many amputees do not have an anchor point for the muscles in their residual limb. If myodesis is performed, the proximal Golgi tendon receptors are able to sense tension in the muscle. Cineplasties may also be used to link the tendon of muscle to outside connections (Weir, 2003). Although a person with an upper limb amputation cannot move their nonexistent joint, they can contract the muscles that originally actuated the joint. The force produced by this contraction has been shown to have a monotonic relationship to the root mean square of the resulting myoelectric signal, for isometric contractions (Heckathorne, 1978, Heckathorne & Childress, 1981).

Muscle and nerve atrophy, coupled with cortical reorganization, alter neuromuscular physiology of persons with an amputation. Muscle atrophy ranges between 40-60% in sectioned muscles, resulting from reduction in muscle mass at amputation combined with inadequate mechanical fixation of muscles (Gottschalk, 2004).

## 2.1 Physiology

Nerves are typically buried in the muscle belly of remaining muscle to prevent painful neuromas from developing. In an experimental protocol, Kuiken (2003) has physically reorganized the neuromuscular system by taking nerves that stimulated amputated muscle and rewiring the nerves to denervated muscles. These muscles may then be used as amplifiers of neural commands to obtain independent MES signals.

### **2.1.3 Mimicking muscle properties in prostheses**

Many of the attributes summarized in section 2.1.1, including intrinsic muscle resistance to position and velocity perturbations, reflexive feedback loops, adaptive internal dynamic compensation, force scalability by muscle fiber recruitment, and variable joint impedance, appear desirable in prosthetics, though some are more practical than others. The scalability of the actuators will not be addressed in this proposal, though research in creation of artificial muscles (Ashley, 2003, Bar-Cohen, 2004, Kornbluh et al., 2002) or use of animal muscles (Herr & Dennis, 2004) offers promise for the future.

Work in areas such as genetic algorithms (Lipson & Pollack, 2000) or adaptive clustering algorithms (Theodoridis & Koutroumbas, 1999) offer promise for the future of robotic adaptive internal dynamics. In the field of prosthetics, however, the author feels that adaptive internal dynamics are inherently satisfied. The internal dynamics of the actuator itself are constant, and as such, may be defined a priori. The internal dynamics of the entire system, which will change with the task, may be learned by the subject, such that the subject is once again in control of the learning process of predicting internal dynamics. Thus, it is the

author's opinion that in the field of prosthetics, adaptive internal dynamics are realized through the end user. As a result, the adaptability of internal dynamics will not be specifically addressed in this proposal.

Physiologically appropriate force feedback of electric prostheses, although outside of the scope of this proposal, is integral to prosthetic control, and is being examined by the author. Childress (1980) and Patterson and Katz (1992) offer comprehensive overviews of historic work in this area. Position feedback has been previously examined through the concept of extended physiological proprioception (Doubler & Childress, 1984): physically coupling the position of the limb segment to a portion of the user's body. This technique has met with success in some instances, but in terms of position tracking, perturbations have inhibited the ability of the user to remain on task (Weir, 1995). Remote feedback has been attempted in numerous ways, including vibration (Shannon, 1976) and functional electrical stimulation (Almstrom, Anani, Herberts & Korner, 1981, Nohama, Lopes & Cliquet, 1995, Riso, Ignagni & Keith, 1991, Sabolich & Ortega, 1994, Scott, et al., 1980, Shannon, 1979, Wang, Zhang, Zhang & Gruver, 1995).

These latter forms of feedback provide feedback using a different modality than the one that they sense. As a result, although providing information to the user, it is likely that it comes at the cost of increased mental load and low level of information transfer. Phillips (1988) has suggested that the feedback signal must fit the stimulus modality of the missing limb. This thought is not new; Rosset (1916) filed a patent in the beginning of the last century for a

## 2.1 Physiology

device that applied pressure when pressure was sensed, and Patterson and Katz (1992) have recently created a similar setup, obtaining better qualitative feedback with pressure to pressure feedback than with pressure to vibratory or electrical stimulation feedback. An adaptive process is still involved, since the subject must learn to associate pressure in one area with pressure in another area. Ideally, the sensory nerve endings of the amputated area would be fed to another muscle so that they might be appropriately stimulated in that area, and the work of Kuiken (2003) has made this concept feasible. Kuiken, Sensinger, and Weir (2005) have recently tested this concept of physiologically appropriate force feedback with positive initial results.

Three areas are left, and all will be addressed in this proposal. The inherent stability of spring-like muscles will be mimicked by introducing a compliant element in the actuator, which resists increasing position perturbations with increased force. A position and velocity dependent reflex mechanism will be mimicked by a proportional, derivative, and integral feedback loop.

The variable impedance of human actuators will be mimicked through a control paradigm known as impedance control, which will be discussed in the following section. Before impedance control is addressed, however, it is noteworthy that English and Russells (1999a, 1999b) have suggested creating antagonistic pairs of spring-like actuators to physically mimic the adaptive impedance found in human actuators. The benefits of doing so include the lack of delay from computing the correct impedance as well as the ability to shut the motors off once

## 2.1 Physiology

the correct impedance has been achieved. Two actuators are required, however, to achieve these results. They must be precisely synchronized, and the combined weight and size of an additional motor is not practical in the field of prosthetics.

## **2.2 Control**

Methods of robotic control suitable to interaction with humans will now be reviewed.

### **2.2.1 Control of Prostheses**

*Body Powered Prostheses:* The majority of upper limb prostheses are body powered. Body powered prostheses are traditionally stimulated by switches or Bowden cables, which transmit position and force information to another joint, providing feedback at the same time. Most body powered prosthesis arrangements allow a closed loop to the user: something that electrically powered prostheses struggle to do. Perhaps their largest drawback, and the largest reason that electrically powered prostheses are still explored, is that this arrangement typically forces the user to control one joint at a time, using a switch to alter the degree of freedom to be moved. This control paradigm is used because there are limited motions, such as bicipital abduction or glenohumeral rotation, that are not typically used for other functional activities. The number of these joints decreases with the level of amputation, while the number of joints needed to be controlled in the prosthesis increases with the level of amputation. Thus, it is hoped that by using electrically powered prostheses simultaneous independent movement of numerous joints may be achieved.

*Electrically Powered Prostheses:* Electrically powered prostheses are typically controlled using open-loop velocity control. This control paradigm is used for DC motors because it presents an easily realized control scheme, because the voltage applied across a motor is roughly

proportional to the speed of the motor. The user typically controls the speed of the prosthesis by changing muscle myoelectric amplitudes, triggering electromechanical switches, or pressing against force sensitive resistors.

Doubler and Childress (1984) found proportional position control to be preferable to proportional velocity control for pursuit tracking tasks when using force transducers as input signals. Proportional position control is more difficult to implement with DC electric motors because it requires some form of feedback to regulate the position of the prosthesis. As a result, it is not commonly employed. With the introduction of microcontrollers in the field of prostheses (Lake & Miguelez, 2003) proportional position control has become a more readily available option. The Hosmer<sup>i</sup> NY Electric Elbow and the Liberating Technologies<sup>ii</sup> Boston Digital Arm System use velocity control, whereas the Motion Control<sup>iii</sup> Utah Arm 3 has the option of position control or velocity control. No commercially available electric prostheses allow the user to control the force generated by the prosthesis or the relationship between movement and force.

*Selection:* If a person has a unilateral amputation, they will tend to use their remaining limb to do virtually all tasks that require dexterity or power. If their dominant arm has been amputated, they will quickly become proficient with the other one. Thus, for a person with a unilateral amputation, control of the prosthesis is only important for those tasks that require co-manipulation between the limbs. The majority of these persons prefer body powered prostheses for functionality, unless the person has a high-level amputation. For persons with a

## 2.2 Control



high-level unilateral amputation, a hybrid system has found success in which an electric hand and a body powered elbow are used (Childress & Weir, 2004). If a person has a bilateral amputation, it is common to fit them with one body powered prosthesis and one electrically powered prosthesis, using the body powered prosthesis for fine manipulation and the electrically powered prosthesis for power. An added advantage in using this hybrid system for persons with a bilateral amputation is that control of the body powered prostheses is decoupled from control of the electrically powered prosthesis, allowing the use of more control sites (Weir, 2003).

### **2.2.2 Impedance Control**

Expectations for control of upper limb prostheses have always been high because of the standard established by able-bodied dexterity. Factors to be improved include the number of joints that may be manipulated, as well as the ability to simultaneously and accurately control motion of those joints. Another factor that plays an integral role in able-bodied movement and that is not implemented in prostheses is the control of impedance, or the relationship between forces and movements.

Impedance plays an integral role in regulating human movement. The modulation of impedance in able-bodied persons allows various optimization paradigms to be used including reduction of power consumption, minimization of trajectory error in the presence of perturbations, and smooth movement (Hogan, 1985a). Control of impedance may be useful in designing biomimetic (life-like) actuators, and the ability to modulate impedance based on the

task seems beneficial. Muscle architecture appears to intrinsically modulate the impedance of joints based on position and speed, while allowing humans to change that impedance depending on the task (Kandel, Schwartz & Jessell, 2000).

Impedance control, as defined by Hogan (1985a), is a generalization of stiffness control, first developed by J.K. Salisbury (1980). In impedance control, forces are generated in response to the difference between the sensed and desired position. To properly generate this force, accurate position sensing and accurate torque generation are required, as shown in Table 2.1. Because the input signal to the controller is position, impedance control is a subset of motion control. In user-modulated impedance control, the user determines the desired position and the desired impedance, where the impedance is the relationship between position perturbations and resultant force. The desired position and impedance are fed to the actuator, which calculates a torque based on the desired impedance and the difference between the actual position of the limb segment and the desired position. The torque required to compensate for the internal dynamics of the system, detailed in Appendix 12.4, should also be included in the generated torque, but it is seldom included in practice for the sake of simplicity. The actuator generates the calculated torque and the position of the limb segment is fed back to the actuator controller, as illustrated in Figure 2.1.

## 2.2 Control

**Table 2.1**  
**Alternative Control Paradigms**

		Control	
		Sense Position	Sense Force
Generate	Position	Position Control Extended Physiological Proprioception	Admittance Control
	Force	Impedance Control	Force Control

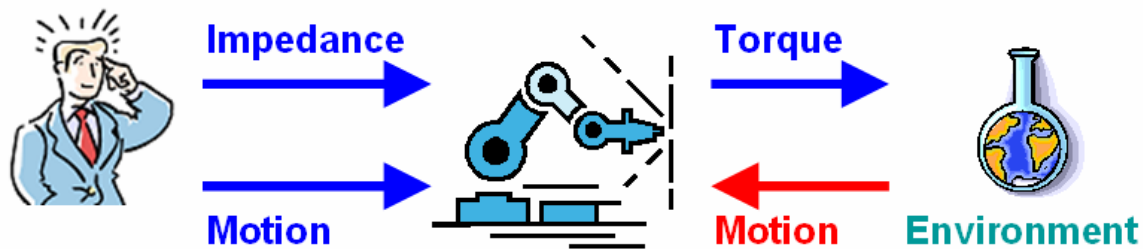


**Figure 2.1: Impedance Control**

The user defines the desired motion and impedance.

The actuator generates a torque based on the difference between the actual and desired motion, and the intended impedance.

The actuator senses the actual motion.

There are generally three variables in impedance control: a static stiffness term  $K_c$ , a dynamic viscosity term  $b_c$ , and an inertial term  $J_c$ . The generated torque is a function of these terms:

$$T_{gen} = K_c (\theta - \theta^*) + b_c \omega + J_c \alpha \quad (2.1)$$

## 2.2 Control

where  $T_{gen}$  is the torque generated,  $\theta$  is the actual position, and  $\theta^*$  is the desired position. Rotational damping coefficient  $b_c$  of the impedance controller is often set to obtain a critically damped system, such that unstable oscillations do not occur. Stiffness term  $K_c$  defines the tradeoff between precise movement trajectories and allowable forces, as previously illustrated in comparing a pencil with an egg. It is desirable to vary this parameter depending on the task. Controller inertial coefficient  $J_c$  effectively acts as a sensitivity gain: if the controller inertia is decreased, a given input signal will produce a larger response, and if the controller inertia is increased, the signal will produce a smaller response. Thus, the inertial term of the impedance controller changes the sensitivity of the controller such that precise movements and large sweeping movements may be produced when needed. The user would ideally independently control all three of the modulating parameters:  $K_c$ ,  $b_c$ , and  $J_c$ , in addition to motion. In practice, however, independently controlling these three variables would make control too burdensome in the field of prosthetics.  $b_c$  can be set to create a critically damped response  $b_c = 2\sqrt{KJ}$ . Determining whether to modulate  $K_c$ ,  $J_c$ , or some function of the two is not so easily accomplished. Historically they have been preset by the programmer (Hogan, 1987) or calculated based on sensed loads, independent of the task at hand (Blaya & Herr, 2004). Hogan (1985a) has advocated various metrics that may be used to reduce the number of variables. The author has shown in Appendix 12.3, however, that these metrics do not reduce the number of variables, or are not truly optimal. In addition, the user must then control which metric is to be used. As a result, it seems best to determine empirically which portion of impedance is

## 2.2 Control

most valuable to be modulated by the user, or some predetermined relationship of variables, leaving the other variables at a predetermined relationship or constant value.

Implementation of impedance control does not require any additional sensors to be placed on patients. Patients are already fit with two myoelectric (MES) sensors on agonist/antagonist muscle pairs. MES signals are created as a byproduct of muscle contraction and are broadly proportional to the amplitude of contraction. They are commonly used in agonist/antagonist muscle pairs to control prostheses. The sum of a pair, which controls movements in both directions, could be used to control impedance as well. Thus, impedance control may be quickly integrated into prosthetic systems.

*Hogan's impedance modulation.* Hogan's laboratory has allowed the user to modulate the stiffness term, but only for a very small range of stiffness (.5-7Nm/rad), and only in a constrained environment. (Abul-Haj & Hogan, 1987, Abul-Haj, 1987, Abul-Haj & Hogan, 1990a, Abul-Haj & Hogan, 1990b, Popat, et al., 1993). A frameless DC motor with a 7:1 belt drive and spur gear transmission was used to supply torque. Backlash was reduced by eccentric bushings on the gear shaft. The actuator was backdrivable, with a 9Nm stall torque, and a 13 rad/sec no-load speed. This actuator is very fast and weak compared to actuators in traditional prostheses, and a result of the very low gear ratio. The low gear ratio allows for more precise torque control. Torque was measured by strain gauges on a restraining gear, position was measured by a potentiometer, velocity was measured by differentiating the

## 2.2 Control

position, and current was measured by the motor amplifier. The user was able to modulate the stiffness between 0.5 and 7 Nm/rad by co-contracting their muscles; the damping coefficient was fixed at .5, and inertia was fixed at .05 kg m<sup>2</sup> (similar to that of able-bodied humans). The maximum MES levels were calculated every time the subject donned the socket.

Co-contraction modulation was observed when impedance control was used, but not when velocity control was used. It was also observed that impedance control smoothed velocity transitions, although no kinematic differences existed between the two controllers (Abul-Haj & Hogan, 1990a). No difference between impedance control and velocity control was observed when cutting meat, donning a sock, or rolling dough.

There are several points worthy of comment. First, in any control paradigm, there is both a motion paradigm and an impedance paradigm. For the motion paradigm, traditionally velocity control is used, although position control may be also used. For a given motion paradigm, an impedance paradigm is overlaid: either one that may be modulated, or one that is always stiff. Unfortunately, in the experiments just described, position control was used as the motion paradigm for impedance modulation control, but velocity control was used as the motion paradigm for a constant stiff impedance paradigm. Thus, the results obtained may be caused not by the impedance paradigm, but rather by the difference in motion paradigm. Second, able-bodied subjects modulate their stiffness between 2 and 120 Nm/rad, as detailed in 12.1.1. Confining the range of impedance modulation to 0.5 – 7 Nm/rad is really an example of a low impedance paradigm, not a modulated impedance paradigm. Finally, it is doubtful, in

## 2.2 Control

the author's experience, whether an actuator with a true stiffness of 7 Nm/rad would even be capable of cutting meat: The difference between the desired and actual position would have to be very large to generate sufficient torques.

### 2.2.3 Admittance Control

Admittance control is similar to impedance control, in that the relationship between movement and forces rather than independent components is regulated. In admittance control, however, force is input, and position is output, as illustrated in Figure 2.2.

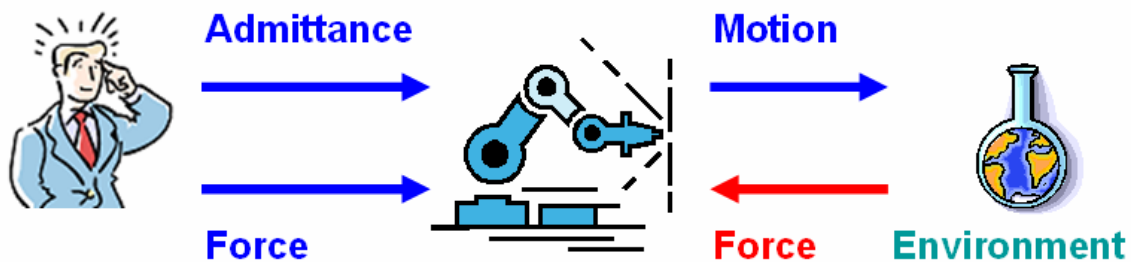


**Figure 2.2: Admittance Control**

Motion is generated instead of force, and force is sensed instead of motion

Obtaining admittance control is not as challenging as obtaining impedance control, since accurate position is easily obtained using reduction gear transmissions. For rigid systems precise modeling of the internal dynamics is required (Clover, 1999, Huang & Schimmels, 2004, Schimmels, 1997, Schimmels & Peshkin, 1994, von Albrichsfeld & Tolle, 2002). Methods of compensating for internal dynamics are reviewed in Appendix 12.4.

A popular example of admittance control is the HapticMaster (Van der Linde, Lammertse, Frederiksen & Ruiter, 2002), which has accurate force control, a large dynamic range of controllable forces, and a quick response time.

#### **2.2.4 Choosing Between Impedance Control and Admittance Control**

There has been some debate over whether or not environments behave as an impedance or an admittance (Hogan, 1985a, Hogan, 1985b, Hogan, 1985c, Robinson, 2000) and if the causality of various elements such as friction make one method of control better than the other. The elements required to obtain each control paradigm are perhaps more important. For instance, increased compliance will allow reflected inertia to be minimized but will decrease the saturation envelope of large torque oscillations. Although neither impedance control nor admittance control require increased compliance, increased compliance lends itself to impedance control, and as a result, impedance control is often thought to be better at minimizing reflected inertia, and worse at large-amplitude high frequency control. It should be emphasized that these are merely attributes of the physical system used: compliance may be introduced in an admittance actuator to achieve these same results, and use of a direct drive motor may allow decreased compliance in impedance control. In looking at the causality of actuators and environments it is easy to become caught up in the impedance versus admittance debate. There is, however, a simple distinction to make between the two of them: any time position control is desired, impedance control should be used. Any time force control is desired, admittance control should be used. This choice does not seem intuitive at first,



because impedance controlled actuators generate force, and thus seem likely to be used for force control. The fact remains that impedance control senses position, and as such, is primarily intended for use as a position controller. The opposite is true of admittance control. Accurate positions may be obtained using admittance control: they do, because they do generate position. Accurate forces may be generated using impedance control: they do after all, control force. But both modes of control are inherently set up to do what they do best, and given that there are two available options, it does not make sense to use one in the realm where the other excels.

## 2.2 Control

### **2.3 Technologies**

Upper-limb prostheses are typically used to grasp an object, position it, and then leave it in that position while the user performs a task (Heckathorne, 2004). As a result, commercial electric prosthetic elbows use a non-backdrivable gear transmission to conserve power during those times when the prosthesis is not moving. A prosthesis with a backdrivable gear transmission continuously consumes power ( $IR^2$ ) during such a task, whereas a prosthesis with a non-backdrivable transmission may be shut off when the prosthesis is not moving. Commercially available prostheses move slowly (2-5 rad/sec), but advances in technology are allowing them to increase their speed. Non-backdrivable transmissions present a dangerous environment to the user during collisions at high speeds (Zinn, Khatib, Roth & Salisbury, 2004a) due to the high impact forces they can create, and as such, despite the controller design used, new mechanical designs must be chosen that limit the impedance of the prosthesis at high frequencies to ensure safety.

High fidelity versions of conceptually classical robots have often been used for interaction with persons because they are capable of achieving high torques and speeds. Many term these robots as having low-impedance if their actuator's impedance is low in the controllable bandwidth. At uncontrollable high frequencies that result from unplanned collisions, however, conventional robots – even ones with high force fidelity – have high impedance and become hazardous to persons. The problem is exasperated by the low torque densities

common in electromagnetic motors, which require high gear ratios to obtain acceptable torque densities. These high gear ratios significantly amplify the inertia of the actuator, creating high impedance systems. Perhaps the most common remedy in conventional robotics is to soften the blow of the robot with a compliant cover. As Zinn et al. have illustrated (Zinn, Roth, Khatib & Salisbury, 2004b), however, more than five inches of cushioning would be needed to generate sufficient compliance to make a robot such as the Puma 560 safe when interacting with persons. This bulkiness is unacceptable for many human-robot applications.

Several methods are being investigated to achieve safer robot interaction with humans, including electromagnetic motor alternatives, inertia reduction, passive impedance modulation, joint torque control, and increased actuator compliance. These methods are examined below. All of these methods attempt to minimize one or more of the components of impedance. Impedance ( $Z$ ) is generally considered to have stiffness ( $k$ ), viscous ( $b$ ), and inertial ( $m$ ) components, although many methods focus solely on the stiffness or inertia of the system.

### **2.3.1 Electromagnetic Motor Alternatives:**

Popular torque generating alternatives to electromagnetic motors include pneumatic or hydraulic motors, McKibben muscles, shape memory alloys, and electroactive polymers (Hollerbach, Hunter & Ballantyne, 1991, Hunter, Hollerbach & Ballantyne, 1992). All of these actuators have been investigated in anthropomorphic systems to some degree, but they

have largely failed because of practical issues such as power consumption, low efficiency, slow response time, weight, and volume. Pneumatic actuators are especially appealing because they are intrinsically compliant (and thus have low impedance at high frequencies). Both pneumatic actuators and hydraulic actuators, however, require compressed sources of air or fluid that are practically difficult to obtain and recharge. Pneumatic actuators have been used in prostheses in the past, but are currently not used because of these self-containment and accessibility difficulties.

### **2.3.2 Inertia reduction**

One way to reduce the impedance of an actuator is to reduce the inertia of the actuator, a technique used by the PHANToM arm (Massie, 1993), WAM hand (Salisbury, Townsend, Eberman & DiPietro, 1988), and the base stage of the DM<sup>2</sup> (Zinn et al., 2004b). The inertia may be reduced by placing the actuators at the base of the robot and using a cable system to transfer power to the endpoint. This placement of the motors successfully reduces the inertia of the endpoint, as illustrated in Figure 2.3, although at higher frequencies the impedance remains high. The physical characteristics of cabling make large gear ratios difficult to obtain (Williamson, 1995), reducing torque density and thus power efficiency. In addition, the nature of cabling electric prosthetic components makes them impractical in prosthetic situations.

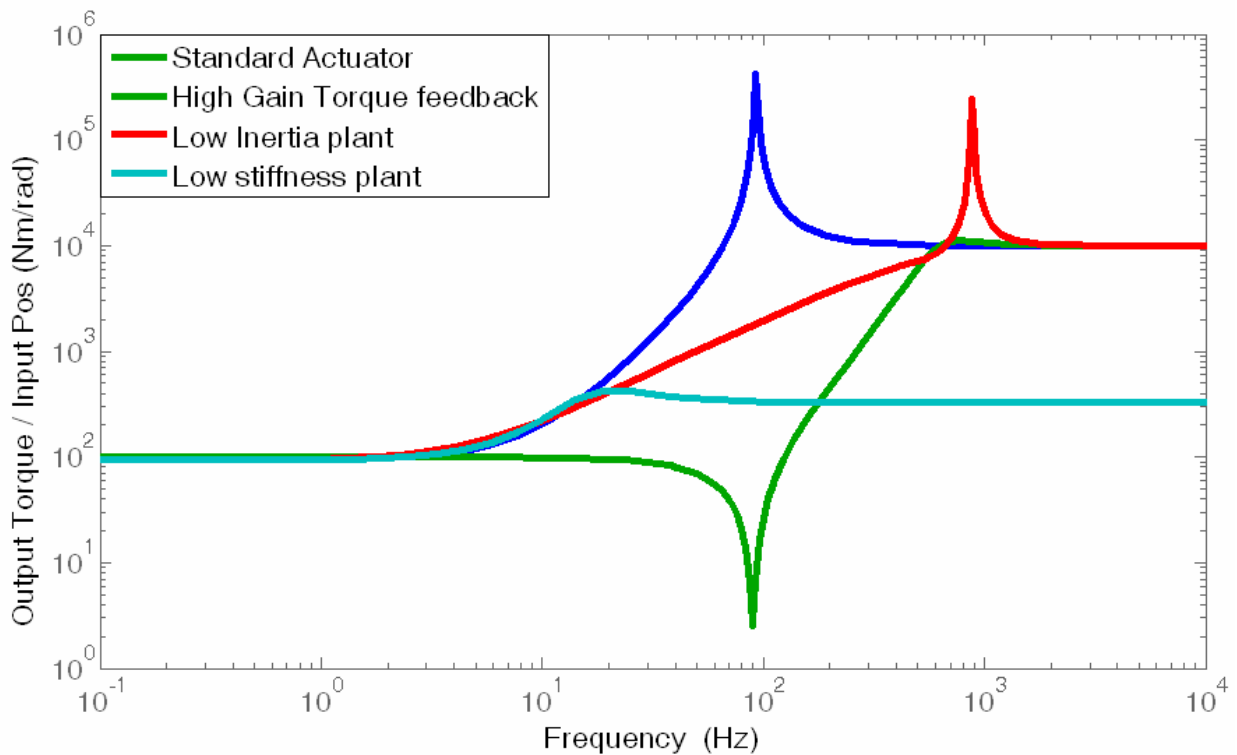


**Figure 2.3: Different solutions to minimize high frequency impedance**

### 2.3.3 Passive impedance modulation

Several groups have created actuators that decouple the stiffness of an actuator from its force or position through nonlinear springs (English & Russell, 1999a), spring length reduction (Hollander, Sugar & Herring, 2005), or other approaches (Bicchi & Tonietti, 2004, Morita & Sugano, 1996, Ozawa & Kobayashi, 2003). These approaches successfully limit the impedance of the actuator. They all, however, require a second motor to decouple the stiffness from the

motion of the actuator. This additional motor increases the size, weight, and power consumption of the robot.

### **2.3.4 Joint Torque Control**

Joint Torque Control (JTC) attempts to create high fidelity torque control by using high performance motors with minimal friction coupled with advanced controllers to achieve high torque performance at each joint in their controllable bandwidth. A recent example is the German DRL II (Butterfass, et al., 2004). The impedance of JTC controlled actuators above the controllable bandwidth, however, remains high, as shown by the “High Gain Torque Feedback” line in Figure 2.3, and it is precisely at this region where the effects of inertia dominate. As a result, JTC controlled actuators are still unsafe for unexpected collisions with humans.

Direct drive motors (Asada & Youcef-Toumi, 1987), a subset of JTC, exclude the gear transmission completely in an effort to minimize the motor inertia and achieve high fidelity torque control. They offer excellent force control by minimizing friction and backlash. Kotoku, Husler, Tanie and Fujikawa (1990) produced a direct drive motor that used adaptive impedance. Hogan (1987) originally used this method to implement control as well. Hogan used a parallel link mechanism to increase the torque and reduce the inertia of the actuator. Hogan indirectly used current control by driving the motor with transconductance amplifiers with high-gain internal current feedback. Control of the torque using electrical current offers a simple and practical way to generate torque, but the size and weight requirements of the

motor are not practical in prostheses, and the backdrivable nature of the actuator means that they need to continuously consume power to maintain position, another limitation in prostheses.

### **2.3.5 Increased Compliance**

Compliance may be used in two different manners: passively and actively, as illustrated in Figure 2.4. If passive compliance is used, the actuator is controlled by position control and a compliant element is inserted on the end of the actuator. Because position control is monitored before the insertion of the compliant element, stability is maintained (Cannon & Schmitz, 1984). The introduction of compliance reduces control instabilities when the actuator transitions from free movement to constrained movement. A popular illustration of the introduction of compliance is the Honda P3 robot (Hirai, 1999). Hirai acknowledged that increased compliance achieved impact absorption at the cost of difficulty in determining the position of the robot with respect to coordinate axes. Attempting to adequately achieve both goals simultaneously, his group chose a compliance such that in the absence of any external forces the output of the gear transmission maintained the correct position, but that in the presence of large ground reaction forces, would yield enough to sufficiently absorb those forces (Hirose, et al., 1995). Passive compliance does reduce contact instabilities, but the magnitude of compliance is fixed: it may not be modulated by the controller. Thus adaptive

impedance control may not be achieved solely by the introduction of a physically compliant member.

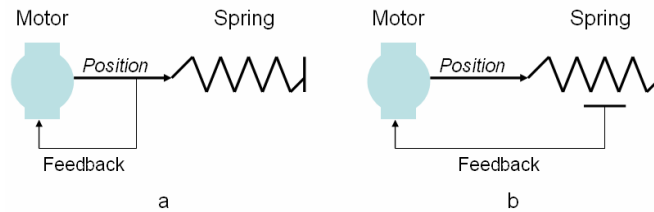


**Figure 2.4: Intentional Compliance in Robots**

Traditional position feedback is used, but a spring is placed on the end of the actuator. The compliance of the spring may not be changed, as used in the Honda P3.

The spring is instrumented, and the force output fed back to the motor to create a Series Elastic Actuator. The overall compliance of the actuator may be varied since the force on the spring is monitored, as pioneered by Pratt and Williamson, and used in this proposal.

The intentional increase of instrumented compliance in electromagnetic motors has been investigated in the past (Andeen & Kornbluh, 1988), and has recently gained support through the work of Pratt et al. (Pratt, et al., 1995), who have termed the concept a *series elastic actuator*. The concept has recently been explored by other groups (Okada, Nakamura & Ban, 2001, Okada, Nakamura & Hoshino, 2000, Zinn et al., 2004b), and is illustrated in Figure 2.5.

## 2.3 Technologies



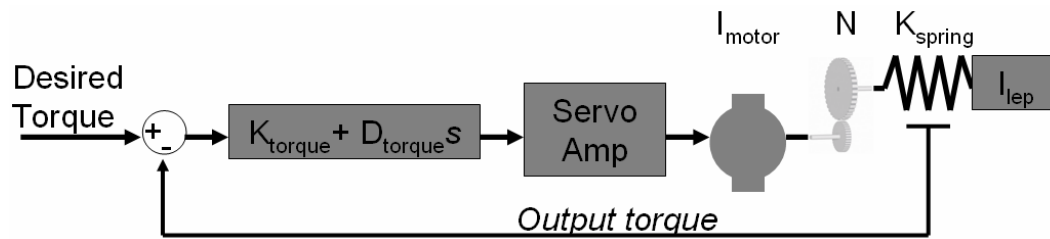


**Figure 2.5: Series Elastic Actuator**

Control system consists of proportional gain  $K_{\text{torque}}$  and derivative gain  $D_{\text{torque}}$ . The dominant feature of the motor is inertia, given the high gear ratio  $N:1$ . Spring has stiffness  $K_{\text{spring}}$ , and interacts with the end-point of the actuator, with inertia  $I_{\text{ep}}$ .

Figure 2.5 initially appears to be a classic example of non-collocated control (Cannon & Rosenthal, 1984) because there is compliance between the sensor and the motor. It should be kept in mind, however, that the sensor in parallel with the compliant element is a torque sensor, not a position sensor. Position control is collocated, because the position sensors used (Hall effect sensors) are located on the motor. Force control is likewise collocated, even in the presence of a non-backdrivable transmission. The position on the input and output of the gear transmission are the same despite stiction. The torsional spring converts this accurate position into an accurate torque. The force at the input and output of the torsional spring are identical, preserving collocated control and ensuring a stable system.

It should be noted that although this torsional spring is compliant compared to traditional actuators, it is still stiff enough such that it appears rigid to the casual observer. In fact, the “compliant” torsional spring used in this proposal (350 Nm/rad) has a stiffness larger than the maximum stiffness of a human joint under co-contraction [3–120 Nm/rad] (DeGoede &

### 2.3 Technologies

Ashton-Miller, 2003, Popescu, Hidler & Rymer, 2003). That level of compliance is still significant in the field of robotic control, and compliance has historically decreased the stable bandwidth in control loops for robotics. Compliance becomes even more problematic in the presence of stiction and backlash (Armstrong-Hélouvry, Dupont & Canudas de Wit, 1994), which are typically present in non-backdrivable transmissions. As such, Williamson and Pratt were forced to use a backdrivable reciprocal ball screw journal to avoid backlash and large levels of stiction. Backdrivable transmissions are not practical in prostheses, because they consume too much power. A backdrivable prosthetic limb may not maintain a fixed position in the presence of an external force without consuming power, and thus the prosthesis must be continuously powered. The author has solved this problem through the introduction of a non-backdrivable backlash free gearing system: Harmonic Drives. The author has shown that non-backdrivable series elastic actuators may be realized, providing a means to produce adaptive impedance control in a manner that may be practically used in prostheses (Sensing, 2005, Sensinger & Weir, 2005, Sensinger & Weir, 2006d).

Harmonic Drives<sup>®</sup>, which have some compliance in their middle gear, have also been used for torque control. Unfortunately, the torque ripples caused by the sinusoidal nature of their elliptical rotation have disrupted sensor readings enough to make torque control unfeasible. Godler et al. has created a tuning algorithm that attempts to correct this problem, but the method does not satisfactorily reduce torque ripple for small torque loads (Godler, Hashimoto, Horiuchi & Ninomiya, 2001, Godler, Horiuchi, Hashimoto & Ninomiya, 2000,

### 2.3 Technologies

Godler, Ninomiya & Horiuchi, 2001). The author has further reduced torque ripple, but still found it to be unsatisfactory for torque control (Sensing, 2005, Sensinger & Weir, 2006c).

Increasing compliance is desirable for two distinct reasons: 1) increased compliance increases force fidelity in the controllable frequency bandwidth, allowing for near-zero impedance, and 2) increased compliance limits the impedance of the actuator to the stiffness of the spring at frequencies above the controllable bandwidth, as illustrated in Figure 2.3. This impedance limiting permits the inclusion of high impedance dynamics on the motor side of the spring, such as a power conserving non-backdrivable transmission, with no effect on the overall output impedance of the system. The introduction of compliance does not come without cost, however. The inclusion of compliance impairs the ability of the actuator to generate large-amplitude, high-frequency torque oscillations. Each of these reasons is further explained below.

**High Fidelity Force Control:** High proportional gains decrease the effects of nonlinearities such as stiction, improving force fidelity. If proportional gains are set too high, however, the system becomes unstable. A simple definition by Whitney (1976) will be sufficient to illustrate the stability region:

$$0 < \tau K_{Control} K_{plant} < 1 \quad (2.2)$$

where  $\tau$  is the sampling period,  $K_{Control}$  is the controller gain, and  $K_{plant}$  is the combined stiffness of the actuator and environment. For a given sampling time, in order to increase the

### 2.3 Technologies

proportional controller gain it is necessary to decrease the actuator or environmental stiffness. It should be noted that the overall stiffness of the robot, from a control perspective, is not changed: it is merely shifted from the physical system to the controller. This increase in controller gain minimizes plant nonlinearities such as friction, creating better force fidelity.

This increased force fidelity does come at a cost, however. All actuators have a torque-speed saturation envelope, an example of which is shown in Figure 2.6a. This envelope, when examined in light of the stiffness of the actuator, may also be thought of as a force-frequency force envelope ( $\text{torque frequency} = \text{spring stiffness} * \text{speed}$ ), as shown in Figure 2.6b. It may be seen that by reducing the stiffness of the actuator, the torque-frequency saturation for a given force is reduced. Thus, through the introduction of compliance, the torque-frequency saturation envelope of the actuator is lowered. Provided the actuator is operating beneath the envelope, increased compliance does not introduce any deleterious effects: it is only when the actuator reaches saturation that performance is reduced.

### 2.3 Technologies

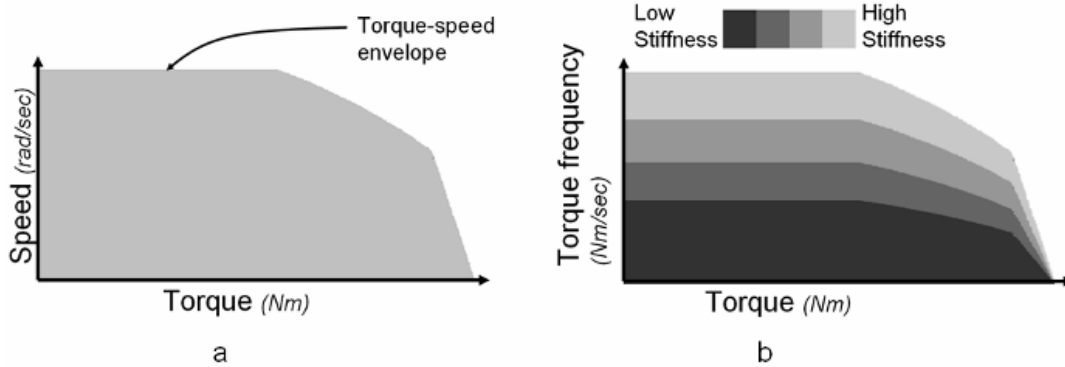


**Figure 2.6: Effect of Compliance on Torque Frequency Saturation.**

All motors have a speed-torque saturation nonlinearity (a), which limits the speed of the motor, dependent on the applied torque. The speed of the motor, combined with the stiffness of the actuator, illustrates the torque frequency of the actuator (Torque frequency = spring stiffness \* speed). As seen in (b) decreasing the stiffness decreases the torque-frequency saturation envelope for a given applied torque. As long as the motor is used inside the envelope, no decrease in torque frequency is observed for decreased stiffness.

**Impedance Saturation above controllable bandwidth:** The impedance of the actuator given in Figure 2.5 may be approximated by the second order model below:

$$\frac{F(s)}{X(s)} = \frac{K_{spring} s^2 N^2 J_{motor}}{s^2 N^2 J_{motor} + K_{spring} + N(K + Ds)} \quad (2.3)$$

At high frequencies, the  $s^2$  terms dominate and the impedance reduces to:

$$\frac{F(s)}{X(s)} \approx \frac{K_{spring} s^2 N^2 J_{motor}}{s^2 N^2 J_{motor}} \approx K_{spring} \quad \text{as } s \rightarrow \infty \quad (2.4)$$

### 2.3 Technologies

As a result, by intentionally decreasing the stiffness of the actuator, the impedance of the actuator is limited to the stiffness of the spring above the controllable bandwidth: not to the stiffness or inertia of the non-backdrivable gear transmission. Despite the fact that the impedance of series elastic actuators is saturated by the stiffness of the spring, allowing for the presence of a non-backdrivable transmission, series elastic actuators have historically used a backdrivable transmission.

**In summary, there are various ways to obtain accurate torque control, a necessary requirement to implement impedance based position control. Few of these options may be practically realized in prostheses. Non-backdrivable series elastic actuators appear to be a reasonable compromise between obtaining high fidelity impedance control and practically implementing the design in prostheses.**

### 2.3 Technologies

### 3 Socket-Residual Limb Interface Rotational Stiffness

The performance of prosthetic components depends on the interface between the prosthesis and the user, illustrated in Figure 3.1. For example, in the presence of a perturbation or static load, a stiff prosthetic elbow will still be displaced if the prosthetic elbow is in series with a compliant socket-residual limb interface. Many biomimetic control paradigms used in prostheses (Abul-Haj & Hogan, 1990a, Popat et al., 1993, Sensinger & Weir, 2006b, Sensinger & Weir, 2006d) assume a rigid socket-residual limb interface. If the socket-residual limb interface is compliant, or the socket-residual limb interface stiffness may be modulated by the user, such control paradigms become superfluous. These examples illustrate the need that engineers have for knowledge of the rotational stiffness of the socket-residual limb interface, to ensure that they do not over-design prostheses at the expense of increased cost, complexity, and development time. Specifically, what is the rotational stiffness of a socket-residual limb interface, and how much influence does co-contraction by the subject have on the rotational stiffness?

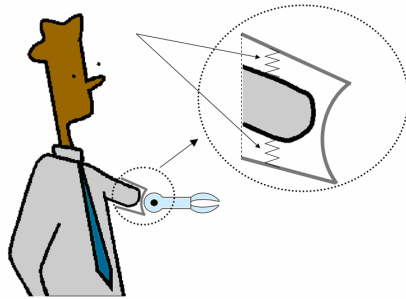


**Figure 3.1: Socket-residual limb interface compliance between socket and residual limb.**

The interface is not rigid: some compliance is present (illustrated here by a pair of springs), and affects control of the prosthesis.

Clinical fitting of subjects and socket design are also improved by properly understanding the effect of variables that significantly influence socket-residual limb interface stiffness. Questions such as what effect does the amputation length have on stiffness, does myodesis improve stiffness, how large of an effect does creating a distal window in the socket have on stiffness, and what effect does the conformity of the fit have on the prosthesis, may be answered if an accurate model of the socket-residual limb interface stiffness is available.

The rotational stiffness of the socket-residual limb interface is a function of the material properties and anthropomorphic parameters of the residual limb. Accordingly, the first portion of this paper will develop mathematical and finite element models of the socket-residual limb interface and analyze the sensitivity of the models to each of the variables. The second portion of the paper will empirically measure the rotational stiffness of the socket-residual limb interface for four subjects with a transhumeral amputation, using fluoroscopy (X-Ray movie frames) to measure bone deformation. These results are compared to the

### 2.3 Technologies



models, using X-Ray slides to obtain accurate anthropomorphic measurements of the parameters.

### **3.1 Modeling**

Modeling of the socket-residual limb interface rotational stiffness significantly depends on the value used for Young's modulus ( $E$ ). Young's modulus is a measure of the ratio of stress to strain, for small strains. Numerous studies have characterized Young's modulus for soft tissue using mechanical indentation tests and ultrasound. Zheng et al. (2001) present a good review of many of the studies that specifically examine residual limb soft tissue. Although tissue deformation is nonlinear (Silver-Thorn, 1999, Zheng, Mak & Lue, 1999), the variance in linear Young's modulus due to co-contraction (Krouskop, Dougherty & Vinson, 1987) is significantly larger than any recorded nonlinear effects. Mak et al. (1994) have shown that there is no difference in Young's modulus between the amputated limb and the intact limb. There is a large difference, however, depending on age and gender. Older subjects (57-78 years old in the study) can only change their Young's modulus by 24%, whereas younger subjects (25-35 years old in the study) can change their Young's modulus by 43% (Mak et al., 1994), presumably because older subjects cannot co-contrast their muscles as much as younger subjects. Male subjects had a mean modulus 40% higher than female subjects (Zheng & Mak, 1999). Krouskop et al (1987) have demonstrated that subjects with a trans-radial (below elbow) amputation can modulate their Young's modulus from 6kPa to 100 kPa by co-

contracting their muscles. In a similar study of able bodied subjects, Zheng et al. (1999) found a Young's modulus range of 10-60 kPa on the forearm. No studies have been done of trans-humeral (above-elbow) residual limb soft tissue, but the range of Young's modulus for trans-radial is the same as for transfemoral, and as a result, this range seems applicable to trans-humeral soft tissue.

It may be thought that myodesis, in which residual muscle is attached to the residual bone, is required to allow for modulation of the stiffness. This is not the case, however. It is unlikely that all of the subjects in Krouskoup's study (Krouskop et al., 1987) had myodesis, yet a Young's modulus range was found of 6-100 kPa. Zheng et al. (2005) has been able to achieve pattern recognition results using the morphological shape of trans-radial residual limb tissue, indicating that the muscle tenses, rather than merely shifting. Abboudi et al. (1999), using a similar pressure dependent recognition system, have measured a pressure range of 0-55 kPa for subjects without myodesis. As a result, it seems likely that all subjects can modulate the stiffness of their residual limb.

### **3.1.1 Mathematical Modeling**

The stiffness of an object may be represented as a function of the area, depth, and Young's modulus of the object. The force exerted by a discrete volume within the object is equal to the stiffness, multiplied by the amount of deformation. The force may be represented by the following equation:

#### 3.1 Modeling

$$F = \frac{EA\Delta d}{d} \quad (3.1)$$

where  $F$  is the force exerted by the tissue against the socket,  $E$  is Young's modulus,  $A$  is the area under consideration,  $\Delta d$  is the deformation of tissue, and  $d$  is the original depth of the tissue to the bone, as illustrated in Figure 3.2.

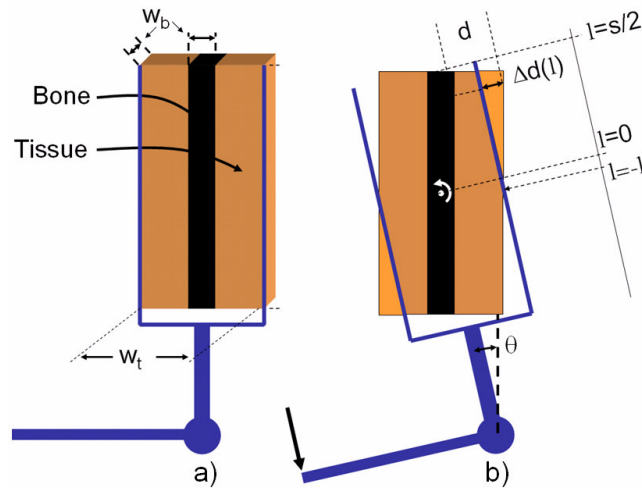


**Figure 3.2: Deformation of tissue when a load is applied to the socket.**

a) Undeformed socket-residual limb interface.  $b$  is the diameter of the bone,  $f$  is the diameter of the soft tissue, and  $s$  is the length of the socket.

b) Deformed socket-residual limb interface.

To calculate the force exerted at a specific point,  $A$  may be separated as the product of length  $l$  and bone width  $w_b$ , and the force may be differentiated with respect to length:

$$dF = \frac{Ew_b\Delta d}{d} dl \quad (3.2)$$

### 3.1 Modeling

$d$  and  $\Delta d$  are given by the following:

$$d = \frac{w_t - w_b}{2 \cos \theta} \quad (3.3)$$

$$\Delta d = l \tan \theta \quad (3.4)$$

Substituting equations 3.3 and 3.4 into 3.2, and simplifying:

$$dF = \frac{2Ew_b l \sin \theta}{w_t - w_b} dl \quad (3.5)$$

The moment at point  $l$  is obtained by multiplying  $dF$  by  $l$ . The majority of the moment across  $l$  acts in one direction. There is a small portion, however, that acts in the opposite direction.

This transition occurs when:

$$l = l' = \frac{w_t (1 - \cos \theta)}{2 \sin \theta} \quad (3.6)$$

The sum of the moments above and below the center of rotation is:

$$M = 2 \left( \int_0^{s/2} \frac{2Ew_b l^2 \sin \theta}{w_t - w_b} dl - \int_0^{l'} \frac{2Ew_b l^2 \sin \theta}{w_t - w_b} dl \right) \quad (3.7)$$

When integrated, this equation becomes:

### 3.1 Modeling

$$M = -Ew_b \frac{w_t^3 \cos^2 \theta - \cos \theta \sin \theta S^3 - 2w_t^3 \cos \theta + w_t^3 - \sin \theta S^3}{6(w_t - w_b)(\cos \theta + 1)} \quad (3.8)$$

By ignoring the portion of the moment that acts in the opposite direction (of which both the displacements and moment arm are small, producing small torques) and simplifying the trigonometry to act near  $\theta = 0$ , the equation simplifies to a format that may easily be displayed in stiffness form as:

$$K = E \frac{w_b S^3}{6(w_t - w_b)} \quad (3.9)$$

The tissue directly in front of the bone will deform by the same amount that the bone deforms. As a result, equation 4 adequately captures the resulting force caused by the tissue directly in front of the bone, because the amount of deformation is known. The amount of deformation of the surrounding tissue, however, is unknown. The resulting deformation will be greatest near the edge of the bone, and minimal near the skin. The deformation, illustrated in Figure 3.3, will be determined by that geometry which minimizes the stored energy, where energy is a function both of the compressive and shear forces resulting from the displaced tissue.

### 3.1 Modeling

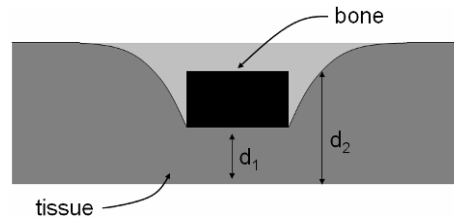


**Figure 3.3: A transverse plane depiction of tissue deformation.**

The deformation at  $d_1$  is known, because the bone determines the amount of deformation. The deformation at  $d_2$ , however, is unknown. Some deformation will occur, because the tissue is connected to the tissue directly in front of the bone. The amount of deformation may be calculated by finding that shape which minimizes the total energy stored at that segment.

Biaxial compressive forces and shear forces are applicable to this shape, for which:

$$dU_{compression} = \frac{E}{2(1-\nu^2)} (\epsilon_x^2 + \epsilon_y^2 - 2\nu\epsilon_x\epsilon_y) dV \quad (3.10)$$

and

$$dU_{shear} = \frac{G\gamma^2}{2} dV \quad (3.11)$$

where  $G$  is the shear modulus, and equals  $\frac{E}{2(1+\nu)}$ ,  $\epsilon_x$  and  $\epsilon_y$  are the strains,  $dV$  is the

discrete volume being analyzed, and  $\gamma$  is the angle of shear deformation. An exponential curve was found to best minimize the sum of energy over the entire residual limb. The power of the

### 3.1 Modeling

exponent depends on the subject's anthropomorphic parameters and the amount of deformation at the boundary of the bone. As a result, the equation cannot be algebraically solved, but may be solved using discrete algebraic code. The results of this mathematical equation are given in the results section.

### **3.1.2 Finite Element Modeling**

A finite element model of the socket-residual limb interface was created using Pro/Engineer Wildfire 2.0<sup>®iv</sup>. Static analysis of tetrahedral solid P elements using Multi-Pass Adaptive (MPA) element fitting was performed for all analyses. MPA analysis records the maximum error at element intersections in Von Mises stress (distortion energy) and strain energy error, increasing the order of the polynomials used to fit the geometry until the errors are all less than ten percent. The amount of acceptable error may be lowered, but lowering this limit results in a dramatic increase in computational time, since the boundary of contact interface is complex. The setup is illustrated in Figure 3.4. Contact points were created at equally spaced intervals along the interface. The inside of the tissue, which interfaces with bone, was grounded, and a force was applied to the end of the prosthesis to realistically mimic a torque on the elbow. Analyses were done using upper and lower estimates of both Young's modulus and Poisson's ratio.

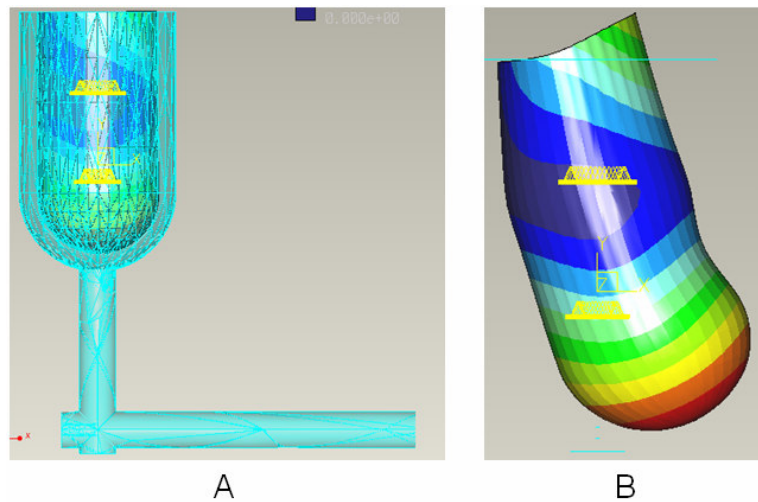


**Figure 3.4: Finite Element Model**

A) FEA p-mesh of CAD geometry.

B) shows the shape of the deformed tissue inside of the socket for a 2.8 Nm load, where  $E=10$  kPa and  $\nu=0.4$ .

### **3.2 Fluoroscopy**

To empirically measure the rotational stiffness of socket-residual limb interfaces, the deformation between the humerus and socket was measured in four subjects using fluoroscopy: a type of low-dosage X-ray. The protocol was approved by the Northwestern University Institutional Review Board, and all patients signed informed consent forms.



### 3.2.1 Subjects

Four subjects, including three males and one female, were included in this study. Socket type, age, and anthropomorphic data are given in Table 3.1. Graphical representations of their residual limb are given in Figure 3.5

**Table 3.1**  
**Subject Anthropomorphic data**

All measurements are in cm

Subject (age)	Socket Type	Bone Dia.	Limb Dia.	Distance from Elbow to:	
				distal end of bone	proximal end of socket
A (27)	Harness	2.3	8.5	19	33
B (39)	Harness	2.9	10.3	19	35
C (43)	Suction	2.4	10.0	17	34
D (50)	Suction	1.7	10.0	9	29

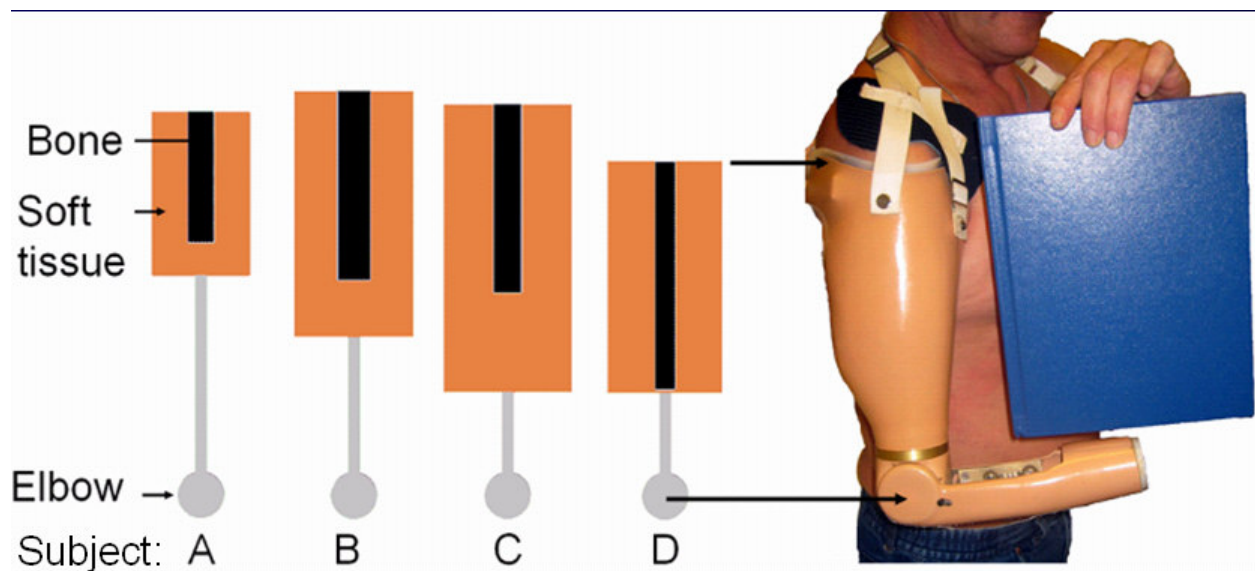


**Figure 3.5: Graphical representation of subject residual limb.**

Anthropomorphic parameters were measured from X-Ray slides of the residual limb.

### 3.2 Fluoroscopy

### 3.2.2 Apparatus & Procedures

Fluoroscopy slides (a rapid series of low-radiation X-Rays) were recorded at 5-8 Hz using a Philips Easy Diagnost Super 80CP digital RF system. The sampling frequency was verified in a separate experiment, described in Appendix 12.2.1. Force data were collected using an Omega<sup>v</sup> LCFA-50 tension/compression load cell and recorded in Matlab<sup>vi</sup> at 40 Hz. An illustration of a slide is given in Figure 3.6.

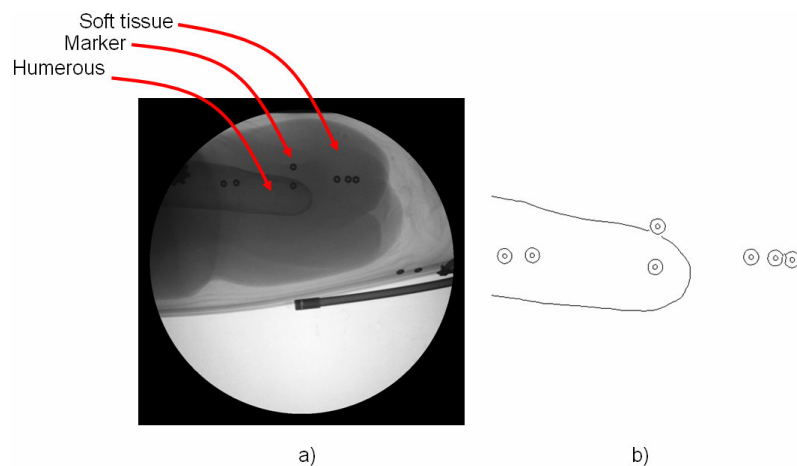


**Figure 3.6: Fluoroscopy images**

- a) Fluoroscopy slide of socket-residual limb interface.
- b) Edges obtained on a cropped version using Matlab's edge command.

The experimental setup for this study did not permit the examination of co-contraction modulation by subjects. Because the viewing window of the fluoroscopy machine was small (13 cm diameter), subjects had to maintain the position of their residual limb in the presence

### 3.2 Fluoroscopy

of force perturbations. As a result, their muscles were always moderately co-contracted to maintain this position.

### 3.2.3 Data Analysis

An edge-detecting filter was applied to a cropped version of each slide using Matlab's *edge* function with a canny filter. The humerus was then manually aligned in each slide. The angular deformation of the markers with respect to the aligned humerus was recorded. The inertial force on the load cell from the prosthesis was calculated based on the inertia of the prosthesis ( $0.4 \text{ kg m}^2$ ) and the calculated rotational acceleration. Empirical measurement of the prosthesis inertia is described in Appendix 12.2.2. The inertial component of forces was subtracted from the force data, and the remaining force was compared to the deformation in position. Due to the low frequency of oscillation, the inertial load was small for all subjects (.01% - 10%).

Because there is noise present in the marker measurements obtained from the X-Ray slides, rotational stiffness may either be found by using a linear least squares regression of the compliance, and then inverting the slope to obtain rotational stiffness, or by calculating the first principal component using principal component analysis – both techniques yielded the same result. This principle is described in more detail in Appendix 12.2.3.

### 3.3 Results

#### 3.3.1 Mathematical model

Sensitivity studies were done using the discrete math model to see how significantly it diverged from the simple math model, which did not consider the effect of surrounding tissue. Each of the anthropomorphic variables was individually varied for each subject, over a range larger than that encountered across all four subjects ( $S = 0.10 - 0.25$  m,  $w_b = 0.01 - 0.03$  m,  $w_t = 0.08 - 0.12$  m). Bone and residual limb diameter did not have large effects on the resulting rotational stiffness. The socket length, however, did have a significant effect, and the rotational stiffness may be accurately represented across subjects as the following function:

$$K = [0.13 - 0.15]ES^{[2.7-2.75]} \quad (3.12)$$

Where  $E$  is Young's Modulus and  $S$  is the socket length.

For estimates of the socket-residual limb interface outside of this variable range, such as for children, a scaling factor was found between equation 3.9, which did not consider the effect of surrounding tissue, and the more robust mathematical model. This scaling factor was found to be 5.5, with a  $r^2$  value of 0.63. The resulting equation should serve as an estimate for socket-residual limb interfaces outside of the range of:  $S = 0.10 - 0.25$  m,  $w_b = 0.01 - 0.03$  m,  $w_t = 0.08 - 0.12$  m.

$$K = 5.5E \frac{w_b S^3}{6(w_t - w_b)} \quad (3.13)$$

### 3.3.2 Mathematical model compared with FEA model

The math model and FEA model are compared with each other in Table 3.2 for subject A, using several values for Poisson's ratio and Young's modulus. These sensitivity studies were only done for a single subject since each analysis took a substantial amount of time to complete.

**Table 3.2**  
**Results of Math & FEA analysis for a sample subject**

		Modeled Young's Modulus for Subject A					
		E=10 kPa			E=70 kPa		
		Math	FEA	Error	Math	FEA	Error
Poisson's Ratio	$\nu=0$	6.9	N/A	N/A	K=48.6	K=41.3	18%
	$\nu=0.4$	K=5.9	K=6.8	13%	K=41.5	K=48.8	15%
	$\nu=0.5$	K=5.8	K=7.8	26%	K=40.8	N/A	N/A

K is in units of Nm/rad. These results were calculated for an applied torque of 2.8 Nm

From this table it may be seen that in the math model, rotational stiffness is proportional to Young's modulus for the math model, and almost proportional to Young's modulus for the FEA model. The range of Poisson's ratio encountered in soft tissue (0.4-0.5) has a small effect on the rotational stiffness. The math model corresponds well to the FEA model.

### 3.3.3 Empirical Results

Stiffness results for each subject are shown in Figure 3.7 - Figure 3.10 Figure 3.10, and the mathematical, FEA, and empirical rotational stiffness for each subject are tabulated in Table

3.3.

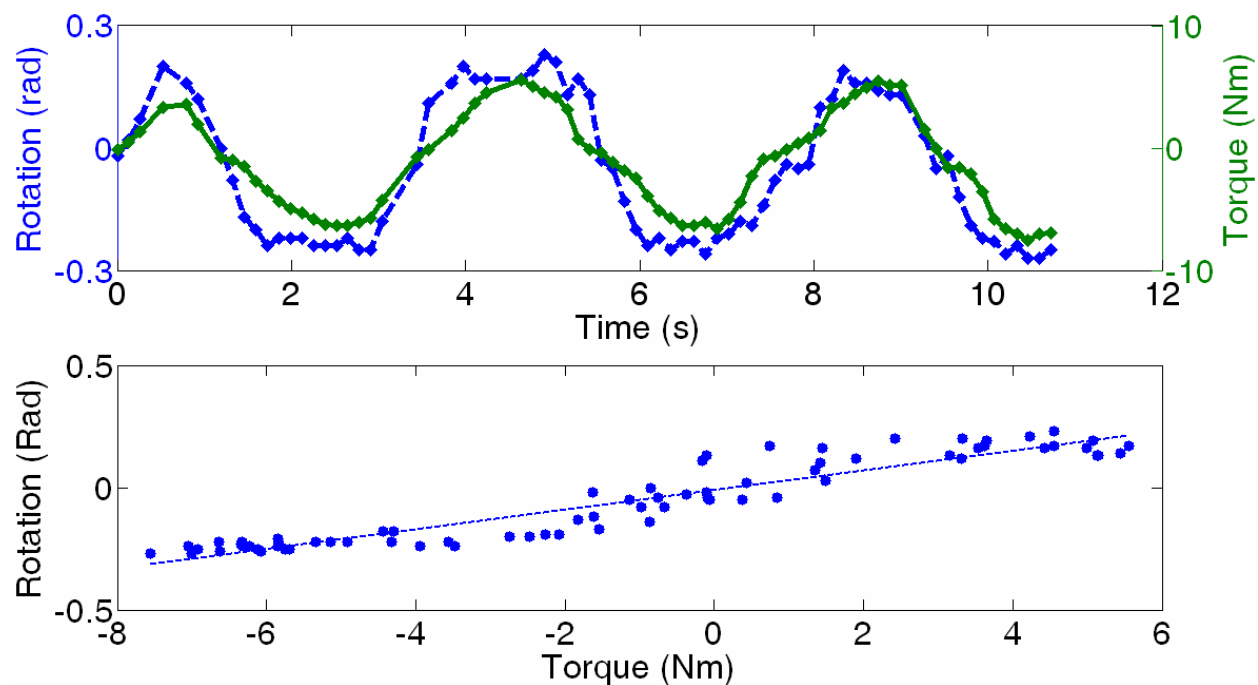


**Figure 3.7: Empirical rotational stiffness of socket-residual limb interface for subject A**

$K=25 \text{ Nm/rad}$ , [23-28 Nm/rad] 95% confidence interval.  $r^2=0.87$

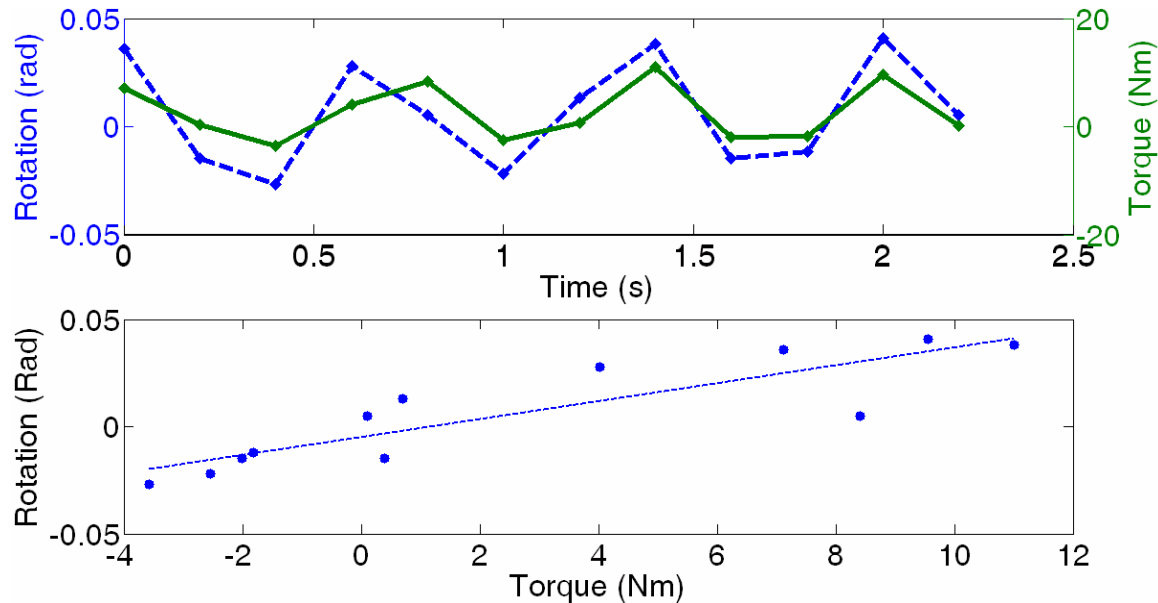


**Figure 3.8: Empirical rotational stiffness of socket-residual limb interface for subject B**

$K=240 \text{ Nm/rad}$ , [172-395 Nm/rad] 95% confidence interval.  $r^2=0.76$

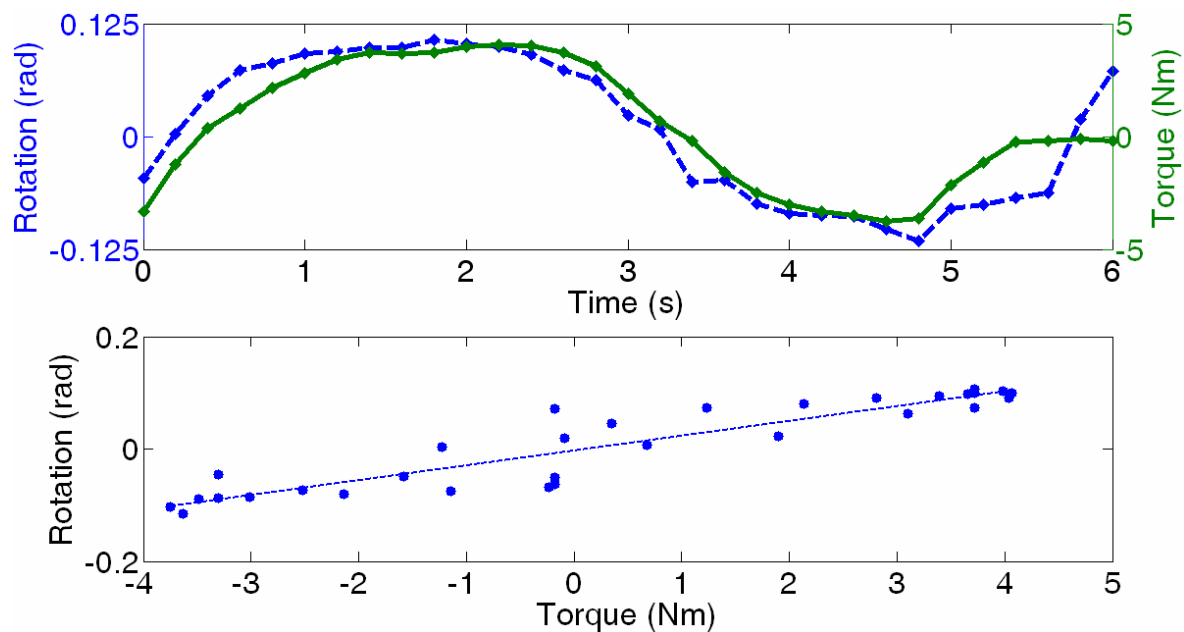


**Figure 3.9: Empirical rotational stiffness of socket-residual limb interface for subject C**

$K=38 \text{ Nm/rad}$ , [32-45 Nm/rad] 95% confidence interval.  $r^2=0.85$ .

### 3.3 Results

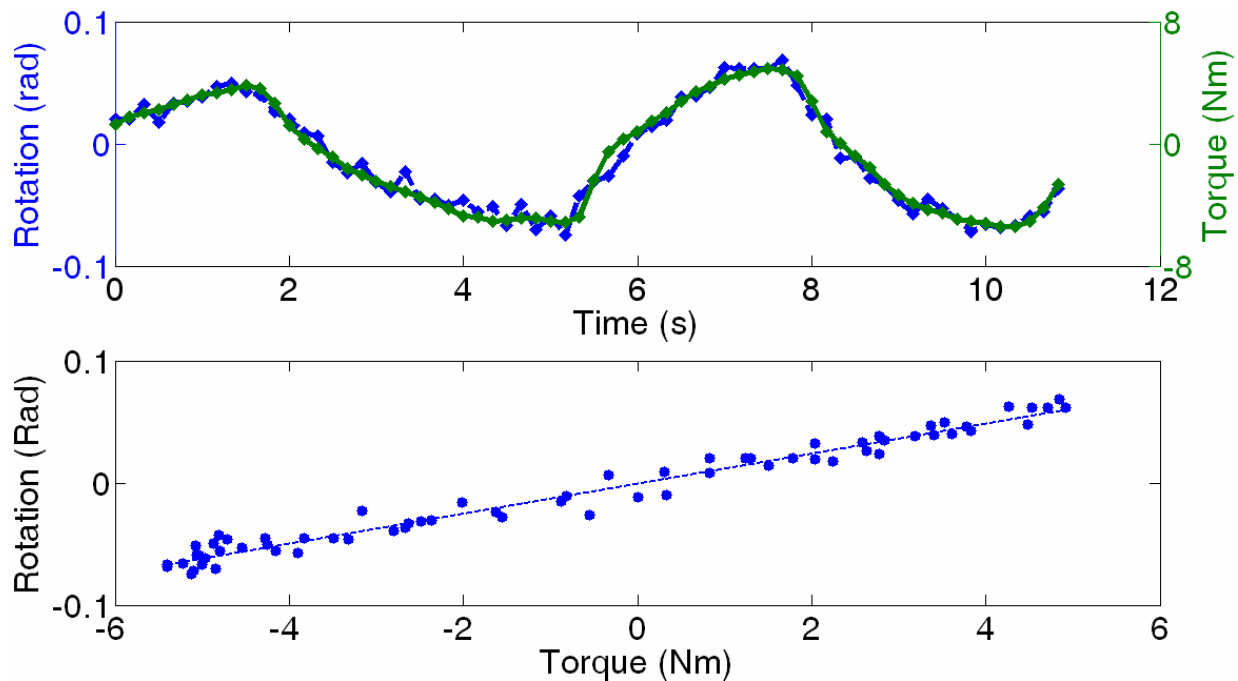


**Figure 3.10: Empirical rotational stiffness of socket-residual limb interface for subject C**  
 $K=81 \text{ Nm/rad}$ , [78-85 Nm/rad] 95% confidence interval.  $r^2=0.97$ .

**Table 3.3**  
**Modeled and Measured Socket-residual limb interface Rotational Stiffness for 4 subjects**

Subject	Stiffness (Nm/rad)				
	Math relaxed – cocontracted	FEM relaxed – cocontracted	Measured		
			Average	95% Confidence range	$r^2$
A	4-59	4-70	<b>25</b>	23-28	0.87
B	6-103	6-100	<b>138</b>	96-244	0.84
C	6-99	5-83	<b>38</b>	32-45	0.85
D	9-156	14-227	<b>81</b>	78-85	0.97

3.3 Results



### **3.4 Discussion**

Rotational stiffness of the socket-residual limb interface is proportional to Young's modulus and significantly smaller than the rotational stiffness of conventional prosthetic elbows. As a result, even in the presence of a stiff prosthetic elbow the overall rotational stiffness of the elbow and socket-residual limb interface may be controlled by co-contraction of the subject. Because of this inherent ability of subjects to modulate the stiffness of their socket-residual limb interface, it appears that control paradigms that implement impedance control directly distal to the socket-residual limb interface are superfluous. These paradigms are still useful, however, on joints that are distally removed from the socket-residual limb interface, since those joints do not have a low-impedance component directly in series with them. For example, the stiffness of the wrist joint is unaffected by the stiffness of a trans-humeral socket-residual limb interface. Likewise, the stiffness of an elbow joint is unaffected by the stiffness of a socket-residual limb interface at higher amputation levels, such as shoulder disarticulation. As a result, impedance control still merits investigation.

Whether Poisson's ratio is 0.4 (nearly incompressible) or 0.5 (completely incompressible) does not have a large effect on the rotational stiffness of the socket-residual limb interface compared to the change in rotational stiffness that results as Young's modulus changes with co-contraction. Because the models correspond well with the empirical measurements, local estimations of Young's modulus may be applied to a global socket-residual limb interface.

This finding should extend the results found in this paper to other joints, for which Young's modulus is locally known, but where global models have not yet been made.

### 3.4.1 Clinical Implications

The discrete math model accurately captures the main effects of the FE model, with the exception of Poisson's ratio. As a result, the adjusted math model (equation 11) provides a simple model of the effect of anthropomorphic factors on the socket-residual limb interface rotational stiffness. This equation may be used to evaluate prosthetic components, control algorithms, and socket techniques.

For example, the socket-residual limb interface rotational stiffness significantly increases as the socket length increases. The effect becomes more dramatic as the socket length increases. As a result, creating a distal window in the socket may relieve discomfort without affecting the subject's ability to provide torque. It does, however, decrease the stiffness of the socket-residual limb interface by 4-20 Nm/rad for every 1 cm of window, depending on the original length of the socket. A distal window reduces the stiffness more for long sockets than for short sockets. Conversely, salvaging an extra cm of distal bone increases the stiffness of the socket-residual limb interface by 4-20 Nm/rad. Likewise, proximally extending the socket increases the stiffness by 4-20 Nm/rad.

As another clinical example, the math models indicate that tissue medial and lateral to the bone have a large effect on the stiffness of the socket. As a result, creating large medial and lateral windows in the socket will have an impact on the rotational stiffness of the socket-

residual limb interface. Creating small windows, however, will not affect the stiffness, as long as they are limited to the sagittal plane.

### **3.5 Conclusion**

The measured socket-residual limb interface stiffness of four subjects is within the modeled range of stiffness predicted using math and FE models, using Young's moduli available in the literature. This same technique may be applied to other joints. From these models, it appears that persons can modulate the rotational stiffness of their socket-residual limb interface over a wide range of values. The floor and ceiling of this range depend significantly on socket length and co-contraction levels, but not on residual limb diameter or bone diameter. Measured trans-humeral socket-residual limb interface rotational stiffness values ranged from 24-140 Nm/rad for the four subjects tested in this study. Control paradigms that modulate the stiffness of a joint are unnecessary when directly in series with this socket-residual limb interface, but may still prove to be useful when implemented in joints that are more distal or when the level of amputation is more proximal.

## 4 Improvements to Series Elastic Actuators

In section 2.3, the case was made for series elastic actuators as an appropriate technology. Series elastic actuators provide accurate torque control using simple components already used for the most part in prostheses, and they are inherently safe above the controllable frequency range. The analysis of them in section 2.3.5, however, only considered a linear system, and any system used in prostheses will most likely have friction and noise in compensation for reduced weight and compactness. As a result, further increases in performance may be possible once these nonlinearities are acknowledged. Two design decisions will be analyzed below in light of these nonlinearities: sensor placement and inner control loop of the motor.

### 4.1 *Modeling Sensor Placement*

Although it is always advantageous to minimize friction in an actuator, different actuator technologies respond better or worse in the presence of friction. Series elastic actuators (SEAs) offer substantial improvements for actuators that have high levels of friction (Robinson, Pratt, Paluska & Pratt, 1999), yet previous series elastic actuators have used virtually frictionless reciprocating ball screw transmissions or low gear ratios to avoid high levels of friction. Although reducing friction has improved their performance, it has potentially masked optimal sensor placement.

SEAs have been conventionally instrumented with a displacement sensor in parallel with the compliant element, taking advantage of the increased motion of the compliant member to

produce a high fidelity signal. In linear series elastic actuators a linear potentiometer is placed in parallel with the spring, as illustrated in Figure 4.1a. Linear potentiometers offer cleaner signals than load cells, which require high levels of amplification. The higher fidelity of potentiometers compared to load cells is not intuitive: potentiometers are often thought of as poor sensors. In the presence of large position changes due to the compliant member the potentiometers are coupled with, however, they offer precise and clean control.

Robinson et al. (1999) have demonstrated that any stiction on the motor side of the sensor is mitigated by the inclusion of a compliant torsional spring. It is important to note, however, that any friction source between the sensor and the environment is not affected by the stiffness of the spring or the value of the feedback gain. As a result, a tradeoff exists between DC and AC error. A potentiometer will offer high fidelity control, but will not account for stiction (DC error). A load cell will offer low fidelity control, but will account for stiction. Thus for high levels of stiction, using a low fidelity load cell should increase performance. As a result, series elastic actuators should not automatically be fit with a position sensor in parallel with the compliant element; anticipated stiction in the design should play a crucial role in determining the optimal sensor location.

#### 4.1 Modeling Sensor Placement

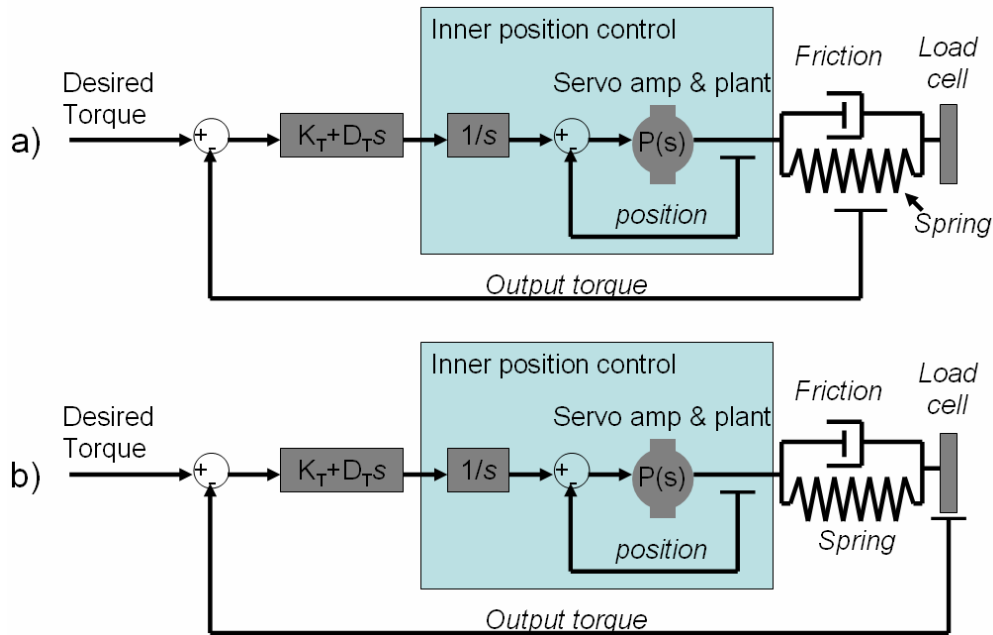


**Figure 4.1: Sensor placement**

a) Traditional parallel placement of a potentiometer offers a high fidelity signal, but cannot differentiate between parallel or distal friction sources and accurate force.

b) Serial placement of a load cell provides a poor signal due to high levels of required amplification, but may provide superior force control if it is placed distal to friction sources within the actuator.

## 4.2 Modeling Feedback control

Pratt and Williamson (1995) have historically used an inner torque control loop since they are ultimately controlling torque. Because series elastic actuators convert the accurate position output of a high impedance motor into a reliable force through the compliance of the spring, an inner velocity loop would appear to be a better choice. An inner velocity loop will attempt to attenuate the inertia of the rotor, effectively providing a flow source. As a result, as long as

the motor is not saturated, an internal velocity loop should provide a higher fidelity position output with decreased system dynamics. Pratt et al. (2004) recently demonstrated that this is the case. An inner velocity control loop is illustrated in Figure 4.2a.

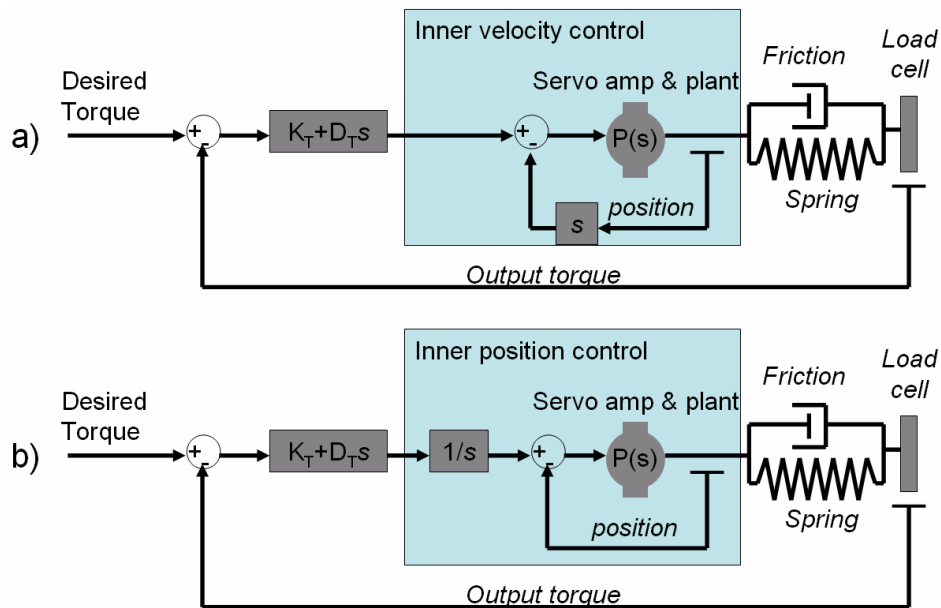


**Figure 4.2: Internal feedback**

a) The inclusion of an inner velocity control loop improves overall force control. The velocity signal is an integration of the measured position, obtained by Hall Effect sensors.

b) Internal position feedback: The inclusion of an inner position control loop should improve performance, since internal position control integrates the force error signal, rather than differentiating the position signal of the motor Hall effect sensors. Differentiating a signal amplifies high frequency (noise) components.

As illustrated in Figure 4.2a, force error, which is proportional to velocity, is fed to the inner velocity control loop. Internal velocity control takes the position reading of linear Hall-effect sensors in the motor and differentiates it to achieve a velocity signal. Noise, which tends to dominate high frequencies, is amplified by differentiating the position signal. Differentiation

#### 4.2 Modeling Feedback control

of the position signal is not required, however: one may also integrate the force error signal and use an internal position control loop, as illustrated in Figure 4.2b

Both of these methods will attempt to attenuate the inertia of the rotor by commanding a desired velocity, regardless of rotor inertia. An inner position loop should do so without adding increased noise. As a result, it should provide better force fidelity. There is a difference in the dynamic response as well, as illustrated by the transfer function for internal velocity control (Eq. 4.1) and internal position control (Eq. 4.2). As further shown by an illustrative zero-pole diagram and bode plot, using position control should increase both stability and phase lag, especially at higher frequencies.

$$TF_v = \frac{P(s)}{sP(s)+1} \quad (4.1)$$

$$TF_p = \frac{P(s)}{sP(s)+s} \quad (4.2)$$

## 4.2 Modeling Feedback control



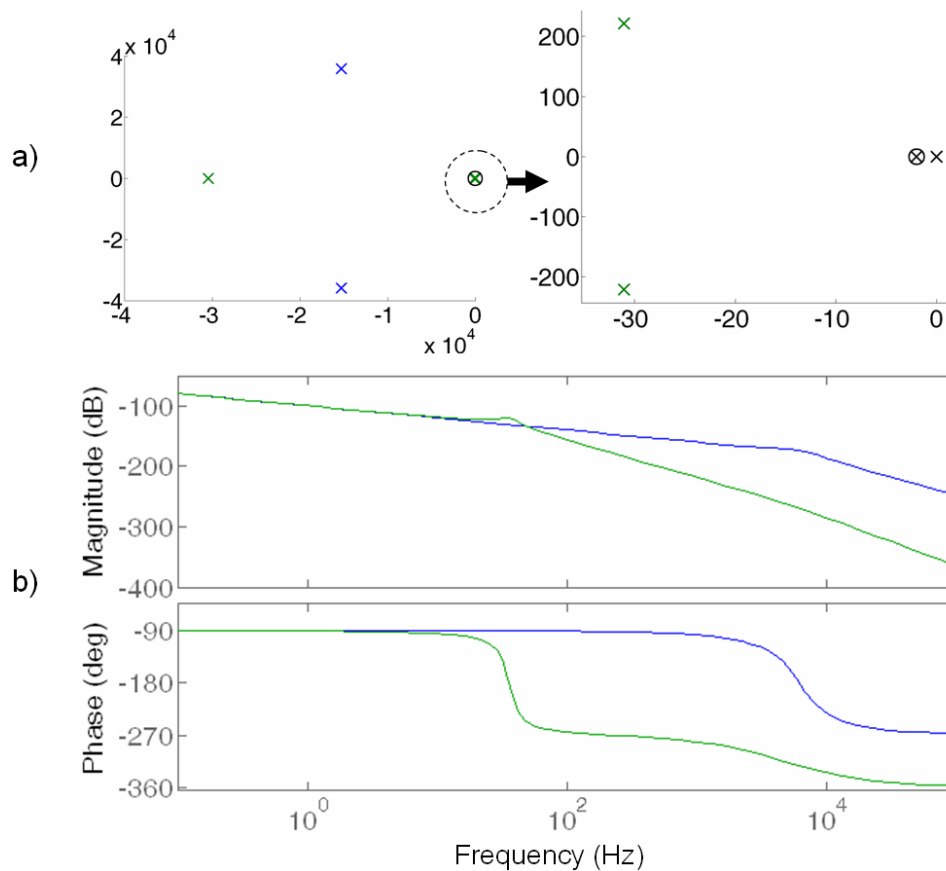


**Figure 4.3: Effect of inner control loop on system dynamics**

a) Pole-Zero diagram of inner velocity feedback (blue) and inner position feedback (green). Poles or zero in common are plotted in black.

b) Frequency response of inner velocity feedback (blue) and inner position feedback (green).

At low frequencies, the two inner control loops are indistinguishable. At higher frequencies, inner velocity control is less stable, but has decreased phase lag.

As a result, using an internal position loop should provide better performance than an internal velocity loop. The author has conducted experiments to examine these hypotheses, as detailed below.

## 4.2 Modeling Feedback control

### 4.3 Experiment Setup

A linear actuator was constructed using a MicroMo<sup>vii</sup> 1628T012 brushless motor with a 16:1 planetary gear transmission and a McMaster-Carr<sup>viii</sup> Acme 0.25"/rev lead screw, as illustrated in Figure 4.4. The actuator was non-backdrivable below 5.8 N. Both a 2-quadrant MicroMo BLD-3502 servo amp and a 4-quadrant MicroMo MCBL 2805 motion controller were used to control the motor at 24V. Due to the lead screw and lack of bearings, this simple and inexpensive actuator has substantial amounts of friction that made force control impossible: proportional gains high enough to overcome friction proved to be too high to ensure stability, and frictional modeling (Johnson & Lorenz, 1992) was of little help. This friction is due to lack of bearings in the output shaft. A compliant 2100 N/m compression spring was placed in series with the actuator to allow for a higher proportional gain. This introduction of compliance created a stable actuator, and in the process provided what may be thought of as a worst-case series elastic actuator. Both a Load Cell Central<sup>ix</sup> VLPB-10lb load cell and an ETI<sup>x</sup> LCP8S-10-10 k $\Omega$  linear potentiometer ( $F \propto \Delta x$ ) were used to sense output force.

All controller gains were tuned using Ziegler and Nichols's (1942) stability criterion for controller gains, as reviewed by Franklin et al. (2002). A 1N step response input against a stiff environment was used to tune the feedback terms. This method was chosen to obtain simple yet objective comparisons.

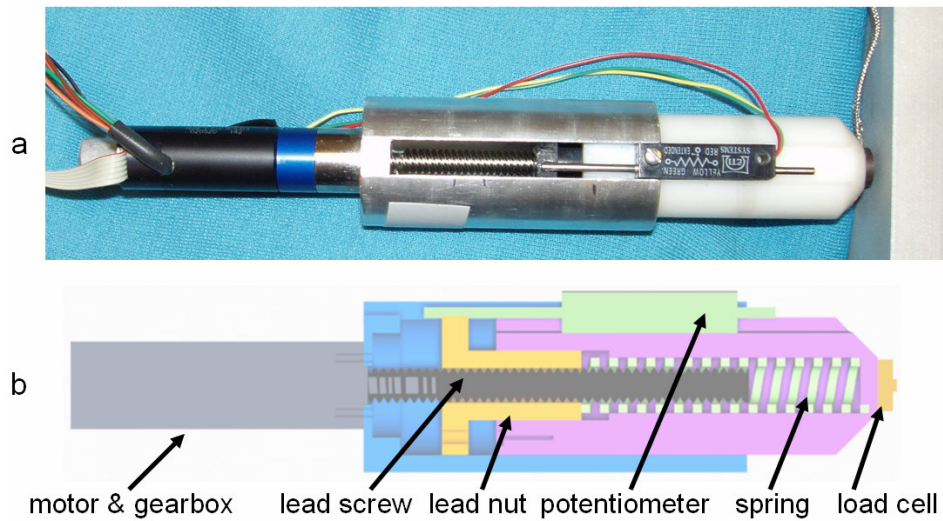


**Figure 4.4: Linear SEA with high levels of friction.**

High levels of friction in shaft made force control difficult, providing an ideal environment to examine the strengths and weaknesses of series elastic actuators.

- a) Picture of actual actuator
- b) CAD rendering of actuator

#### **4.4 Results: Sensor placement**

To examine sensor placement, the SEA was fit with a 10 k $\Omega$  linear potentiometer. When the system was tuned using the linear potentiometer, a proportional gain of 1.68 was achieved, significantly lower than the proportional gain of 9 achieved using the low fidelity load cell. The results are illustrated in Figure 4.5.

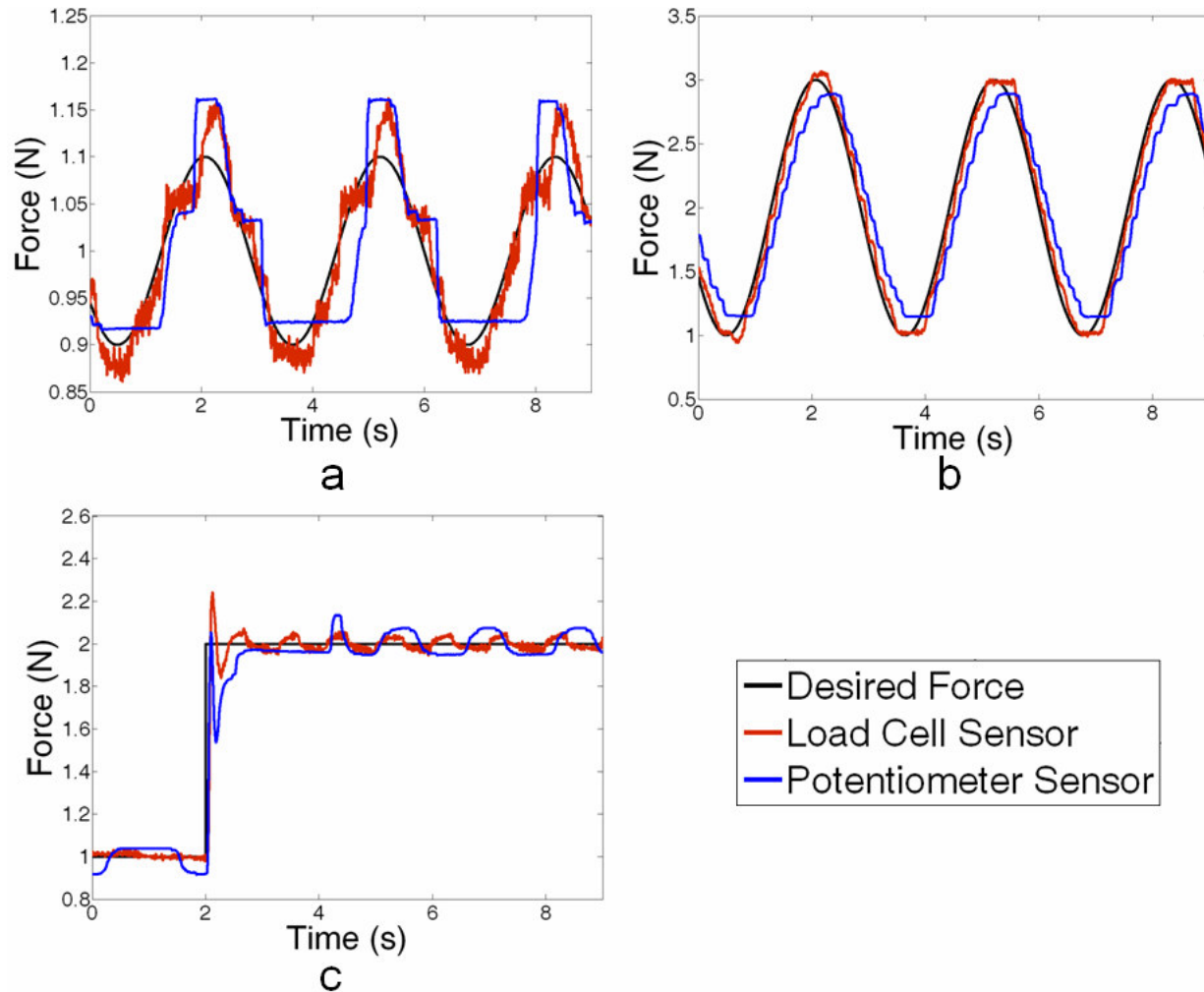


**Figure 4.5: Comparison of sensor placement**

a) Small amplitude oscillations. b) Large amplitude oscillations. c) Step response.

Notice the high amount of noise present in the load cell sensor compared to the potentiometer. Despite this increased noise, the load cell has better resolution and decreased phase lag, since it is distal to any friction sources.

Controller gains for potentiometer: Proportional force gain (K) = 1.68, Derivative force gain (D) = 0.382.

Controller gains for load cell: Proportional force gain (K) = 9.0, Derivative force gain (D) = 0.3125.

Controller gains were determined using the Nichols and Zeigler stability tuning method.

#### 4.4 Results: Sensor placement

## 4.5 Results: Inner control

Figure 4.6 illustrates the results of force control for the linear SEA. The fact that stable force control is achievable at all is impressive given the high levels of friction, but the high levels of friction, combined with the introduction of compliance, create a system that is under-damped for increasing forces and over-damped for decreasing forces.

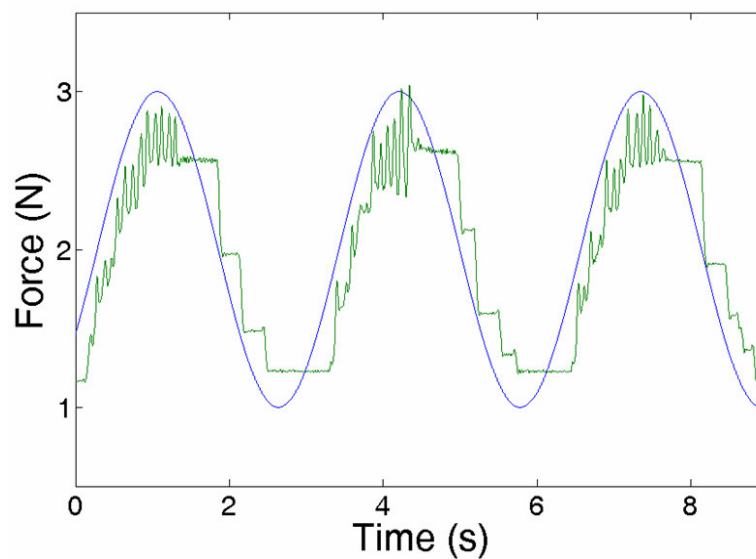


**Figure 4.6: Force control of a linear SEA with no internal control**

No stable force control was achievable without the inclusion of a spring, illustrating the ability of increased compliance to compensate for high levels of friction. High levels of friction combined with compliance create an under-damped system for increasing forces and an over-damped system for decreasing forces.

Controller gains: Proportional force gain ( $K$ ) = 0.258, Derivative force gain ( $D$ ) = 0.006, as determined using the Nichols and Zeigler stability tuning method.

Adding an internal proportional-integral (PI) velocity feedback loop significantly increases performance, as illustrated by the improvement of Figure 4.7c compared to Figure 4.6. When

an internal position loop is used, the force feedback proportional gain is increased 9 times and the -3dB frequency bandwidth is tripled compared to an inner velocity control loop, as shown in Table 4.1. Thus, it seems advisable to use inner position control as opposed to inner velocity control.

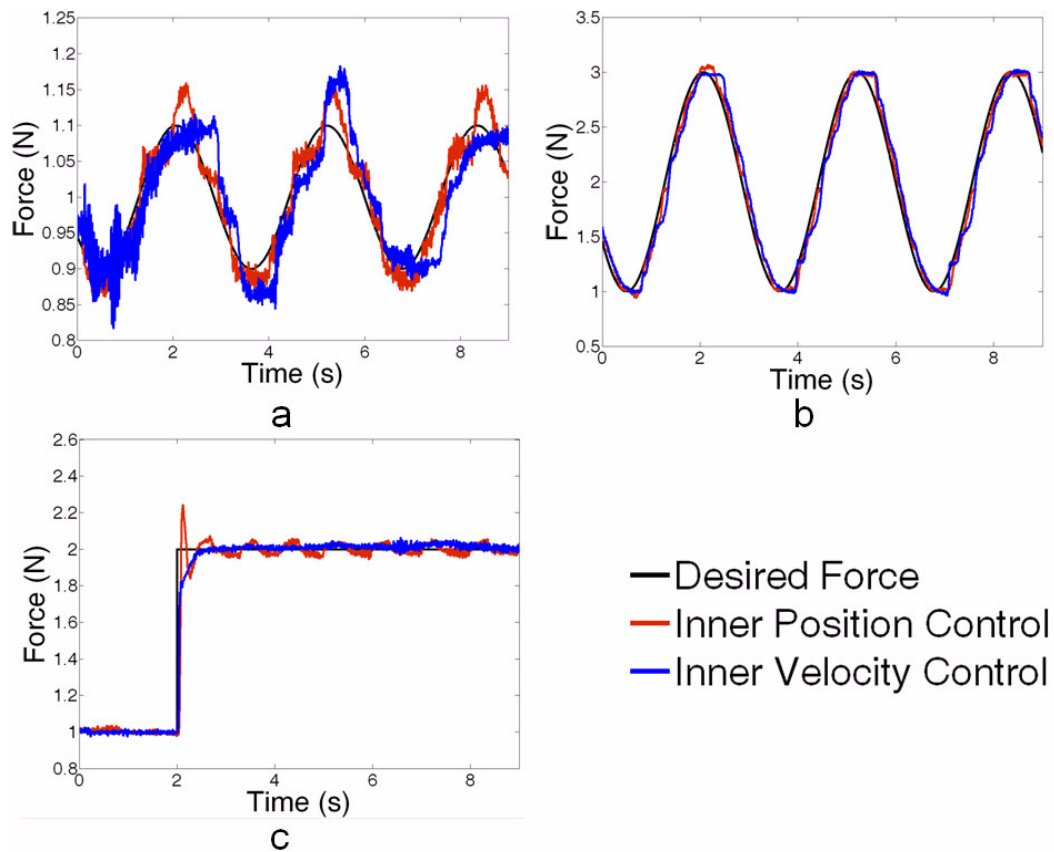


**Figure 4.7: Internal Control loops.**

a) Small amplitude oscillations. b) Large amplitude oscillations. c) Step response.

Controller gains for inner position control: Proportional force gain ( $K$ ) = 9.0, Derivative force gain ( $D$ ) = 0.3125

Controller gains for inner velocity control: : Proportional force gain ( $K$ ) = 1.0, Derivative force gain ( $D$ ) = 0.014

Controller gains were determined using the Nichols and Zeigler stability tuning method.

#### 4.5 Results: Inner control

## 4.6 Summary of results

Table 4.1 reports proportional gain and measured -3 dB frequency bandwidth of the various control schemes. From these results, it seems apparent that introduction of compliance, internal position control, and a sensor in series with the actuator distal to any friction sources provide the highest fidelity force control.

**Table 4.1**  
**Comparison of different control schemes**

Stiffness	Inner loop	Sensor	Proportional gain	Frequency bandwidth
$\sim \infty$	No inner loop	Load cell	No stable gain	N/A
	Position control	Load cell	.192	N/A
2100 N/m	No inner loop	Load cell	.258	N/A
	Velocity control	Load cell	1	3 Hz
	Position control	Load cell	<b>9</b>	<b>10 Hz</b>
		Potentiometer	1.68	1 Hz

Inner loop position control, coupled with a load cell and a compliant element, provides the highest proportional gain and frequency bandwidth.

## **4.7 Discussion**

The addition of an inner position control loop as opposed to an inner velocity control loop seems logical. Velocity sensors such as tachometers are only accurate at high speeds. Although robotic actuators can operate at high frequencies, they often operate at low velocities, even in the presence of reduction gear ratios. As a result, position information acquired through encoders or Hall Effect sensors is usually differentiated or filtered to obtain velocity data. It makes more sense to use the original, accurate position information obtained by the position sensors in the motor.

The placement of a displacement sensor in series with the actuator distal to any friction sources, as opposed to in parallel with the compliant element, also makes sense. At some point, there is a tradeoff between noise level and friction. The high levels of friction present in this actuator have tipped the balance in favor of noisy torque control. Low levels of friction might tip the balance in favor of indiscernible friction. It should also be acknowledged that for a linear series elastic actuator, a load cell is substantially more expensive than a linear potentiometer. The increase in performance must be balanced against the increase in cost. In conclusion, providing an inner position loop and using a sensor distal to all friction sources provides increased proportional gain, better force fidelity, and higher controllable bandwidths.



## 5 Design of the Prosthetic Elbow

Two general areas of design will be addressed: design of the physical actuator and the control scheme used to operate it. These two areas are intricately linked: mechanical design decisions in terms of compliance, friction, and inertia will significantly influence control design. As a result, detail has been applied to the mechanical design in an attempt to simplify the control design. Specifically, the compliance of the mechanical design has been closely monitored, inertia has been reduced wherever possible, and parts have been integrated to reduce the number of moving parts, in hope of reducing friction. Detailed reviews of the mechanical and controller designs are given below.

### 5.1 Mechanical Design Principles

There are several important factors when designing a series elastic prosthetic elbow. The prosthesis must be able to generate accurate torque over the frequency bandwidth used by humans, be moderately close in size to a human elbow, and be non-backdrivable to conserve power. In terms of prosthetic components, there must be a channel through the prosthesis to route wires through the prosthesis, physical and electrical limits of rotation, and some means of integration with a prosthetic socket. All of these demands will be addressed below.

*Torque generation:* A novel torsional spring is used to convert accurate position control of an electric motor to accurate force control. The spring is instrumented with rosette strain gauges to sense strain. Based on previous modeling (Sensinger, 2005), a spandrel shape shown

in Figure 5.1 is used to increase resiliency. The sensors are in parallel with the compliant member, rather than distal to it, because the motion is rotary. As a result, distal friction is minimal compared to linear actuators.



**Figure 5.1: Spandrel Cross section**

Fillets are extended to the edges of the shape, slightly increasing the stiffness while significantly decreasing the maximum shear stress, thus increasing the geometric resiliency of the shape.

The torsional spring is made from Ph17-4 stainless steel. This particular stainless steel alloy was chosen because it has high yield strength in its cold rolled state (1210 MPa) with no need for heat-treating. Other alloys such as steel alloy 4340 offer higher yield strengths when heat-treated (1620 MPa), but the unstable nature of the alloy coupled with the thin geometric shape can cause substantial warping during heat-treating.

The geometric parameters of the spring have been chosen to prevent the spring from plastically deforming for a 20 Nm load. This specification, coupled with other design requirements, has given the spring a predicted torsional stiffness of 350 Nm/rad.

*Size reduction:* Previous Series Elastic Actuator designs (Pratt & Williamson, 1995, Robinson, 2000, Williamson, 1995) have added considerable length to their designs by placing

the spring at the output of the gear stage. Torsional springs for this use are traditionally two inches or more in length, thus adding significant length to the actuator. Both the frameless motor and the gear transmission used in the author's design have a hollow shaft. These hollow shafts have allowed the author to insert the spring back through the transmission and motor, thus not adding any additional space to the actuator as illustrated in Figure 5.2a. In addition to wrapping the spring through other components, the rotor has been integrated with the rest of the design, excluding the need for a shaft. Through similar techniques of parts integration, the overall size of the actuator has been further reduced such that it is the same size as the Boston Elbow III.

*Non-backdrivable:* An upper limb prosthesis user will often pick up an object and carry it with them (Heckathorne, 2004). The actuator should be turned off after the proper position has been achieved to conserve power. A backdrivable system would consume power during the entire time that the object is held, whereas a non-backdrivable system could maintain the desired position without power. Because portable power sources have a limited power capacity, backdrivable actuators are not practical for use in prosthetics.

In the presence of compliance, however, a non-backdrivable motor is not desired given backlash and stiction traditionally associated with non-backdrivable gear transmissions. These unwanted features quickly diminish desired force control, and as such, series elastic actuators have traditionally used backdrivable transmissions (Pratt & Williamson, 1995, Robinson, 2000, Williamson, 1995). The author has found that non-backdrivable series elastic actuators

## 5.1 Mechanical Design Principles

may be used if a backlash free gear transmission is used (Sensing, 2005, Sensinger & Weir, 2005).

There are three ways to achieve a non-backdrivable transmission. In the first method, a high gear ratio is used, exploiting the inherent friction in the gear transmission to create a non-backdrivable transmission. This method is only non-backdrivable for moderate torques and does not save energy in typical activities (Sensing & Weir, 2006d). A subset of this approach used in linear actuators is the lead screw. With sufficient pitch, linear forces are always within the friction cone, ensuring that the transmission is non-backdrivable for all forces. In the second method, a clutch is used to provide a non-backdrivable transmission. A clutch increases the inertia of the motor and introduces backlash. As long as the roller clutch is placed on the input side of the gear transmission, backlash is significantly attenuated. This method can save energy compared to a backdrivable system, provided the inertia of the clutch is kept low. Finally, a brake may be used to prevent motion during those times when the actuator is not in use. Of these methods, the use of a high ratio gear transmission was used to achieve moderate levels of non-backdrivability in a rotary actuator for the purposes of this thesis.

The author chose a Harmonic Drive as a non-backdrivable backlash free gear transmission. Harmonic Drives are only non-backdrivable for small torques ( $< 6\text{Nm}$ ). In order to increase the range of non-backdrivable actuation, a custom designed roller clutch has been inserted before the input portion of the Harmonic Drive. There is a small amount ( $3^\circ$ ) of backlash in

this roller clutch. The amount of backlash is reduced to less than  $0.02^\circ$  by the high reduction gear ratio of the Harmonic Drive, which attenuates position. Recent modeling by the author (Sensing & Weir, 2006d) has indicated that for tasks of daily living, the energy saved by inclusion of this roller clutch is negligible, due to the substantial increase in inertia required to make the elbow non-backdrivable. The inertia may easily be decreased in future designs, however, without affecting mechanical integrity. This decreased inertia will allow the roller clutch to provide substantial energy savings.

## **5.2 Mechanical Design**

A customized Emoteq<sup>xi</sup> HT02500 frameless brushless motor capable of producing 2.8 Nm stall torque and a 160:1 gear ratio Harmonic Drive LLC<sup>xii</sup> CSD 20 gear transmission were used, controlled by a Faulhaber<sup>xiii</sup> BLD7010 servo amplifier capable of handling large currents and a 13.5 V power supply. The gear transmission is non-backdrivable up to 6 Nm. A spandrel shape torsional spring (Figure 5.2e) with a stiffness of 327 Nm/rad was used to provide compliance. This cross section is an optimization of the existing cross-shaped torsional spring (Figure 5.2d) and provides increased geometric resilience: the ability to absorb energy without plastically deforming (Sensing, 2005, Sensing & Weir, 2005).

The torsional spring was instrumented with two Omega SG-4/350-TY31 rosette foil strain gauges with a 5-volt power supply to provide torque control. The strain gauges were configured in a Wheatstone bridge and fed through an instrumentation amplifier with a 1065

differential gain to use the full range of the data acquisition system. Matlab's Simulink XPC and Real-time toolboxes were used at a sampling frequency of 10 kHz to control the actuator.

Position was measured using Hall effect sensors with 3800 bits/rev. Velocity was obtained by differentiating the position signal  $\left(\omega = \frac{s}{0.01s+1}\theta\right)$  and passing it through a 100 unit/sec rate limiter. Acceleration was likewise calculated by differentiating the non-rate limited velocity, and rate limiting the acceleration at 100 units/sec. This method provides a clean and accurate signal, with superior information at low speeds such as those used with a prosthesis, which moves between 0 and 2.5 rad/sec.

Because a frameless motor and a hollow gear transmission were used, the torsional spring was passed back through the middle of the actuator, achieving high compliance without increasing the size of the actuator, as illustrated in Figure 5.2a-b.

## 5.2 Mechanical Design

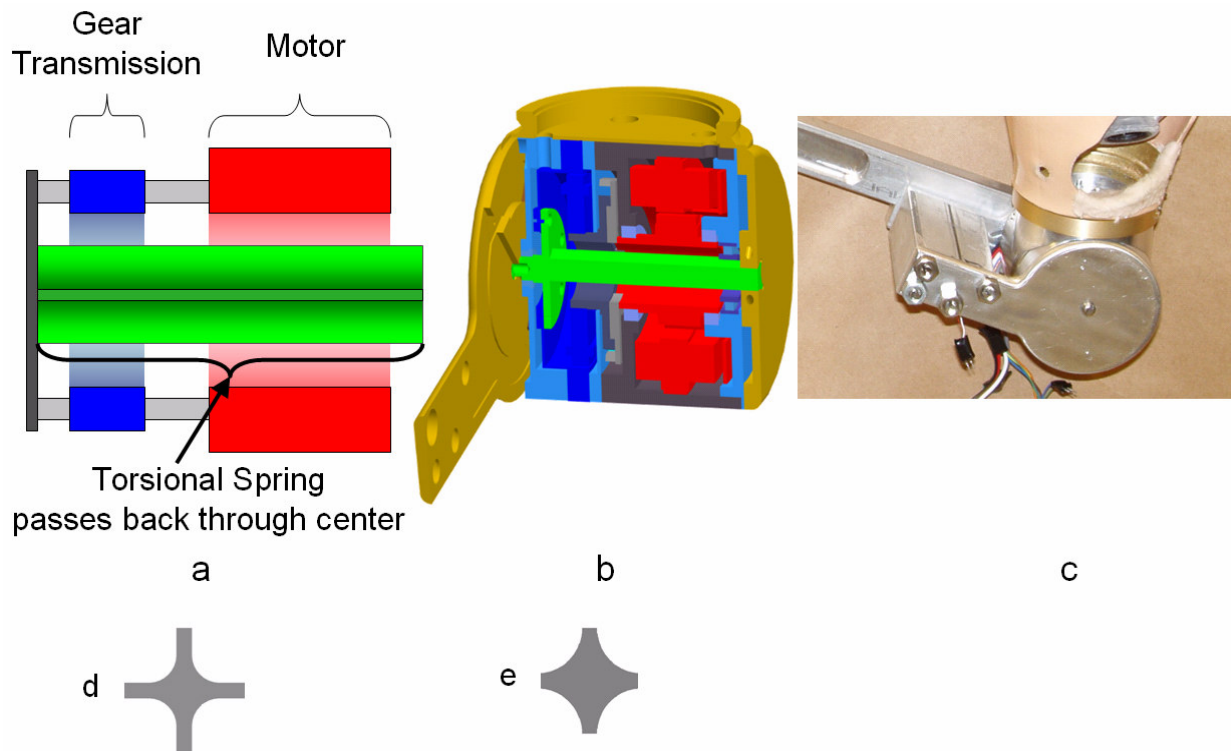


**Figure 5.2: Prosthetic Elbow**

- a) Torsional spring passed back through the middle of the harmonic drive and frameless motor.
- b) CAD rendering of SEA prosthetic elbow
- c) Photograph of the SEA elbow
- d) shows the conventional cross section of the torsional spring
- e) shows a more resilient cross shape, termed a spandrel, that may deform more without plastically deforming.

*Requirements of the prosthesis:* Physical and electrical limit switches have been included to prevent the torsional spring from deflecting more than 3.3 degrees. Physical limits will allow subjects to lift heavier loads than the spring is capable of lifting without breaking the spring.

A channel has been included to allow proximally located wires to be fed through the

## 5.2 Mechanical Design

prosthetic elbow on their path to prehension devices, and the design allows sufficient space for the wires to move as the elbow rotates. Finally, an interface similar to that of the Boston Digital Arm has been incorporated to allow the prosthetic elbow to be interfaced with the socket. This interface will allow patients who use the Boston Digital Arm to maintain the same socket. Schematics of the machined parts are illustrated in Appendix 12.7. Data sheets for purchased parts are presented in Appendix 12.11.

The initial roller clutch design did not properly engage when a load was applied, despite numerous modifications to the size of the rollers. As a result, the studies presented in this thesis did not employ a non-backdrivable roller-clutch. The prosthetic elbow was still non-backdrivable below 6 Nm of torque, due to the inherent stiction in the Harmonic Drive. The components of the roller clutch remained in place, and as a result, the increased inertia due to a roller clutch was present in this design. A second roller clutch was fabricated using a design theory created by Otto Bock (Puchhammer, 2006). This design theory is simple and elegant, and the resulting roller clutch worked very well. The design theory is a trade secret of Otto Bock, and as a result, it is not explained in this thesis.

### **5.3 Controller Design**

Control of the actuator may be grouped into three different stages: *Signal Processing*, *Impedance Control*, and *Torque Control*, as illustrated in Figure 5.3. Detailed schematics of each control block are provided in Appendix 12.8 and Appendix 12.9.

#### 5.3 Controller Design



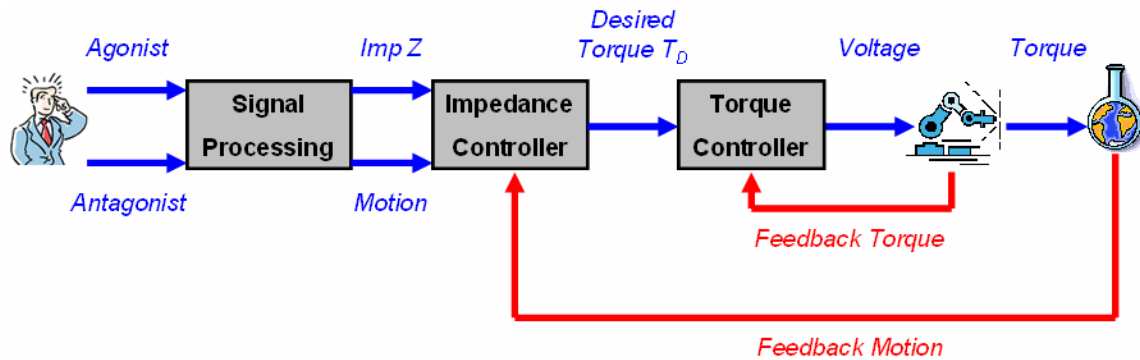


**Figure 5.3: Expanded Impedance Control Diagram**

Three controller blocks convert subject muscle activity to torque

Torque is fed back using strain gauges on a compliant torsional spring

Motion is fed back using Hall effect sensors in the motor

### 5.3.1 Signal Processing

Otto Bock 13E200 MYOBOCK<sup>®</sup> electrodes calculate the root mean square (RMS) of raw myoelectric (MES) activity from a pair of agonist/and antagonist muscles. MES signals are created as a byproduct of muscle contraction and are roughly proportional to the amplitude of isometric force during muscle contraction (Heckathorne, 1978, Heckathorne & Childress, 1981). The RMS of muscle voltages corresponds well with isometric exerted force (Basmajian & De Luca, 1985). In the *Signal Processing* block these RMS signals are calibrated to set a noise threshold and to make their maximum amplitudes equivalent. The desired position or velocity, depending on the motion control paradigm, is proportional to the difference between the RMS of the two signals. The impedance signal  $Z$  is proportional to the amount that they are both activated, which is simply the amplitude of the lesser signal, as illustrated in Figure 5.4. Thresholds and buffer zones are calibrated for each subject.

#### 5.3 Controller Design

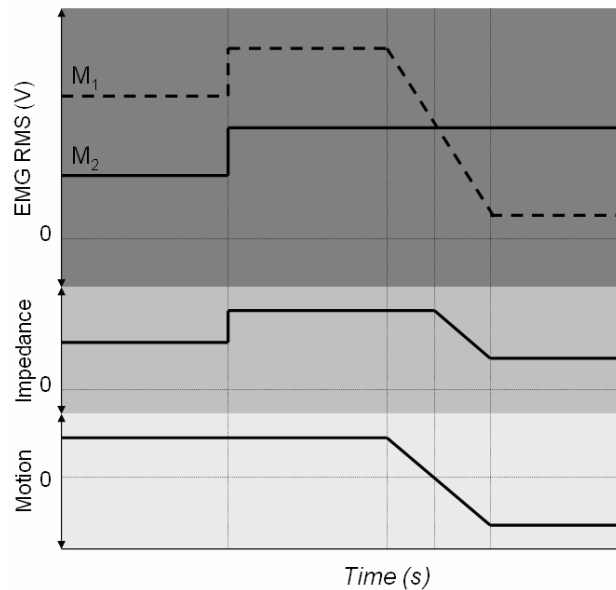


**Figure 5.4: Extraction of Motion and Impedance from MES RMS Signals**

For MES data, dashed and solid lines represent a pair of muscles ( $M_1$ ,  $M_2$ )

Impedance  $\sim \min(M_1, M_2)$

Motion  $\sim M_1 - M_2$

Thresholds & buffer zones will be calibrated for each subject

It may make more sense to some persons to think of impedance as the sum of opposing muscle forces. Unfortunately, the sum of muscle forces does not decouple impedance from velocity. For example, to move a joint while maintaining the same level of impedance, the level of force generated by one of the muscles must be increased such that they no longer sum to zero. If impedance is defined as the sum of the two muscle forces, this action will result in a rise in impedance where none is warranted. If one looks at the minimum level of force, the level of impedance will not change.

### 5.3 Controller Design

In section 12.1.1 it is observed that the impedance of human joints is dependent on the magnitude and direction of velocity: two effects that the above control scheme does not mimic. MES signals will ideally be controlled by isometric contractions, which do not have a velocity component. Thus, the transfer from muscle contractions to an impedance signal shown in Figure 5.4 should be adequate. At the same time, the mechanical properties of the motor will introduce a similar velocity dependent torque. As a result, the overall system will mimic velocity dependent impedance found in human joints.

In this control scheme, as impedance increases, the maximum motion signal decreases. This effect is also observed in human joints: if a muscle can only generate so much force, and most of that force is balanced by the antagonist muscle, less force is available to move the joint. Thus low impedance is generally observed during voluntary movements (Popescu et al., 2003).

### **5.3.2 Impedance Controller**

The output of the Signal-processing block contains two scalar values: motion and impedance. Motion may be adequately represented by a scalar value, and as such may be quickly passed on to later control blocks. Impedance must be further broken up into stiffness, viscous damping, and inertial terms. Metrics such as trajectory pursuit or maximum power transfer have not provided any reduction of independently controlled variables. As a result, each of these variables is independently tested in subjects while setting the other impedance variables to a predefined constant.

### 5.3.3 Torque Controller

Based on the difference between the desired and actual motion and the desired impedance, a desired torque is sent to the torque controller. A proportional feedback loop ensures accurate torque. Speed  $\omega$  is calculated from Hall effect sensor position information. The motor used has 8 poles, or 4 electrical cycles per mechanical revolution. With 6 commutation steps per electrical cycle, there are 24 counts per revolution, or  $15^\circ$  resolution. Reduced by a 160:1 gear ratio, this resolution equates to  $0.09^\circ$  of resolution, or 3800 bits per revolution. The author used this method of position and velocity sensing based on size constraints. Pratt, Willison, Bolton, and Hofman (2004) recently used the technique, justifying their reasoning by writing that accurate joint position information was not required in the presence of high fidelity force recordings. They obtained high fidelity impedance control at low frequencies using the Hall effect sensors as velocity sources.

This design offers a compact series elastic actuator with the capability to modulate impedance. Whether or not the design is successful at modulating the impedance, however, remains to be seen, and will be examined in the following chapter.

## 6 Impedance Modulation Evaluation

Series elastic actuators offer very good force control in a constrained environment, because the increase in compliance has no effect on overall dynamics while increasing the fidelity of the control (Robinson, 2000). The effect of increasing the compliance in an unconstrained environment, however, is not as simple: the stiffness of the elastic element linearly affects the resonant frequency of the system (Robinson, 2000). Imposing a virtual impedance on an unconstrained series elastic actuator becomes even more problematic. As a result, it may be useful to model the system before examining a prototype.

Pratt et al. (2004) have used a series elastic actuator to perform impedance control, but only for low (1-2 Hz) frequencies in an unconstrained state. Although this frequency range may be adequate given the limited unconstrained frequency range of humans (Chan & Childress, 1990, Sheridan & Ferrell, 1974), there may also be situations when higher frequencies are desired. As such, the author wanted to investigate impedance control at higher frequencies.

### 6.1 *Plant modeling*

Both Pratt et al. (2004) and the author have found that internal voltage regulation performs better than torque regulation. Internal voltage regulation complicates modeling, however, because if the electrical wiring of the motor is not included in the model, a velocity source will mitigate any dynamic effect of the inertial portion of the rotor, due to the effects of derivative causality. The inertial portion of the rotor is a significant term given the high gear

ratio. As a result, the model must include the resistance and inductance of the wire, along with the inertia and the viscosity of the rotor in order to preserve the effect of the rotor inertia on the dynamic response. Such a model is shown in Figure 1 in bond graph form, which allows for the fact that each stage of the system is not necessarily a high impedance stage. The dynamic characterization is significantly different from that of a simplified model.

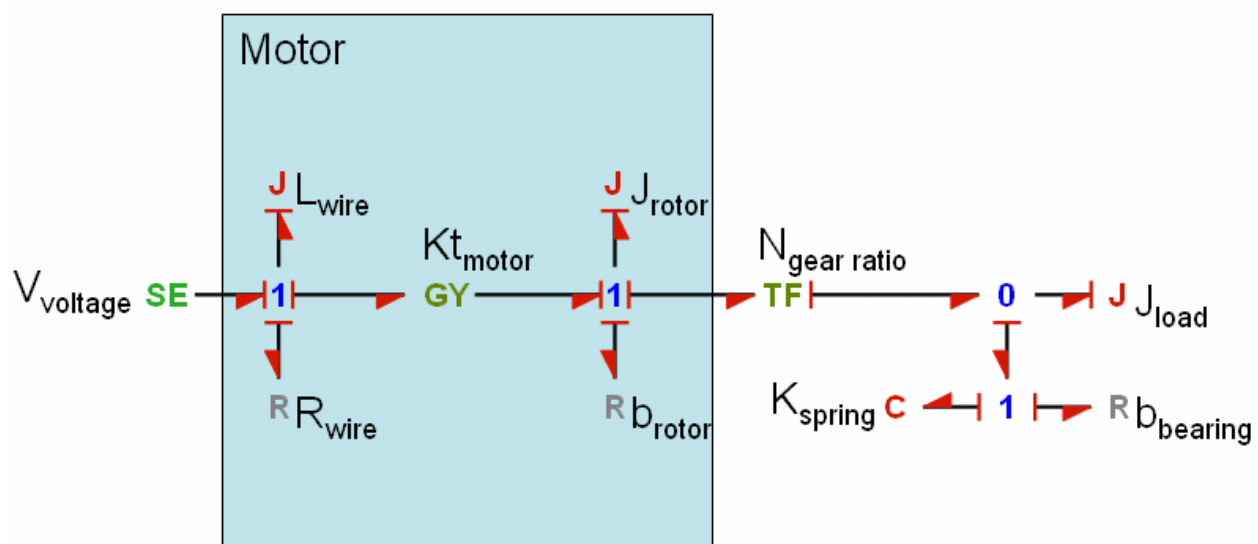


**Figure 6.1: Bond graph of system prosthetic elbow**

The motor wiring must be modeled in order to preserve the dynamic effect of the rotor inertia, because a velocity source is used to drive the motor.

The strain on the torsional spring is sensed, and fed back to a torque controller, as shown in Figure 6.2. The low stiffness of the torsional spring allows for a high proportional gain ( $K_{\text{torque}}$ ). This high proportional gain in turn increases the torque fidelity of the system. Once the actuator is capable of accurately generating a desired torque, a desired impedance, or interaction between forces and movements, may be constructed. A force is generated in

response to the difference between the desired and actual position, multiplied by the desired stiffness ( $K$ ) of the system. This force is added to a viscous ( $b$ ) and inertial term ( $J$ ), using the actual velocity and acceleration of the actuator. The viscous term could be applied to the difference between desired and actual signals instead of being applied to the actual velocity: this would effectively place the viscous element in parallel with spring. Placement of the viscous element within the feedback loop would result in a faster response and higher overshoot than if the actual velocity is used (Franklin et al., 2002).

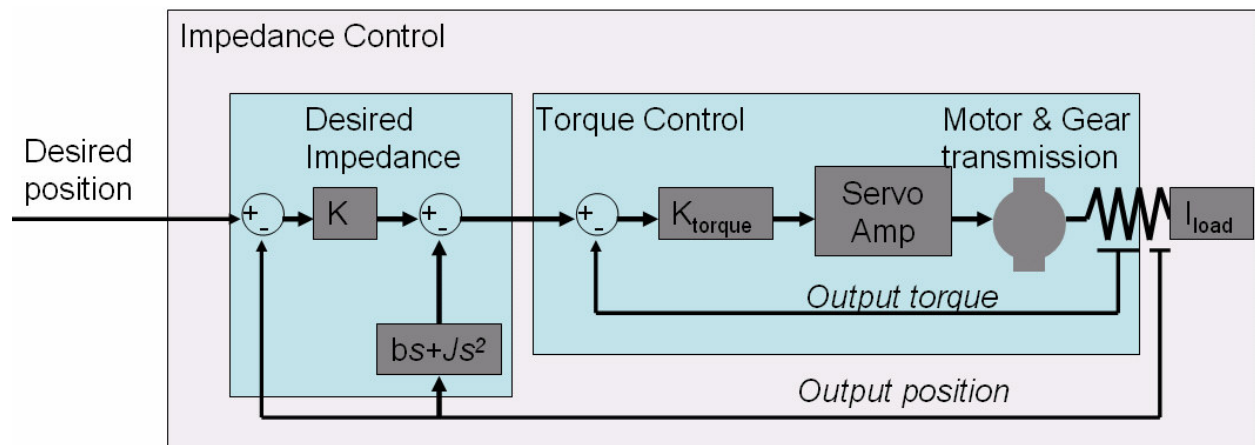


**Figure 6.2: Control system**

The inner torque control loop senses the torque applied on the compliant torsional spring, and feeds the error between the desired and actual force into a proportional gain. The outer impedance loop creates an impedance for the actuator to mimic, consisting of stiffness  $K$ , viscosity  $b$  and inertia  $I$ .

Due to the complexity of the model and control system, the transfer functions of control for this system are lengthy. Simplification does not adequately represent the dynamic response.

## 6.1 Plant modeling

Root locus plots offer an effective tool to understand the effects of a single variable on the dynamics of a system (Franklin et al., 2002). If several variables of interest affect the system's dynamic response, each of these variables may be examined using a root locus plot while keeping the other variables constant. Keeping the other variables constant, however, neglects the fact that the effect of one variable may be heavily dependent on the value of other variables.

## ***6.2 2D projection of a multivariate root locus***

One way the author has solved this problem is to choose a range for each variable, and then to calculate the poles for numerous iterations, each using a random value of each of the variables of interest (Sensinger & Weir, 2006a). In this way, a root locus region may be shown over which the system behaves in that range of variables, as shown in Figure 6.3.



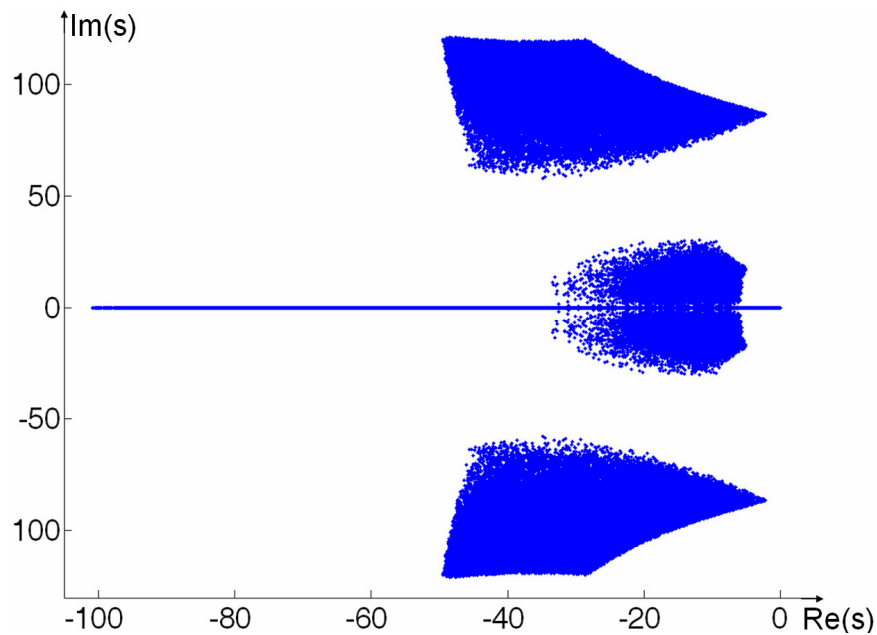


**Figure 6.3: Scatter plot of poles for the random variation of 3 variables**

This technique allows for a root-locus space over which the system dynamics are constrained, no matter what the particular value of an individual control variable.

Although this approach shows the range of the system dynamics, it does not address how individual variables affect that range. In an effort to answer that question, the author have overlaid an additional scatter plot on top of Figure 6.3, in which the variable of interest is set to be either the floor or the ceiling of that variable's range, while all other variables are randomly determined. An example of this overlaid approach is shown in Figure 6.4.

## 6.2 2D projection of a multivariate root locus

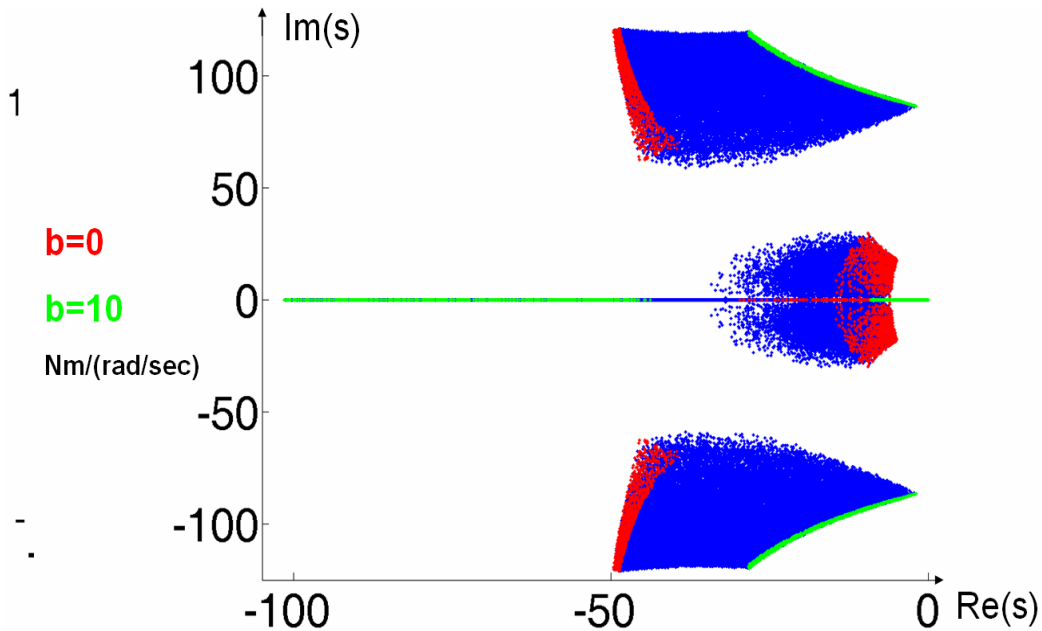


**Figure 6.4: The endpoints of 1 variable overlaid on a scatter plot of all variables**

From this figure, it can be seen that this particular variable has a significant effect on both sets of poles. As  $b$  is increased, the real portion of the outer poles decreases, indicating a decreased settling time. The middle pole becomes over-damped as  $b$  increases. It is worth noting that  $b$  does not have a significant effect on the imaginary portion of the poles, indicating that it has no significant effect on the rise time.

Using this approach, the effect of each variable may be determined on each pole, despite complicated dynamic equations. A final example showing the effect of 3 variables is shown in Figure 6.5.

## 6.2 2D projection of a multivariate root locus

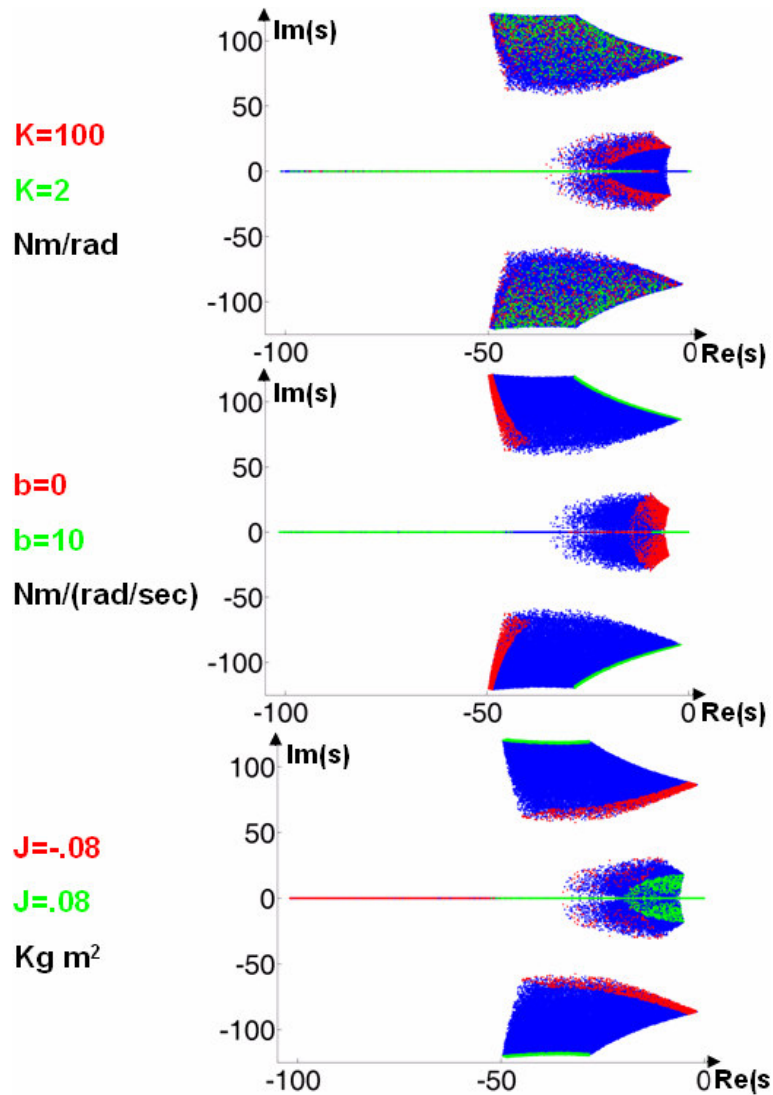


**Figure 6.5: Scatter plot, showing the effect of three variables**

Root locus of Impedance terms.  $K_{\text{torque}} = 1$ .

a) Red( $K=100$  Nm/rad), Green ( $K=2$  Nm/rad)

b) Red( $b=0$  Nm/(rad/sec)), Green ( $b=10$  Nm/(rad/sec))

c) Red( $J=-.08$  kg m<sup>2</sup>) Green ( $J=.08$  kg m<sup>2</sup>)

## 6.2 2D projection of a multivariate root locus

This method is a fairly simple and straightforward approach to obtain a grasp of how the system dynamics are affected by multiple variables, taking into account the other variables.

It may be seen in Figure 6.3 that the system is stable for the range of desired impedances. As expected, the system becomes under-damped as the stiffness increases (Figure 6.3a), the viscosity decreases (Figure 6.3b), or the inertia decreases (Figure 6.3c).

It should be noted that negative desired inertias are allowed. This decision was decided based on work regarding the IBM TrackPoint (Barrett, Selker, Rutledge & Olyha, 1995), which suggests that a negative inertia of the actuator, coupled with a positive inertia of muscle activation of the user, multiply together to create a system with little if any overall inertia. As our impedance controlled system remains stable for a negative inertial term, it seemed beneficial to allow it.

### **6.3 Empirical Testing**

The actuator described in Chapter 5 was tested using a commanded impedance of  $K_{\text{Desired}}=100$  Nm/rad,  $b_{\text{Desired}}=0$  Nm/rad/sec, and  $J_{\text{Desired}}=0$  kg m<sup>2</sup>. The stiffness was also lowered to  $K=2$  Nm/rad, keeping both the desired viscosity and inertia at 0.

The actuator behaves well at low frequencies, as illustrated in Figure 6.6. This observation is in agreement with the results of Pratt et al. (2004), in which they successfully created a stiffness an order of magnitude less than the actual stiffness of their actuator. As seen in Figure

6.7, the ability to generate a stiffness of 2 Nm/rad, over two orders of magnitude less than the actual stiffness of 327 Nm/rad, demonstrates the ability of series elastic actuators to provide high fidelity force control. The actuator is not able to entirely mitigate the inherent effects of damping at that low stiffness level, but still provides effective impedance control.

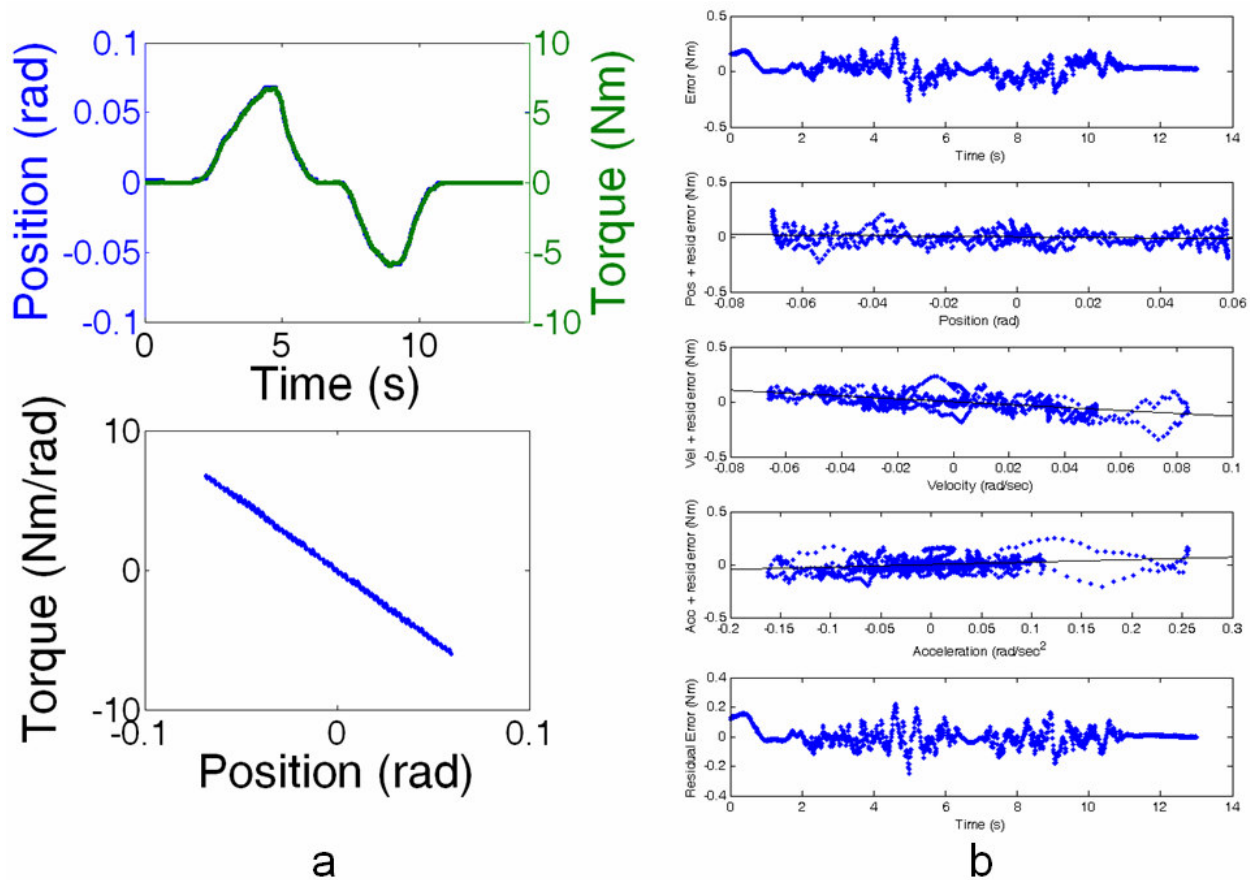


**Figure 6.6: Unconstrained Impedance Control**

$K_{\text{Desired}}=100 \text{ Nm/rad}$ ,  $b_{\text{Desired}}=0 \text{ Nm}/(\text{rad}/\text{sec})$ ,  $I_{\text{Desired}} = 0 \text{ kg m}^2$

b) The error between the desired and actual impedance is:  $K_{\text{error}}=0.3 \text{ Nm/rad} \cdot \theta$ ,  $b_{\text{error}} = 1.3 \text{ Nm}/(\text{rad}/\text{sec}) \cdot \omega$ ,  $J_{\text{error}} = 0.2 \text{ Nm}/(\text{rad}/\text{sec}^2) \cdot \alpha$ .

### 6.3 Empirical Testing

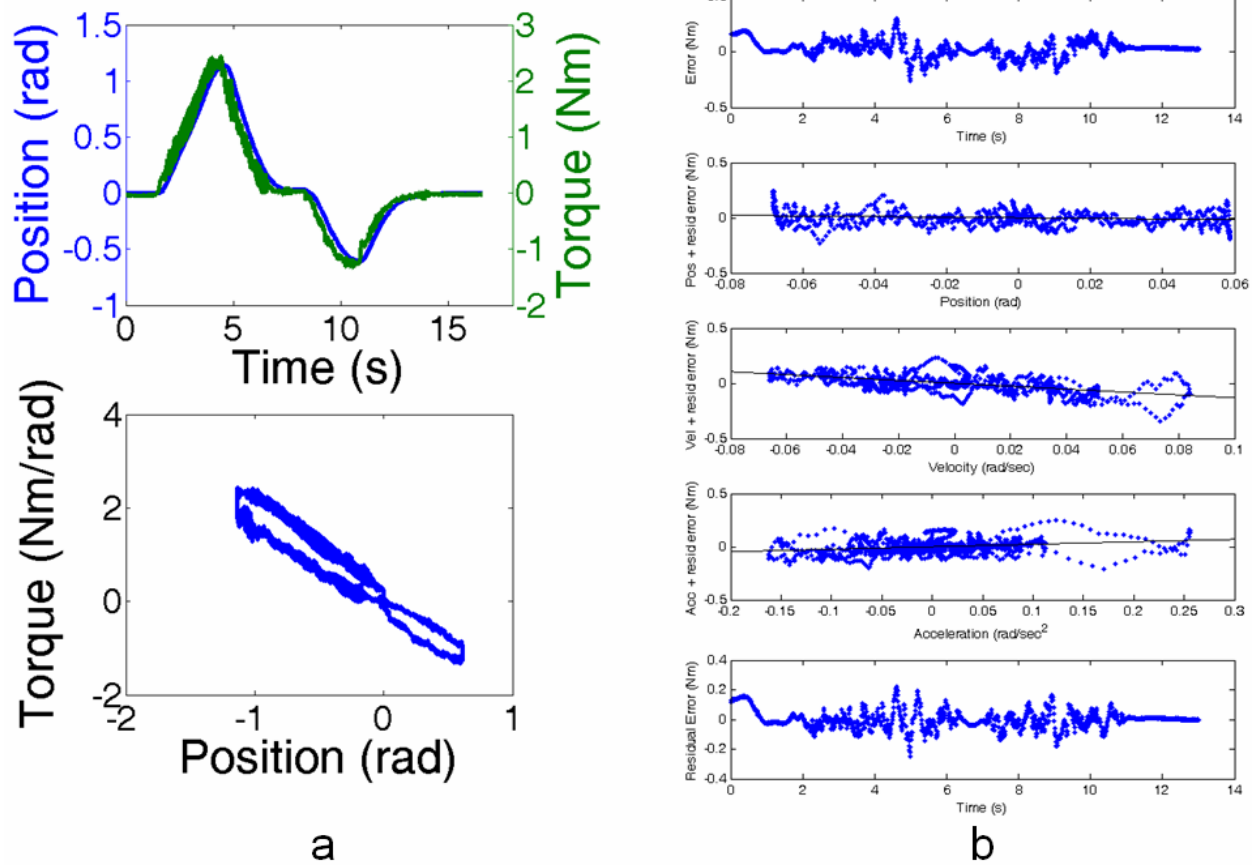


**Figure 6.7: Unconstrained Impedance Control:**

Commanded  $K_{\text{Desired}}=2 \text{ Nm/rad}$ ,  $b_{\text{Desired}}=0 \text{ Nm/(rad/sec)}$ ,  $J_{\text{Desired}} = 0 \text{ kg m}^2$

The error between the desired and actual impedance (shown on the right of the figure) is:  $b_{\text{error}} = 0.65 \text{ Nm/(rad/sec)} \cdot \omega$ ,  $J_{\text{error}} = 0.09 \text{ Nm/(rad/sec}^2) \cdot \alpha$ . There was no significant error in stiffness. This stiffness is over 2 orders of magnitude less than the actual stiffness of 327 Nm/rad, yet the actuator still does a reasonable job of mimicking the low stiffness. It is not able to completely mitigate the inherent damping of the system at this low stiffness.

### 6.3 Empirical Testing

Although the actuator behaves well at low frequencies, however, an unusual oscillation develops when the unconstrained system is commanded at frequencies near the natural frequency of the system, as illustrated in Figure 6.8.

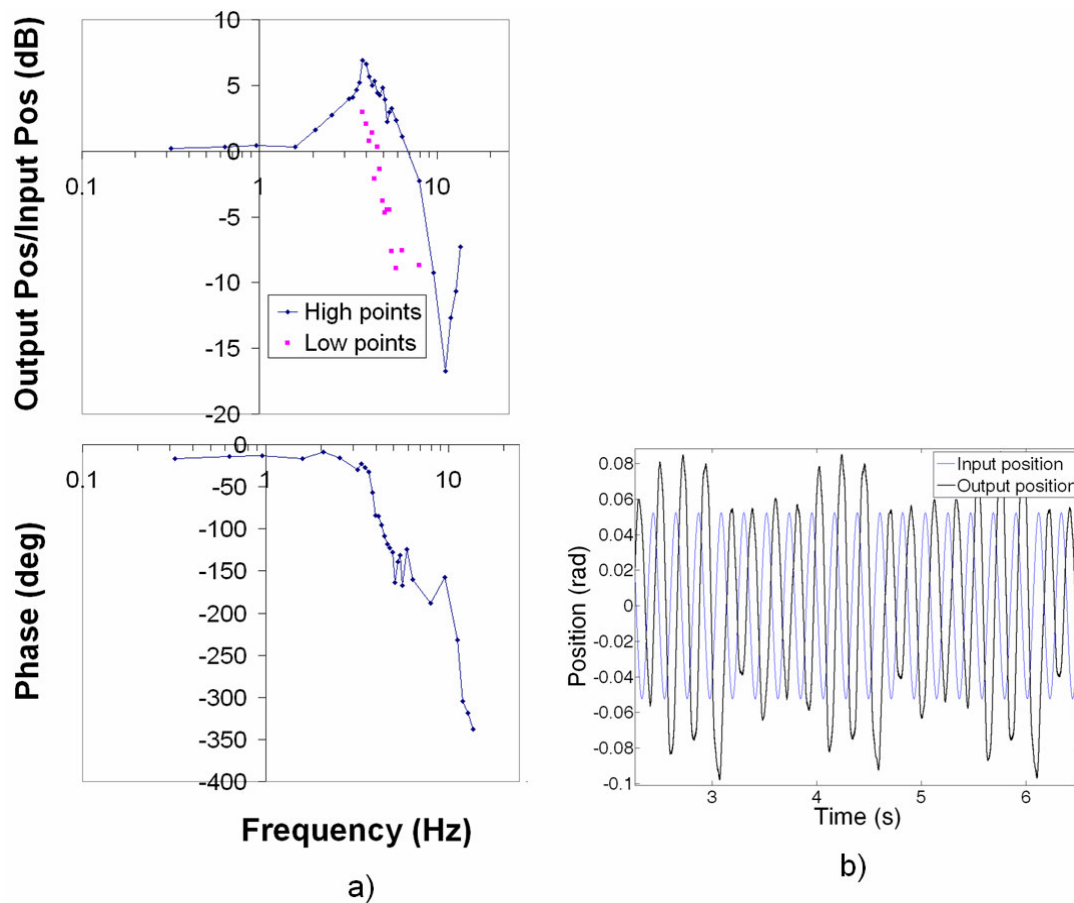


**Figure 6.8: Bode plot of position response of the unconstrained actuator using impedance control**

$K_{\text{Desired}} = 100 \text{ Nm/rad}$ ,  $b_{\text{Desired}} = 0$ ,  $J_{\text{Desired}} = 0$ .

a) Frequency response of unconstrained actuator.

b) 4.3 Hz signal

The system developed secondary oscillations, as shown by the low points in the frequency response. Such a signal is illustrated by b). The system is still stable at these frequencies, but does not output a pure sine wave.

### 6.3 Empirical Testing

These nonlinear oscillations appear to be a result of backlash at the output of the torsional spring. A nonlinear model predicts a similar effect under the same conditions, as illustrated in Figure 6.9. Thus, at moderate frequencies, nonlinear oscillations will arise when the commanded oscillation is the same magnitude as the amount of backlash in the system: this feature is not an instability, however, but merely backlash in the system. Future designs will prevent this backlash by using a steel mating part instead of an aluminum mating part, which plastically deforms over time.

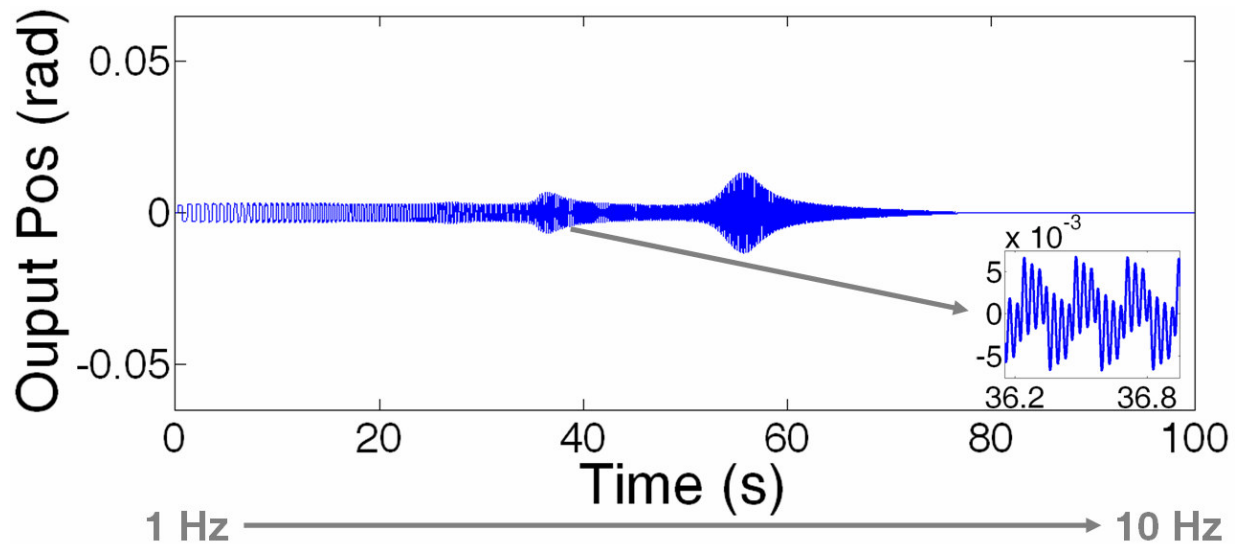


**Figure 6.9: The modeled effect of output backlash on the system's ability to maintain a stiffness of 100 Nm/rad**

### 6.3 Empirical Testing



## **6.4 Discussion**

In order to preserve stability, a low torque feedback gain of 1 has been required for  $K_{\text{torque}}$ . This feedback gain is an order of magnitude lower than required for the constrained case, resulting in loss of fidelity. Introducing a derivative term in the inner torque loop, which usually acts as a damper, only amplifies this instability in the unconstrained state.

Despite these nonlinear dynamics at moderate frequencies, the system is stable, and it has adequately performed in an unconstrained state during recent subject testing of user-modulated impedance control. It is controllable in the 0.5-1 Hz frequency bandwidth of human tracking (Chan & Childress, 1990, Sheridan & Ferrell, 1974). Thus, it seems suitable for human interfaces. The impedance controller controls stiffness and inertia better than viscosity. Using a faster viscous response by placing the viscous element within the feedback loop may rectify this problem, and future experiments will investigate this modification to the control scheme.

These findings highlight the limits of previous studies: Popat et al. (1993) only tested impedance control on a constrained system, citing subject safety as their motivation, and Pratt et al. only looked at unconstrained impedance control at 1-2Hz frequencies. Impedance control appears to work well when either constrained (in which case it is essentially force control) or at low frequencies, but may not be a good choice for use above 3 Hz, either due to signal attenuation (as predicted by modeling) or the development of secondary oscillations (as observed during testing).

## **6.5 Conclusion**

Series elastic actuators offer high force fidelity in their controllable bandwidth and intrinsic low impedance above their controllable frequency bandwidth, making them useful in impedance control and safe for human interaction. The high level of compliance coupled with an inertia load make them unsuitable for moderate frequency use in an unconstrained state. For use with humans, however, who do position tracking below 2 Hz, they offer a safe and high fidelity solution to providing impedance control.

The terms impedance control and non-backdrivable have traditionally been incompatible. There is no conceptual difficulty, however, with accepting a low impedance non-backdrivable actuator. These empirical results, coupled with the author previous finding that high fidelity force control using a non-backdrivable gear transmission is possible, should allow for the syntheses of non-backdrivable transmissions and impedance control in future robotic actuators.

## **7 Critical Decisions required to Implement Impedance Control**

The prosthetic elbow is capable of modulating impedance over the desired range of values. Two questions related to user-modulated impedance control must be answered prior to examining whether or not this capability is useful to subjects. These two questions are: what underlying motion paradigm should be used, and what should be the default impedance? This chapter will address these questions.

### ***7.1 Questions to Address***

In impedance control, two variables determine the output force generated by the actuator: the desired motion, and the desired impedance. Before analyzing desired impedance paradigms, it is necessary to select an underlying desired motion paradigm.

Myoelectric (MES) signals from a pair of agonist/antagonist muscles are often used clinically to control the motion of electric prostheses. MES signals are created as a byproduct of muscle contraction and are broadly proportional to the amplitude of contraction (Heckathorne & Childress, 1981). The velocity of the joint has conventionally been proportional to the amplitude of the rectified, 3 Hz -3dB low-pass filtered MES signals (Weir, 2003). This relationship between speed and MES signals is called proportional velocity control (PVC). A different motion control paradigm, proportional position control (PPC), sets the position of

the joint proportional to the amplitude of the rectified, 3 Hz -3dB low-pass filtered MES signals. PPC has been found to be better than PVC (Doubler & Childress, 1984, Weir, 1995) in pursuit tracking tasks, but these studies used force transducers as opposed to MES signals as inputs. The high level of noise present in MES signals may mitigate any inherent advantage in PPC.

Popat et al. (1993) used PVC for their conventional paradigm and PPC for their impedance modulation paradigm. Thus, the effects of the impedance paradigm and motion paradigm were confounded. In order to decouple the motion paradigm from the impedance paradigm, all impedance paradigms were tested in this study using both PVC and PPC to determine which motion paradigm is better for impedance control.

Able bodied subjects typically have minimal stiffness in their elbow joint (Popescu et al., 2003), most likely because it requires less energy expenditure than continuously co-contracting their muscles. Using computer based impedance control, however, the relaxed state of the subject may be set to an arbitrary impedance: either low if subjects prefer low impedance most of the time, or high if subjects prefer high levels of impedance most of the time. Although co-contracting muscles to lower stiffness does not mimic human physiology, it may provide better control with less energy expenditure than mimicking human physiology. While exact values are not necessary for further experiments, an understanding of whether low or high impedances are preferred would aid future experiments.

## 7.1 Questions to Address

In order to answer this question, it is necessary to decouple the subject's preferred co-contraction level from subject's preferred impedance of the prosthesis. All impedance paradigms were tested for two co-contraction states to decouple these two variables. If the subject's co-contraction level changes when the co-contraction state changes, then it may be inferred that the subject was willing to change their co-contraction level to maintain a preferred impedance. If the co-contraction level does not change when the co-contraction state changes, it may be inferred that the subject is either incapable of changing their co-contraction state, or that the subject does not have a preferred impedance.

## ***7.2 Experimental Apparatus***

The protocol was approved by the Northwestern University Institutional Review Board, and all patients signed informed consent forms. Four able bodied subjects (mean age 28 +/- 3 years) including two males and two females were enrolled in this preliminary study. Subjects remotely controlled the prosthesis by tensing a pair of agonist and antagonist muscles. The amount that subjects co-contracted was set proportional to impedance. The amount one muscle was contracted more than the other was set proportional to speed. Otto Bock<sup>xiv</sup> 13E200 electromyography (MES) sensors were used to record MES signals. Otto Bock's 13E200 electrodes use a 100-400 Hz bandpass filter and a 60 Hz notch filter. The resulting signal is rectified and low-pass filtered. The electrodes were located on the lateral head of the triceps brachii and the long head of the biceps brachii, over the center of the muscle belly.

Subjects wore an elbow orthosis to maintain 90 degrees of elbow flexion, and held onto a fixed pole to allow for the use of isometric contractions.

Subject's MES signals were used to calibrate eight thresholds, shown in Figure 7.1. The first four thresholds involved the maximum and minimum levels of the agonist and antagonist muscles. The final four thresholds involved the maximum and minimum values of the motion signal and impedance signal. The voltages corresponding to minimum and maximum muscle contraction were proportionally scaled to 0-1 for both muscles. The scaled muscle signals were then sent to the motion and impedance blocks, where the maximum and minimum motion and impedance were each proportionally scaled to 0-1. Subjects were asked to exert moderate contractions with each muscle to calibrate the maximum setting of each muscle, in order to avoid fatigue. To determine the minimum thresholds for each muscle, subjects were asked to alternate between a moderate contraction of one muscle and a moderate contraction of the other muscle. The level they contracted the relaxed muscle was set as the minimum threshold, so that impedance would not be activated by involuntary antagonist muscle contraction.

## 7.2 Experimental Apparatus

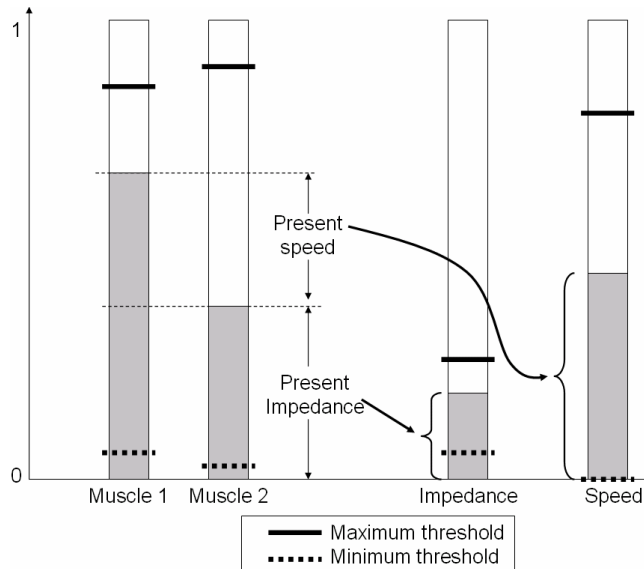


**Figure 7.1: Calibrating Signal thresholds.**

Maximum and Minimum thresholds were set for each muscle. These thresholds were scaled to 0-1, and then fed into Impedance and speed blocks, where maximum and minimum thresholds were again calibrated. These thresholds were likewise scaled to 0-1.

To ensure that the thresholds were correctly set, subjects were asked to track a moving target on a computer screen while exerting three levels of co-contraction: minimum, medium, and maximum. In addition, subjects were asked to co-contrast at two different levels shown on the screen. The maximum impedance threshold was adjusted to allow subjects to accurately but easily control their impedance value without affecting their performance. Impedance maximum thresholds ranged from 20 to 40% of the maximum co-contraction range. The maximum velocity threshold was set to 80% of the maximum velocity signal, allowing subjects to obtain maximum co-contraction at maximum velocity. The minimum velocity threshold was set to 0.

## 7.2 Experimental Apparatus

In order to decouple the motion paradigm from the impedance paradigm, all impedance paradigms were tested using both PVC and PPC to determine which motion paradigm is better for impedance control. For PVC, the desired velocity was set proportional to the MES signals. This velocity signal was then integrated to obtain the desired position necessary to implement impedance control. Integration served the added function of inherently low-pass filtering the signal, such that no additional filtering was required. For PPC, a position range double that of the range of the elbow was set proportional to the range of the MES signals. This position signal was then rate limited to 0.6 rad/sec to ensure stability. Rate limiting provided more responsive control than implementing a low pass filter. Without rate limiting, the elbow could not be accurately controlled using proportional position control, due to the high noise levels inherent in the MES signals.

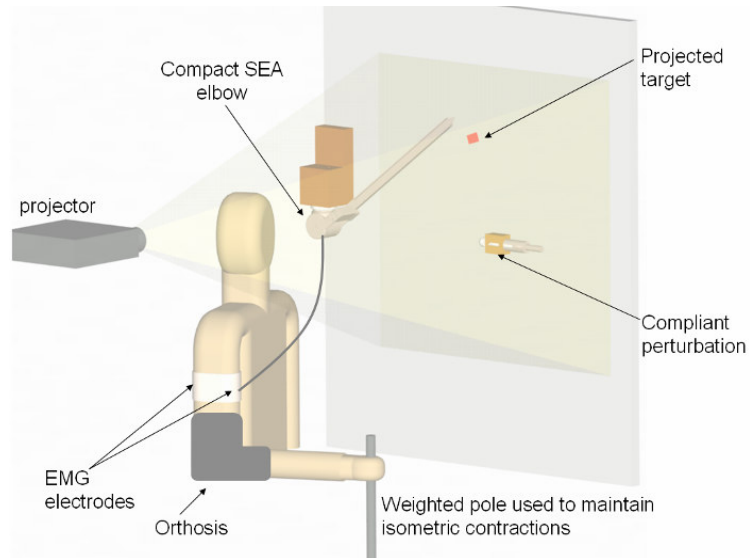
All impedance paradigms were tested for two co-contraction states. In the first co-contraction state, the default impedance corresponded to low impedance, with co-contraction raising the impedance. In the second co-contraction state, the default impedance corresponded to high impedance, with co-contraction lowering the impedance. This second co-contraction state is not biomimetic, in that the derivative of control does correspond to physiological systems, where co-contracting always increases impedance. It is impossible to decouple the derivative of these variables, and as a result, the derivative had to remain non-biomimetic, in an effort to decouple co-contraction from desired impedance.

## 7.2 Experimental Apparatus



The task was designed to mimic real life situations, in which the majority of tasks are unconstrained, but where perturbations may be encountered. Subjects remotely controlled the prosthetic elbow while trying to position its endpoint on stationary projected targets. Subjects were asked to arrive at the targets as accurately and quickly as possible. A compliant perturbation in the middle of the target space impeded movement. The experimental apparatus is shown in Figure 7.2.

## 7.2 Experimental Apparatus



a



b

### Figure 7.2: Experimental Apparatus.

a) A projector projects targets onto the display board. The compact SEA elbow is mounted to the display board, and remotely controlled by the subject's MES signals. A fixed compliant perturbation impedes movement. Subjects are fit in an orthosis and they grasp a weighted pole to exert isometric contractions. The position of the target changes with each trial.

b) A picture showing the actual setup

## 7.2 Experimental Apparatus

The computer displayed a new target at a different location when the subject's velocity reversed direction or stopped near the target. The computer also recorded the time taken to arrive from the previous target, the angular error between desired and actual endpoint position (based on where the subject stopped or reversed direction), and the average impedance throughout the entire movement. Average angular velocity was calculated based on the time required to reach the target and the actual distance covered.

The task was performed for a series of target diameters and trajectory lengths in an attempt to provide a Fitts' law analysis of the task. The resulting data did not meet the requirements for a Fitts' model, however: the relationship between time and index of difficulty was not sufficiently linear ( $r^2 < 0.81$ ), and the linear intercept between the two variables was too large ( $b > 0.4$  s). For the sake of clarity, these results are not presented in this chapter, because they are not relevant to the critical decisions required to implement impedance control. These results are presented and discussed in Appendix 12.5.

Subjects were given a practice run for each motion paradigm. Subjects completed the task for 50 targets for each combination of paradigms. Only the last 40 targets were analyzed for each trial. Subjects were encouraged to try modulating their co-contraction level during the first 10 targets to see if it helped or hurt their performance.

Subjects were independently tested for stiffness modulation and inertia modulation, as well as a control paradigm in which the impedance was fixed regardless of co-contraction levels.

## 7.2 Experimental Apparatus

These impedance paradigms were tested using both motion paradigms and both co-contraction states. Subjects were blinded to all paradigm variations. **The Simulink control blocks used to implement this experiment are shown in Appendix 12.8, and the Matlab code used to run the experiment is presented in Appendix 12.10.**

## **7.3 Results**

### **7.3.1 Performance of Underlying Motion Paradigm**

Speed, endpoint error, and co-contraction levels are compared between proportional position control (PPC) and proportional velocity control (PVC) in Figure 7.3. There is a significant increase in speed using PVC ( $p \leq 0.01$ ) compared to PPC. This increase in speed is largely attributable to the fact that the speed of PPC hit a ceiling due to rate limiting. This effect will be discussed in section 7.4. There is no significant difference in error between the two motion paradigms ( $p=0.66$ ) or in co-contraction levels ( $p=0.17$ ), although there does appear to be a trend towards higher co-contraction levels in PVC control that might be found to be significant by examining larger numbers of subjects. For the purpose of this preliminary study, however, the fact that there is a significant increase in speed without a significant increase in error is sufficient to recommend PVC as the underlying motion paradigm.

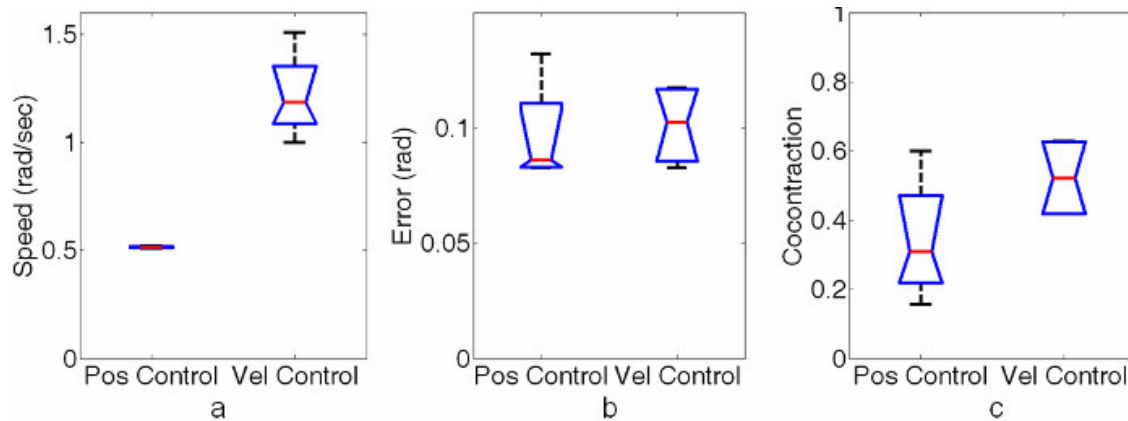


**Figure 7.3: Boxplot comparison of motion paradigms.**

Proportional velocity control reached targets faster, with similar error to proportional position control. The speed ceiling reached in PPC is discussed in section 7.4.

### 7.3.2 Impedance Baselines

Figure 7.4 illustrates subject's co-contraction and impedance ranges using **proportional position control (PPC)**. In Fixed Impedance, where co-contraction had no effect on the impedance, subjects had low levels of co-contraction. For the Stiffness modulation paradigm, there was a noticeable difference in co-contraction levels depending on the co-contraction state. When the co-contraction state had a default of low stiffness, subjects co-contracted to raise the stiffness. This effect bordered on statistical significance ( $p=0.058$ ) for four subjects.

There was a similar effect in inertia levels, although it was not as pronounced. This effect was also not statistically significant ( $p=.071$ ) for four subjects. Qualitatively, subjects did not mind positive inertia, but did not like negative inertia, and these results confirm that: subjects co-contracted to maintain positive inertia when given a negative inertia baseline.

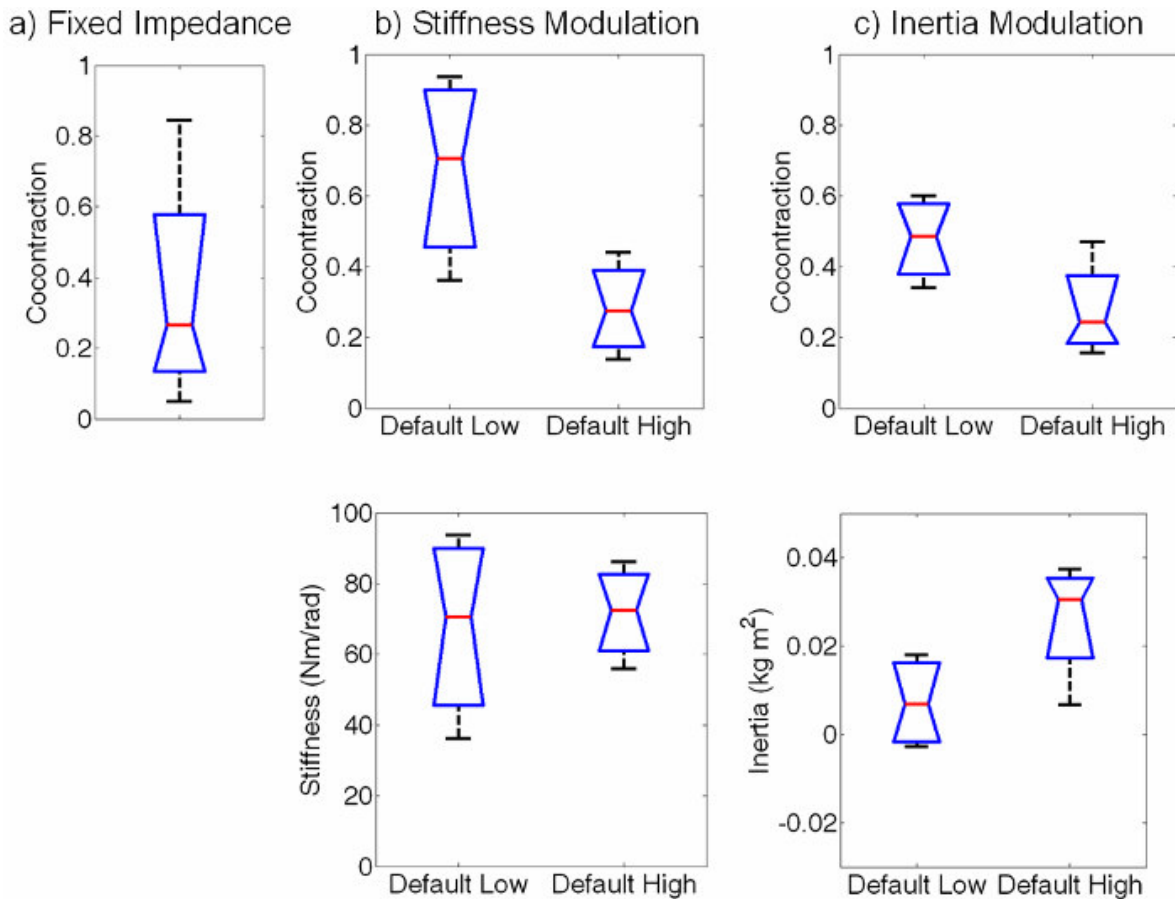


**Figure 7.4: Co-contraction & Impedance Modulation Ranges for Proportional Position Control (PPC).**

a) shows the range of co-contraction and impedance modulation for the Fixed Impedance paradigm, where co-contraction had no effect on the impedance of the prosthetic elbow.

b) shows the range of co-contraction and impedance modulation for the Stiffness modulation paradigm for two co-contraction states. In the first (Default Low), the default stiffness was low, and co-contraction increased the stiffness. In the second (Default High), the default stiffness was high, and co-contraction lowered the stiffness. For Default Low, subjects co-contracted to raise the stiffness. For Default High, they remained at low co-contraction levels. Thus, it appears that subjects preferred higher stiffness.

c) shows the range of co-contraction and impedance modulation for the Inertia modulation paradigm for the two co-contraction states. For Default Low, subjects co-contracted to make the inertia non-negative. For Default High, subjects did not behave differently than the Fixed Impedance paradigm. Thus, it appears that subjects preferred non-negative inertia.

### 7.3 Results

Figure 7.5 illustrates subject's co-contraction and impedance ranges using **proportional velocity control (PVC)**. In Fixed Impedance, where co-contraction had no effect on the impedance, subjects co-contracted more than they did for the same paradigm in PPC. For the Stiffness modulation paradigm, there was a noticeable difference in co-contraction levels depending on the co-contraction state, although less pronounced than in PPC, in which subjects raised the stiffness regardless of the co-contraction state. This effect was not statistically significant for four subjects ( $p=0.17$ ). There was not a noticeable difference in inertia levels, and no statistical difference ( $p=0.31$ ).

### 7.3 Results

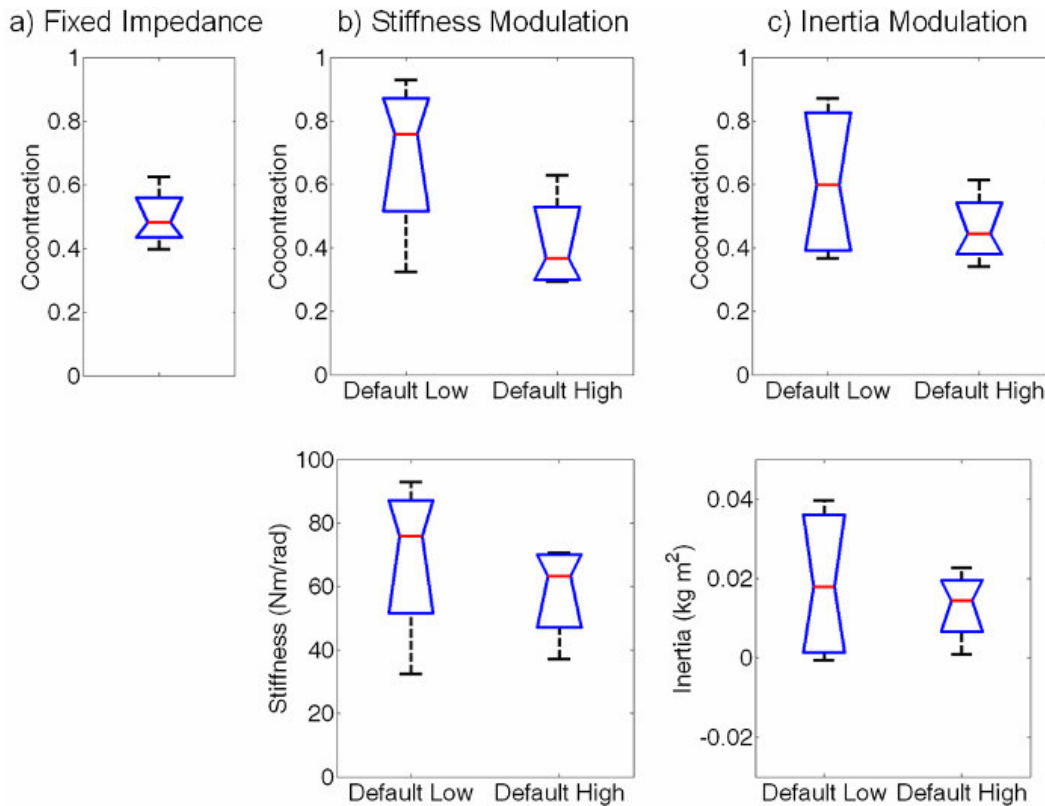


**Figure 7.5: Co-contraction & Impedance Modulation Ranges for Proportional Velocity Control (PVC).**

a) shows the range of co-contraction and impedance modulation for the Fixed Impedance paradigm, where co-contraction had no effect on the impedance of the prosthetic elbow.

b) shows the range of co-contraction and impedance modulation for the Stiffness modulation paradigm for two co-contraction states. In the first (Default Low), the default stiffness was low, and co-contracting increased the stiffness. In the second (Default High), the default stiffness was high, and co-contracting lowered the stiffness. For Default Low, subjects co-contracted to raise the stiffness. For Default High, they co-contracted less than they did for the Fixed Impedance paradigm, which again raises the stiffness. Thus, it appears that subjects preferred higher stiffness.

c) shows the range of co-contraction and impedance modulation for the Inertia modulation paradigm for the two co-contraction states. There is not a noticeable difference between the two co-contraction states, and thus no apparent preferred inertia baseline for this task.

### 7.3 Results



## **7.4 Discussion**

Proportional position control has been found in the past to provide better performance for pursuit tracking tasks (Doubler & Childress, 1984, Weir, 1995). It relies on clean, accurate command signals, however, such as those provided by position or force transducers (Doubler & Childress, 1984, Simpson, 1974). Electromyography signals commonly used to control electric prostheses are not clean signals. As a result, either the prosthesis is uncontrollable, or the speed of the prosthesis must be severely limited when using proportional position control. The author chose to limit the speed to the fastest speed at which the prosthesis could be controlled at all. Using a rate limiter allowed for a higher cutoff frequency with less phase lag than using a low-pass filter (0.7 Hz -3dB cutoff) to achieve the same stability criterion. Whereas it is not surprising that subjects moved at the speed determined by the rate limiter, the fact that their accuracy was not improved over velocity control demonstrates that proportional velocity control provides better control of the prosthetic elbow. An adaptive low pass filter, in which the signal is smoothed more at lower speeds (Jacobsen, Meek & Fullmer, 1984), may allow for better accuracy using proportional position control during slow movements, but not faster movements such as those tested in this study, as the frequency cutoff was determined during movements. In summary, stable proportional velocity control is just as accurate, and significantly faster, than stable proportional position control when using MES electrodes: thus it should be used as the motion paradigm for MES-based impedance control. This finding is in agreement with qualitative feedback from the subjects, who

preferred the more stable and faster velocity control. Subjects also felt that this motion paradigm was more intuitive: In order to move the elbow from full flexion to medium flexion, it made more sense to tense the antagonist muscle than to relax the tension in the agonist muscle.

It also seemed evident that subjects prefer high stiffness and non-negative inertia, although this is not statistically shown. Subjects consciously co-contracted to maintain high stiffness levels when presented with a paradigm that made the relaxed state low impedance. This finding also makes sense: increased stiffness provides increased position accuracy. In humans, increased stiffness requires excessive power consumption, but for a prosthesis, increased stiffness can easily be achieved without power consumption by the user, affording more accurate control for less work. This effect, while present in PVC, was weaker than in PPC. This weaker contrast may be a result of the naturally higher co-contraction levels in PVC, which brought subjects closer to their desired impedance regardless of the co-contraction state. In the case of inertia control, if subjects naturally co-contracted 50%, then they would never encounter a negative inertia, and thus have no reason to alter their co-contraction levels. While future studies that test more subjects may suggest differently, this certainly suggests a good starting baseline of high stiffness levels and non-negative inertia.

#### 7.4 Discussion

## **7.5 Conclusion**

Using the prosthetic elbow described in previous chapters, a motion paradigm of MES driven proportional velocity control was found to provide faster control than MES driven proportional position control, without an increase in error. Subjects are willing to co-contract to maintain high stiffness and non-negative inertia. Thus, the default stiffness should be high (50-100 Nm/rad) and the default inertia should be nonnegative. Future studies will use these conditions to evaluate the usefulness of user-modulated impedance control.

## **8 User Modulated Proportional Impedance Control by Able Bodied Subjects**

The author has designed a prosthetic elbow that is capable of mimicking a variety of impedances. In addition, he has shown that subjects can modulate impedance without impairing performance. Whether the ability to modulate impedance improves performance compared to using predefined optimal values remains to be seen. Two tasks were evaluated in order to assess whether or not subjects prefer to modulate impedance within and between tasks, using a variety of impedance modulation paradigms. The protocol was approved by the Northwestern University Institutional Review Board, and all patients signed informed consent forms. Fifteen subjects (median age 37 +/- 14 years) including eight males and seven females were enrolled in this study.

The procedure described in section 7.2 was used for **Signal Acquisition and Calibration**.

### **8.1 Control Paradigms**

Each component of impedance, including stiffness, viscosity, and inertia, was independently modulated by the subject while keeping the other impedance components fixed. The subject also used a control paradigm, in which all impedance components were fixed. Impedance component ranges included stiffness modulation ( $K = 2-102 \text{ Nm/rad}$ ), viscosity modulation

( $b = 0-10 \text{ Nm}/(\text{rad}/\text{sec})$ ), positive inertia modulation ( $J = 0-0.05 \text{ kg m}^2$ ) and negative inertia modulation ( $J = 0 - -0.03 \text{ kg m}^2$ ), using velocity control as the motion paradigm. The fixed state of impedance components when they were not being modulated, or when the subject was completely relaxed, were  $k = 102 \text{ Nm}/\text{rad}$ ,  $b = 0 \text{ Nm}/(\text{rad}/\text{sec})$ ,  $J = 0 \text{ kg m}^2$ . These default values at the relaxed state, as well as the motion paradigm used, were based on the results of Chapter 7. Both the subjects and the experimenters were blind to the variable being tested in each paradigm, and the order was randomly determined for each subject.

## **8.2 Experimental Tasks**

In order to evaluate the usefulness of impedance modulation for control of a prosthesis, two tasks were designed to mimic real life situations, in which the majority of activities are unconstrained, but where perturbations may be encountered. In the first task, which was a pointing task, subjects remotely controlled the prosthetic elbow while trying to position its endpoint on discrete projected targets, as shown in Figure 8.1. Subjects were asked to arrive at the targets as accurately and quickly as possible. A compliant perturbation in the middle of the target space impeded movement.

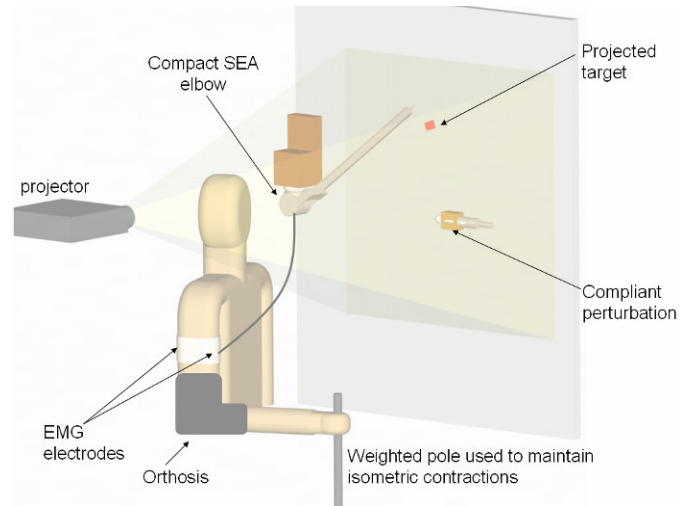


**Figure 8.1. Experimental apparatus for pointing task.**

A projector projects targets onto the display board. The compact SEA elbow is mounted to the display board, and remotely controlled by the subject's MES signals. A fixed compliant perturbation impedes movement. Subjects are fit in an orthosis and they grasp a weighted pole to exert isometric contractions. The position of the target changes with each trial.

The computer displayed a new target at a different location when the subject's velocity reversed direction or stopped near the target. The computer also recorded the time taken to arrive from the previous target, the angular error between desired and actual endpoint position (based on where the subject stopped or reversed direction), and the average impedance throughout the entire movement. The average impedance during three segments of movement, including movement initiation, free swing, and movement termination, was also recorded. Average angular velocity was calculated based on the time required to reach the target and the actual distance covered.

## 8.2 Experimental Tasks

One trial consisted of 50 targets. Only the last 40 targets were analyzed for each trial. Subjects were encouraged to modulate their co-contraction level during the first 10 targets to see if it helped or hurt their performance. Two trials were done for each paradigm. For one of these trials, subjects were required to complete the Stroop task (Stroop, 1935) in parallel with the pointing task. In this Stroop task, a word was displayed next to the target. The word spelled a color, but was projected in a different color. Subjects were given such a word at the beginning of the experiment to see if they would intuitively say the text or the color of the word. Throughout the remainder of the experiment, subjects were asked to say the opposite, in an attempt to add an additional mental load. Whether or not the mental load trial was done first or second was randomly determined.

For the second task, subjects were asked to track a continuously moving target in an attempt to simulate a partially constrained task, such as raising the sail on a sailboat. The position of the target was determined by a 100 Hz band limited white noise generator, which was passed through a 0.3 Hz eighth order low-pass Butterworth filter. A pulley system conveyed the output of the prosthetic arm to an unseen weight rack, where 0.08 kg, 0.76 kg, or 1.445 kg was supported by the prosthetic arm, depending on its position. This setup is illustrated in Figure 8.2. **The Simulink control blocks used to implement this experiment are shown in Appendix 12.9, and the Matlab code used to run the experiment is presented in Appendix 12.10**

## 8.2 Experimental Tasks

The average impedance over the entire one-minute task was recorded, as well as the average detrended error between the actual and desired angular position.

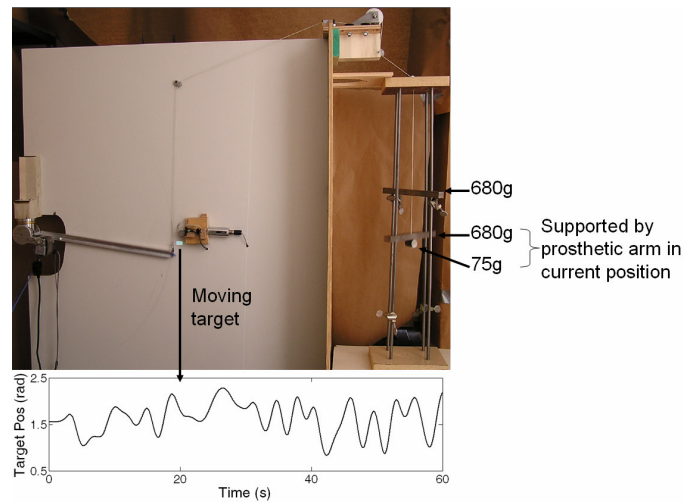


**Figure 8.2: A picture showing the tracking task.**

The prosthetic arm is connected through a pulley system to a weight rack. The arm must pull between 75g and 1,435g, depending on the position of the elbow. The user must track the target, which continuously moves at 0.3 Hz. The fixed perturbation slides backwards for this task, so that it does not interfere with the prosthesis.

At the beginning of the experiment, subjects performed the pointing task once to become used to the proportional-velocity-control motion paradigm without any data being recorded or analyzed. For each paradigm, the pointing task was done twice in succession: once in parallel with the Stroop task and once without (in random order). Subjects then completed

## 8.2 Experimental Tasks



the second task, and then a new paradigm was presented. This sequence is illustrated in Figure 8.3. Subjects were informed each time a new paradigm was presented.

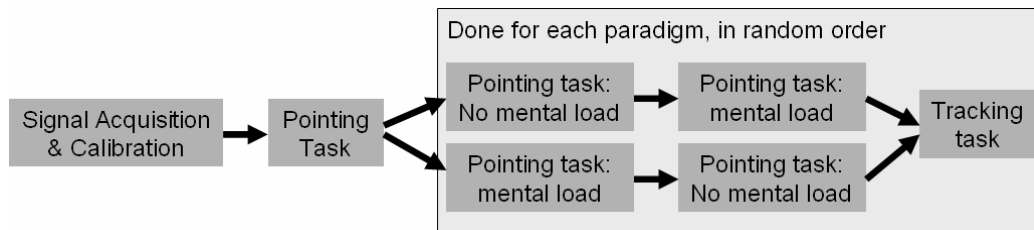


**Figure 8.3: Experiment Sequence.**

After Signal Acquisition & Calibration, subjects completed the pointing task once to become used to the motion paradigm. Then, for each paradigm, subjects completed the pointing task twice, and then the tracking task once. For the pointing task, subjects had to complete an additional task for one of the trials. The order of these two trials was randomly determined.

### 8.3 Results

Inter-subject variables included impedance paradigm and mental load. Between-subject variables included age group and gender. There was no statistical difference for speed or error based on age ( $p > 0.1$ ), gender ( $p > 0.27$ ), or paradigm order ( $p > 0.19$ ). The addition of the mental load task decreased mean speed across paradigms from 0.74 rad/sec to 0.69 rad/sec ( $p = .04$ ), but had no statistically significant effect on error ( $p = 0.28$ ). With the additional mental load task, the spread of co-contraction levels for a given trial of a given subject increased dramatically. As a result, any statistical comparisons had  $p$  values of around 0.9, since the co-contraction levels essentially became white noise. As a result, only the results for

the no-mental load condition are presented below, since the addition of a mental load effectively prevented subjects from having any control over their co-contraction levels.

The co-contraction levels of individual targets are shown in Appendix 12.6.

### **8.3.1 Co-contraction**

The co-contraction levels of individual subjects were analyzed across paradigms for the 40 trials in the pointing task, using a 1X5 repeated measures ANOVA with a Bonferroni correction factor to compare main effects. Every subject had at least one pair of paradigms with statistically different ( $p < 0.05$ ) median co-contraction, and 12 subjects had at least one paradigm that had a statistically different ( $p < .05$ ) median co-contraction level than the median co-contraction level of all the other paradigms. Four subjects had at least 3 statistically different ( $p < 0.05$ ) groupings of paradigm co-contraction levels. Three of these subjects were retested on different days, but none of these subjects maintained the distinct groupings of co-contraction levels between paradigms. Thus, co-contraction results were not repeatable.

The median co-contraction levels of the subjects are shown in Figure 8.4 for both tasks. The difference in co-contraction levels across paradigms is not statistically significant ( $p > .27$ ) for either task using a 1X5 repeated measures ANOVA.

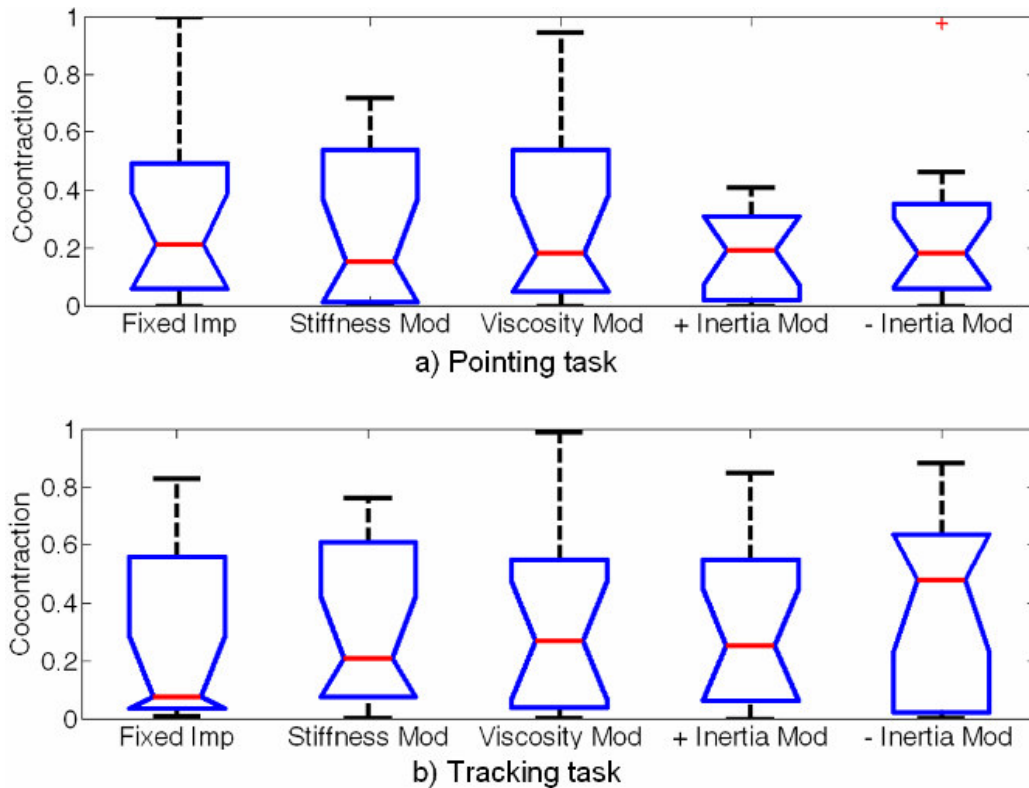


**Figure 8.4: Impedance Modulation, compared by paradigm.**

$p = 0.27$  for pointing task and  $0.50$  for tracking task. Subjects did not have a consensus for the optimal impedance

A significant difference in the co-contraction levels between the two tasks is expected if subjects modulate impedance levels based on the particular task. The difference between the median co-contraction levels of both tasks for each impedance paradigm is shown in Figure 8.5. There was no statistical significance between the tasks using a paired student's t-test, except for the negative inertia modulation paradigm ( $p=0.01$ ), in which subjects co-contracted more during the tracking task than during the pointing task.

### 8.3 Results

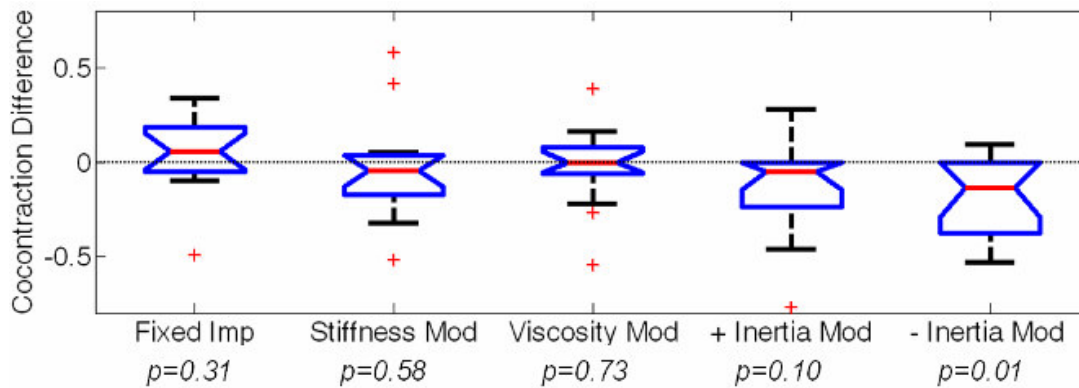


**Figure 8.5: Impedance Modulation, compared by task.**

There was no difference in the level of impedance modulation between the two tasks, except for negative inertia modulation, in which subjects co-contracted more in the tracking task, providing inertia that is more negative.

Co-contraction levels were also analyzed within three movement regions for each movement: movement initiation, free swing, and termination, as illustrated in Figure 8.6. Subjects co-contracted more at movement initiation (0.182) and termination (0.210) than during free swing (0.088), regardless of paradigm ( $p=0.011$ ), even when co-contraction had no influence on motion control.

### 8.3 Results

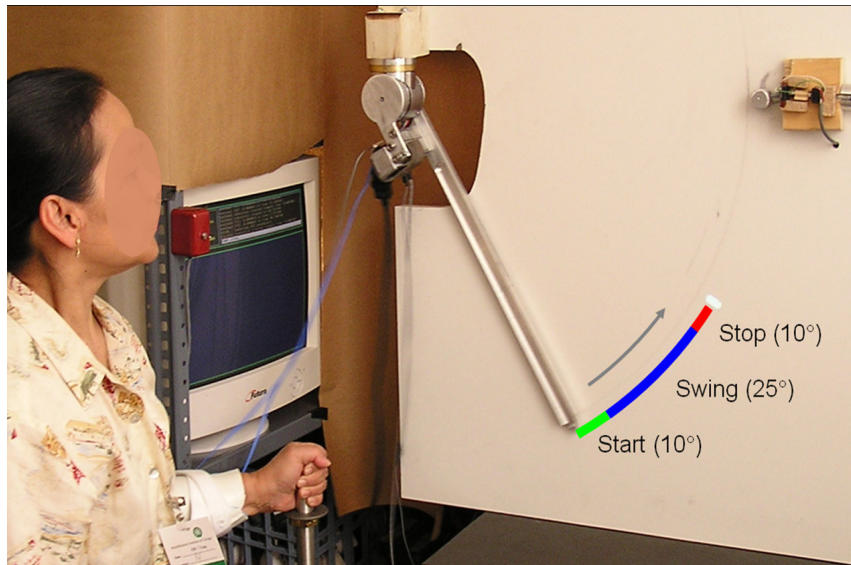


**Figure 8.6: Co-contraction across movement regions.**

Average impedance was recorded for three movement regions: Movement initiation, free swing, and movement termination. Subjects co-contracted more during the start and stop of each movement than in the middle, regardless of the impedance paradigm.

### 8.3.2 Performance

From the results of section 8.3.1, it may be inferred that subjects did not actively modulate their impedance to improve their performance. The level that they did modulate their impedance, however, may have had an effect on their performance. As a result, median performance metrics were compared across impedance paradigms to see if subjects performed better using a particular impedance paradigm. A linear regression was also done between optimum performance metrics and their corresponding co-contraction levels for each paradigm, to see if impedance values affected performance.

## 8.3 Results

Median performance metrics are shown in Figure 8.7. There was a significant difference between the paradigms for both error ( $p = <.001$ ) and speed ( $p = .001$ ), where error is defined as the difference between the desired and actual endpoint position. Using a post-hoc analysis of the main effects, it was found that the Fixed and Viscosity paradigms had lower error than the other paradigms ( $p < 0.05$ ), and that the speed of the two inertia paradigms was higher than that of the others ( $p < 0.02$ ).

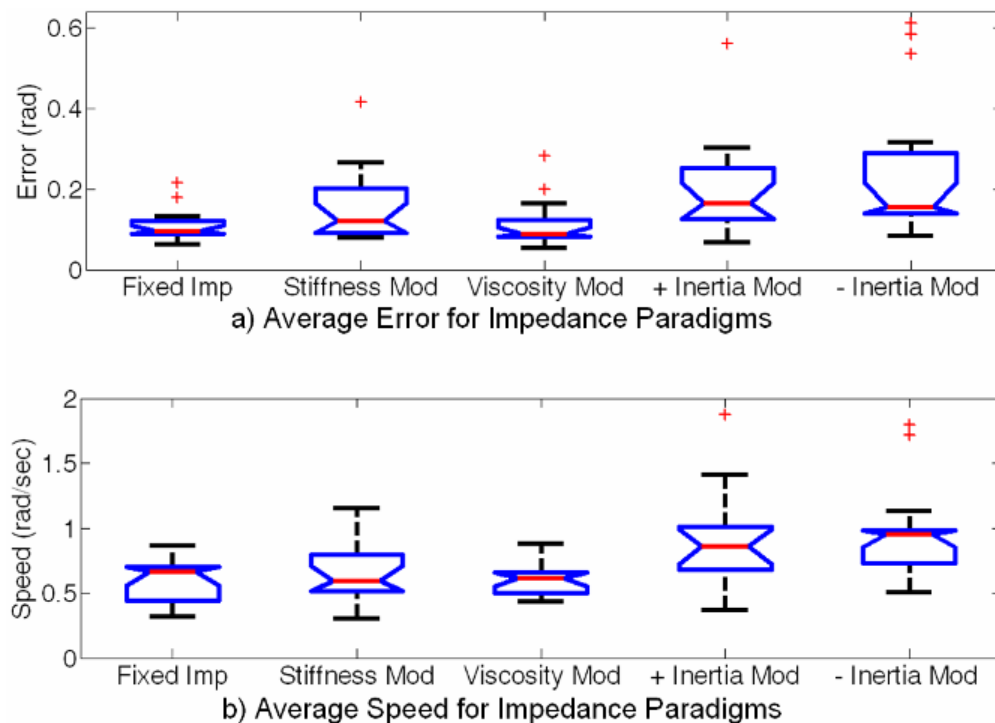


**Figure 8.7: Impedance paradigm effect on performance.**

The co-contraction level corresponding to the optimum performance (minimum error, maximum speed) is shown in Figure 8.8. Linear regressions were done between optimum performance and the co-contraction level corresponding to it across subjects. There was no

significant correlation between co-contraction levels and performance, except for the error of the Fixed Impedance paradigm ( $\text{Error} \sim .05 * \text{Co-contraction}$ ) and the speed of positive inertia ( $\text{Speed} \sim 0.91 * \text{Co-contraction}$ ).

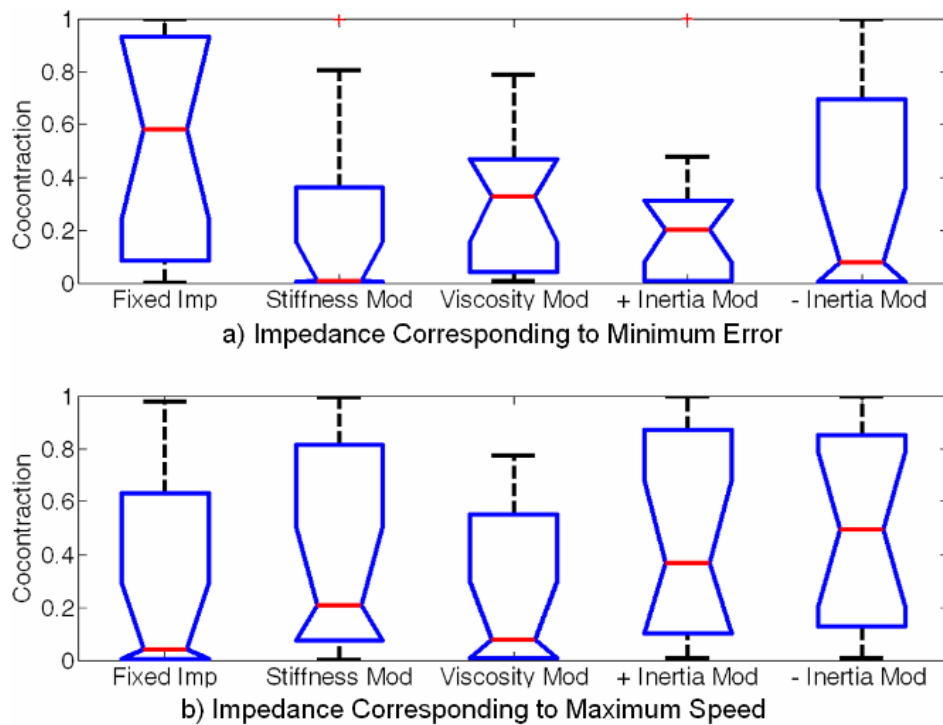


**Figure 8.8: Impedance effect on performance.**

Co-contraction had a small, but significant effect on error ( $\text{Error} \sim .05 * \text{Co-contraction}$ ) for the Fixed Impedance Paradigm and a large effect on speed ( $\text{Speed} \sim .91 * \text{Co-contraction}$ ) for positive Inertia. Other than those, co-contraction did not have a significant effect on the performance.

## 8.4 Discussion

If the default impedance provides poor enough control of the prosthesis, the results of Chapter 7 have indicated that subjects are willing to co-contrast to change the impedance.

However, no consensus was found in this study. In this study, the baseline impedance was set to the preferred impedance of the previous study. As a result, it seems likely that subjects are either unwilling, or unable to fine-tune their impedance once a generally acceptable impedance is obtained.

For each impedance paradigm, subjects were only allowed to evaluate the preferred impedance for 10 movements. It is feasible that if subjects were given several hours to learn each impedance paradigm, differences between paradigms might be more apparent, and subjects might gain more fine-tune control of the impedance level. Due to the noisiness of MES, this is unlikely, but future studies are required to rule this possibility out.

It is useful to note that increased co-contraction only had a small impact on performance. This means that co-contraction level may be used in the future to control a separate variable. MES signals are noisy, however, even when they are severely low-pass filtered. As a result, co-contraction does not present a viable method for fine-tuning any parameters in a prosthesis. It may be used to coarsely adjust a feature, but if an approximation of the ideal parameter is known a priori, this prior knowledge will yield a more finely tuned impedance setting than having the subject adaptively tune the impedance. As a result, allowing the subject to control the modulation of impedance does not seem useful. Having several states of predefined impedance, that the user may switch to by flipping a switch, or using co-contraction to act as a switch, seems a much easier solution, and one that will provide more accurate control with a lower mental load.

#### 8.4 Discussion



The choice of tasks likely also contributed to subject's lack of impedance modulation. If objective tasks had been found in which the impedance was actively modulated, subjects may have modulated their impedance. The authors were unable to devise an experiment in which impedance modulation was intuitively beneficial, although both of the tasks used in this experiment attempted to do so. There are very few tasks that may be objectively measured using a bench-top prototype in which impedance modulation makes sense. Giving subjects more time to learn each impedance modulation paradigm may have likewise allowed them to better use impedance modulation. However, such training sessions were outside the scope of this thesis.

Subjects qualitatively voiced their preference for fixed impedance, stiffness control, and viscosity control. Both positive and negative inertia control were difficult to control. These qualitative findings are in agreement with the performance results shown in Figure 8.7

## **8.5 Conclusion**

There was no collective agreement on the optimal state of any impedance parameters, most likely a result of the inability to fine-tune the impedance using MES signals as a control signal. Stiffness control and viscosity control presented the most stable results. Both positive and negative inertia control were very difficult to control by the subjects. Future studies should allow the user to switch between impedance states, rather than allowing subjects to proportionately modulate impedance.

## **9 User Modulated Proportional Impedance Control by Subjects with an Amputation**

The experiments described in chapter 8 were also performed on two subjects with a shoulder disarticulation and two subjects with a transhumeral amputation. All of these subjects had targeted reinnervation, and had controlled electric prostheses using myoelectric sensors for at least six months. The protocol was approved by the Northwestern University Institutional Review Board, and all participants signed informed consent forms. The protocol was the same as the one described in chapter section 8, except that subjects wore the prosthesis for the second task.

One of the subjects with a transhumeral amputation did not satisfactorily complete the signal calibration phase, in which subjects isolate co-contraction from individual muscle action. This subject was unable to co-contract while simultaneously controlling movement. Of the remaining three subjects, both subjects with a shoulder disarticulation attempted to complete the second task, in which the prosthetic elbow was attached to their socket. One of them did not feel comfortable wearing the prosthesis since its terminal device was connected to a series of weights, however, and as a result, only one of them completed the second task. There were technical difficulties with the electrodes used by the second subject with a transhumeral amputation, and as a result, although he did complete the second task, he had to do so remotely, using Otto Bock electrodes. As a result, his results for the second task are not

presented below. The co-contraction levels for the three subjects who remotely completed the first task and for the one subject with a shoulder disarticulation who completed the second task while wearing the prosthetic elbow are shown below in Figure 9.1.

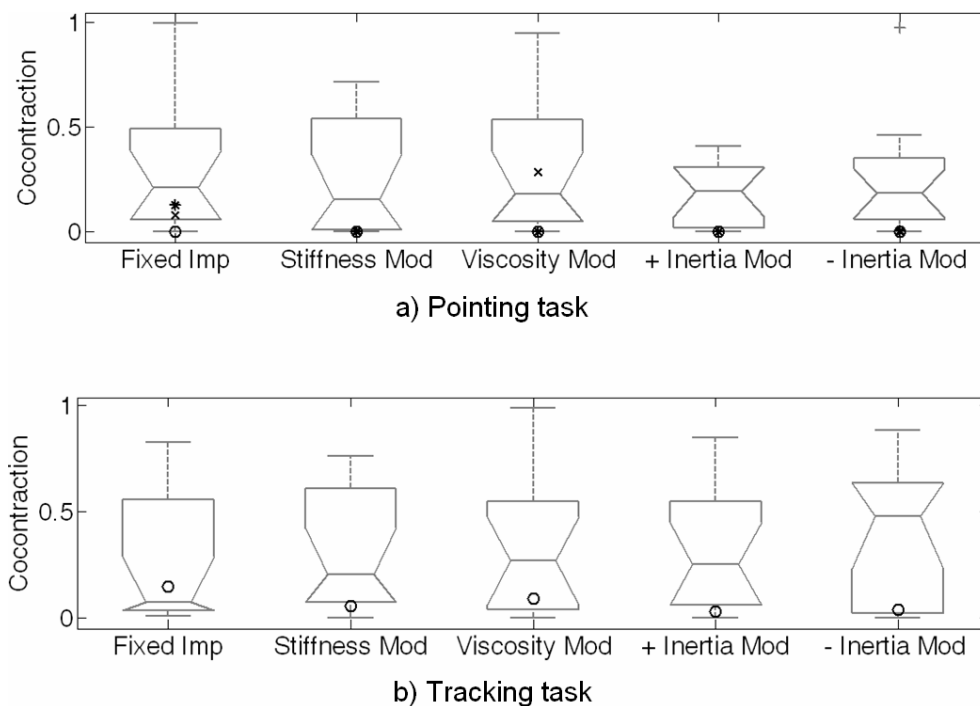


**Figure 9.1: Co-contraction levels for subjects with an amputation.**

Co-contraction levels for the three subjects with an amputation are shown with point markers. They are overlaid against a background of able-bodied box-plots for each paradigm.

Only one subject was able to complete the second task.

Both subjects with a shoulder disarticulation rarely co-contracted, even during those initial movements where they were encouraged to co-contrast. The subject with a transhumeral amputation, shown with an x marking in Figure 9.1, did co-contrast during the initial

movements, but only intentionally co-contracted during the fixed Impedance paradigm and the viscosity impedance paradigm. Subjects who control prostheses using myoelectric control are trained to relax their antagonist muscles. While they may use co-contraction to act as a switch, they never intentionally co-contrast throughout a movement. As a result, it was likely to detrain themselves to intentionally co-contrast their muscles. The one subject who performed the second task did co-contrast more when the prosthesis was attached to his socket, but only minimally.

For the second task subjects had to move 15 N in a tracking task, using a 0.5 m lever arm. In retrospect, this weight was too heavy to ask subjects to move in a sinusoidal manner. Subjects had to brace themselves to prevent themselves from being tipped over, and one of the smallest and lightest subjects was uncomfortable with the amount of torque required, and as such did not complete the experiment. Future experiments should use less weight, and adjust the lever arm to be anthropomorphically appropriate for the subject.

## **10 Conclusions**

The measured socket-residual limb interface rotational stiffness for four subjects with a transhumeral amputation ranged from 24-140 Nm/rad. Finite element modeling indicates that these subjects should be able to modulate their impedance at least between 14 and 70 Nm/rad by co-contracting their muscles. Able-bodied subjects can modulate the stiffness of their elbow between 3 and 140 Nm/rad. As a result, the rotational stiffness range of the socket-residual

limb interface sufficiently overlaps the range of able-bodied elbows to render impedance control of the elbow superfluous. Impedance control of more distal joints is not affected by the stiffness of the elbow socket-residual limb interface, however, and still merits investigation. Impedance control of the elbow for subjects with a shoulder disarticulation is also unaffected by the stiffness of the socket-residual limb interface, and merits investigation.

A compact series elastic actuator has successfully been designed and created that accurately mimics a range of impedances less than its actual impedance for frequencies less than 4 Hz. It has been found that inner position control and a sensor distal to sources of friction improve the fidelity of the system. These improvements were not included in this design, however, for reasons discussed in Chapter 5. Regardless of whether impedance control is implemented or not, the physical impedance of the prosthetic elbow should always be limited by inserting a compliant element distal to the gear transmission, to ensure safety to the user.

A pilot study involving four subjects found that subjects prefer proportional velocity control to proportional position control as an underlying motion paradigm to implement impedance control. Proportional velocity control may be controlled more accurately at higher speeds than proportional position control. This study also found that subjects could decouple co-contraction from motion control when presented with an undesirable impedance baseline, and that subjects prefer high stiffness and nonnegative inertia.

A study involving fifteen able bodied subjects and four subjects with an amputation found that subjects do not actively modulate their impedance when given an acceptable baseline impedance. Stiffness control and viscosity control provided the most stable control. Subjects with an amputation tended not to co-contract, even during the initial segment of each trial, when they were encouraged to co-contract. As a result, they may require additional training to learn to use co-contraction as an additional signal in parallel with motion control.

In summary, allowing subjects to actively modulate their impedance using MES signals, while they simultaneously controlled the motion of the prosthesis, did not prove to be useful. While allowing subjects to use co-contraction as a switch to change between large groupings of impedance may be useful, proportional impedance control of an unconstrained or semi-constrained prosthesis is not advantageous.

## 11 Future Work

Although user-modulated proportional impedance control has not proven useful, it may still be useful to allow subjects to switch between impedance states such as high and low stiffness, using co-contraction as a switch. Viscosity control seems to hold the most promise, followed by stiffness control. Future experiments should use a low (2 Nm/rad) and high (70-100 Nm/rad) stiffness state, or a low (0 Nm/(rad/sec)) and a high (5 Nm/(rad/sec)) viscosity state.

Now that the design concepts of the prosthetic elbow have been proven, it would be useful to create a second generation of prototypes that may be taken home by subjects and worn for several months. This would allow subjects with an amputation sufficient time to adjust to the new paradigms, and assess if they like them in real activities of daily living. By monitoring the amount of time they stay in each state, it would be possible to quantitatively assess how much they used each state.

Adjustable impedance control also seems useful in body-powered prostheses, especially for the wrist. Future research may design a wrist capable of adjusting both the stiffness and the viscous friction by turning two disks. The impedance could be set for a particular task, and then left alone while the subject performed the task.

The intentional insertion of compliance allows for energy storage. As a result, forces may be exerted that do not fluctuate with small movement perturbations, removing the need for external power sources. This concept lends itself to a subset of body-powered terminal devices

termed voluntary closing (VC) terminal devices, where the user generates a force to close the terminal device. These devices typically have clutches to allow the user to relax once they have grasped an object: otherwise, the user would constantly have to exert force on the terminal device to preserve the force. These clutches are seldom successful, however, because all force is lost if any amount of slip is present. The terminal devices function more poorly with time as clutch parts wear down, and as a result, they can seldom be used to grasp noncompliant objects, such as a piece of paper. This problem may be solved by inserting a compliant element distal to the clutch – in effect making the terminal device itself compliant. By introducing a nonlinear stop, higher forces may be exerted. For moderate to low forces, however, the force will remain stable even in the presence of small position perturbations. Future work will investigate the implementation of this design.

Finally, although it now seems apparent that user-modulated proportional impedance control is not useful, a converse paradigm may prove interesting. Instead of having the subject change the inertia, it may be useful for the prosthesis to appear to have the same inertia, regardless of the load in the terminal device. This may be accomplished by implementing a load-sensitive continuously variable transmission. The author has created a design that simply accomplishes this goal in a body-powered prosthetic elbow and a body-powered prosthetic terminal device (Sensinger & Weir, 2007), and future research will fabricate these devices and explore subject's perception of them.



## References

- Abboudi, R.L., Glass, C.A., Newby, N.A., Flint, J.A., & Craelius, W. (1999). A Biomimetic Controller for a Multifinger Prosthesis. *IEEE Transactions on Rehabilitation Engineering*, 7 (n), 121-129.
- Abul-Haj, C., & Hogan, N. (1987). An Emulator System for Developing Improved Elbow-Prosthesis Designs. *IEEE Transactions on Biomedical Engineering*, 34 (9), 724-737.
- Abul-Haj, C.J. (1987). Elbow-prosthesis emulation--a technique for the quantitative assessment of an assistive device. *Department of Mechanical Engineering* (p. 173). Cambridge: Massachusetts Institute of Technology.
- Abul-Haj, C.J., & Hogan, N. (1990a). Functional Assessment of Control-Systems for Cybernetic Elbow Prostheses - Part 2: Application of the Technique. *IEEE Transactions on Biomedical Engineering*, 37 (11), 1037-1047.
- Abul-Haj, C.J., & Hogan, N. (1990b). Functional Assessment of Control-Systems for Cybernetic Elbow Prostheses - Part I: Description of the Technique. *IEEE Transactions on Biomedical Engineering*, 37 (11), 1025-1036.
- Almstrom, C., Anani, A., Herberts, P., & Korner, L. (1981). Electrical-Stimulation and Myoelectric Control - A Theoretical and Applied Study Relevant to Prosthesis Sensory Feedback. *Medical & biological engineering & computing*, 19 (5), 645-653.
- Andeen, G.B., & Kornbluh, R. (1988). Design of Compliance in Robots. *International Conference on Robotics and Automation* (pp. 276-281).
- Armstrong-Hélouvy, B. (1993). Stick Slip and Control in Low-Speed Motion. *IEEE Transactions on Automatic Control*, 38 (10), 1483-1496.
- Armstrong-Hélouvy, B., Dupont, P., & Canudas de Wit, C. (1994). A Survey of Models, Analysis Tools and Compensation Methods for the Control of Machines with Friction. *Automatica*, 30 (7), 1083-1138.
- Asada, H., & Youcef-Toumi, K. (1987). *Direct-drive robots: theory and practice*. (Cambridge, MA: MIT Press.
- Ashley, S. (2003). Artificial Muscles. *Scientific American*, 289 (4), 53-59.
- Bagesteiro, L.B., & Sainburg, R.L. (2003). Nondominant Arm Advantages in Load Compensation During Rapid Elbow Joint Movements. *Journal of Neurophysiology*, 90, 1503-1513.
- Bar-Cohen, Y. (2004). Electroactive polymer (EAP) actuators as artificial muscles: reality, potential, and challenges. *SPIE Press monograph* (pp. xvii, 765). Bellingham, WA: SPIE Press.
- Barrett, R.C., Selker, E.J., Rutledge, J.D., & Olyha, R.S. (1995). Negative Inertia: A Dynamic Pointing Function. *ACM/SIGCHI Conference on Human Factors in Computing Systems* (Denver, CO).
- Basmajian, J., & De Luca, C. (1985). *Muscles alive: their functions revealed by electromyography*. (Baltimore, MD: Williams and Wilkins.

- Bhushan, N., & Shadmehr, R. (1999). Computational nature of human adaptive control during learning of reaching movements in force fields. *Biological Cybernetics*, 81, 39-60.
- Bicchi, A., & Tonietti, G. (2004). Fast and soft arm tactics. (vol 11, pg 22, 2004). *IEEE Robotics & Automation Magazine*, 11 (3), 61-61.
- Bizzi, E., Hogan, N., & Mussa-Ivaldi, F.A. (1992). Does the Nervous-System use Equilibrium-Point Control to guide single and multiple joint movements. *Behavioral Brain Science*, 15 (4), 603-613.
- Bizzi, E., Polit, A., & Morasso, P. (1976). Mechanisms Underlying Achievement of Final Head Position. *Journal of Neurophysiology*, 39 (2), 435-444.
- Blaya, J.A., & Herr, H. (2004). Adaptive control of a variable-impedance ankle-foot orthosis to assist drop-foot gait. *IEEE Transactions on Neural Systems and Rehabilitation Engineering*, 12 (1), 24-31.
- Brooks, R.A. (1991). How To Build Complete Creatures Rather Than Isolated Cognitive Simulators. In: K. VanLehn (Ed.) *Architectures for intelligence* (pp. x, 436 p.). Hillsdale, NJ: L. Erlbaum Associates.
- Brooks, R.A., & Connell, J. (1986). Asynchronous Distributed Control System for a Mobile Robot. *Proceedings of SPIE's Cambridge Symposium on Optical and Optoelectronic Engineering* (pp. 77-84). Cambridge, MA.
- Butterfass, J., Fischer, M., Grebenstein, M., Haidacher, S., & Hirzinger, G. (2004). Design and Experiences with the DLR Hand II. *Proceedings of the World Automation Congress* (Seville, Spain).
- Calvert, J.B. (2001). Jacobi's Theorem. ([www.du.edu/~jcalvert/tech/jacobi.htm](http://www.du.edu/~jcalvert/tech/jacobi.htm)).
- Cannon, R.H., & Rosenthal, D.E. (1984). Experiments in control of flexible structures with noncolocated sensors and actuators. *AIAA Journal of Guidance and Control*, 3
- Cannon, R.H., & Schmitz, E. (1984). Initial Experiments on the Endpoint Control of a Flexible One-Link Robot. *International Journal of Robotics Research*, 3 (3), 62-75.
- Chan, R.B., & Childress, D.S. (1990). On Information-Transmission in Human-Machine Systems - Channel Capacity and Optimal Filtering. *IEEE Transactions on Systems Man and Cybernetics*, 20 (5), 1136-1145.
- Childress, D., & Weir, R.F. (2004). Control of Limb Prostheses. In: D.G. Smith, J.W. Michael, & J.H. Bowker (Eds.), *Atlas of Amputations and Limb Deficiencies* (Rosemont, IL: American Academy of Orthopaedic Surgeons).
- Childress, D.S. (1980). Closed-Loop Control in Prosthetic Systems - Historical Perspective. *Annals of biomedical engineering*, 8 (4-6), 293-303.
- Clover, C. (1999). A control-system architecture for robots used to simulate dynamic force and moment interaction between humans and virtual objects. *IEEE transactions on systems, man and cybernetics. Part C, Applications and reviews*, 29 (4), 481-493.
- Da Vinci, L. (1519). *The Notebooks*. (Dover, NY).
- DeGoede, K.M., & Ashton-Miller, J.A. (2003). Biomechanical simulations of forward fall arrests: effects of upper extremity arrest strategy, gender and aging-related declines in muscle strength. *Journal of Biomechanics*, 36, 413-420.

- Doubler, J., & Childress, D.S. (1984). An analysis of extended physiological proprioception as a control technique. *Journal of Rehabilitation Restorative Devices*, 21 (1), 5-18.
- English, C.E., & Russell, D. (1999a). Mechanics and stiffness limitations of a variable stiffness actuator for use in prosthetic limbs. *Mechanism and Machine Theory*, 34 (1), 7-25.
- English, C.E., & Russell, D. (1999b). Mechanics and stiffness limitations of a variable stiffness actuator for use in prosthetic limbs. *Mechanism and Machine Theory*, 25, 7-25.
- Feldman, A.G. (1966a). Functional Tuning of Nervous System During Control of Movement or Maintenance of a Steady Posture .3. Mechanographic Analysis of Execution by Man of Simplest Motor Tasks. *Biophysics-Ussr*, 11 (4), 766.
- Feldman, A.G. (1966b). Functional Tuning of Nervous System with Control of Movement or Maintenance of a Steady Posture .2. Controllable Parameters of Muscles. *Biophysics-Ussr*, 11 (3), 565.
- Feldman, A.G. (1986). Once More on the Equilibrium-Point Hypothesis ( $\lambda$  Model) for Motor Control. *Journal of Motor Behavior*, 18 (1), 17-54.
- Fitts, P.M. (1954). The information capacity of the human motor system in controlling the amplitude of movement. *Journal of Experimental Psychology*, 47, 381-391.
- Franklin, G.F., Powell, J.D., & Emami-Naeini, A. (2002). Feedback control of dynamic systems. (pp. xvii, 910 p.). Upper Saddle River, NJ: Prentice Hall.
- Godler, I., Hashimoto, M., Horiuchi, M., & Ninomiya, T. (2001). Performance of gain-tuned Harmonic Drive torque sensor under load and speed conditions. *IEEE/ASME Transactions on Mechatronics*, 6 (2), 155-160.
- Godler, I., Horiuchi, M., Hashimoto, M., & Ninomiya, T. (2000). Accuracy improvement of built-in torque sensing for harmonic drives. *IEEE/ASME Transactions on Mechatronics*, 5 (4), 360-366.
- Godler, I., Ninomiya, T., & Horiuchi, M. (2001). Ripple Compensation for Torque Sensors Built into Harmonic Drives. *IEEE Transactions on Instrumentation and Measurement*, 50 (1), 117-122.
- Gottschalk, F. (2004). Transfemoral Amputation: Surgical Management. In: D.G. Smith, J.W. Michael, & J.H. Bowker (Eds.), *Atlas of Amputations and Limb Deficiencies* (Rosemont, IL: American Academy of Orthopaedic Surgeons.
- Guiard, Y., & Beaudouin-Lafon, M. (2004). Fitts' law 50 years later: applications and contributions from human-computer interaction - Preface. *International Journal of Human-Computer Studies*, 61 (6), 747-750.
- Heckathorne, C.W. (1978). A study of the cineplastic human biceps: relationship of the surface electromyogram to force, length, velocity and contraction rate. (
- Heckathorne, C.W. (2004). Components for Electric-Powered Systems. In: *Atlas of Amputations and Limb Deficiencies* (pp. 145-172). Rosemont, IL: American Academy of Orthopaedic Surgeons.
- Heckathorne, C.W., & Childress, D.S. (1981). Relationships of the Surface Electromyogram to the Force, Length, Velocity, and Contraction Rate of the Cineplastic Human Biceps. *American Journal of Physical Medicine & Rehabilitation*, 60 (1), 1-19.

- Herr, H., & Dennis, B.A. (2004). A Swimming Robot Actuated by Living Muscle Tissue. *Journal of NeuroEngineering and Rehabilitation*,
- Hill, A.V. (1938). The heat of shortening and the dynamic constants of muscle. *Proceedings of the Royal Society*, 126, 136-195.
- Hinder, M.H., & Milner, T.E. (2003). The case for an internal dynamics model versus equilibrium point control in human movement. *Journal of Physiology*, 549 (3), 953-963.
- Hirai, K. (1999). The Honda humanoid robot: development and future perspective. *Industrial Robot*, 26 (4), 260-266.
- Hirose, M., Gomi, H., Takahashi, H., Takenaka, T., Nishikawa, M., & Takahashi, T. (1995). Legged mobile robot and a system for controlling the same. (p. 28). United States: Honda Giken Kogyo Kabushiki Kaisha.
- Hirshberg, C. (2002). My Mother, the Scientist. *Popular Science*, April
- Hogan, N. (1985a). Impedance Control - an Approach to Manipulation .1. Theory. *Journal of Dynamic Systems Measurement and Control*, 107 (1), 1-7.
- Hogan, N. (1985b). Impedance Control - an Approach to Manipulation .2. Implementation. *Journal of Dynamic Systems Measurement and Control*, 107 (1), 8-16.
- Hogan, N. (1985c). Impedance Control - an Approach to Manipulation .3. Applications. *Journal of Dynamic Systems Measurement and Control*, 107 (1), 17-24.
- Hogan, N. (1987). Stable Execution of Contact Tasks using Impedance Control. *IEEE International Conference on Robotics and Automation* (pp. 1047-1054). Philadelphia.
- Hollander, K.W., Sugar, T.G., & Herring, D.E. (2005). A Robotic 'Jack Spring' for Ankle Gait Assistance. *ASME International Design Engineering Technical Conference & Computers and Information in Engineering Conference* (Long Beach, California).
- Hollerbach, J.M., Hunter, I.W., & Ballantyne, J. (1991). A comparative analysis of actuator technologies for robotics. In: *Robotics Review 2* (pp. 299-342). Cambridge, MA: MIT Press.
- Huang, S.G., & Schimmels, J.M. (2004). Admittance selection for force-guided assembly of polygonal parts despite friction. *IEEE transactions on robotics*, 20 (5), 817-829.
- Hunter, I.W., Hollerbach, J.M., & Ballantyne, J. (1992). A comparative analysis of actuator technologies for robotics. In: O. Khatib, J.J. Craig, & T. Lozano-Pérez (Eds.), *The Robotics Review 2* (pp. x, 372 p.). Cambridge, MA: MIT Press.
- Jacobsen, S.C., Meek, S.G., & Fullmer, R.R. (1984). An Adaptive Myoelectric Filter. *IEEE EMBS Conference* (pp. 15-17). Los Angeles, California.
- Johnson, C.T., & Lorenz, R.D. (1992). Experimental Identification of Friction and its Compensation in Precise, Position Controlled Mechanisms. *IEEE Transactions on Industry Applications*, 28 (6), 1392-1398.
- Kandel, E.R., Schwartz, J.H., & Jessell, T.M. (2000). Principles of neural science. (pp. xli, 1414). New York: McGraw-Hill Health Professions Division.
- Karnopp, D. (1985). Computer Simulation of Stick-Slip Friction in Mechanical Dynamic Systems. *Journal of Dynamic Systems Measurement and Control-Transactions of the ASME*, 107 (1), 100-103.

- Kornbluh et al., R. (2002). Engineering a Muscle: An Approach to Artificial Muscle Based on Field-Activated Electroactive Polymers. In: J. Ayers, J.L. Davis, & A. Rudolph (Eds.), *Neurotechnology for biomimetic robots* (pp. xiv, 636 p.). Cambridge, MA: MIT Press.
- Kotoku, T., Husler, E., Tanie, K., & Fujikawa, A. (1990). The Development of a direct drive master arm. *Journal of Mechanical Engineering Laboratory*, 44 (6), 199-210.
- Krouskop, T.A., Dougherty, D.R., & Vinson, F.S. (1987). A pulsed Doppler ultrasonic system for making noninvasive measurements of the mechanical properties of soft tissue. *Journal of Rehabilitation Research and Development*, 24 (2), 1-8.
- Krylow, A.M., Sandercock, T.G., & Rymer, W.Z. (1995). Muscle Models. In: M. Anbib (Ed.) *The Handbook of Brain Theory of Neural Networks* (pp. 609-613). Boston: Bradford Books, MIT Press.
- Kuiken, T.A. (2003). Consideration of nerve-muscle grafts to improve the control of artificial arms. *Journal of Technology and Disability*, 15, 105-111.
- Kuiken, T.A., Sensinger, J.W., & Weir, R.F. (2005). Phantom Limb Sensory Feedback through nerve transfer surgery. *Myoelectric Controls Symposium* (New Brunswick).
- Lake, C., & Miguez, J. (2003). Comparative Analysis of Microprocessors in Upper Limb Prosthetics. *Journal of Prosthetics and Orthotics*, 15 (2), 48-63.
- Lipson, H., & Pollack, J.B. (2000). Automatic design and manufacture of robotic lifeforms. *Nature*, 406 (6799), 974-978.
- Mah, C. (2001). Spatial and temporal modulation of joint stiffness during multijoint movement. *Experimental Brain Research*, 136, 492-506.
- Mak, A.F.T., Liu, G.H.W., & Lee, S.Y. (1994). Biomechanical assessment of below-knee residual limb tissue. *Journal of Rehabilitation Research and Development*, 31 (3), 188-198.
- Massie, T.H. (1993). Design of a three degree of freedom force-reflecting haptic interface. (Massachusetts Institute of Technology).
- Morita, T., & Sugano, S. (1996). Development of 4-D.O.F. Manipulator Using Mechanical Impedance Adjuster. *International Conference on Robotics and Automation* (pp. 2902-2907). Minneapolis, Minnesota.
- Nohama, P., Lopes, A.V., & Cliquet, A. (1995). Electrotactile Stimulator for Artificial Proprioception. *Artificial organs*, 19 (3), 225-230.
- Okada, M., Nakamura, Y., & Ban, S. (2001). Design of programmable passive compliance for humanoid shoulder - Towards skill of compliance of humanoid robots. *Experimental Robotics VII*, 271, 31-40.
- Okada, M., Nakamura, Y., & Hoshino, S.-i. (2000). Design of Active/Passive Hybrid Compliance in the Frequency Domain - Shaping Dynamic Compliance of Humanoid Shoulder Mechanism. *International Conference on Robotics and Automation* (pp. 2250-2257). San Francisco, California.
- Ozawa, R., & Kobayashi, H. (2003). A New Impedance Control Concept for Elastic Joint Robots. *International Conference on Robotics and Automation* (pp. 3126-3131). Taipei, Taiwan.

- Patterson, P.E., & Katz, J.A. (1992). Design and Evaluation of a Sensory Feedback-System that Provides Grasping Pressure in a Myoelectric Hand. *Bulletin of prosthetics research*, 29 (1), 1-8.
- Phillips, C.A. (1988). Sensory Feedback-Control of Upper-Extremity and Lower-Extremity Motor Prostheses. *Critical reviews in biomedical engineering*, 16 (2), 105-140.
- Popat, R.A., Krebs, D.E., Mansfield, J., Russell, D., Clancy, E., Gillbody, K.M., & Hogan, N. (1993). Quantitative Assessment of 4 Men Using above-Elbow Prosthetic Control. *Archives of Physical Medicine and Rehabilitation*, 74 (7), 720-729.
- Popescu, F., Hidler, J.M., & Rymer, W.Z. (2003). Elbow impedance during goal-directed movements. *Experimental Brain Research*, 152, 17-28.
- Popescu, F., & Rymer, W.Z. (2000). End points of planar reaching movements are disrupted by small force pulses: an evaluation of the hypothesis of equifinality. *Journal of Neurophysiology*, 84, 2670-2679.
- Pratt, G.A., & Williamson, M.M. (1995). Series elastic actuators. *IEEE/RSJ International Conference on Intelligent Robots and Systems*, 2 (pp. 399-406). Pittsburgh, PA: IEEE Computer Society Press.
- Pratt, G.A., Williamson, M.M., Dillworth, P., Pratt, J.E., Ulland, K., & Wright, A. (1995). Stiffness isn't everything. *Fourth International Symposium on Experimental Robotics* (Stanford).
- Pratt, G.A., Willisson, P., Bolton, C., & Hofman, A. (2004). Late Motor Processing in Low-Impedance Robots: Impedance Control of Series-Elastic Actuators. *Proceeding of the 2004 American Control Conference* (pp. 3245-3251). Boston, MA.
- Puchhammer, G. (2006). Personal communication regarding classified roller clutch design theory. (Vienna: Otto Bock).
- Reynolds, O. (1886). On the theory of lubrication and its application to Mr. Beauchamp Tower's experiments, including an experimental determination of the viscosity of olive oil. *Philosophical Transactions of The Royal Society*, 177, 157-234.
- Riso, R.R., Ignagni, A.R., & Keith, M.W. (1991). Cognitive Feedback for use with FES Upper Extremity Neuroprostheses. *IEEE transactions on bio-medical engineering*, 38 (1), 29-38.
- Robinson, D.W. (2000). Design and analysis of series elasticity in closed-loop actuator force control. *Mechanical Engineering* (p. 123): Massachusetts Institute of Technology.
- Robinson, D.W., Pratt, J.E., Paluska, D.J., & Pratt, G.A. (1999). Series Elastic Actuator Development for a Biomimetic Walking Robot. *IEEE/ASME International Conference on Advanced Intelligent Mechanisms* (pp. 561-568).
- Rosset, F. (1916). Artificial Limbs. (Germany).
- Sabolich, J.A., & Ortega, G.M. (1994). Sense of Feel for Lower-Limb Amputees: A Phase-One Study. *Journal of Prosthetics and Orthotics*, 6 (2), 36-41.
- Sainburg, R.L., & Schaefer, S.Y. (2004). Interlimb Differences in Control of Movement Extent. *Journal of Neurophysiology*, 92, 1374-1383.
- Salisbury, J.K. (1980). Active Stiffness Control of a Manipulator in Cartesian Coordinates. *IEEE Conference on Decision and Control* (New Mexico).

- Salisbury, J.K., Townsend, W.T., Eberman, B.S., & DiPietro, D.M. (1988). Preliminary design of a whole-arm manipulation system (wam). *1988 IEEE International Conference on Robotics and Automation* (Philadelphia).
- Schimmels, J. (1997). A linear space of admittance control laws that guarantees force-assembly with friction. *IEEE transactions on robotics*, *13* (5), 656-667.
- Schimmels, J.M., & Peshkin, M.A. (1994). Force-Assembly with Friction. *IEEE transactions on robotics*, *10* (4), 465-479.
- Scott, R.N., Brittain, R.H., Caldwell, R.R., Cameron, A.B., & Dunfield, V.A. (1980). Sensory-feedback system compatible with myoelectric control. *Medical & biological engineering & computing*, *18*, 65-69.
- Sensinger, J.W. (2005). Design & Analysis of a Non-backdrivable Series Elastic Actuator for use in prostheses. *MSC Thesis, Biomedical Engineering* (p. 135). Evanston: Northwestern University.
- Sensinger, J.W., & Weir, R.F.ff. (2005). Design and Analysis of Non-backdrivable Series Elastic Actuators. *IEEE 9th International Conference on Rehabilitation Robotics* (Chicago).
- Sensinger, J.W., & Weir, R.F.ff. (2006a). 2D Projection of a Multivariate Root Locus. *IEEE/ASME Transactions on Mechatronics, MT06-100, submitted for publication*
- Sensinger, J.W., & Weir, R.F.ff. (2006b). Impedance Control Using a Compact Series Elastic Actuator. *IEEE/ASME International Conference on Mechatronic and Embedded Systems and Applications* (Beijing, China).
- Sensinger, J.W., & Weir, R.F.ff. (2006c). Improved Torque Fidelity in Harmonic Drive Sensors through the Union of Two Existing Strategies. *IEEE/ASME Transactions on Mechatronics*, *11* (4), 457-461.
- Sensinger, J.W., & Weir, R.F.ff. (2006d). Non-backdrivable Impedance Control. *Robotics: Science and Systems; Robotic Systems for Rehabilitation, Exoskeleton, and Prosthetics Workshop* (Philadelphia, PA).
- Sensinger, J.W., & Weir, R.F.ff. (2007). Inherently Compensating Body Powered Elbow. *12th World Congress of the International Society of Prosthetics and Orthotics* (Vancouver).
- Shannon, G.F. (1976). A comparison of alternative means of providing sensory feedback on upper limb prostheses. *Medical & biological engineering & computing*, *14*, 289-294.
- Shannon, G.F. (1979). A myoelectrically-controlled prosthesis with sensory feedback. *Medical & biological engineering & computing*, *17*, 73-80.
- Sheridan, T.B., & Ferrell, W.R. (1974). *Man-Machine Systems: Introductory Control and Decision Models of Human Performance*. (Cambridge, Massachusetts: MIT Press).
- Silver-Thorn, M.B. (1999). In Vivo Indentation of Lower Extremity Limb Soft Tissues. *IEEE Transactions on Rehabilitation Engineering*, *7* (3), 268-277.
- Simpson, D.C. (1974). The Choice of Control System for the Multimovement Prosthesis: Extended Physiological Proprioception (e.p.p). In: P. Herberts, R. Kadefors, R. Magnusson, & I. Petersen (Eds.), *The Control of Upper-Extremity Prostheses and Orthoses* (pp. 146-150). Springfield, IL: Charles Thomas.
- Smith, D.G., Michael, J.W., & Bowker, J.H. (2004). *Atlas of Amputations and Limb Deficiencies*. (Rosement: American Academy of Orthopaedic Surgeons).

- Soukoreff, R.W., & MacKenzie, I.S. (2004). Towards a standard for pointing device evaluation, perspectives on 27 years of Fitts' law research in HCI. *International Journal of Human-Computer Studies*, 61 (6), 751-789.
- Stroeve, S. (1998). Neuromuscular control model of the arm including feedback and feedforward components. *Acta Psychologica*, 100, 1117-1131.
- Strogatz, S.H. (1994). Nonlinear dynamics and chaos : with applications to physics, biology, chemistry, and engineering. *Studies in nonlinearity* (pp. xi, 498). Cambridge, MA: Perseus Pub.
- Stroop, J.R. (1935). Studies of Interference in Serial verbal reactions. *Journal of Experimental Psychology*,
- Theodoridis, S., & Koutroumbas, K. (1999). Pattern recognition. (pp. xiv, 625 p.). San Diego: Academic Press.
- Todorov, E., & Jordan, M. (2002). Optimal feedback control as a theory of motor coordination. *Nature Neuroscience*, 5 (11), 1126-1235.
- Van der Linde, R.Q., Lammertse, P., Frederiksen, E., & Ruiters, B. (2002). The HapticMaster, a new high-performance haptic interface. *Proceedings Eurohaptics* (pp. 1-5). Edinburgh, UK.
- von Albrichsfeld, C., & Tolle, H. (2002). A self-adjusting active compliance controller for multiple robots handling an object. *Control engineering practice*, 10 (2), 165-173.
- Wang, G., Zhang, X., Zhang, J., & Gruver, W.A. (1995). Gripping force sensory feedback for a myoelectrically controlled forearm prosthesis. *IEEE International Conference on Intelligent Systems for the 21st Century*, 1 (pp. 501-504). Vancouver, BC.
- Weir, R.F. (1995). Direct Muscle Attachment as a Control Input for a Position Servo Prosthesis Controller. *Ph.D. dissertation, Biomedical Engineering* (Evanston: Northwestern University).
- Weir, R.F. (2003). Design of Artificial Arms and Hands for Prosthetic Applications. In: M. Kutz (Ed.) *Standard handbook of biomedical engineering and design* (pp. 32.31-32.61). New York: McGraw-Hill.
- Whitney, D.E. (1976). Force feedback control of manipulator fine motions. *Proceedings of the Joint Automatic Control Conference* (
- Williamson, M.M. (1995). Series elastic actuators. *Electrical Engineering and Computer Science* (p. 80): Massachusetts Institute of Technology.
- Zheng, Y., Chan, M.M.F., Shi, J., Chen, X., & Huang, Q.H. (2005). Sonomyography: Monitoring morphological changes of forearm muscles in actions with the feasibility for the control of powered prosthesis. *Medical Engineering & Physics*,
- Zheng, Y., & Mak, A.F.T. (1999). Effective Elastic Properties for Lower Limb Soft Tissues from Manual Indentation Experiment. *IEEE Transactions on Rehabilitation Engineering*, 7 (3), 257-267.
- Zheng, Y., Mak, A.F.T., & Leung, A.K. (2001). State-of-the-art methods for geometric and biomechanical assessments of residual limbs: A review. *Journal of Rehabilitation Research and Development*, 38 (5), 487-504.



- Zheng, Y., Mak, A.F.T., & Lue, B. (1999). Objective assessment of limb tissue elasticity: Development of a manual indentation procedure. *Journal of Rehabilitation Research and Development*, 36 (2), 71-85.
- Ziegler, J.G., & Nichols, N.B. (1942). Optimum Settings for Automatic Controllers. *IEEE Transactions on Automatic Control*, 64, 759-768.
- Zinn, M., Khatib, O., Roth, B., & Salisbury, J.K. (2004a). Playing it Safe. *IEEE Robotics and Automation Magazine*, 11 (2), 12-21.
- Zinn, M., Roth, B., Khatib, O., & Salisbury, J.K. (2004b). A new actuation approach for human friendly robot design. *International Journal of Robotics Research*, 23 (4-5), 379-398.

## 12 Appendices

### 12.1 Expanded Physiology Review

#### 12.1.1 Muscle Physiology

The physical properties of muscles have a substantial impact on control of movement. Thus, examining the physical attributes of muscles may form an important foundation in the understanding of human control of movement. The properties of muscle described here are explored in greater detail by Kandel, Schwartz and Jessell (2000).

Humans use muscle to generate contractile force. Muscles are linked to bone across one or more joints by tendons, which are moderately compliant. Bones provide the structural framework of motion, and muscles act in antagonistic pairs to move bones. The tendons of muscles tend to be inserted close to joints, allowing large forces and small movements by the muscle to be translated to larger movements and smaller forces by the limb segment.

A muscle is composed of parallel bundles of fibers. Each of these fibers is in turn composed of smaller bundles of fibers termed *muscle fibers*. Each muscle fiber contains bundles termed *myofibrils*. Muscles are activated when electrical action potentials, traveling through nerves, reach a chemical synapse on the muscle fibers termed an endplate. Most muscle fibers are activated by one motor neuron in one place. The group of muscle fibers activated by the same motor neuron is called a motor unit. When an action potential reaches the endplate of a

muscle fiber, acetylcholine, a neurotransmitter, is released in sufficient quantity to depolarize the postsynaptic membrane of the muscle fiber to its threshold. Acetylcholinesterase is released shortly after, so that the muscle fiber is ready for the next action potential. Because of this process, muscle fibers fire in an all or none manner for each action potential. Whereas the action potential of each motor neuron synchronously depolarizes all of its muscle fibers, the action potentials of motor neurons in a given muscle tend to activate asynchronously for non-minimal forces, the sum of which appears to be a smooth generation of force in the presence of mechanical damping, inertia, and compliance.

Once the muscle fiber membrane has been depolarized, a large-current motor unit action potential (MUAP) slowly propagates away from the endplate throughout the muscle fiber. The action potential encounters longitudinally repeating sarcomeres in each myofibril. As the action potential propagates across each sarcomere, a chemical reaction takes place that incrementally ratchets a subcomponent of the sarcomere called myosin across a thinner component called actin. This sliding of the two sub-filaments creates contractile force in muscle. Each ratcheting movement is approximately  $0.06\mu\text{m}$  long. All of the myofibrils in a muscle unit tend to ratchet at the same rate.

In addition to the contractile elements detailed above, each muscle unit has connecting filaments called connectins that form an elastic structure along the length of the muscle, creating some of the spring-like nature of muscle fibers. Connectins align the thick and thin

filaments of sarcomers when they no longer overlap. Collagen also surrounds each muscle fiber, helping to distribute tension and sarcomere length changes evenly.

The total contractile force produced at the tendon is a product of three factors: the rate of stimulation of the muscle nerve, the length of each sarcomere, and the velocity of cross-bridge motion.

*Rate of stimulation:* If an action potential is produced before the muscle fiber has a chance to relax, the muscle fiber exerts even more force for several action potentials, and then levels out to a mean value with a ripple for each action potential. Increasing the rate of action potentials increases the mean force until fused tetanus is achieved. For fused tetanus, the action potential rate is so fast that a constant force without ripple is observed.

*Length of sarcomere:* As the sarcomere length decreases and cross bridges begin to form, the generated force increases linearly with the number of cross bridges. This linear increase in force is masked by the passive force generated by the elastic structural part of the muscle, which acts nonlinearly in this area. As the sarcomere length continues to decrease, the force remains constant because there are no remaining attachment sites for the myosin heads (and thus the number of crossbridges remains constant). As the sarcomere length decreases even more, force decreases linearly as the progressive overlap precludes the binding of advancing myosin heads. See Figure 12.1 for an illustration.

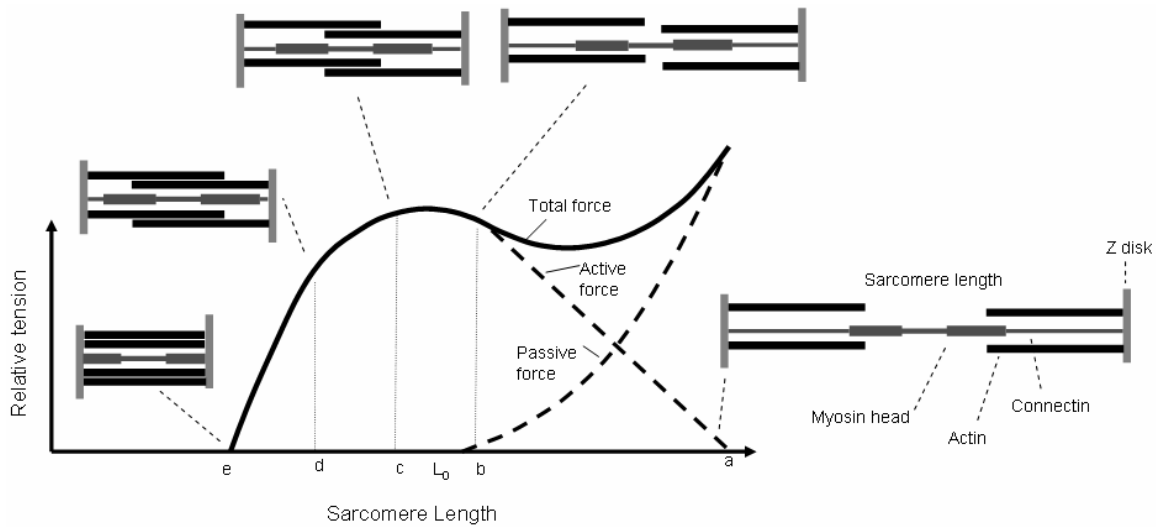


**Figure 12.1: Force Length relationship**

The amount of force generated by muscle fibers depends on the position of the myosin and actin filaments, and the amount of passive force due to structural components of muscle.

Figure traced from (Kandel et al., 2000)

*Velocity:* As the velocity of the contraction increases, the percentage of myosin that are in the process of transitioning, and are thus unattached, increases. As a result, force decreases with velocity. For negative velocities that occur during lengthening, known as eccentric contractions, force increases. In other words, as velocity increases in a given direction, the limb is capable of generating less force in the direction of movement, and more opposition force, as shown in Figure 12.2. In light of this force / velocity relationship, the impedance of human joints is velocity dependent, both in terms of the magnitude and direction of the velocity. The monotonic trend of force from negative velocities to zero velocities to positive velocities will have an important impact on the intrinsic stability of movements, as described

later on. The relationship between force and velocity is relatively independent of the relationship between force and length.

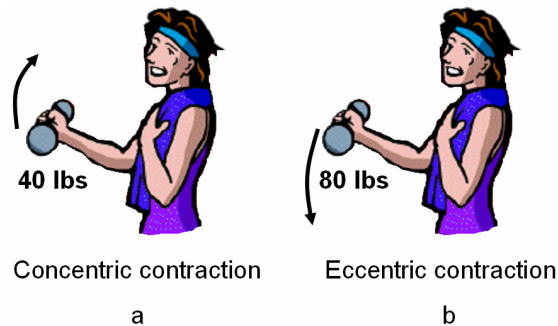


**Figure 12.2: Illustration of Force vs. velocity**

A person can generate more force during an eccentric contraction than during a concentric contraction, creating a velocity dependent effect on the impedance of a joint.

Motor units tend to be recruited in order from weakest to strongest. Size-ordered recruitment makes the random activation of a large force motor unit during a fine motor task less likely by ensuring that the increment of force generated by successively activated motor units will be approximately proportional to the force at which each individual unit is recruited. In order to increase the rate of applied torque, the central nervous system will often activate the agonist muscle with a higher rate of action potentials than is required, and shortly after activate the antagonistic muscle, so that the sum of the two muscles creates the required torque in a shorter space of time than would be possible if only the agonist muscle was used. Thus, increased joint stiffness during rapid movements is not only a reflexive means of postural stability, but also a means to increase the performance of the system.

The relationship between force, velocity, and length creates an intrinsically stable system in the presence of perturbations if co-contraction is present. This inherent stability is necessary because the fastest reflexes having a delay of 50 ms. If a pair of muscles about a joint are co-contracted and a perturbation occurs, the muscle that pulls in that direction is shortened, and thus the force that it exerts intrinsically decreases, whereas the muscle that opposes the perturbation is lengthened, which intrinsically increases its force. The same is true of velocity: the muscle that acts in the same direction of the perturbation increases its velocity, decreasing its force, whereas the muscle opposing the perturbation increases its force the faster it is lengthened. Thus, perturbations are intrinsically damped by the inherent nature of coupled muscles.

*Feedback:* There are four types of somatic sensation: discriminative touch, proprioception, nociception, and temperature sense. Of these, discriminative touch (size, shape, texture) and proprioception (sense of the position of limb segments in space without the aid of vision) are integral in kinematically interacting with an environment. Discriminative touch receptors sense pressure and vibration. Some discriminative touch receptors respond to changes in these parameters, whereas others respond to continuous pressure. Some discriminative touch sensors also sense stretch of skin, which is useful for proprioception as well. Proprioceptive sensors include muscle spindle receptors, Golgi tendon organs, and receptors in joint capsules. Muscle spindle fibers are sensitive to changes of length, whereas Golgi tendon organs are more

sensitive to changes in muscle tension. Golgi tendon organs offer precise feedback regarding the tension in muscles.

Stretch reflexes resist the lengthening of muscle, similar to but not the same as the intrinsic length resisting characteristics of muscle. Most stretch reflexes are monosynaptic circuits, meaning that the sensory neuron and motor neuron are directly connected to each other, decreasing delay time. The lack of an interneuron in between the two neurons makes the reflexes less plastic to modification by the brain. An example is illustrated in Figure 12.3.

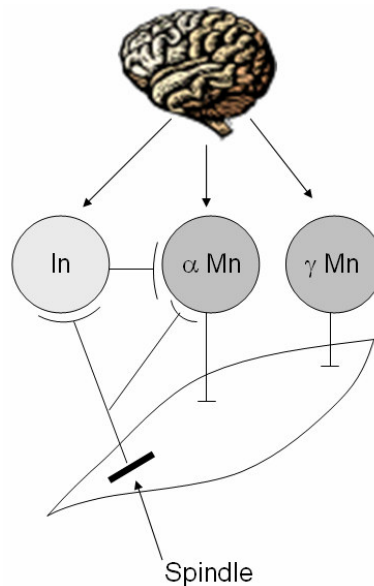


**Figure 12.3: Stretch Reflex**

The central nervous system modulates alpha and gamma motor neurons (Mn), as well as interneurons (In). Spindle fibers in the muscle act as a feedback servo controller, keeping the position constant for a given equilibrium position.



### 12.1.2 Control of Movement

Given an understanding of the physical properties of muscles and the feedback sensors available, it will now be possible to examine control of voluntary movement. Three mechanisms influence human joint kinematics as traditionally understood:

- A feedforward control process which encodes a solution to the inverse dynamics of the desired movement trajectory and the forces which act on the musculoskeletal system
- A feedback control process (reflexive system) which corrects for errors in the feedforward control process as well as environmental perturbations
- Overall impedance of the musculoskeletal system, which includes the stiffness derived by the antagonist muscle pairs, as well as the viscosity components induced by the muscles and other viscoelastic components and the compliance of the muscles.

It is often thought that the feedforward control process acts in advance of the movement. Through methods not yet clearly identified, the feedforward process calculates neural signals to move one point on the body to a different location. The feedback system then provides a closed loop process, in case the feedforward method is based on faulty dynamic assumptions, or fails to take into account environmental perturbations. The interplay of these two processes is not well understood, but their combination does produce fairly accurate results (Bhushan & Shadmehr, 1999, Todorov & Jordan, 2002). Because the feedforward process occurs before the movement it is not hampered by response delays. The feedback process is hampered by response delays that may exceed 200 ms (Bhushan & Shadmehr, 1999). As such,

the mere combination of these two systems is unable to keep a limb on target in the presence of unexpected environmental perturbations.

Before looking at the role that impedance plays between the first two mechanisms in the presence of perturbations, it will be useful to examine a different paradigm of movement: the Equilibrium Point Hypothesis. The Equilibrium Point Hypothesis was first developed by Feldman (1966a, 1966b). Feldman's model relies on tuning of feedback circuits to achieve accurate position. A variant of Feldman's  $\lambda$  model is Bizzi's  $\alpha$  model, which uses input signals to achieve accurate endpoint positions rather than feedback (Bizzi, Polit & Morasso, 1976). Bizzi's model will be described first, since his model looks only at the foundation of movement, whereas Feldman's model looks at movement in its entirety.

*Bizzi's  $\alpha$  model:* The  $\alpha$  model relies on the intrinsic spring-like nature of muscles, and more importantly, on the changing stiffness of muscles as their length changes. By modulating the tension in two antagonistic muscles, a new endpoint position is obtained, as illustrated below in Figure 12.4. Perhaps the strongest evidence that Bizzi gives for this proposal is an experiment that uses deafferented monkeys in which proprioceptive feedback has been deprived (Bizzi, Hogan & Mussa-Ivaldi, 1992). In this experiment, monkeys were asked to move their limb from one position to another. The monkeys were not able to see their limb. Unknown to the monkeys, their limb had already been passively moved to the endpoint trajectory. If monkeys use a forward dynamics trajectory, it follows that they would overshoot the target, as illustrated below in Figure 12.5a. If, however, monkeys use a set of

equilibrium positions to achieve their trajectory, then they would likely move backwards because the virtual endpoint initially had them at the starting point, as illustrated in Figure 12.5b. Bizzi et al. did indeed find that their limbs initially moved towards the starting point before moving to the end position, signifying that the monkeys followed a virtual set of endpoint positions.

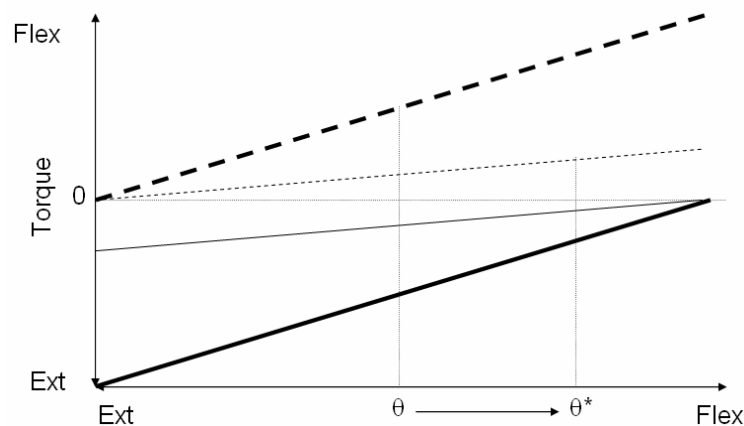


**Figure 12.4: Equilibrium Point Shift**

Dashed lines are antagonist muscles of solid lines

Bold lines are stronger stiffness of each muscle, as modulated by the activation of the muscle

By making both muscles stiffer, the stability force is greater in the presence of a perturbation.

By shifting the stiffness of one muscle relative to another, a new equilibrium position is achieved.

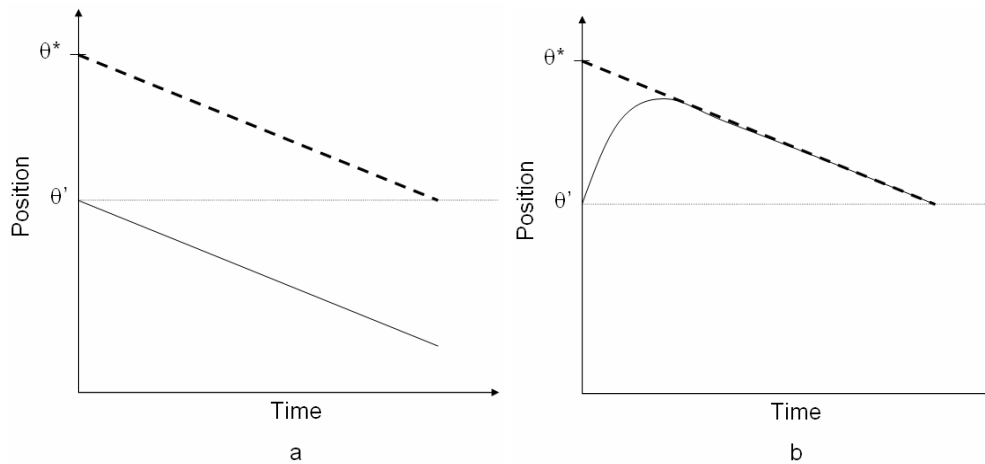


**Figure 12.5: Predicted Trajectories in the absence of proprioceptive feedback**

The monkeys think they start at position  $\theta^*$ , but they actually start at position  $\theta'$ , which is the desired endpoint position. The dashed line represents the path they would have taken if they had started at position  $\theta^*$ .

- a) Predicted Trajectory if monkeys use an Internal Dynamics Model
- b) Predicted trajectory if monkeys use equilibrium points

*Feldman's  $\lambda$  model:* Spindle fibers in muscles send position information to a stretch reflex, which in turn increases the activation of a muscle if the spindle is lengthened, and decreases activation of the muscle if the spindle is shortened. The stretch reflex thus acts as a feedback servo, maintaining a steady state position. Feldman has hypothesized that changing the equilibrium point of the stretch reflex controls movement while quickly attenuating perturbations. Feldman has proposed that the central nervous system controls some independent parameter,  $\lambda$ , in addition to the length of the muscle to elicit force in muscles. If  $\lambda$  is not altered, muscles act like static springs. If  $\lambda$  is altered, smooth movement occurs.  $\lambda$  may be thought of as the virtual or desired position. The generated force may be thought of as

some impedance function of the difference between the actual and desired position. Although not instantaneous, the quick response time of the stretch reflex may modulate movement by changing the desired position and receiving feedback of the actual position (Feldman, 1986).

*Synthesis of the two models:* In many ways the  $\alpha$  and  $\lambda$  equilibrium point models are analogous to the forward dynamics and feedback system commonly thought to exist in motion control. The person desires to move to a specified position. They generate a signal to do so, but rather than generating the torques required to move their limb to that position, they use the  $\alpha$  model to create an equilibrium point at which point the torques will be equal to zero, thus simplifying control. Rather than using complex strategies such as the minimization of jerk to keep their limb on target, they use the  $\lambda$  equilibrium point model of control for feedback, which acts much more quickly than any higher-level controller could operate. Finally, the intrinsic properties of muscle, such as inherent stiffness and damping, coupled with the force-length and force-velocity relationships of muscle further smooth movement and resist perturbations.

Although the equilibrium point hypothesis illustrates an elegant and compelling model of human movement, recent studies have shown that the equilibrium point hypothesis does not perform as well as internal dynamics models. Work by Popescue and Rymer (2000) has shown that for small movements and low stiffness, resulting position errors cannot be explained by the equilibrium point hypothesis. Hinder and Milner (2003) have shown that for large movements and large stiffness, where the equilibrium point hypothesis is supposed to work

best, the hypothesis still cannot predict accurate trajectories in the presence of velocity controlled perturbations. The results obtained by Bizzi and Feldman may be due in part to the intrinsic spring-like characteristics of muscles. It may also be possible that monkeys use some sort of equilibrium point hypotheses, whereas humans predominantly use internal dynamics to allow movement that is more adaptable.

Work in Sainburg's laboratory has recently shown that the nondominant limb may primarily use feedback control, whereas the dominant limb may primarily use internal dynamic control (Sainburg & Schaefer, 2004). As a result, specialization of the dominant arm for controlling limb and task dynamics is specifically related to feedforward control mechanisms, and the nondominant arm has more effective load compensation response than the dominant arm (Bagesteiro & Sainburg, 2003).

As a result, the equilibrium point hypothesis may still be valid in the non-dominant arm. Regardless of whether the equilibrium point hypothesis or internal dynamic argument is correct, impedance of muscles significantly contributes to motion control.

*The Role of Impedance:* Numerous studies (Stroeve 1998; Bhushan and Shadmehr 1999; Novak, Miller et al. 2000; Novak, Miller et al. 2002; Novak, Miller et al. 2003) have examined the role that the higher-level cortex plays in smoothing movements in the presence of environmental perturbations. Unfortunately, neither the higher-level cortex nor neural reflexes can provide instantaneous correction in the presence of perturbations. Impedance

must thus be integrated into models of movement control to correctly understand responses to perturbations.

It is difficult to create a simple yet accurate model of muscle impedance due to the nonlinear properties of muscle described in section 12.1.1. Hill's lumped parameter model (Hill, 1938) attempted to portray these nonlinearities by modeling a contractile element in series with an elastic element, with both of these elements in parallel with another elastic element. The contractile element acts as an active force generator, the series elastic element acts as the combined stiffness of tendons and crossbridges, and the parallel elastic element acts as the passive tissue that contributes to muscle force. The series elasticity is usually modeled as a linear spring. The elastic element due to passive tissue is often modeled in the form of an exponential function that increases with extension, though it is seldom modeled in practice because it only affects the impedance of long muscles. Other nonlinearities exist, in muscle. If active muscle is rapidly stretched, yielding may occur. In addition, muscle force shows hysteresis when measured during increasing neural activation compared with decreasing activation. Fatigue also causes hysteresis. The Hill model does not predict yielding and cannot evaluate varying cross-bridge persistence, which is observed in the presence of hysteresis (Krylow, Sandercock & Rymer, 1995).

Stroeve (1998) found that the intrinsic stiffness of the musculoskeletal system is ten times lower than the stiffness that the Hill model predicts. Extension for dynamic components that add impedance at lower frequencies is needed to compensate for this discrepancy. This

conclusion was reached by developing a neuromusculoskeletal model of the human arm that incorporated feedforward and feedback control, and then comparing the model to experimentally collected myoelectric data and arm impedance.

Hogan (1984) simulated a musculoskeletal system to examine the effect of impedance modulation and reflex mechanisms on stability in the presence of perturbations. Reflex mechanisms expend minimal energy and have long delays. Antagonist muscle contractions expend substantial energy and have no delay. Hogan optimized the interaction of these two terms using dynamic optimization theory. It was assumed in the model that modulation of joint stiffness was accomplished solely through co-contraction of antagonist muscle groups and that the torsional stiffness required by ligaments, which is relatively small compared to gravitational loads, was insignificant. The dynamic optimization strategy used minimized the summation of the time integral of the instantaneous power consumed by the muscle and the square of deviation from the desired posture. An infinitesimal perturbation was added to the system to observe its stability, as a system will appear stable at its bifurcation point unless it is perturbed. The results of this optimization indicated that simultaneous activation of agonist and antagonist muscles was observed under normal physiological conditions, and that the level of antagonist co-contraction increased as gravitational torques increased. Neither feedback control nor stabilization by impedance modulation was found to be superior. A combination of the two provided the optimal solution under a wide range of conditions.



Mah (2001) validated this simulation by observing joint impedance during dynamic movement. Arm impedance was measured during large, slow perturbations and then compared to other models based on fast perturbations. Results were generally similar to the fast perturbation models, though there were several important deviations that needed to be incorporated into the model. It was found that joint impedance undergoes marked changes in magnitude that depend on the direction of movement. In addition, it was found that joint impedance has a strong dependence on joint angle, which is consistent with the mechanical properties discussed in section 12.1.1 but a factor that has not previously been considered. Mah's results agreed with those of Hogan, in that modulation of impedance acted as an energy conserving force field to constrain movement. This constraint of energy conservation allows for simplification of computations on a neural level and provides a balance between energy conservation and response time. Mah found that, rather than consuming more energy, optimum impedance actually conserved energy in humans.

Impedance plays an integral role in regulating human movement. The modulation of impedance allows for different optimization paradigms to be used, ranging from reduction of power consumption to minimization of trajectory error in the presence of perturbations to smooth muscle movement. Control of impedance will be useful in designing biomimetic actuators, and the ability to modulate impedance based on the task seems useful. Perhaps the most useful finding in observations of human impedance is that, similar in concept to subsumption architecture proposed by Brooks and Connell (Brooks, 1991, Brooks & Connell,

1986), muscle architecture intrinsically modulates the impedance of joints based on position and speed, while allowing humans to change that impedance depending on the task.

## ***12.2 Fluoroscopy Notes***

### **12.2.1 Verifying sampling frequency of Fluoroscopy machine**

There was initially some doubt regarding the precision and accuracy of the fluoroscopy machine's sampling time. By accessing time stamps on the digital images, it was possible to determine that the actual sampling frequency was different from the one the technician had thought he had entered in, and that X-Ray slides were occasionally named in improper order, although their time stamps remained in the correct order.

Between the time the problem was noticed and the time the answer was found, a small experiment was done to verify the precision and accuracy of the machine. In this experiment, a clock with a steel hand was constructed to capture the actual sampling time in picture format. The clock was controlled by a MicroMo 1728 brushed motor with a 512 bit/rev encoder and a 159:1 gear transmission. The position of the motor was regulated by a MicroMo MCDC 2805 motion controller. The clock hand spun at 0.9 revolutions per second. The precision of the clock was verified by recording its motion using a Canon Power Shot S45 camera to take a movie at 15 Hz.

Two sets of data were recorded using the fluoroscopy machine. The machine was set to have a sampling frequency of 6 Hz. A sample fluoroscopy image of the clock is shown in Figure 12.6a. The clock hand was outlined using Matlab's *edge* command with a canny filter, shown in Figure 12.6b.

The outline contains both the outline of the clock hand, as well as the outline of the motor shaft. Because the motor is 24 mm long, any small rotation relative to the X-Ray machine will elongate the outline of the motor shaft in the plane of the fluoroscopy machine. This elongation, in turn, will skew the center of the motor shaft, which in turn will bias the orientation of the clock hand. In order to remedy this problem, a circular area must be erased originating from the center of rotation, and containing the skewed outline of the motor shaft. In order to do this, each image was overlaid on top of each other, as shown in Figure 12.6c. The center was found, and then a circular area was deleted from each outline, originating in the center and encircling the motor shaft. The remaining portion of the image is shown in Figure 12.6d. Once the motor shaft had been removed, principal component analysis of the outline was used to determine the orientation of the clock hand.

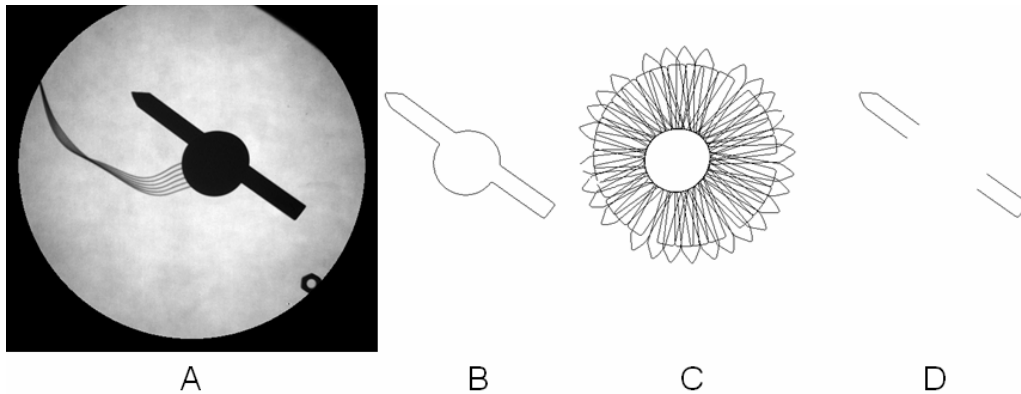


**Figure 12.6: Clock**

- a) An X-Ray image of the clock.
- b) Image is outlined using Matlab's *edge* command with a canny filter.
- c) By superimposing all of the images, the center of rotation may be found.
- d) A circle originating at the center of rotation is erased to delete the outline of the motor shaft. The outline of the shaft may be skewed if the image is taken at a slight slant, so it is necessary to erase the shaft outline so that it does not skew the PCA fit.

The results are tabulated for both runs in Table 12.1. From these results, it may be concluded that the sampling frequency of the fluoroscopy machine is both precise and accurate, especially when making allowance for any variance caused by actual motor position variation and principal component analysis variation.

**Table 12.1**  
**Measured Sampling frequency of fluoroscopy machine**

	Mean Frequency	95% Confidence Interval	Between 2 points:	
			Minimum Frequency	Maximum Frequency
Trial 1	6.025	6.023-6.027	5.95	6.11
Trial 2	6.018	6.017-6.019	5.97	6.07

### 12.2.2 Measuring inertia of a body-powered prosthesis

An object's inertia may be empirically calculated by measuring the frequency at which the object swings as a pendulum. The relationship between oscillation frequency and inertia is shown in Equation 12.1.

$$J = \frac{\tau^2 mgl}{4\pi^2} \quad (12.1)$$

Where  $\tau$  is the period of oscillation,  $m$  is the mass of the object,  $g$  is the gravitational acceleration constant, and  $l$  is the distance between the center of mass and the center of rotation. The center of mass may easily be obtained by finding the intersection of two plumb lines when the object is hung from two different points.

### 12.2.3 Calculating the slope of data

The slope of a line may be calculated using a linear least squares regression, in which:

$$S_x = x_1 + x_2 + \dots x_n \quad (12.2)$$

$$S_{xx} = x_1^2 + x_2^2 + \dots x_n^2 \quad (12.3)$$

$$S_{xy} = x_1y_1 + x_2y_2 + \dots x_ny_n \quad (12.4)$$

and the slope is estimated by

$$\hat{\beta} = \frac{nS_{xy} - S_x S_y}{nS_{xx} - S_x^2} \quad (12.5)$$

Linear least squares regression is robust to Gaussian noise in  $y$ , but it is not robust to Gaussian noise in  $x$ . If there is noise in  $x$ ,  $S_{xx}$  will become biased. This bias results from the fact that in squaring a signal combined with noise, the resulting signal's noise is no longer centered on zero. As a result, the estimated slope will always be less than the actual slope in the presence of noise, no matter how many data points are collected. The magnitude of this bias is proportional to the variance of the Gaussian noise.

If only one of the signals contains noise, this problem may easily be remedied by switching  $x$  and  $y$ , fitting the curve, and then taking the inverse of the slope. Such a method is robust to noise in  $x$ .

Principal component analysis may be used instead, as it is robust to noise in both  $x$  and  $y$ . For the socket-residual limb interface work presented in this thesis, both methods were employed, and the same result was obtained with each method.

### ***12.3 Review of Metrics to Optimize Impedance Control***

The use of impedance control or admittance control, as detailed in section 1.1, may improve actuator interaction with the environment. At the same time, they introduce additional variable that must be controlled. To further complicate control, the desired impedance or admittance of a system is seldom a scalar value: it usually has both a magnitude and a phase

component, which in physical systems result from damping, compliance, and inertia terms. Although modulation of impedance by the user is desirable, giving them control of three separate variables in addition to motion is practically unfeasible and probably not beneficial from an information content perspective. As a result, several optimizations of impedance will be explored below in an attempt to simplify the control of impedance.

*Trajectory Pursuit:* Hogan (1985c) distinguished trajectory pursuit from power transfer, concluding that the two objectives inherently conflict. Trajectory pursuit is defined as the minimization of deviations from desired motions while simultaneously minimizing interface forces. Some tradeoff  $p$  between minimized deviations, which requires maximum actuator impedance, and minimized forces, which requires minimum actuator impedance, must exist:

$$Z_A Z_E = p \quad (12.6)$$

Thus for environments that are unyielding, the actuator should have a low impedance. For environments that do not resist trajectory pursuit, the actuator should have a high impedance. Hogan advocated that this requirement conflicts with maximum power transfer, and this claim will be investigated below. Unfortunately, the result of trajectory pursuit optimization does not reduce the control degrees of freedom because it suggests that impedance as a whole be modulated.

*Maximum power transfer:* Maximum power transfer may provide a useful metric to optimize impedance control, allowing coupling of the stiffness and inertial term of the impedance

controller. The concept of maximum power transfer was first introduced by Moritz von Jacobi (1801-1874), the older brother of the more well known Carl Jacobi, while attempting to maximize the efficiency of his electric boat. Jacobi modeled a voltage source in series with an internal resistor and a variable load resistor, as illustrated in Figure 12.7a. He concluded that in order to maximize power transfer from the voltage source to the variable resistor, the resistance of the load resistor should be matched to that of the internal resistor. Edison later showed that if the internal resistor may be varied, as illustrated in Figure 12.7b, the internal resistor should not be matched to the load resistor. Instead, it should be minimized in order to maximize power transfer to the load resistor (Calvert, 2001).

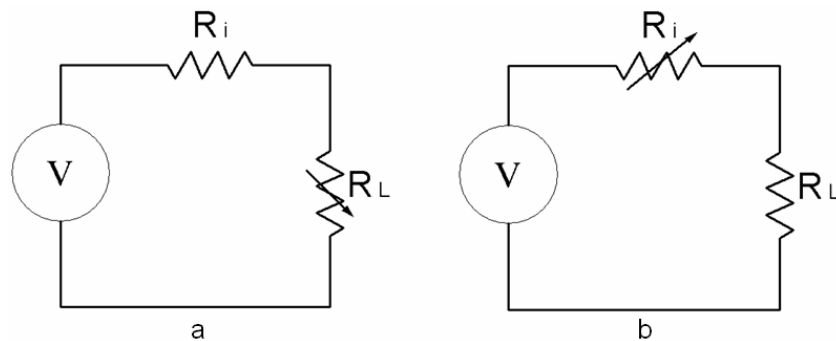


**Figure 12.7: Series Circuit - Maximum power transfer through  $R_L$**

- a) If  $R_L$  may be varied, match  $R_L$  to  $R_i$  to maximize power transfer through  $R_L$
- b) If  $R_i$  may be varied, minimize  $R_i$  to maximize power transfer through  $R_L$

This distinction is worth noting because, although it may easily be shown and has been demonstrated for almost a century, Edison's addition is seldom taught, and as such, the



potential exists to match  $R_i$  to  $R_L$  in an attempt to maximize power transfer. Thus, when looking at the transfer of power, it is important to define which resistor may be varied, as well as for which resistor maximum power is desired.

Hogan (1985a, 1985b, 1985c) has modeled the interaction between an actuator and its environment as the interaction between two impedances<sup>1</sup>. Because impedance control is a subset of position control, Hogan used a current source in parallel with two impedances. This alteration effectively states that the force at the junction between the actuator and its environment is constant, rather than the velocity. The model is similar to that in Figure 12.8a&b.

---

<sup>1</sup> Hogan actually modeled the interaction between actuator impedance and environmental admittance, in order to preserve causality. The same results are obtained in these derivations whether impedance or admittance is used. Because his following derivations did not exploit the causal nature of his restriction, impedance notation will be used instead of admittance notation (1/impedance) because it simplifies the notation.

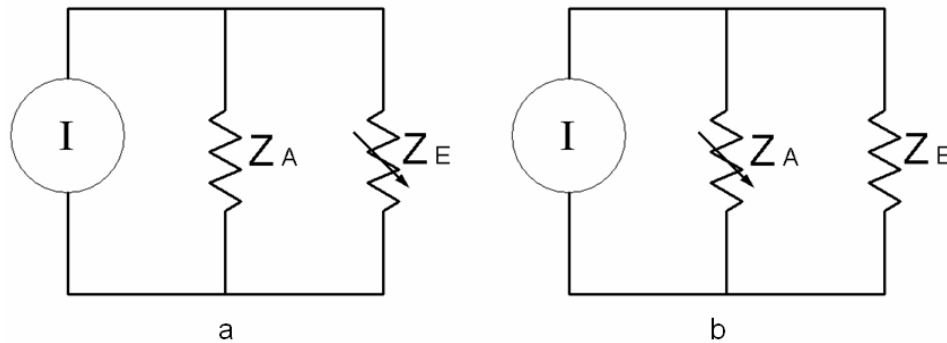


**Figure 12.8 Parallel circuit – Maximum power transfer through  $Z_E$**

- a) If  $Z_E$  may be varied, match  $Z_E$  to  $Z_A^*$  to maximize power transfer through  $Z_E$
- b) If  $Z_A$  may be varied, maximizing power transfer through  $Z_E$  becomes difficult

In his calculations, Hogan did not adequately clarify between the impedance for which power transfer was desired and the variable impedance: a distinction Edison has shown to be critical. As a result, Hogan's conclusion that the actuator impedance should be matched to the environmental impedance to maximize power transfer is incorrect. In addition, Hogan only gave the example of linear dissipative elements, not addressing the complexities of power transfer through impedances. Even if Edison's contribution is acknowledged, if the intricacies of impedance are not addressed one comes to the conclusion that in order to optimize power transfer to the environment while varying the impedance of the actuator, the resistance of the actuator should be maximized; a result that infringes on common sense. In spite of this maximum power transfer as a metric is still worth pursuing.

The topic of maximizing power transfer when the environmental impedance may be adjusted will not be explored because this topic has no bearing on modulating the impedance of the actuator. The impedance of the environment, regardless of the actuator impedance, should always be matched to the impedance of the actuator if maximum power transfer to the environment is desired.

### 12.3.1 Exploration of Impedance Metrics

Although Hogan dealt with impedances, his examples only used dissipative resistance, and as a result, several issues did not need to be addressed in the review of Hogan's work. A fuller representation of impedance will now be used. Impedance may be thought of a general form of resistance, in which effort and flow are related across the frequency spectrum:

$$e = Z(\omega)f \quad (12.7)$$

Impedance is commonly used in electrical circuits, in which resistance (R), inductance (L), and capacitance (C) play a role:

$$Z_E = R + j\left(\omega L - \frac{1}{\omega C}\right) \quad (12.8)$$

Impedance also has its place in rotational physical systems, in which rotational damping (c), inertia (J), and compliance (C) play a role:

$$Z_M = c + j\left(\omega J - \frac{1}{\omega C}\right) \quad (12.9)$$

The concept of power itself is not as trivial for impedances as it was for resistances. The instantaneous power across an impedance is still equal to the product of effort and flow. Because the reactance components may store energy, however, this number will not be a useful metric. Average power is given by  $\bar{P} = \Re(VI^*) = \Re(V^*I)$ , where  $V^*$  and  $I^*$  are the complex conjugates of  $V$  and  $I$ . The average power will provide a more useful metric of the average power distributed to the environment than instantaneous power.

*Maximum Power Transfer for Admittance Control:* Although the author has chosen impedance control as a control paradigm, it will be useful to examine admittance control, both to facilitate future work and to illustrate that it is indeed possible to extract simple impedance relationships without simplifying analysis of impedance. An example of force generation is given in Figure 12.9, in which  $Z_A$  is the impedance of the actuator and  $Z_E$  is the impedance of the environment.

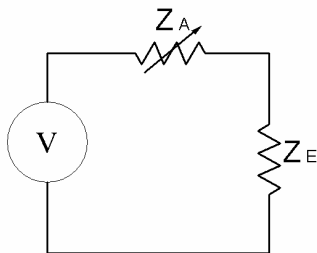


**Figure 12.9 Series Impedance Circuit - Maximum Average Power Transfer Through  $Z_E$**

The current through the circuit is

$$I = \frac{V}{Z_A + Z_E} \quad (12.10)$$

and the voltage across  $Z_E$  is

$$V_E = \frac{Z_E}{Z_A + Z_E} V \quad (12.11)$$

The average power is

$$\begin{aligned}
\bar{P} &= \Re e(VI^*) \\
\bar{P} &= \Re e\left(\frac{Z_E}{Z_A + Z_E} V \left(\frac{V}{Z_A + Z_E}\right)^*\right) \\
\bar{P} &= \Re e\left(V^2 \frac{\left(\frac{R_E + j\left(\omega J_E - \frac{1}{\omega C_E}\right)}{R_E + R_A + j\left(\omega(J_E + J_A) - \frac{C_E + C_A}{\omega C_E C_A}\right)}\right)}{\left(R_E + R_A + j\left(\omega(J_E + J_A) - \frac{C_E + C_A}{\omega C_E C_A}\right)}\right)}\right)^* \\
\bar{P} &= \Re e\left(V^2 \frac{\left(\frac{R_E + j\left(\omega J_E - \frac{1}{\omega C_E}\right)}{R_E + R_A + j\left(\omega(J_E + J_A) - \frac{C_E + C_A}{\omega C_E C_A}\right)}\right)}{\left(R_E + R_A - j\left(\omega(J_E + J_A) - \frac{C_E + C_A}{\omega C_E C_A}\right)}\right)}\right) \\
\bar{P} &= \Re e\left(V^2 \frac{\left(\frac{R_E + j\left(\omega J_E - \frac{1}{\omega C_E}\right)}{\left(R_E + R_A\right)^2 + \left(\omega(J_E + J_A) - \frac{C_E + C_A}{\omega C_E C_A}\right)^2}\right)}{\left(\left(R_E + R_A\right)^2 + \left(\omega(J_E + J_A) - \frac{C_E + C_A}{\omega C_E C_A}\right)^2}\right)}\right) \\
\bar{P} &= V^2 \frac{R_E}{\left(R_E + R_A\right)^2 + \left(\omega(J_E + J_A) - \frac{C_E + C_A}{\omega C_E C_A}\right)^2}
\end{aligned} \tag{12.12}$$

Thus for admittance control, to maximize average power transfer to the environment, the actuator resistance should be minimized, and the compliance and rotary inertia should conform to the following relationship:

$$\omega^2 J_A - \frac{1}{C_A} = \frac{1}{C_E} - \omega^2 J_E \tag{12.13}$$

The relationship between the inductance and capacitance of the actuator for maximum power transfer does not provide any added constraint over that of trajectory pursuit. In addition, the introduction of frequency has complicated the problem, in that a frequency of interest must be selected as well. It does not thus appear as though maximum power transfer will provide a useful metric when it is dealt with in its entirety. For the sake of completeness, maximum power transfer for impedance control is analyzed below to see if it provides additional constraints.

*Maximum Power Transfer for Impedance Control:* An example of motion generation is given in Figure 12.10.

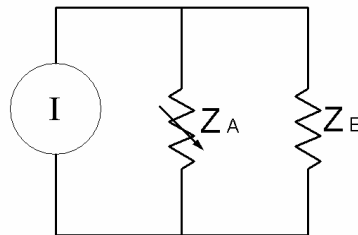


**Figure 12.10 Parallel Impedance Circuit - Maximum Average Power Transfer Through  $Z_E$**

The voltage across  $Z_E$  is

$$V_E = \frac{Z_A Z_E}{Z_A + Z_E} I \quad (12.14)$$

and the current through  $Z_E$  is

$$I_E = \frac{Z_A}{Z_A + Z_E} I \quad (12.15)$$

The average power is

$$\begin{aligned} \bar{P} &= \Re\{VI^*\} \\ \bar{P} &= \Re\left\{\left(\frac{Z_A Z_E}{Z_A + Z_E} I\right)\left(\frac{Z_A}{Z_A + Z_E} I\right)^*\right\} \\ \bar{P} &= \Re\left\{I^2 \frac{\left(\left(R_A + j\left(\omega J_A - \frac{1}{\omega C_A}\right)\right)\left(R_E + j\left(\omega J_E - \frac{1}{\omega C_E}\right)\right)\right)}{\left(R_E + R_A + j\left(\omega(J_E + J_A) - \frac{C_E + C_A}{\omega C_E C_A}\right)\right)} \left(\frac{R_A + j\left(\omega J_A - \frac{1}{\omega C_A}\right)}{R_E + R_A + j\left(\omega(J_E + J_A) - \frac{C_E + C_A}{\omega C_E C_A}\right)}\right)^*\right\} \\ \bar{P} &= \Re\left\{I^2 \frac{\left(\left(R_A + j\left(\omega J_A - \frac{1}{\omega C_A}\right)\right)\left(R_E + j\left(\omega J_E - \frac{1}{\omega C_E}\right)\right)\right)}{\left(R_E + R_A + j\left(\omega(J_E + J_A) - \frac{C_E + C_A}{\omega C_E C_A}\right)\right)} \left(\frac{R_A - j\left(\omega J_A - \frac{1}{\omega C_A}\right)}{R_E + R_A - j\left(\omega(J_E + J_A) - \frac{C_E + C_A}{\omega C_E C_A}\right)}\right)\right\} \\ \bar{P} &= \Re\left\{I^2 \frac{\left(\left(R_A^2 + \left(\omega J_A - \frac{1}{\omega C_A}\right)^2\right)\left(R_E + j\left(\omega J_E - \frac{1}{\omega C_E}\right)\right)\right)}{\left((R_E + R_A)^2 + \left(\omega(J_E + J_A) - \frac{C_E + C_A}{\omega C_E C_A}\right)^2\right)}\right\} \\ \bar{P} &= I^2 \frac{\left(R_A^2 + \left(\omega J_A - \frac{1}{\omega C_A}\right)^2\right)R_E}{\left(R_E + R_A\right)^2 + \left(\omega(J_E + J_A) - \frac{C_E + C_A}{\omega C_E C_A}\right)^2} \end{aligned}$$



The magnitudes of  $R_A$ ,  $C_A$ , and  $J_A$  that maximize  $P$  are not simple expressions, and as such, for impedance control, it does not appear that a simple relationship between the stiffness and inertial term will be found.

### **12.4 Internal Dynamics Compensation**

Due to the physical compliance typically found in impedance control, an internal dynamics model is not necessary to generate appropriate forces (Hogan, 1987, Robinson, 2000, Williamson, 1995). Although this statement is true, an accurate model of the internal dynamics will improve the performance of almost any actuator, and as such, several different internal dynamic parameters will be examined, including inertial, gravitational, and stiction effects, to see if they should be included in the controller of a series elastic actuator.

*Inertia:* The internal inertia of the actuator will be included in the internal dynamics of the actuator, although the coupled inertia of the actuator and environment has the potential to be an input signal in determining the impedance of the actuator.

*Gravity:* Gravity introduces an instability in rotational robots unless the limb segment is at a stable minimum with respect to gravity (Strogatz, 1994). In the field of prosthetics, it will be too difficult to determine the position of the limb with respect to gravity, given that the user may rotate the limb into a different plane, such that the angular position of the actuator no longer corresponds to the gravitational position. As a result, an internal dynamics component

due to gravity will not be included, though it is hoped that the user will adapt to maintain a position in the presence of gravity, just as they would do with an intact limb.

*Friction:* Friction is a nonlinear feature that, although difficult to model, will have a substantial impact on the performance of the actuator. Properly modeling friction allows for increased feedback gains, greater sensitivity, and smoother performance. Stiction plays a significant role in compliant systems such as series elastic actuators (Armstrong-Hélouvy, 1993). Armstrong-Hélouvy, Dupont, and Canudas de Wit (1994) present a good overview of friction. The static and Coulomb friction model typically used was first developed by Leonardo Da Vinci (1519). Reynolds later added a viscous effect (1886), as shown in Figure 12.11a. Negative viscous friction, known as the Stribeck effect, has also been observed, as illustrated in Figure 12.11b.

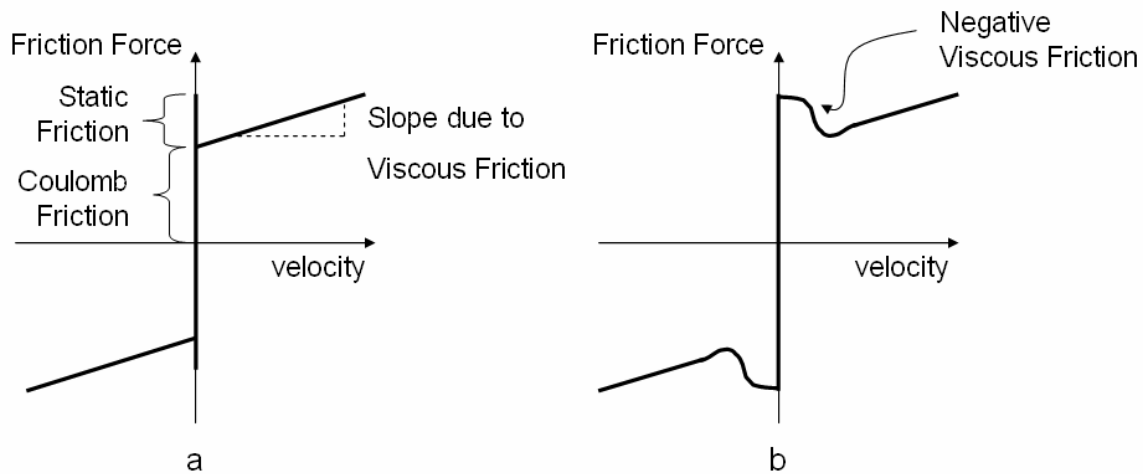


**Figure 12.11: Common Friction Models**

Negative Viscous Friction is also known as Stribeck Friction. It is due to the transition between boundary lubrication to fluid lubrication.

Static Friction is known as Stiction

Various other components may be added, perhaps the most common ones being time constants to account for frictional memory. Although these features may be modeled in the study of tribology, the simple model shown in Figure 12.11a should be sufficient to model the actuator described in this proposal.

A version of this model, shown in Figure 12.11, may be used to reduce algorithm complexity. This model, designed by Karnopp (1985), accounts for stiction while avoiding the search for the switching point. In this method, the frictional force is not always a function of the velocity: for a small neighborhood near zero velocity, the frictional force is a function of the applied force, as given by:

$$F_f(\dot{x}, F) = \begin{cases} \text{sign}(\dot{x})F_c & |\dot{x}| > T_v \\ \text{sign}(F)\min(F, F_s) & \dot{x} \leq T_v \end{cases} \quad (12.16)$$

This model allows for the change in causality that appears to develop around the zero velocity region, allowing stable control, as shown in Figure 12.12.

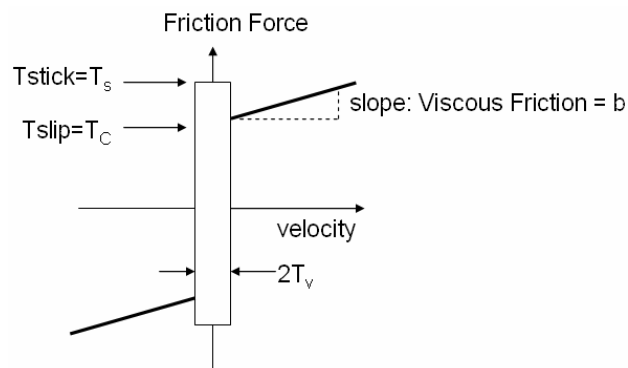


**Figure 12.12: Computationally simple friction model**

This model allows for computational simplicity

*Acquisition of Internal Dynamic parameters:* Johnson and Lorenz (1992) have suggested a simple way to acquire the necessary internal dynamic parameters. A proportional, derivative, and integral feedback loop is used, determined by the Ziegler and Nichols tuning method (1942). A series of trajectories with the same velocity distribution are averaged with respect to velocity, as illustrated in Figure 12.13.

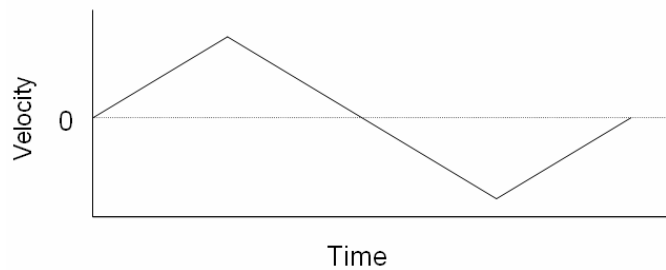


**Figure 12.13: Velocity Profile:**

Position trajectories are generated based on this velocity profile. By changing the length of time of the velocity profile, the position and acceleration are altered.

Results may then be averaged with respect to velocity to obtain a force vs. velocity plot.

These forces may then be accounted for in an internal dynamics model.

The torque signal sent to the actuator is examined with respect to velocity. Any hysteresis may be accredited to the inertia of the actuator, and an appropriate inertial term obtained by measuring the height of hysteresis. Once inertia has been accounted for, viscous damping may be accounted for by measuring the slope of torque with respect to speed.  $T_s$  and  $T_c$  may then be identified by observing the remaining signal of a third trial.

The placement of the internal dynamics model is important (Johnson & Lorenz, 1992). Feedback gains should be amplified by the difference between the desired and actual signal. In contrast with this placement, internal dynamics gains should be amplified by an actual signal. Johnson and Lorenz have shown that better results are obtained near low velocities if internal dynamics are calculated from the feedback signal as opposed to the desired signal, with both options shown in Figure 12.14.

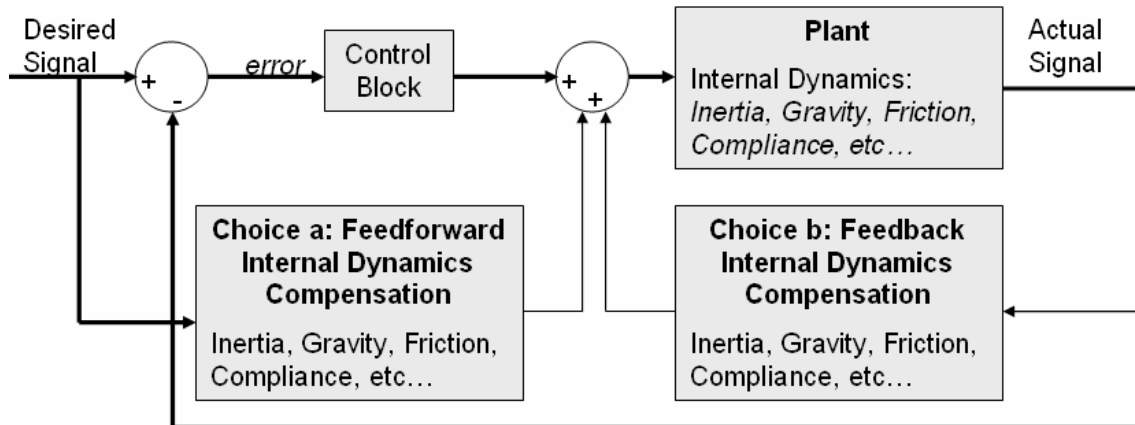


**Figure 12.14: Placement of Internal Dynamics Compensation**

The Internal Dynamics Compensation block may use the desired motion signals or the actual motion signals to calculate internal dynamic forces. If the trajectory is known a priori, internal dynamic compensation forces may be calculated before the task. For real-time execution, a feedforward model has the same processing time as a feedback model.

## 12.5 Pilot Study notes

Fitts' law (Fitts, 1954, Guiard & Beaudouin-Lafon, 2004) was initially used as the performance metric for the pilot study presented in chapter 7 of this thesis. Fitts' law provides a relationship between trajectory distance, accuracy required, and response time. As a result, it is able to distil several variables attributable to performance to a single number for a given pointing device and control scheme. It presents a standardized approach (ISO9241-9) that allows other laboratories to compare the results of different experiments in a quantitative way. As a result, it seemed an ideal performance metric. Soukoreff and MacKenzie (2004) offer an excellent review on standardization suggestions for ISO9241-9.

In accordance with ISO9241-9, data were collected over a range of an Index of Difficulty ( $ID$ ), where  $ID = \log_2\left(\frac{A}{D} + 1\right)$ ,  $A$  is the arc length between movements, and  $D$  is the diameter (width) of the acceptable target. Arc length and diameter for this particular experiment are illustrated in Figure 12.16. Two parameter sets are presented below in Figure 12.16 to illustrate  $ID$  range. Target choice is selected to ensure an index of difficulty range of 2 to 8 in accordance with ISO9241-9, as illustrated in Figure 12.17.

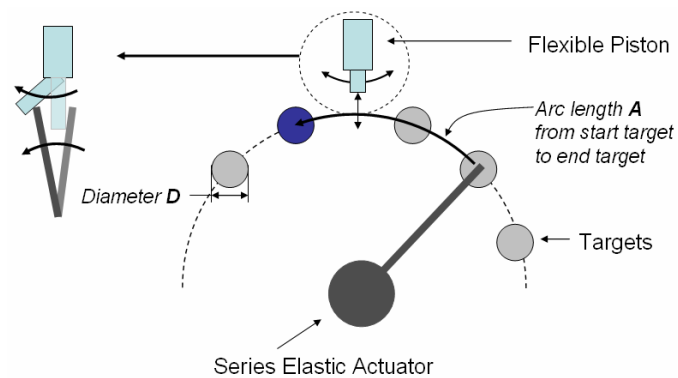


**Figure 12.15: Experiment B Setup**

Targets are projected from a digital projector. The data bit ID is determined by the diameter  $D$  of the target and the arc length  $A$  between targets.

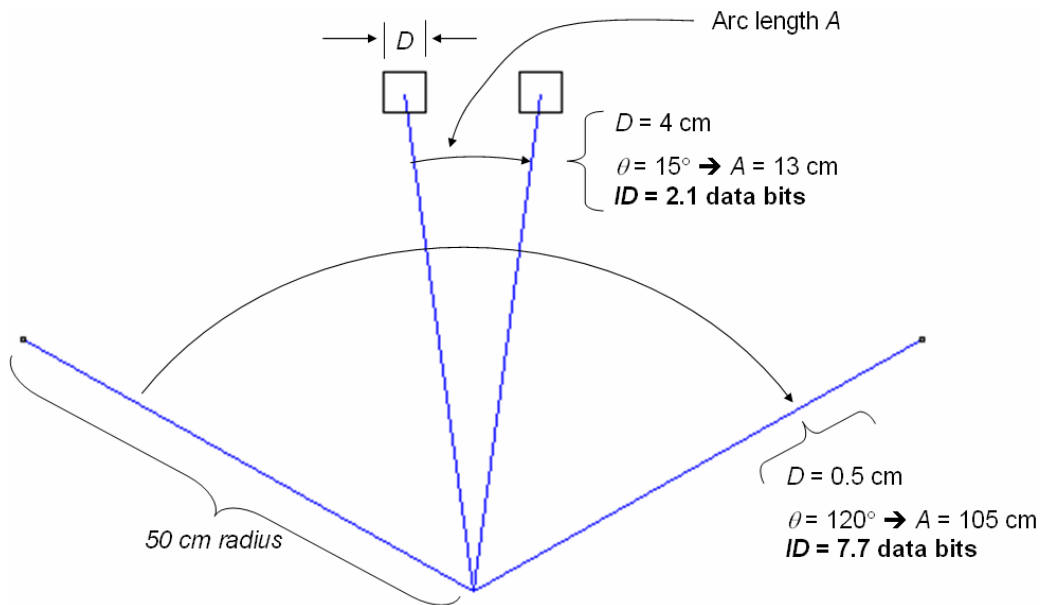


**Figure 12.16: Trajectory & Accuracy Range due to Index of Difficulty Range**

Trajectory arc length  $A$  and target diameter  $D$  are altered to vary index of difficulty  $ID$ .

In order to obtain an Index of Difficulty of 8, very large trajectories and very small targets must be used.



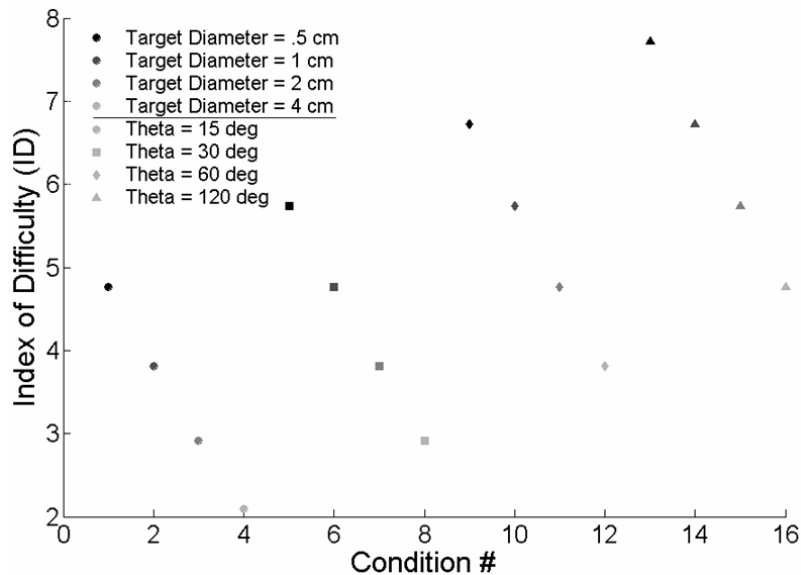


**Figure 12.17: Index of Difficulty Range**

In accordance with Fitts' experiments, a range of  $ID$  values are chosen from 2 – 8 with an average of 5 and a normal distribution.

Although the diameter of successful motions is varied, studies have found that individual subjects have predefined preferences for how accurate a trajectory must be, regardless of target diameter. To account for this fact,  $D$  is corrected for each data bit after testing by finding the standard deviation of movement for a given data bit and correcting as follows:  $D_e = 4.133\sigma$ . This correction is in part why at least 15 movements for each data bit have been found to be necessary.  $A$  is recalibrated as the mean movement distance for a given data bit. To assess differences in control paradigms, these measures will be synthesized into a single index termed

throughput:  $TP = \frac{1}{y} \sum_{i=1}^y \left( \frac{1}{x} \sum_{j=1}^x \frac{ID_{e_{ij}}}{MT_{ij}} \right)$ , where  $y$  is the number of subjects,  $x$  represents the

number of movement conditions, and  $MT$  is the movement time. Throughput has units of bits per second.

In order to evaluate if Fitts' law may be applied to the data, least-squares linear regression is used to find the intercept (a) and slope (b) parameters of the Fitts' law equation  $MT_{Predicted} = a + b * ID$ . If the intercept is positive, it should be between -0.2 and 0.4 seconds, and preferably closer to 0. Likewise the  $r^2$  value of linearity of fit should be greater than 0.81 (Soukoreff & MacKenzie, 2004). For the four subjects tested in this study, none of the paradigms met both acceptance criteria, and most paradigms failed both acceptance criterion, as illustrated in Figure 12.18.

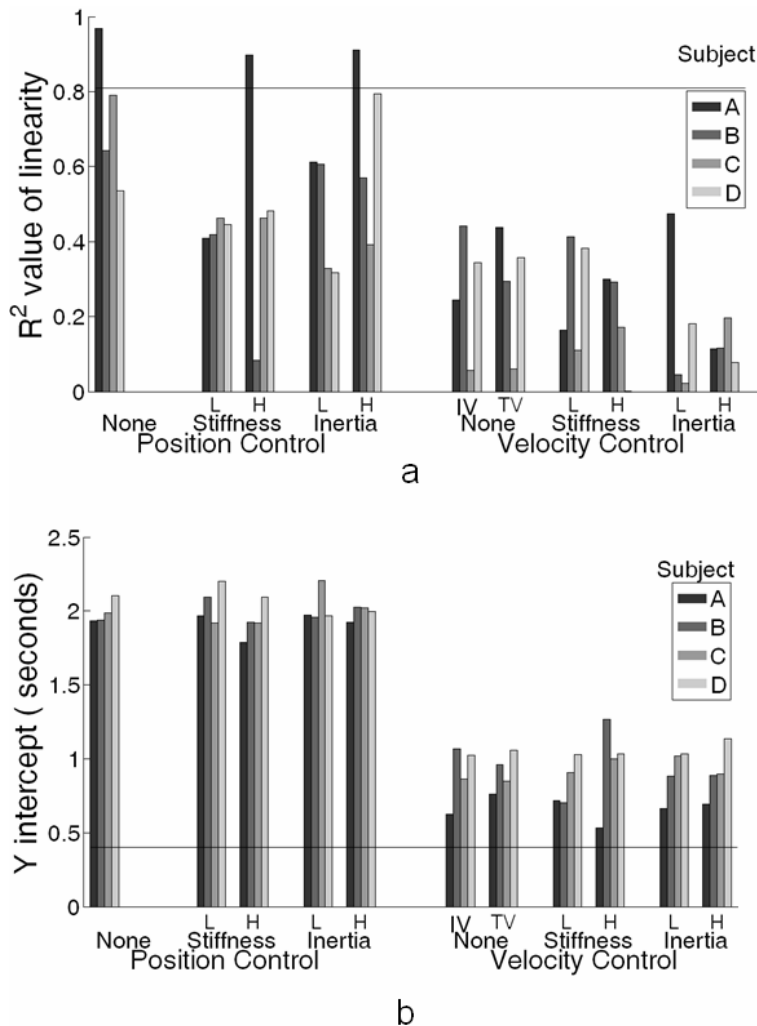


**Figure 12.18: Fitts Law applied to 4 subjects**

The majority of subjects did not meet the acceptance criterion in their movement to be analyzed using Fitts' law, either in terms of linearity of fit or in terms of Y intercept.

The failure of the Y intercept to be close to 0 is likely a result of the maximum speed of the prosthetic elbow of 2.5 rad/sec, combined with the angular distances the prosthetic elbow was required to travel. It is likely, in retrospect, that the prosthesis was unable to maintain constant acceleration during the movement, but quickly reached peak velocity. This

observation is especially true of Position control, where velocity was rate limited to 0.6 rad/sec, but also true of velocity control, indicating that faster prostheses are needed to correctly mimic human elbow physiology. Increased speed comes at the cost of decreased precision, however, given a finite level of control of the prosthesis, and thus most subjects clinically prefer a lower maximum speed setting than that capable by the motor. Thus, more accurate user intent to create better precision is ultimately required to use a prosthetic elbow in a Fitts' task.

## ***12.6 Co-contraction values for individual targets***

The average impedance for each of the 50 targets is shown in each subplot of Figure 12.19 for able-bodied subjects and in Figure 12.20 for subjects with an amputation. The independent axis corresponds to target number: the average impedance of the first target for a given trial is shown on the left, and the average impedance of the 50<sup>th</sup> target for a given trial is shown on the right.

For each subplot, the set of green dots represent the trial where the Stroop task was performed simultaneously with the pointing task. The set of blue dots represent the trial where the Stroop task was absent. The red asterisk represents the average impedance for the tracking task. The gray line marks the tenth target. Calculations were performed on targets 11-50. Targets 1-10 were not analyzed, allowing subjects to experiment with co-contraction. Subjects should have co-contracted at least some of the time in the first 10 trials to evaluate the paradigm. Some subjects, however, rarely co-contracted, even in the first 10 trials.

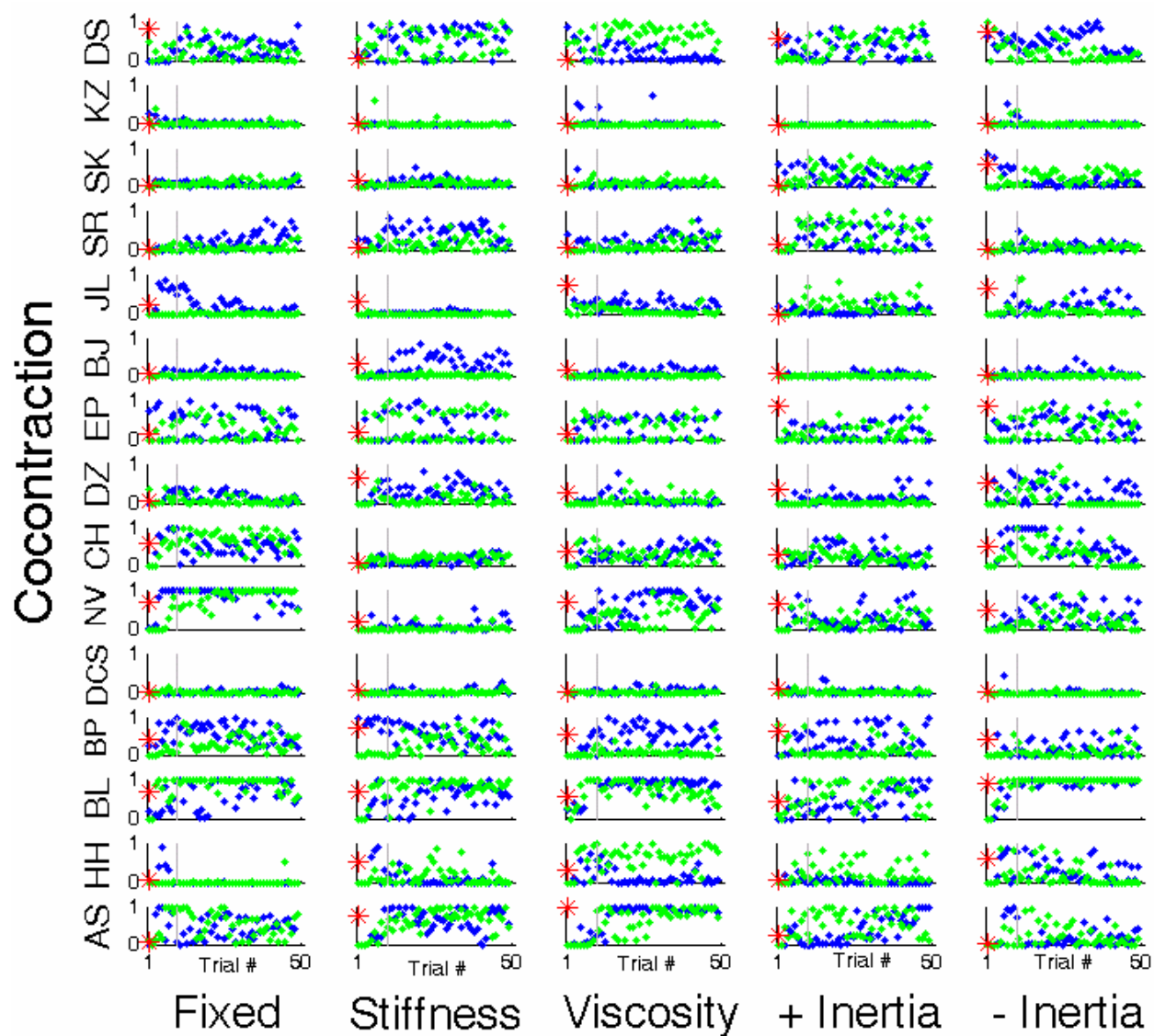


**Figure 12.19: Impedance for individual targets, for able bodied subjects**

See text above the figure for a description of the graph

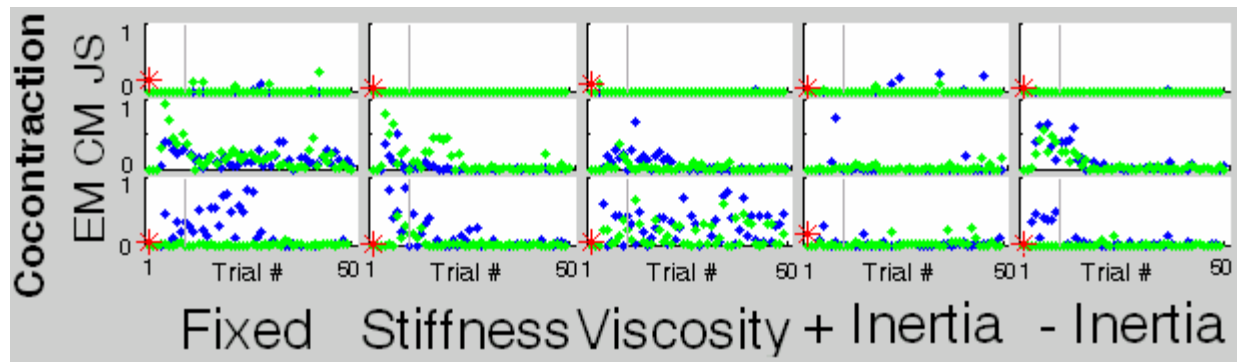


**Figure 12.20 : Impedance for individual targets, for subjects with an amputation**

See text above the set of figures for a description of the graph

The average impedance was also measured for three distinct regions of each target movement: movement start ( $10^\circ$ ), swing ( $25^\circ$ ), and movement stop ( $10^\circ$ ), shown in Figure 12.21.

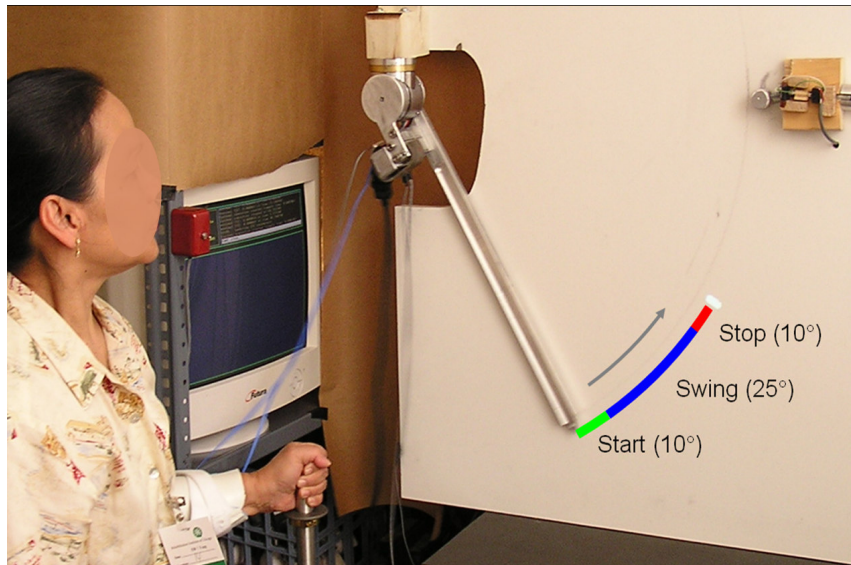


**Figure 12.21: Co-contraction across movement regions.**

Average impedance was recorded for three movement regions: Movement initiation, free swing, and movement termination. Subjects co-contracted more during the start and stop of each movement than in the middle, regardless of the impedance paradigm.

The individual results are shown for the no mental load paradigm (in which the Stroop task was absent), in Figure 12.22 for able-bodied subjects and Figure 12.23 for subjects with an amputation. The set of green dots corresponds to movement start, the set of blue dots corresponds to swing, and the set of red dots corresponds to movement stop.



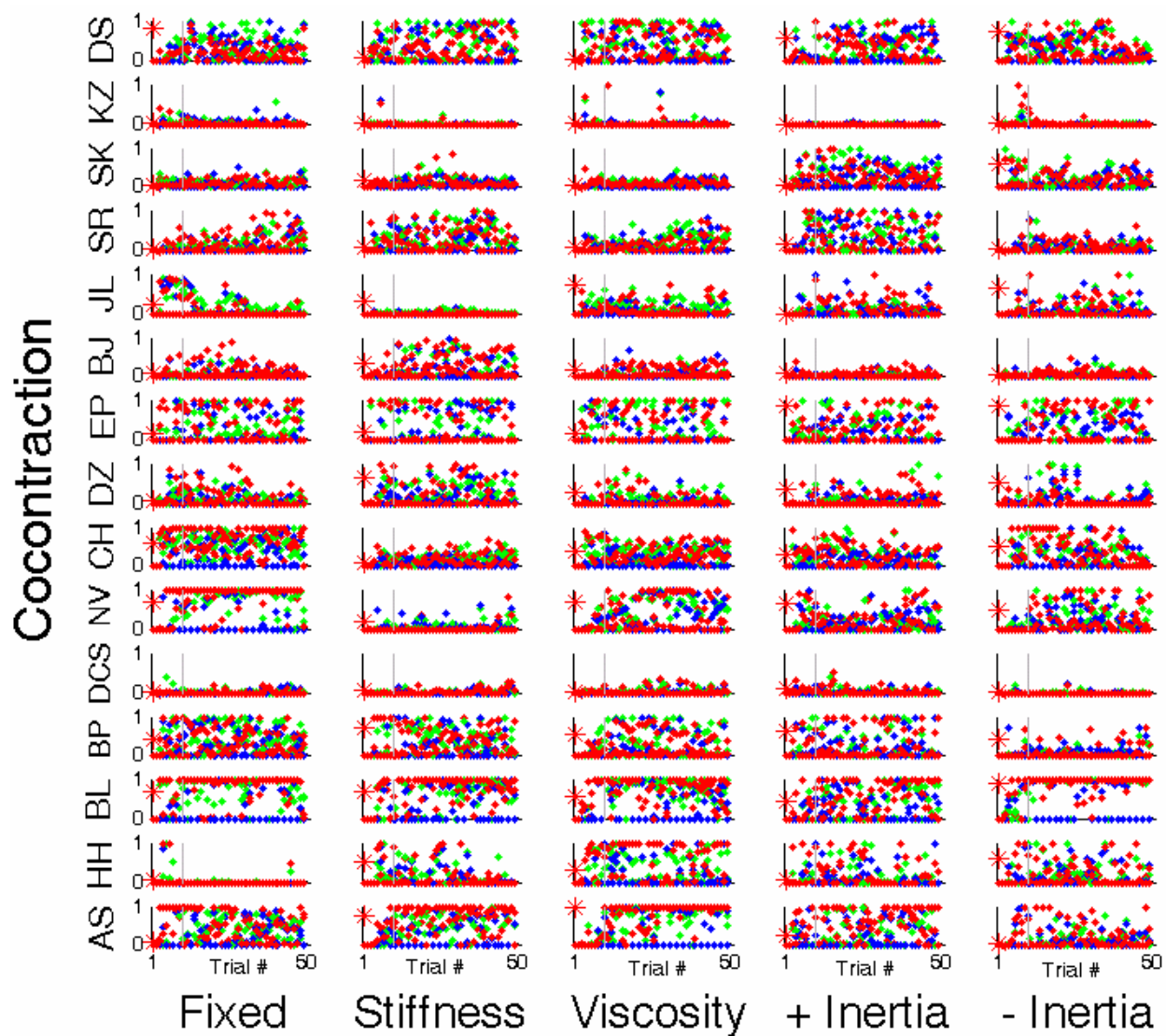


**Figure 12.22 Impedance for individual target *regions*, for able bodied subjects**

See text above the figure for a description of the graph

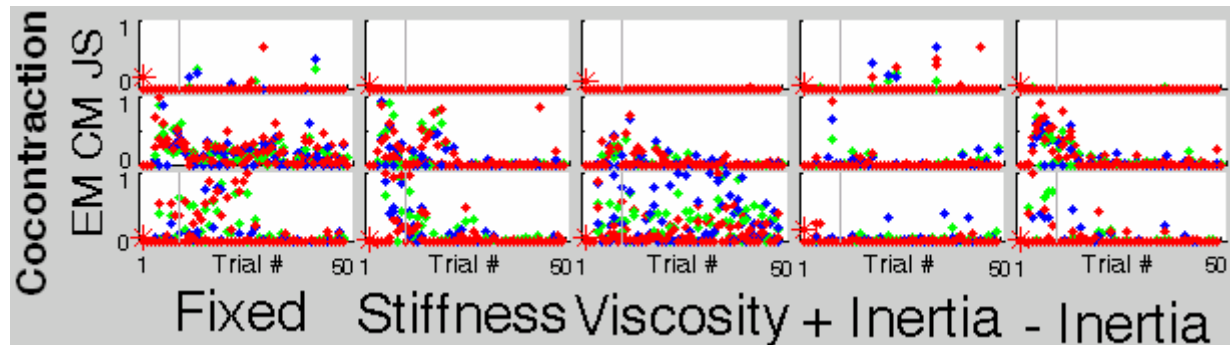


**Figure 12.23 Impedance for individual target *regions*, for subjects with an amputation**

See text above the set of figures for a description of the graph

Figure 12.24 is presented as a visual aid to illustrate what co-contraction levels were distinct between impedance paradigms for individual subjects. Black lines between paradigms indicate that the co-contraction levels across the 40 target movements were not statistically different, at the  $p = 0.05$  level, between the two paradigms. If a subject has no black lines between any paradigms (subject AS comes close), it indicates that they maintained a different level of co-contraction for each impedance paradigm. If a subject has black lines between every single combination of paradigms (subject DCS comes close), it indicates that they did not have any distinction in co-contraction levels between any paradigms.

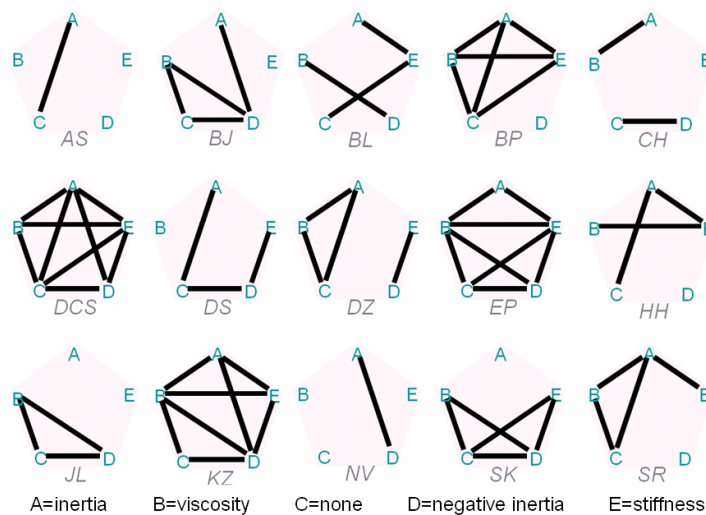


**Figure 12.24: Co-contraction distinctions between paradigms for individual subjects**

See text above figure for a description of the text

While individual subjects had different levels of co-contraction between impedance paradigms, the group as a whole did not have a statistically different level of co-contraction between impedance paradigms. Three of the subjects who had several distinct levels of co-contraction (JL, AS, CH) were retested to see if they would maintain the same groupings of co-contraction. None of the three subjects maintained the same groupings of co-contraction.

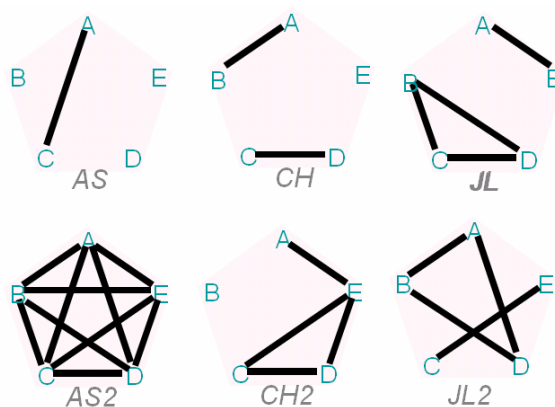
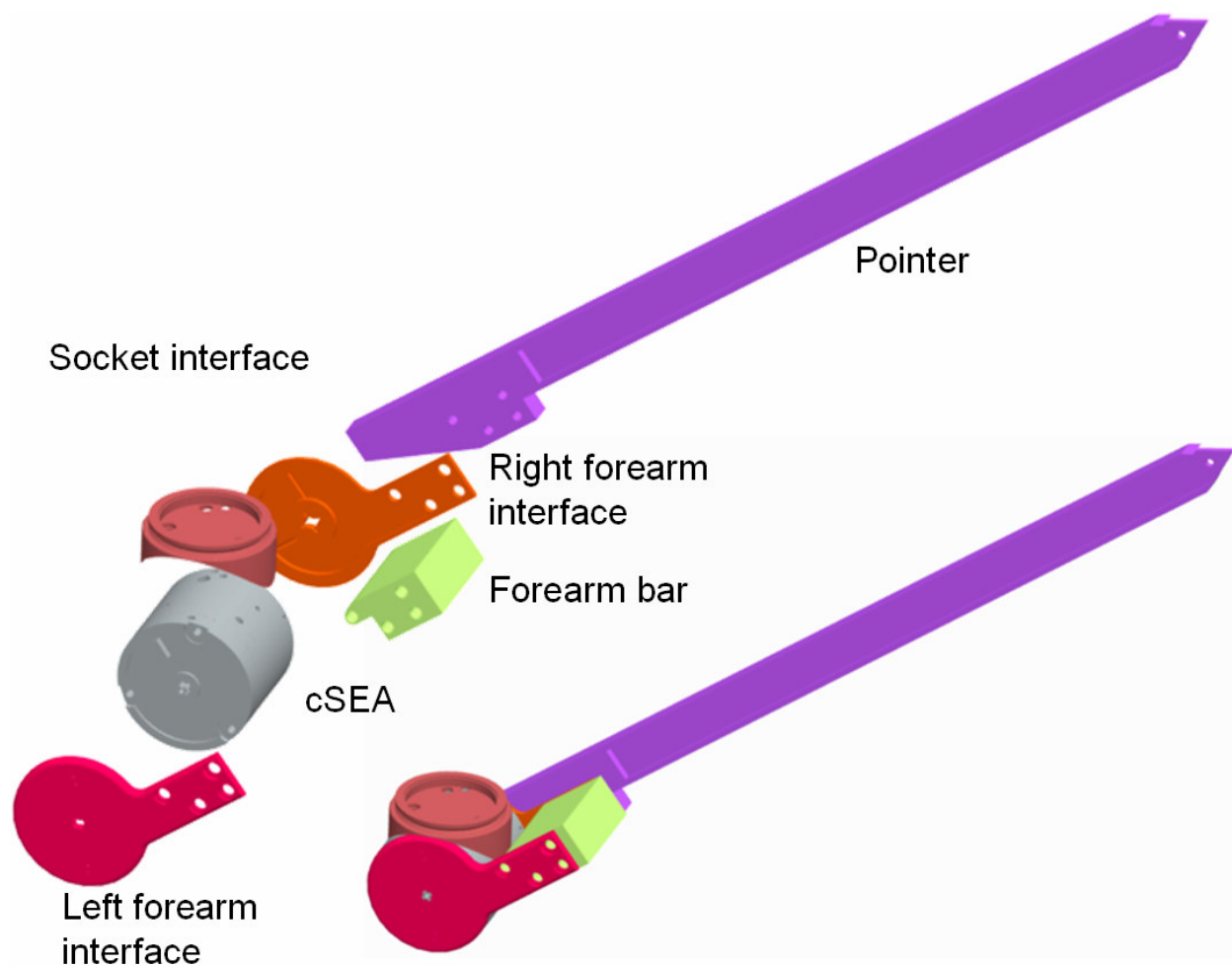


**Figure 12.25: Repeated trials for 3 subjects who demonstrated initial co-contraction distinction between impedance paradigms**

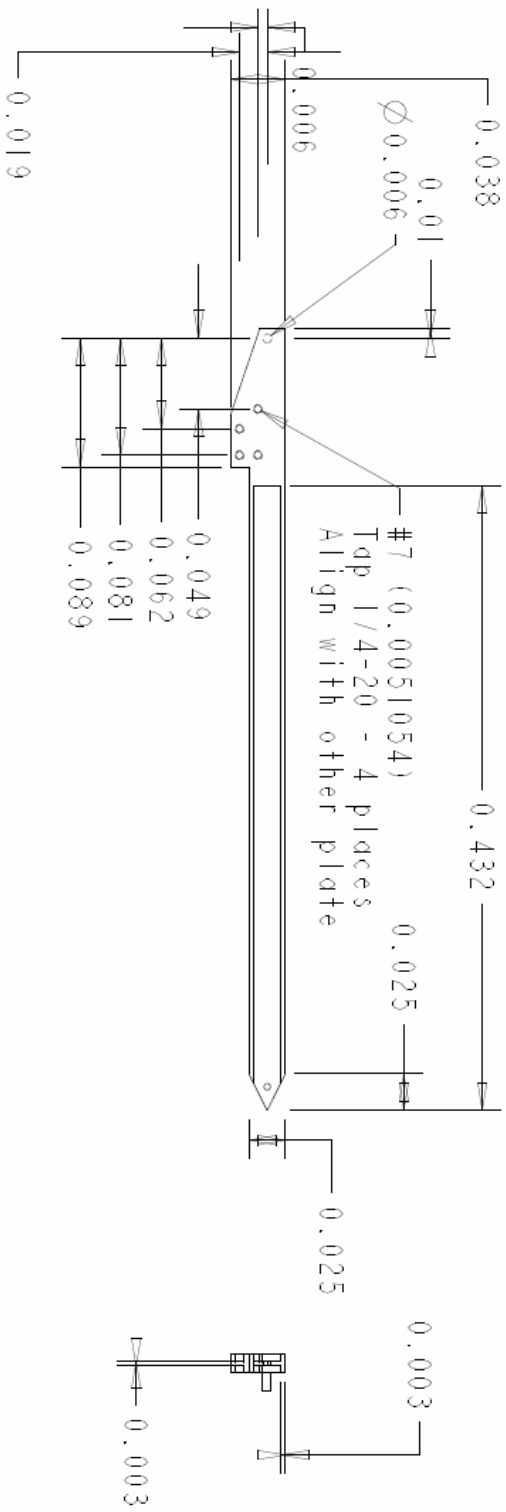
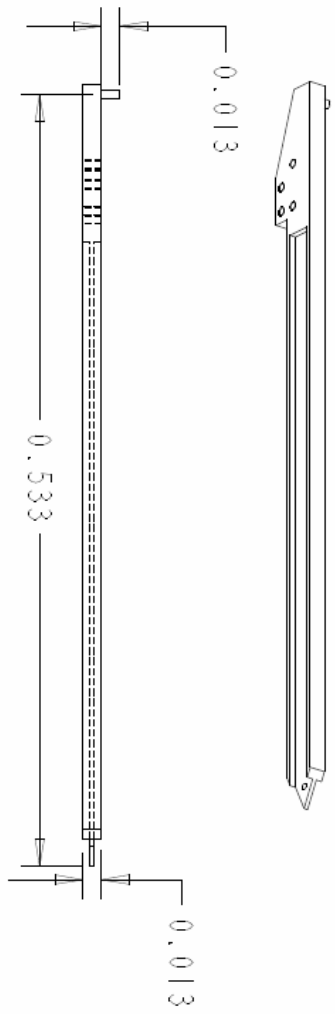
See text above Figure 12.24 for a description. Subjects did not demonstrate repeatable distinctions.

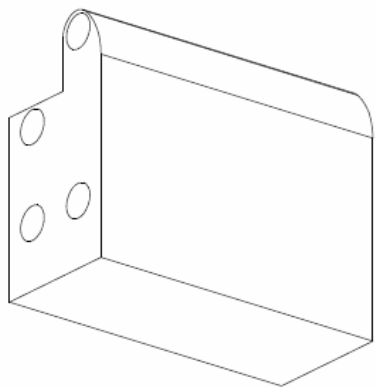
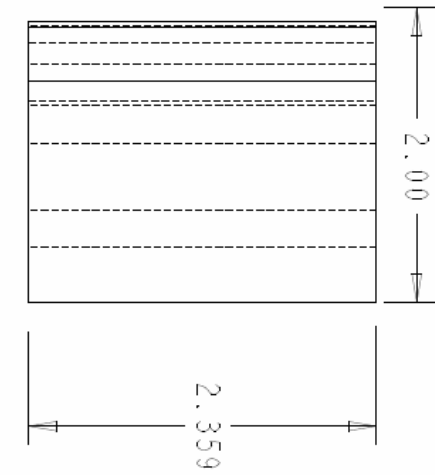
## 12.7 Mechanical Design

	Inertia (g cm <sup>2</sup> )	Output Inertia (kg m <sup>2</sup> )
Arm (1.4 kg)		0.97
Pointer & interface (586 g)		
Pointer (487 g)	1.1E+05	0.01
Pointer (284 g)		
Forearm bar (129 g)		
Screws (62 g)		
Nuts (13 g)		
L forearm interface (47 g)	729	0.00
R forearm interface (53 g)	790	0.00
Socket interface (65 g)		
Socket interface (61 g)		
Screws (3 g)		
<hr/>		
Elbow (740 g)		
Housing top (54 g)		
Screws (8 g)		
Pins (2 g)		
Circular spline (63 g)		
Clutch lip (47 g)		
Harmonic Drive (130 g)		
WG+FS+spring (134 g)		
WG (53 g)	200	0.51
FS (14 g)	65	0.00
Spandrel spring (67 g)	16	0.00
Rest of elbow (434 g)		
Emoteq motor (176 g)	87	0.22
Housing motor (106 g)		
Roller clutch (59)	91	0.23
Casing (19 g)		
Output (27 g)		
Input (10 g)		
Rollers (3 g)		
Housing Bottom (35 g)		
Insert (8 g)		

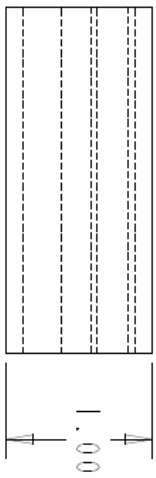
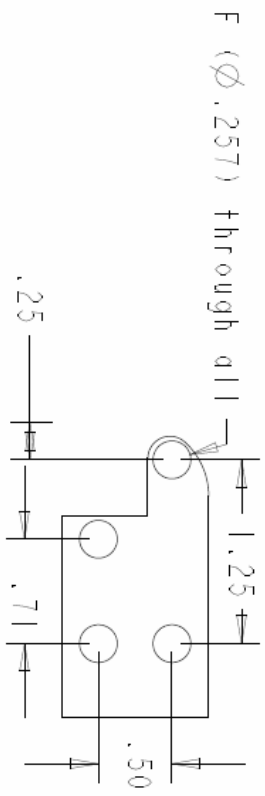


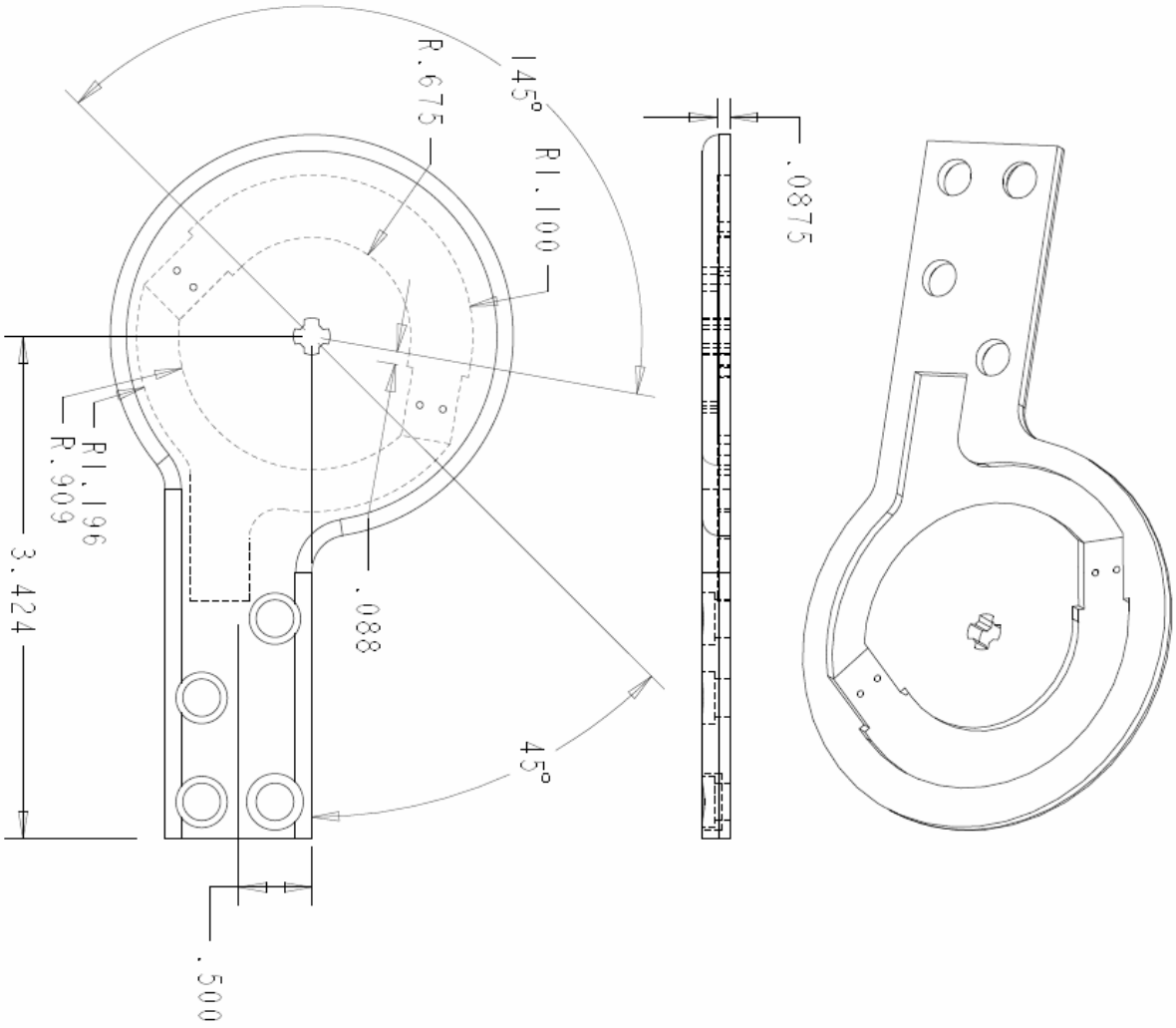
Painter  
Jon Sensinger 06/11/05  
Material: Aluminum  
Units: Inches  
Scale: 0.25





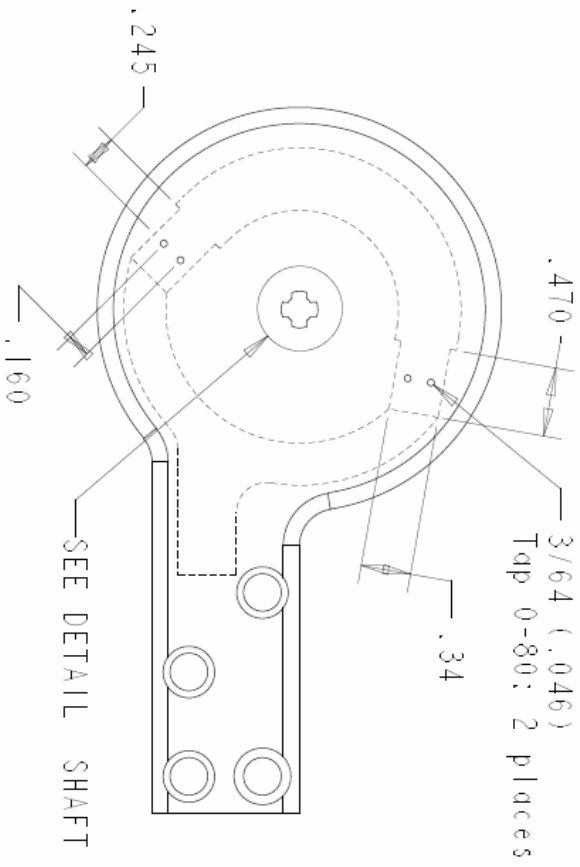
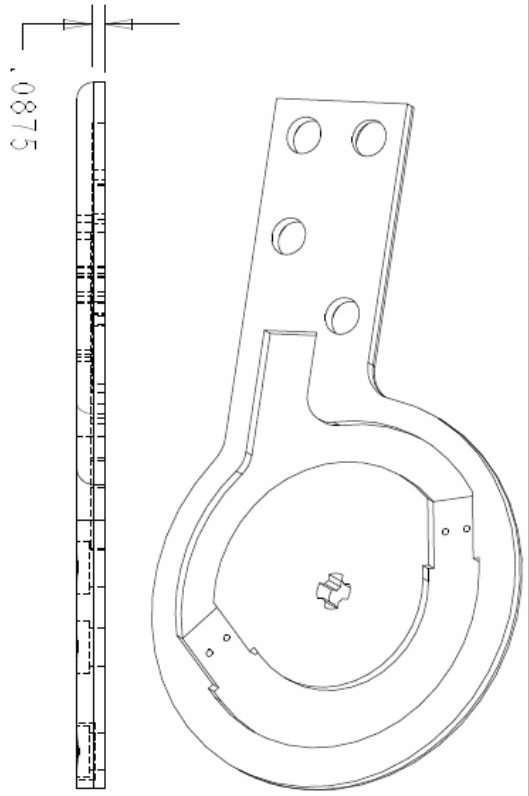
Forearm bar  
Jon Sensinger 01/13/2006  
Material: Aluminum  
Scale: 1  
Units: Inches



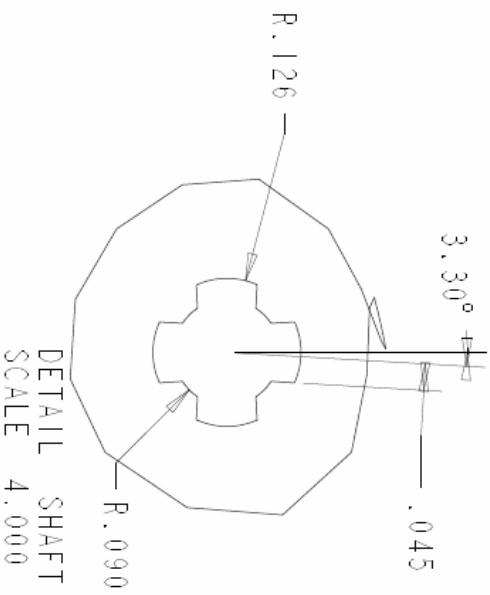


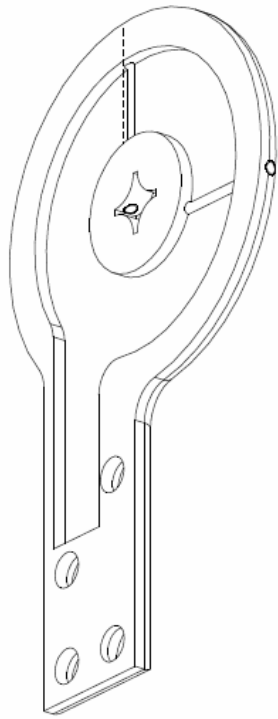
Interface  
Forearm InterfaceL  
Jon Sensinger 03/25/05  
Material: Aluminum  
Units: Inches  
Scale: 1  
Drawing 1 of 2



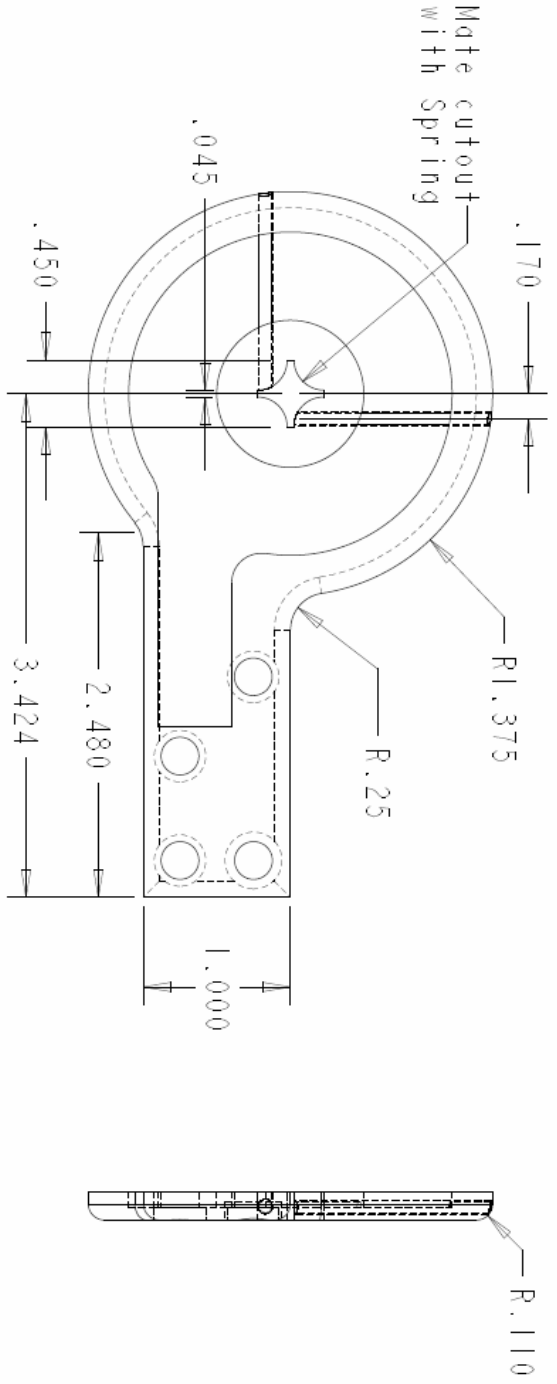
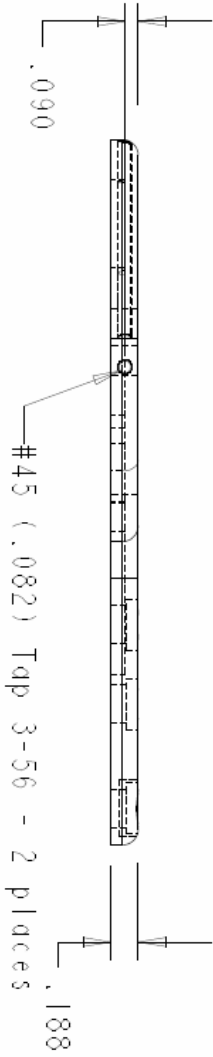


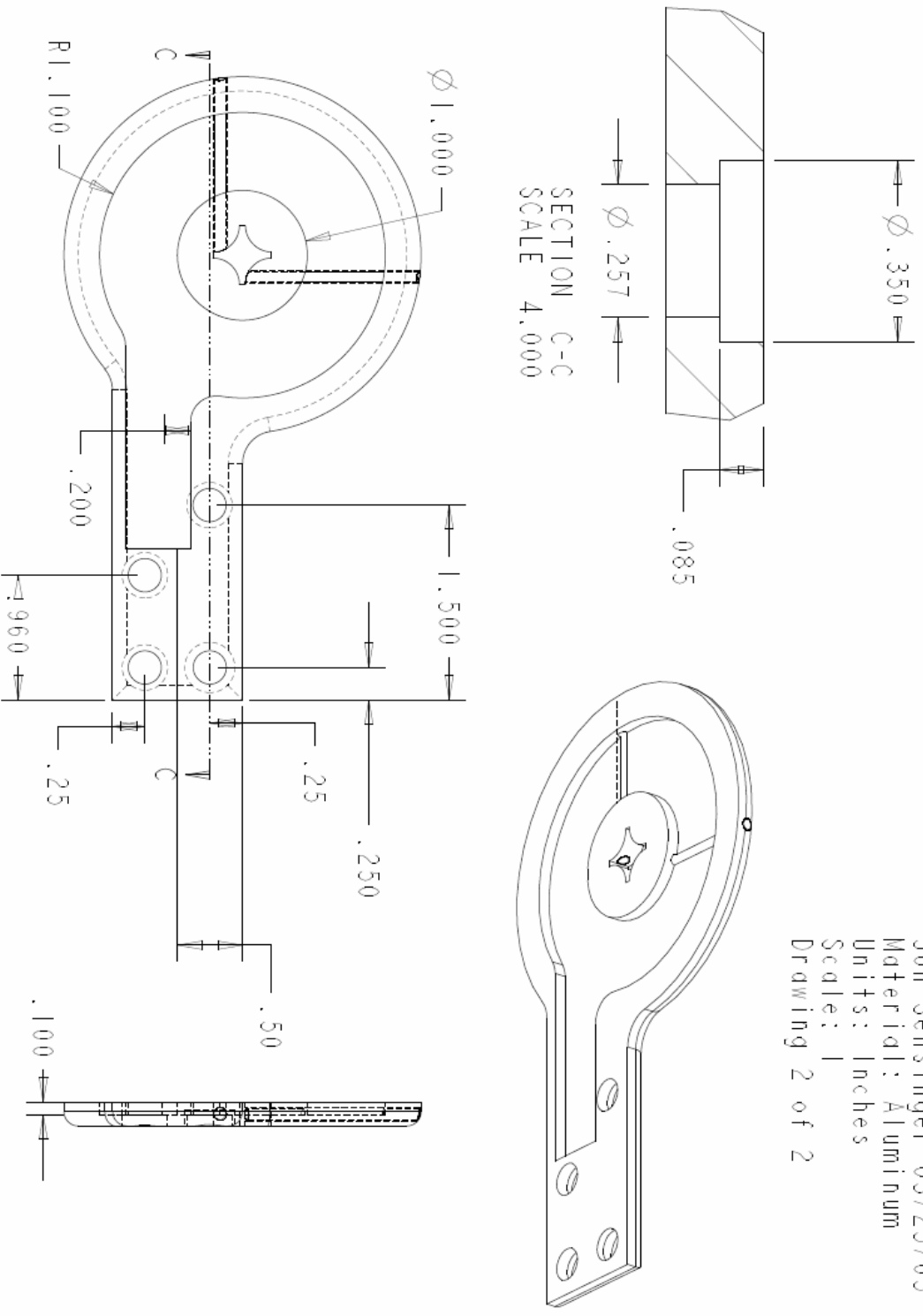
Interface  
Forearm Interfacel  
Jon Sensinger 03/25/05  
Material: Aluminum  
Units: Inches  
Scale: 1  
Drawing 2 of 2



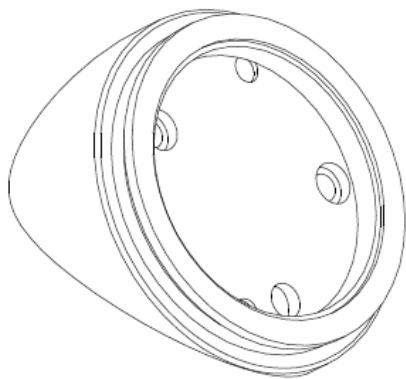
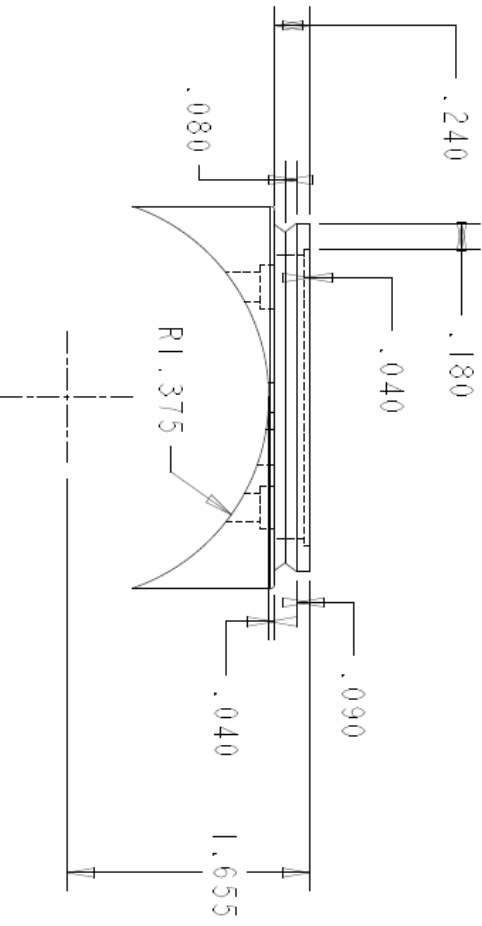
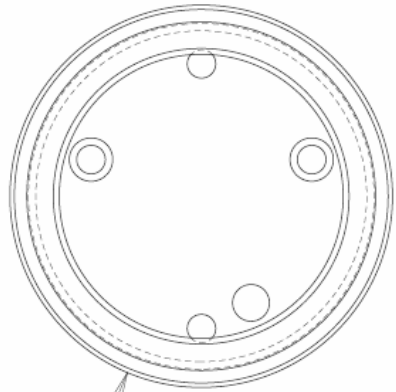
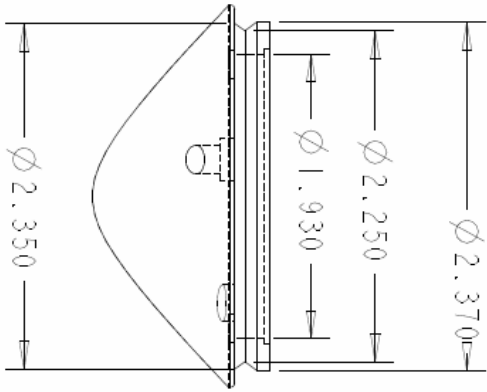


InterfaceR  
Forearm InterfaceR  
Jon Sensinger 03/25/05  
Material: Aluminum  
Units: Inches  
Scale: 1  
Drawing 1 of 2

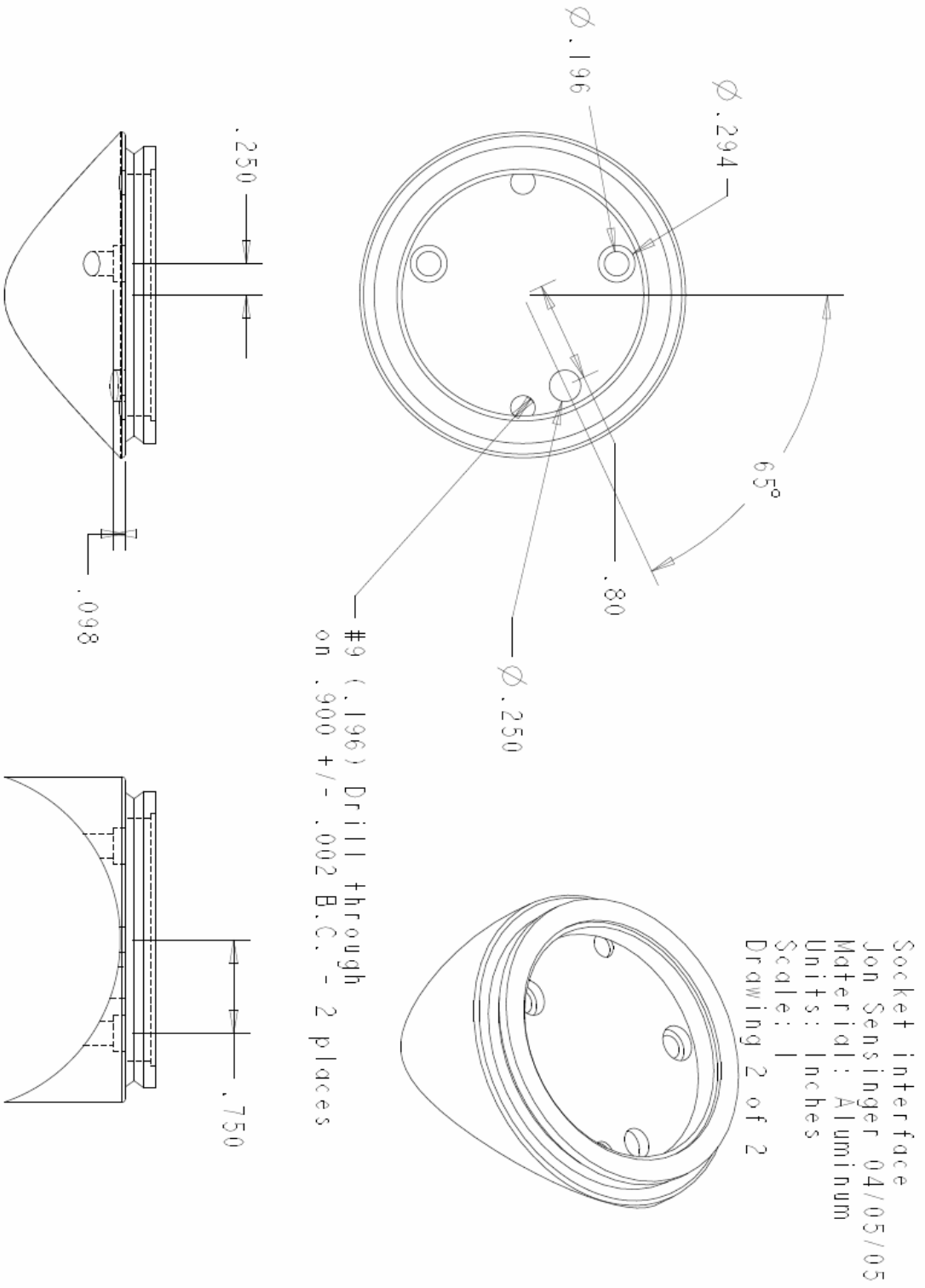


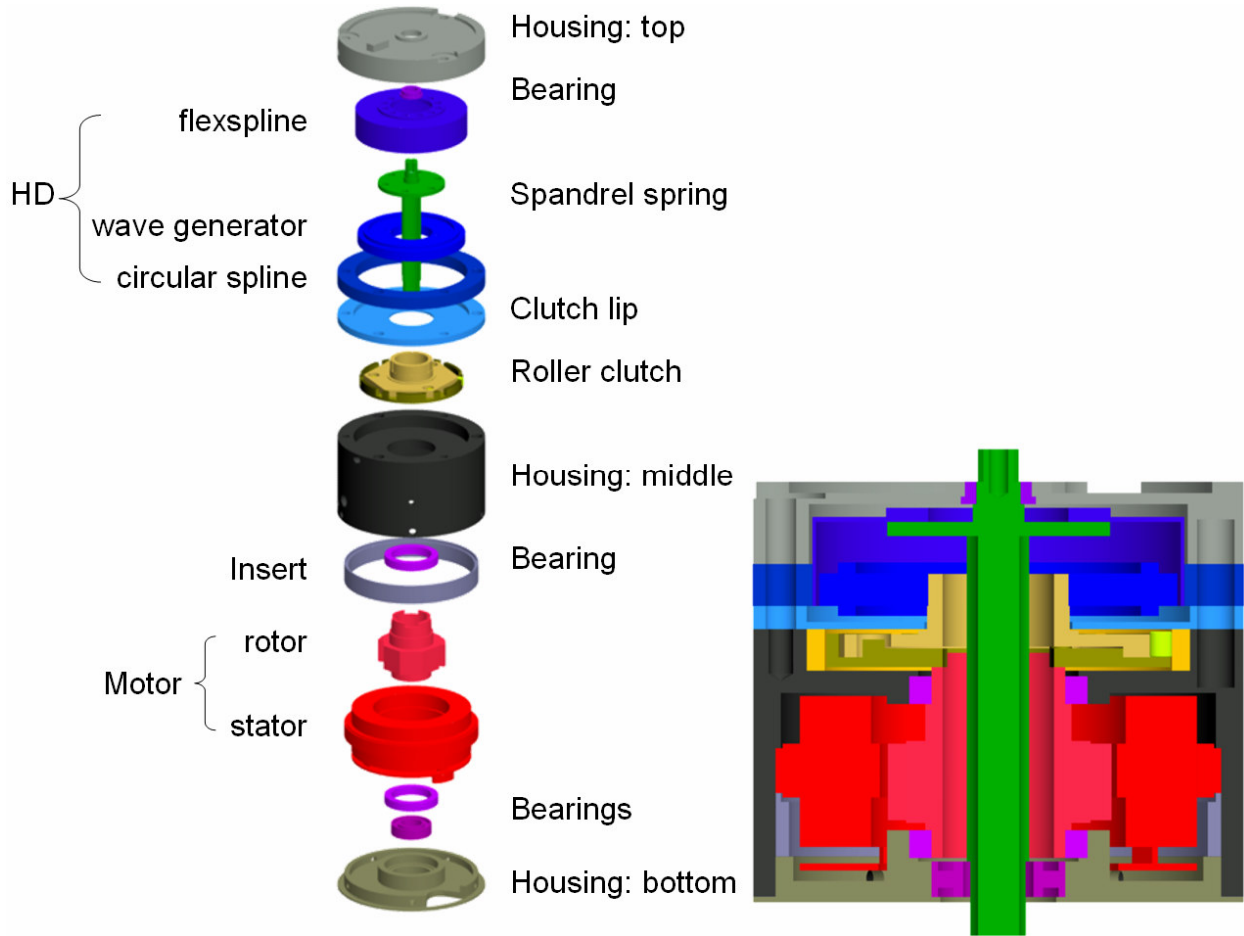


Interface  
Socket InterfaceR  
Jon Sensinger 03/25/05  
Material: Aluminum  
Units: Inches  
Scale: 1  
Drawing 2 of 2

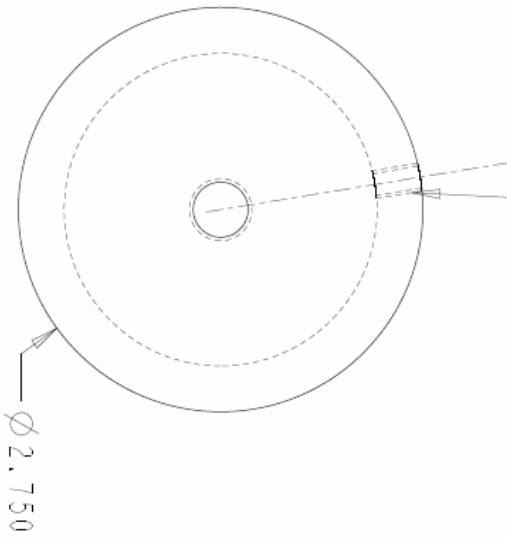


Socket interface  
Jon Sensinger 04/05/05  
Material: Aluminum  
Units: Inches  
Scale: 1  
Drawing 1 of 2

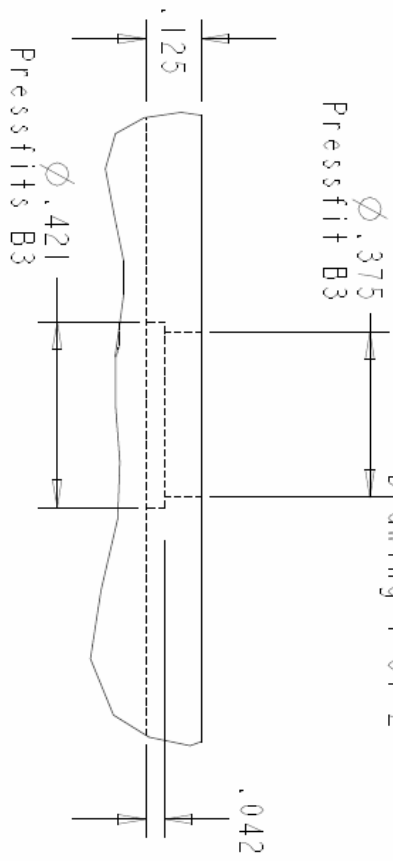




#25 (.1495)  
 Tap 10-24  
 R 1.220 +/- .002 B.C. - 3 places  
 Align with H4 & P1

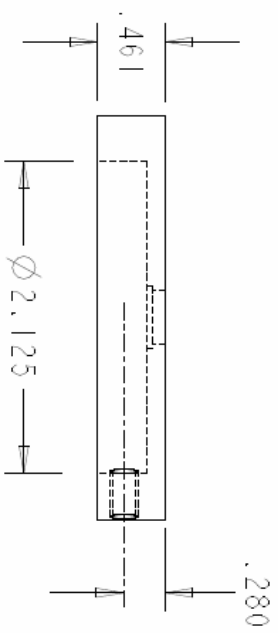
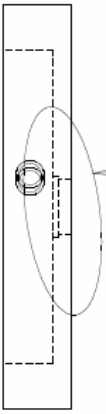


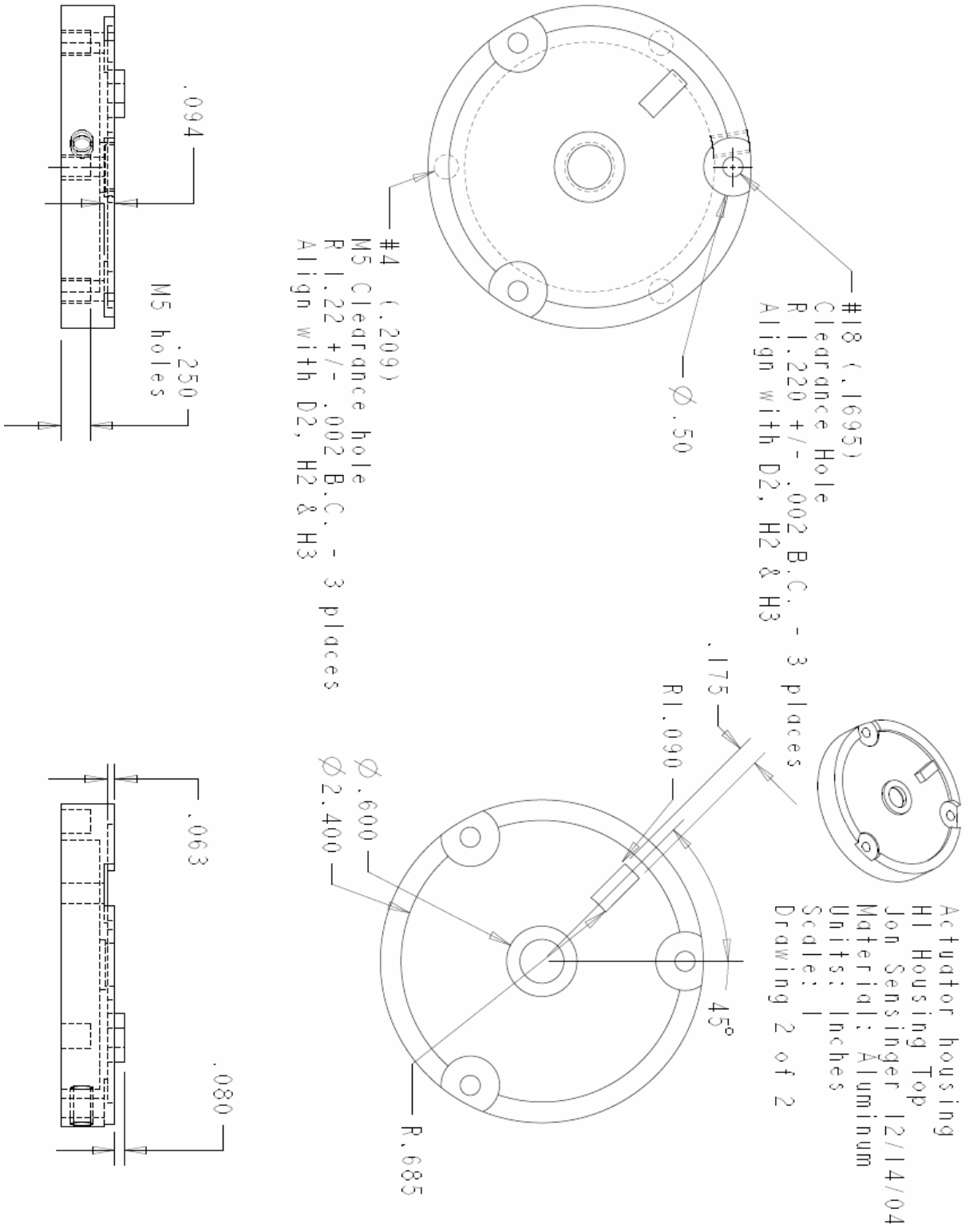
DETAIL BEARING DETAIL  
 SCALE 3.000



Actuator housing  
 H1 Housing Top  
 Jon Sensinger 12/14/04  
 Material: Aluminum  
 Units: Inches  
 Scale: 1  
 Drawing 1 of 2

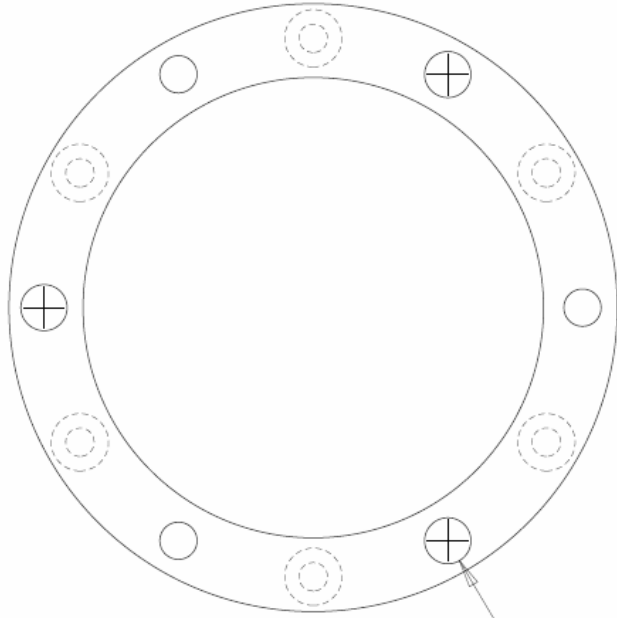
SEE DETAIL  
 BEARING DETAIL



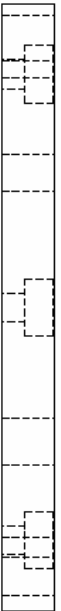
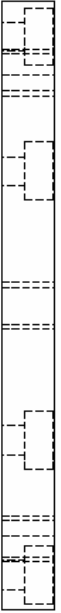


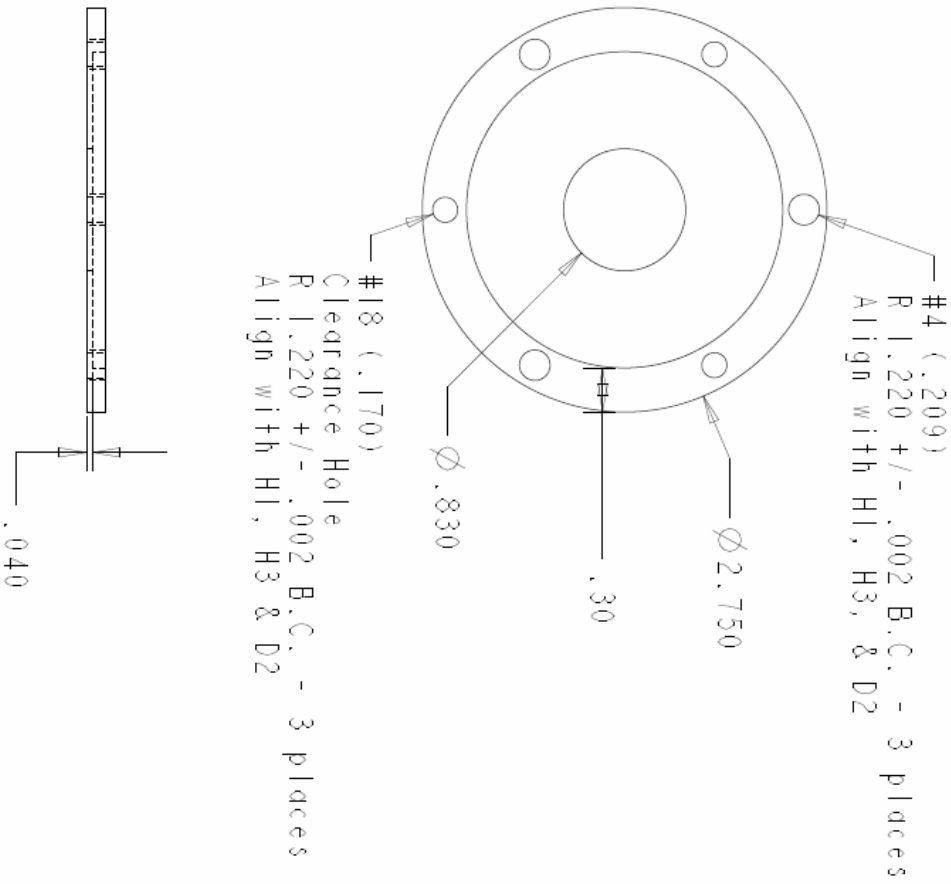


Actuator Housing:  
D2: HD CS(MODIFICATION)  
Jon Sensinger 12/13/04  
Material: Steel  
Units: Inches  
Scale: 1.5



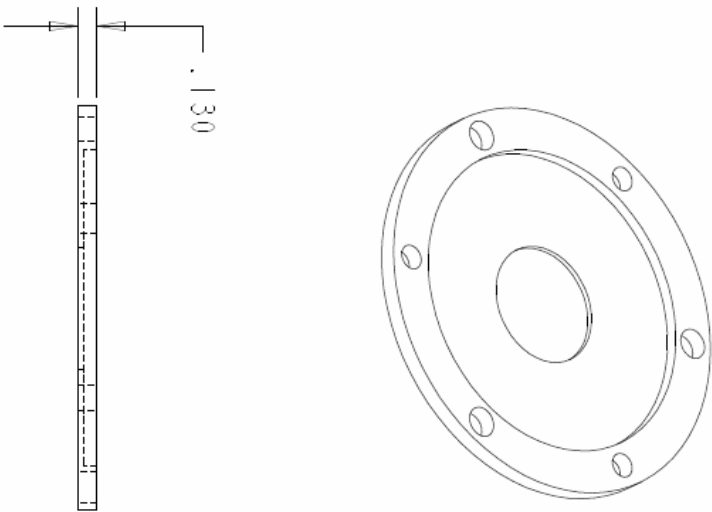
#4 (.209)  
R 1.220 +/- .002 B.C. - 3 places  
Align with H1, H2, & H3

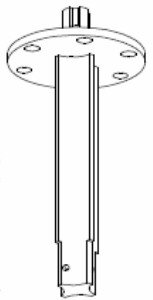




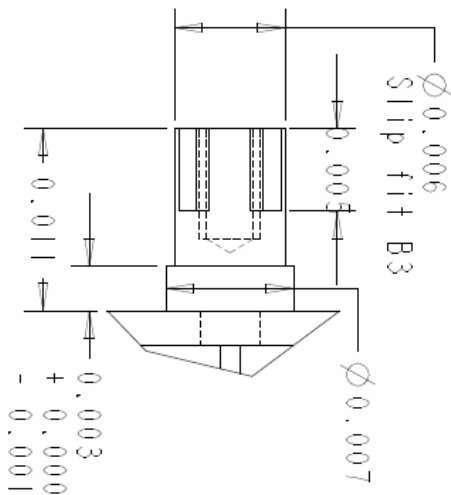
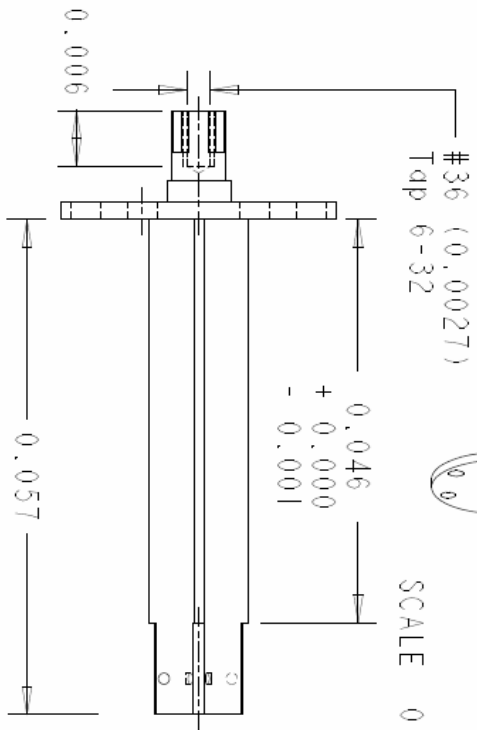
Actuator Housing  
 H2 Clutch Lip  
 Jon Sensinger 12/13/2004  
 Material: Hardened Steel  
 Units: Inches  
 Scale: 1

Split in half to make 2 parts  
 that mate together



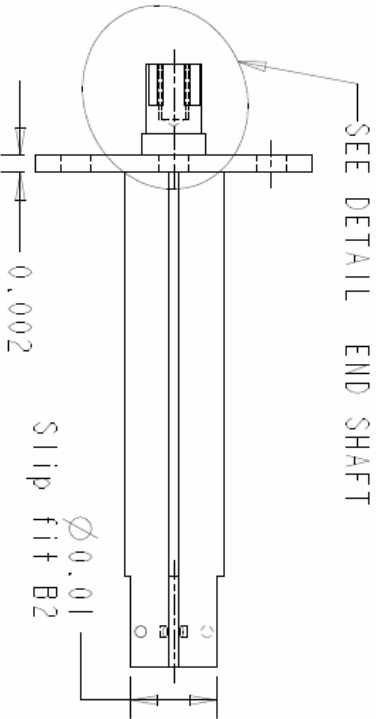


Spandrel Spring 04/07/05  
 Jon Sensinger SS 17-4Ph  
 Material: SS 17-4Ph  
 Oil quenched & tempered (@315 C)  
 Units: Inches  
 Scale: 1.5  
 Drawing 1/2

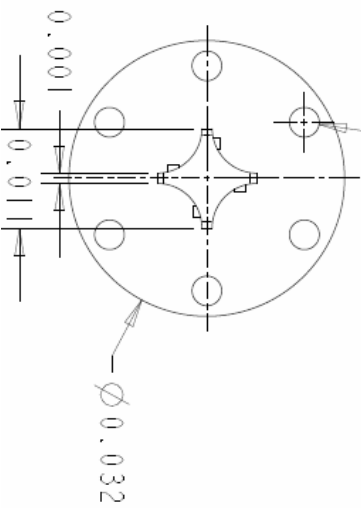


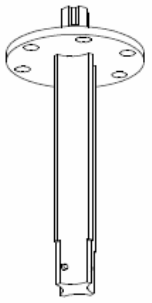
DETAIL END SHAFT  
 SCALE 3.000

$\phi 0.003$  3.4 mm Metric Drill - 3 places  
 $\phi 5/32$  (0.156) - 3 alternating places  
 R 0.013 +/- .002 B.C  
 Mate D1



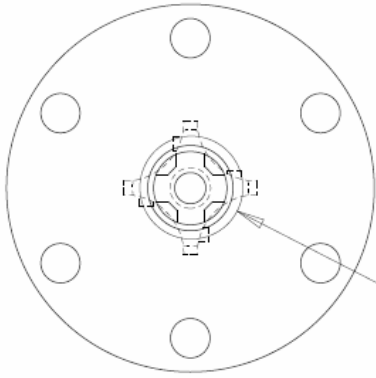
SEE DETAIL END SHAFT



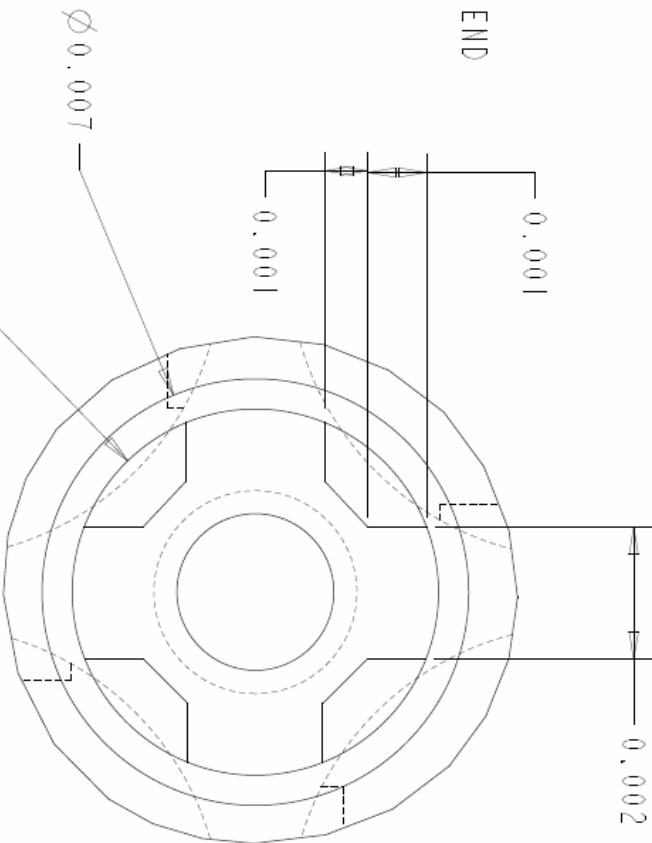


SCALE 0.750

Spandrel Spring  
Jon Sensinger 04/07/05  
Material: SS 17-4Ph  
Oil quenched & tempered @315C  
Units: Inches  
Scale: 2  
Drawing 2 of 2



SEE DETAIL END



$\phi 0.006$   
Slip fit B3

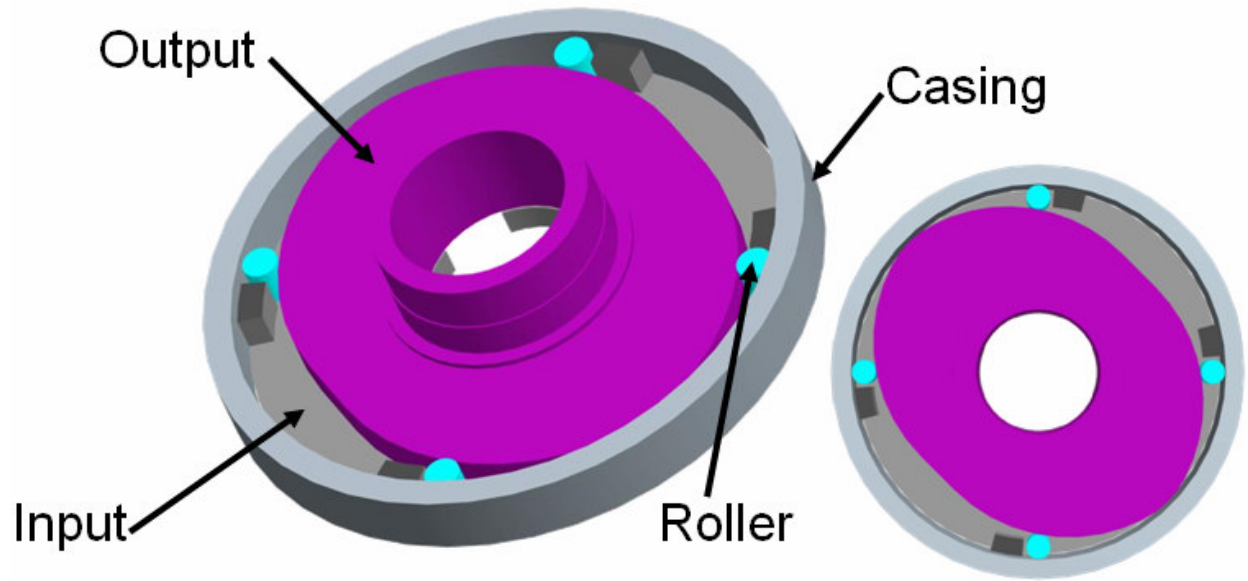
$\phi 0.007$

0.001

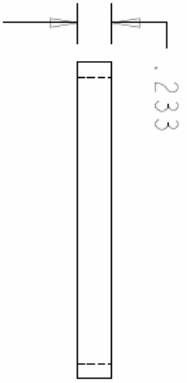
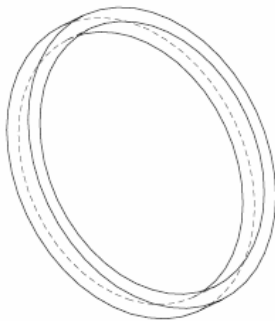
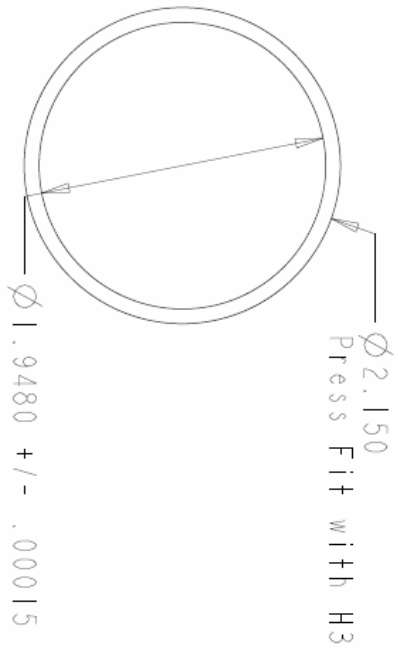
0.001

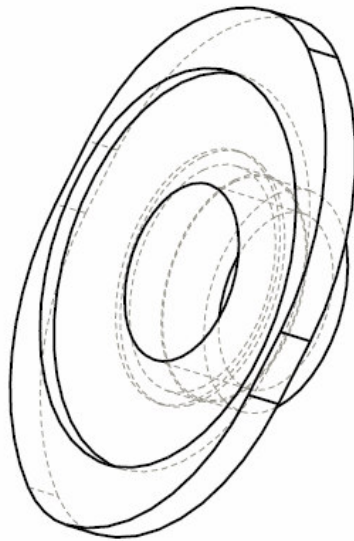
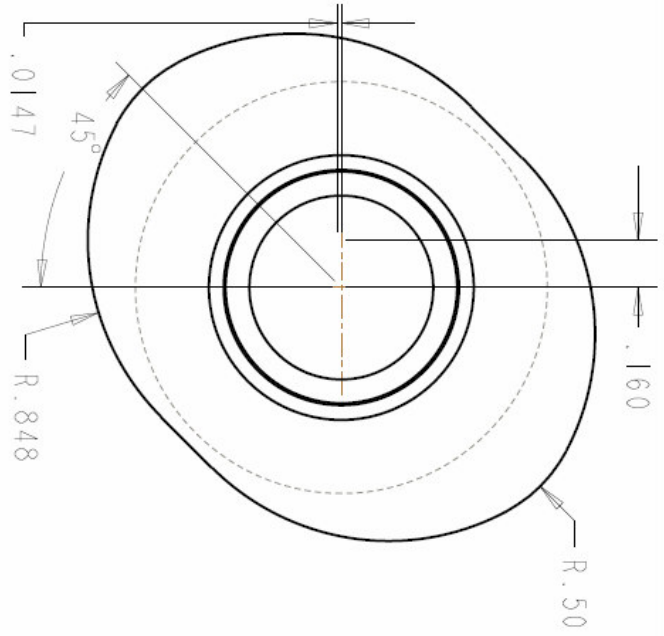
0.002

DETAIL END  
SCALE 10.000

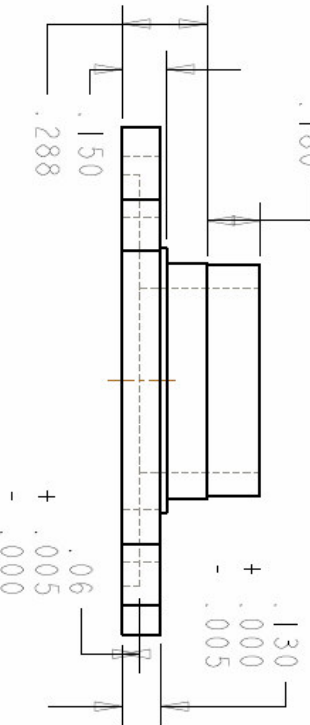
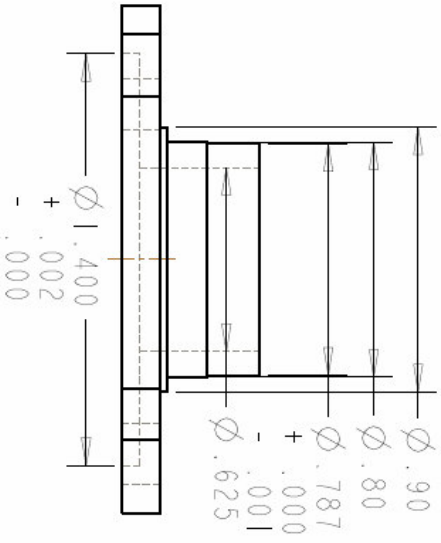


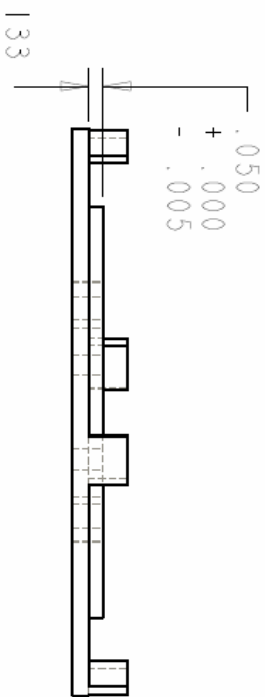
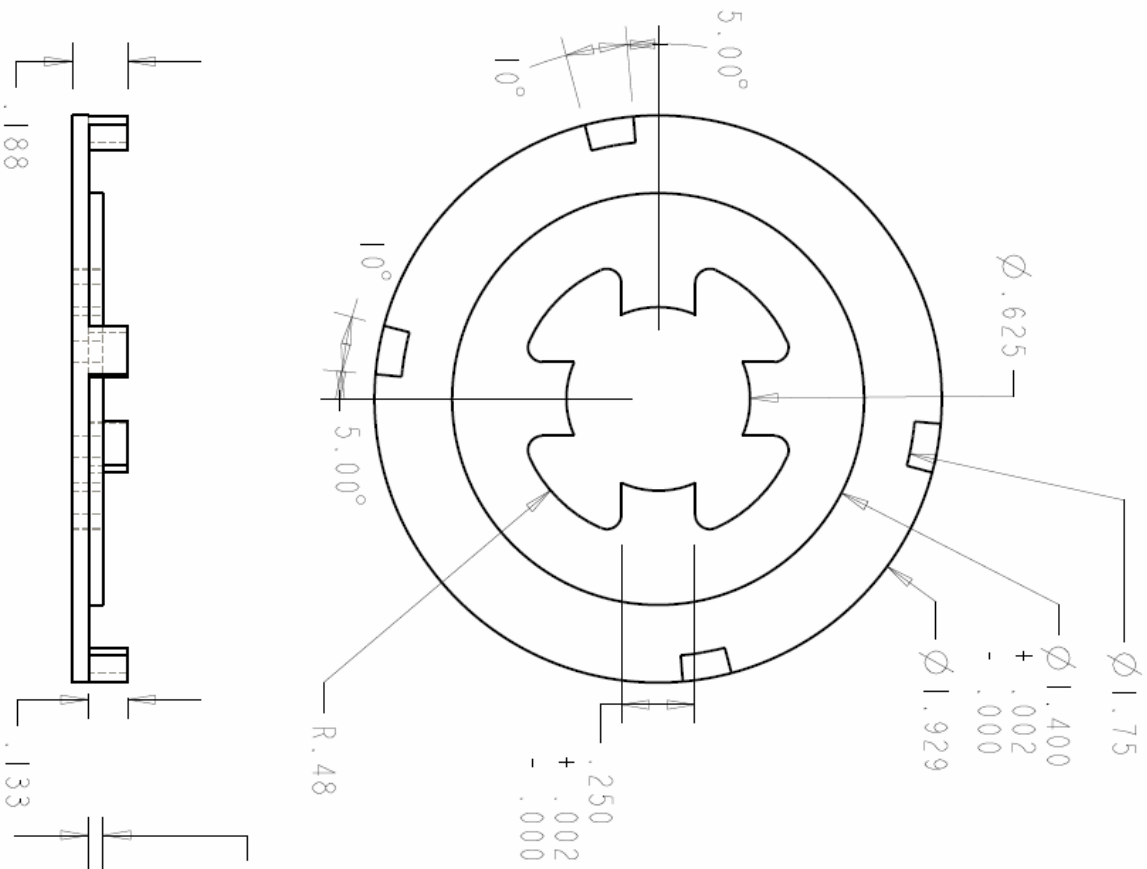
Casing  
Jon Sensinger 12/13/04  
Material: Hardened Steel  
Units: Inches  
Scale: 1





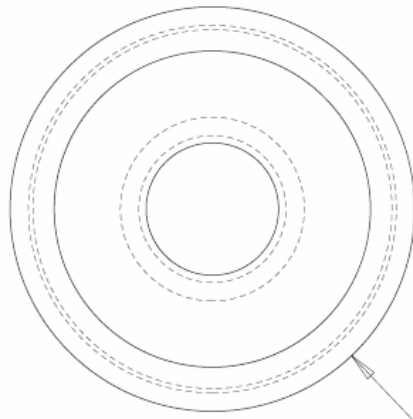
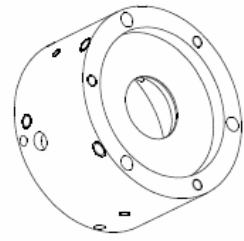
Cam Output  
 Sensinger: NUPRL, 07/11/06  
 Material: Hardened Steel  
 Units: Inches  
 Scale: 2  
 Tolerances: +/- .001 for .XXX  
 +/- .005 for .XX  
 unless otherwise noted



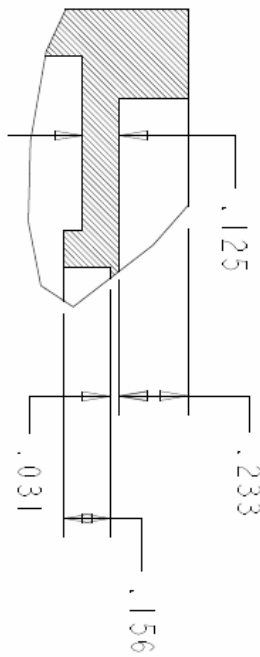
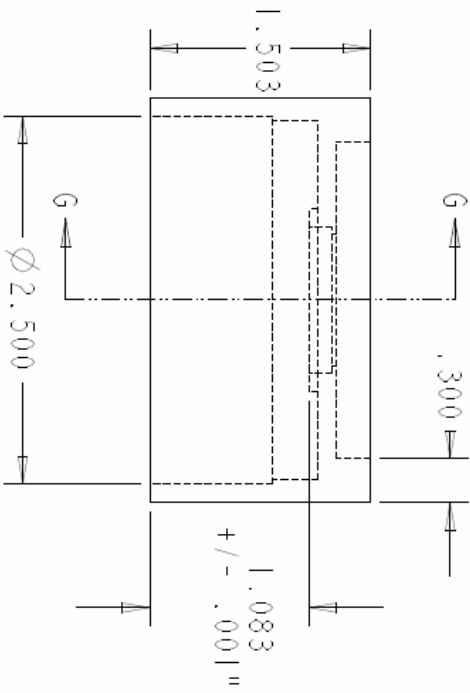


Cam Input  
 Sensinger: NUPRL, 07/11/06  
 Material: Hardened Steel  
 Units: Inches  
 Scale: 2  
 Tolerance: +/- .001 for .XXX  
 +/- .005 for .XX  
 unless otherwise noted

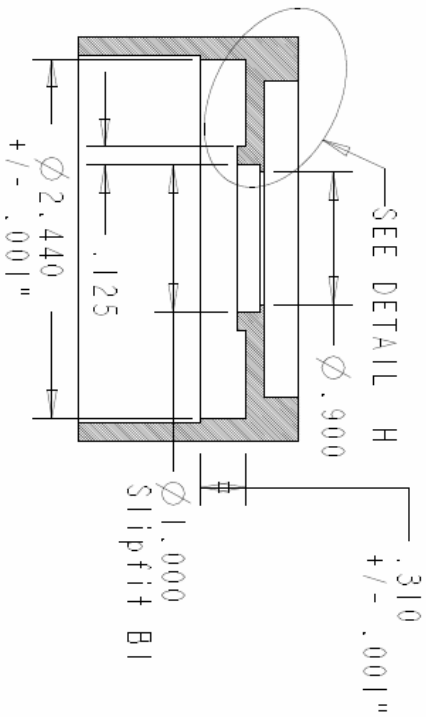




$\phi 2.750$

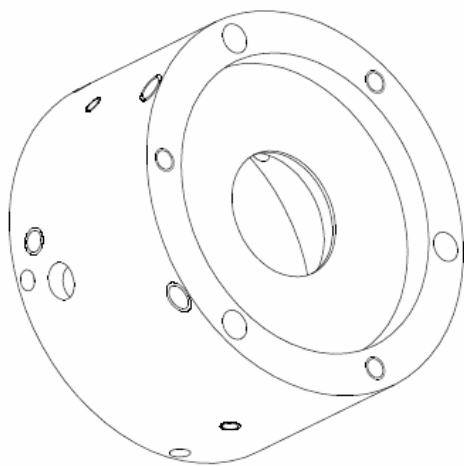
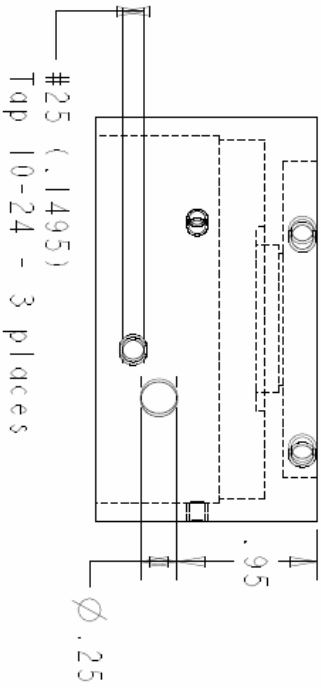
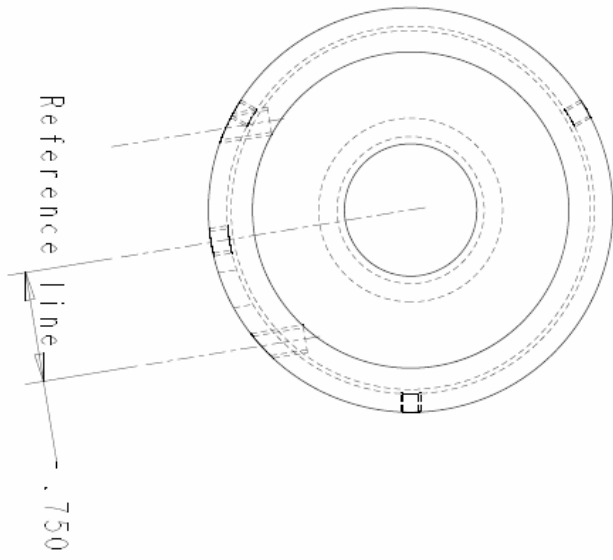


DETAIL H  
 SCALE 2.000

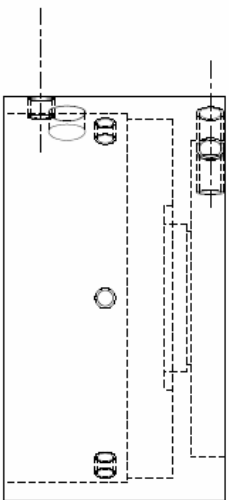


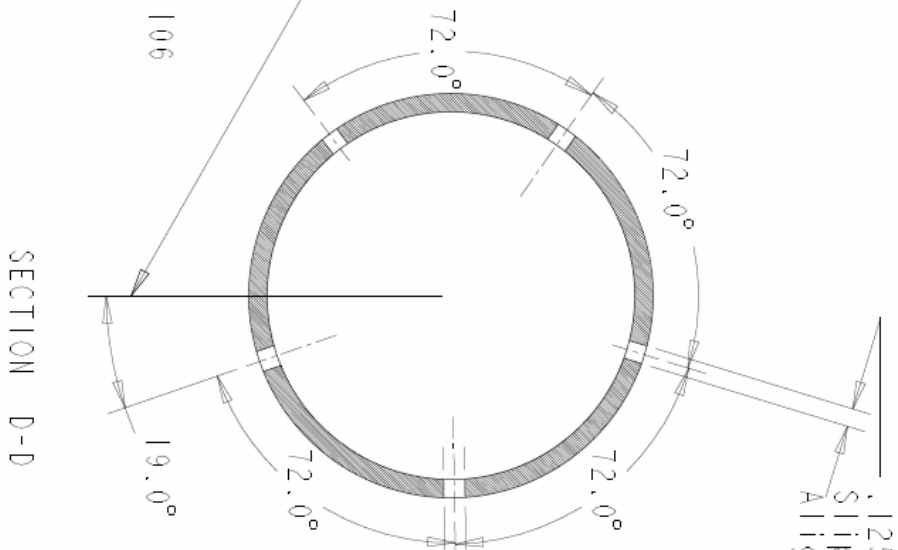
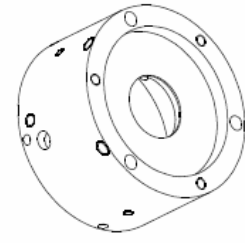
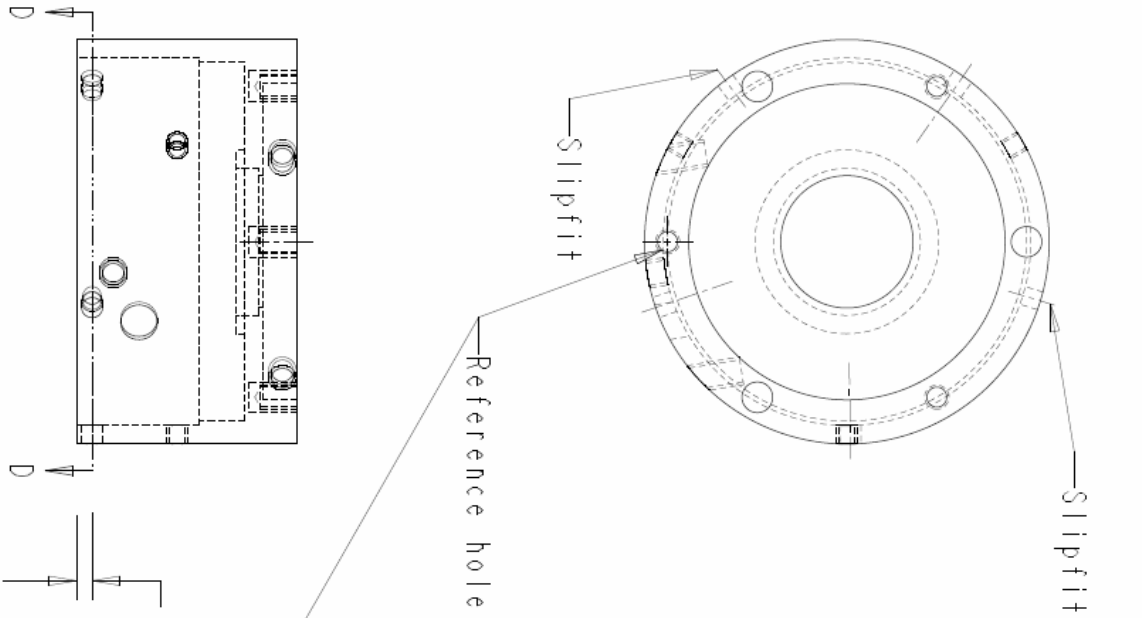
SECTION G-G

Actuator Housing  
 H3 Housing Motor  
 Jon Sensinger 12/13/04  
 Material: Aluminum  
 Units: Inches  
 Scale: 1  
 Drawing 1 of 5



Actuator Housing  
H3 Housing Motor  
Jon Sensinger 12/13/04  
Material: Aluminum  
Units: Inches  
Scale: 1  
Drawing 2 of 5



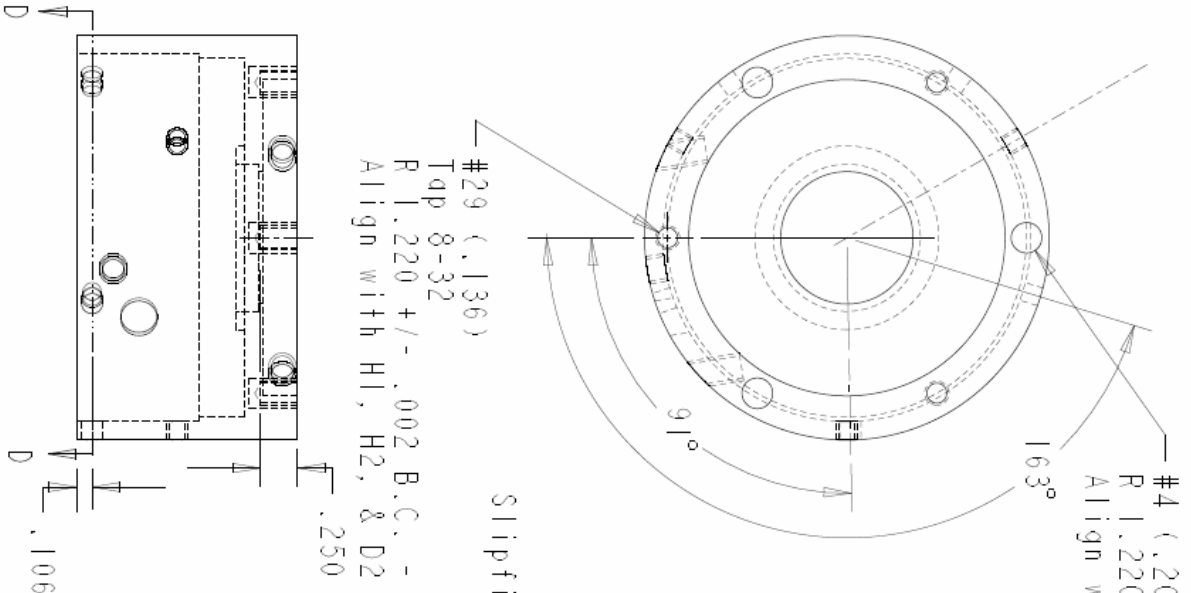


#27 (.144)  
Clearance Hole  
- 3 places  
Align with H4

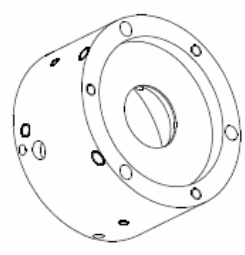
.125  
Slipfit dowel - 2 places  
Align with H4

Actuator Housing  
H3 Housing Motor  
Jon Sensinger 12/13/04  
Material: Aluminum  
Scale: Inches  
Scale: 1  
Drawing 3 of 5





Actuator Housing  
H3 Housing Motor  
Jon Sensinger 12/13/04  
Material: Aluminum  
Scale: Inches  
Scale: 1  
Drawing 4 of 5

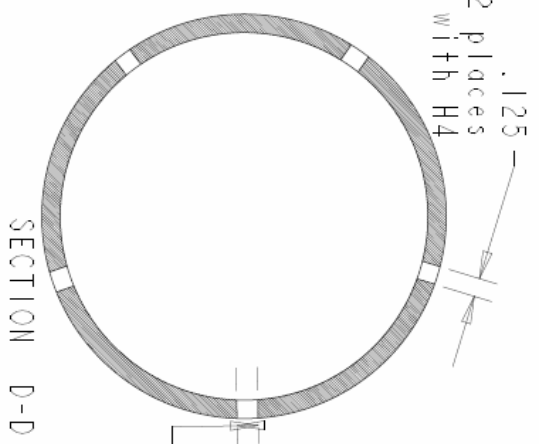


Slipfit dowel - 2 places  
Align with H4

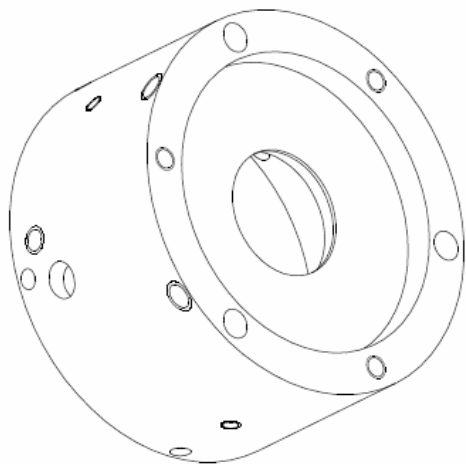
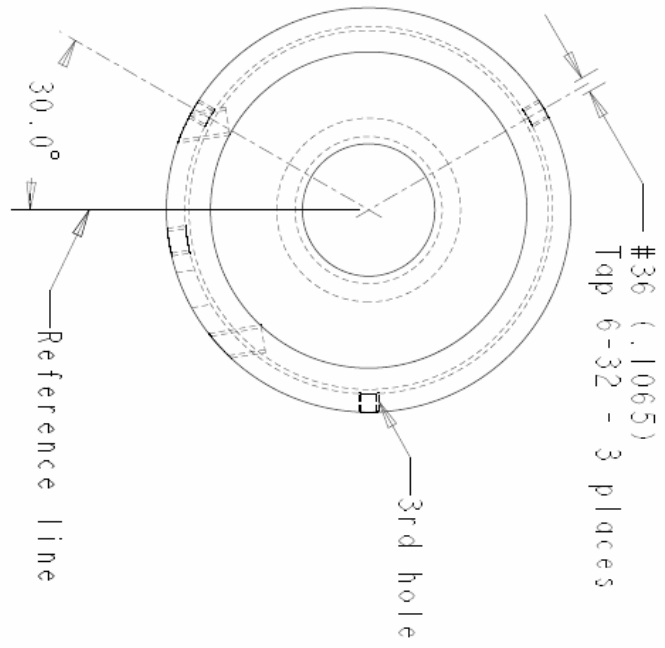
.125

.250

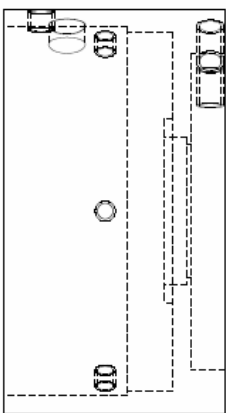
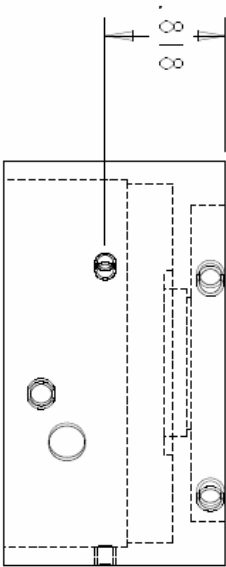
.106

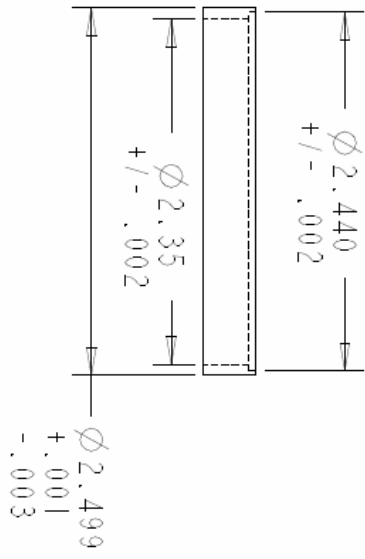
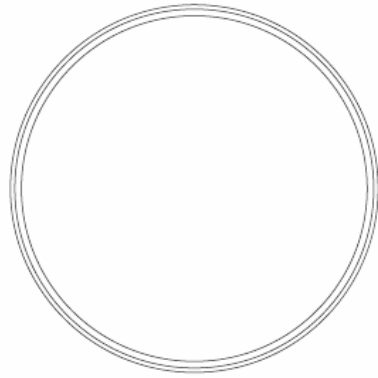


#27 (.144)  
Clearance Hole  
- 3 places  
Align with H4

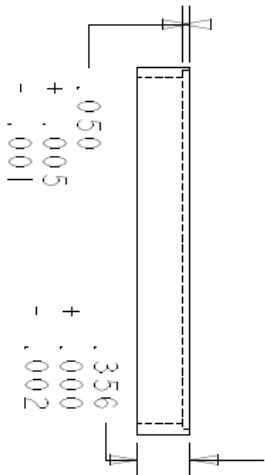
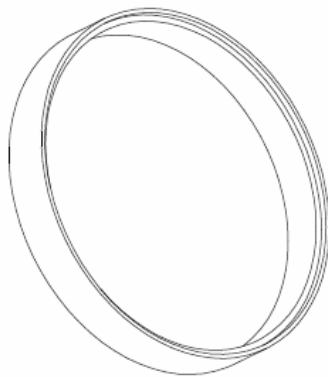


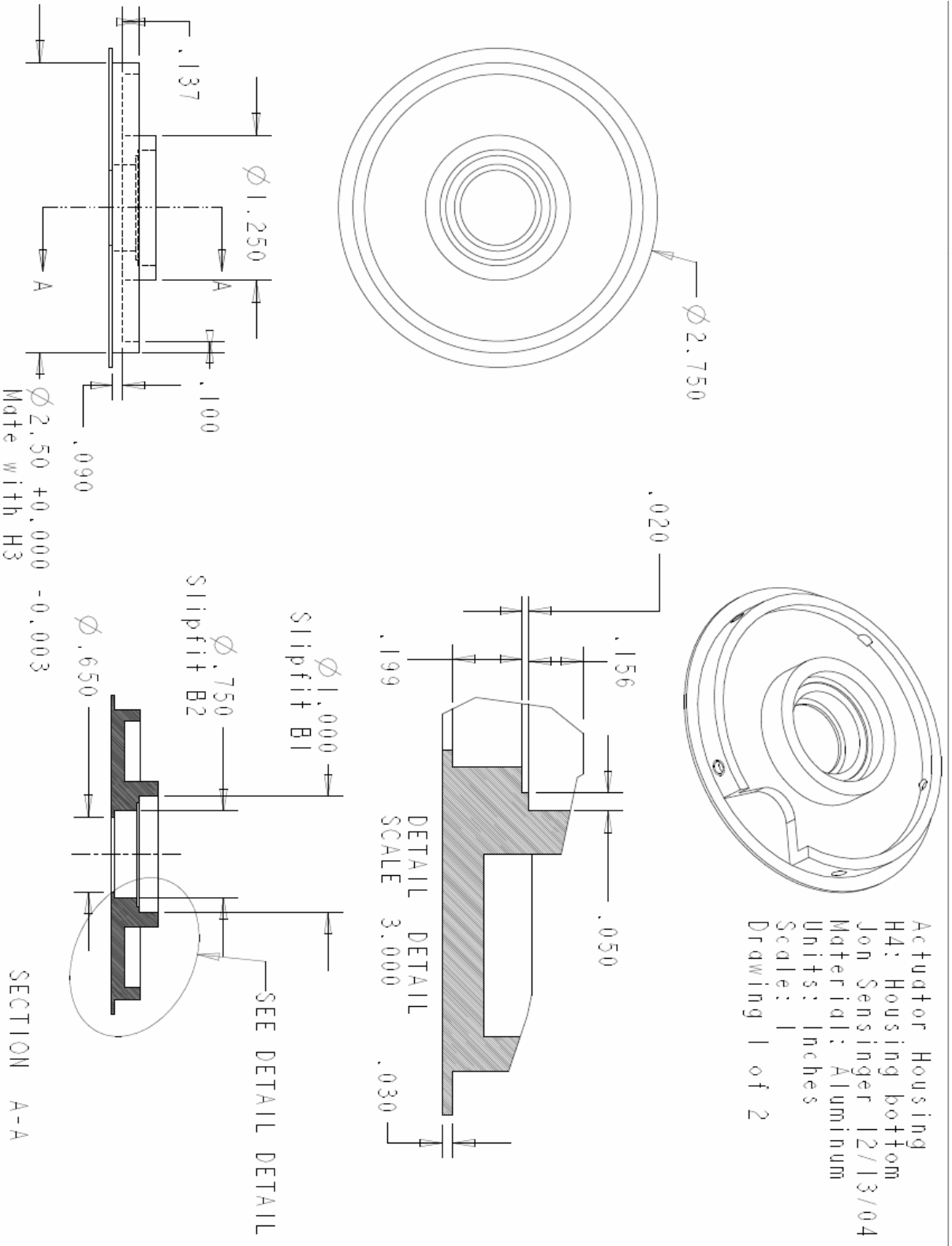
Actuator Housing  
H3 Housing Motor  
Jon Sensinger 12/13/04  
Material: Aluminum  
Units: Inches  
Scale: 1  
Drawing 5 of 5

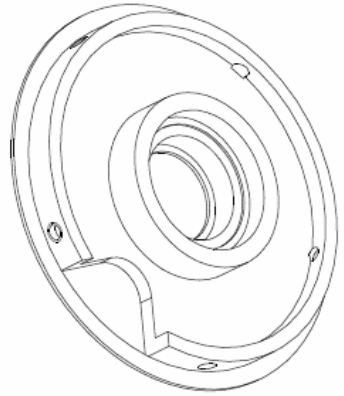
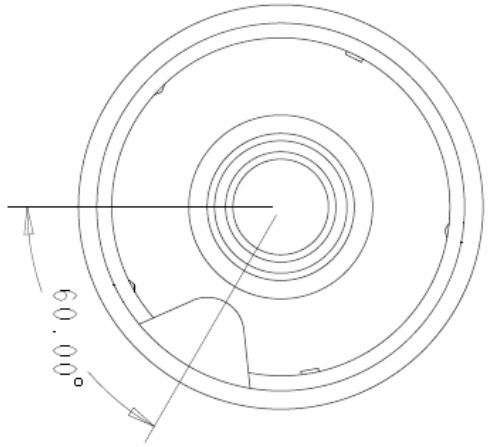




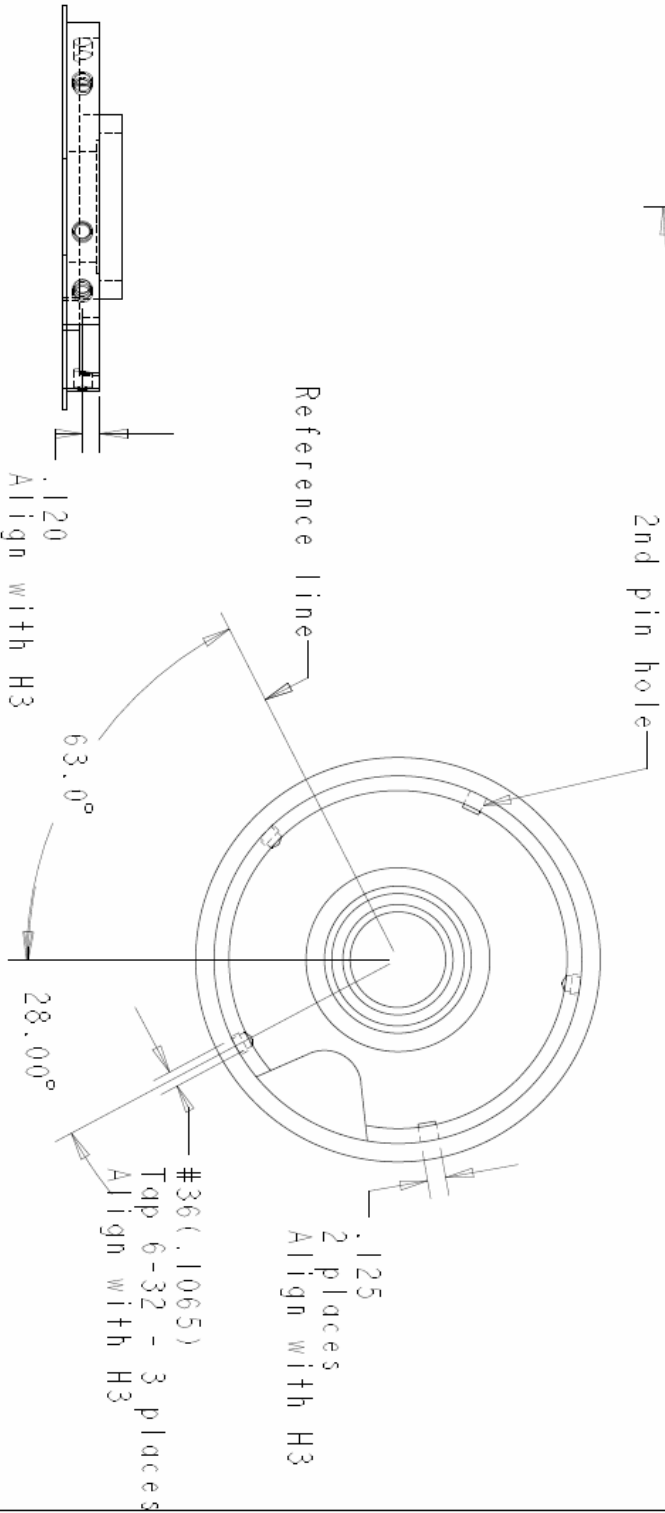
Insert  
Jon Sensinger 04/13/2006  
Material: Aluminum  
Scale: 1  
Units: Inches





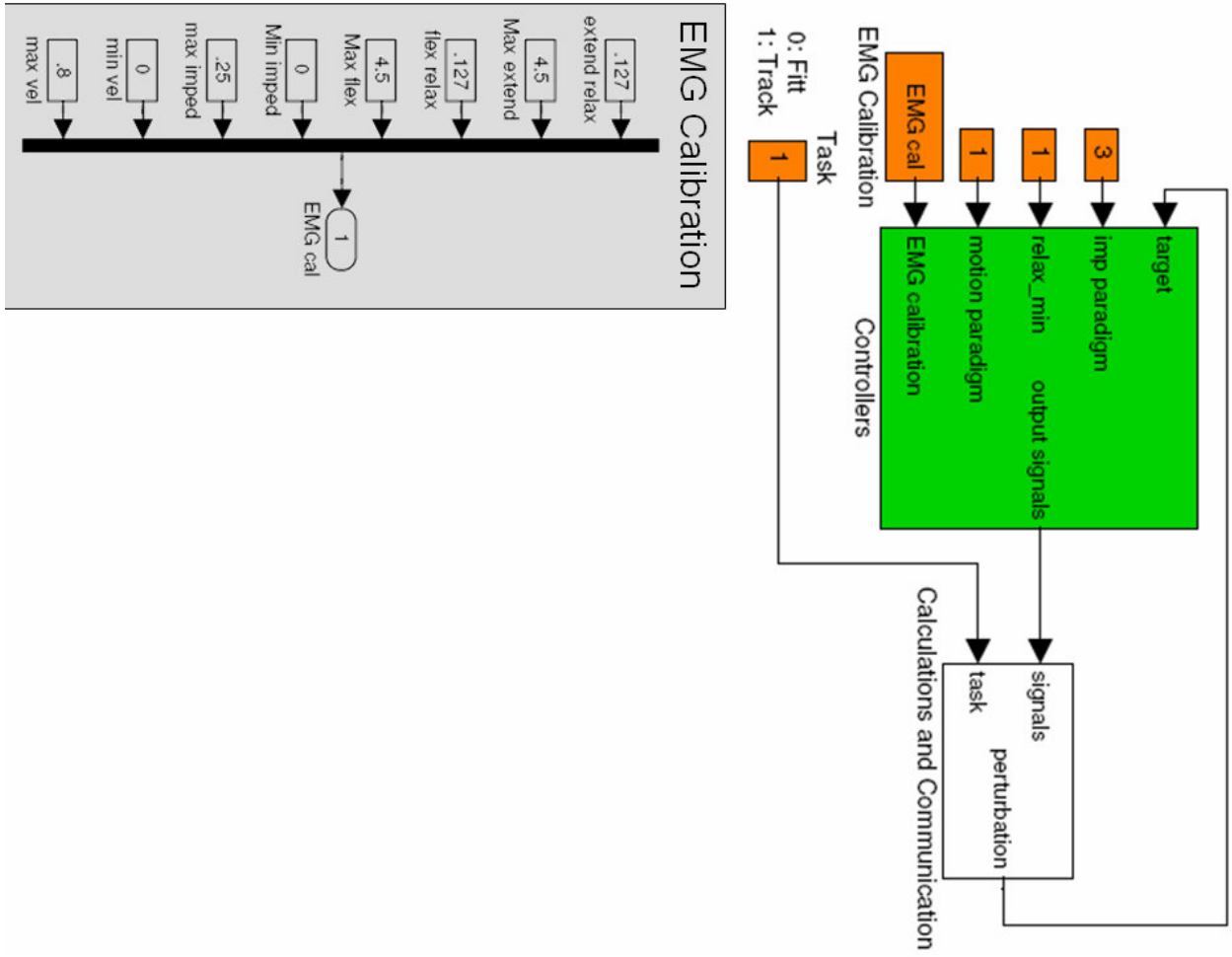


Actuator Housing  
H4: Housing bottom  
Jon Sensinger 12/13/04  
Material: Aluminum  
Units: Inches  
Scale: 1  
Drawing 2 of 2

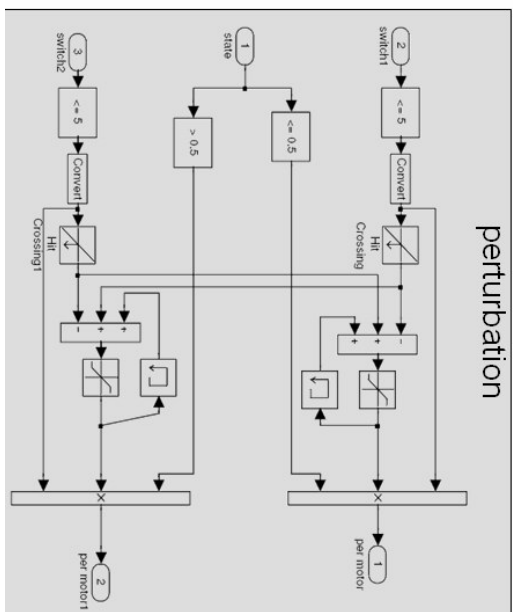
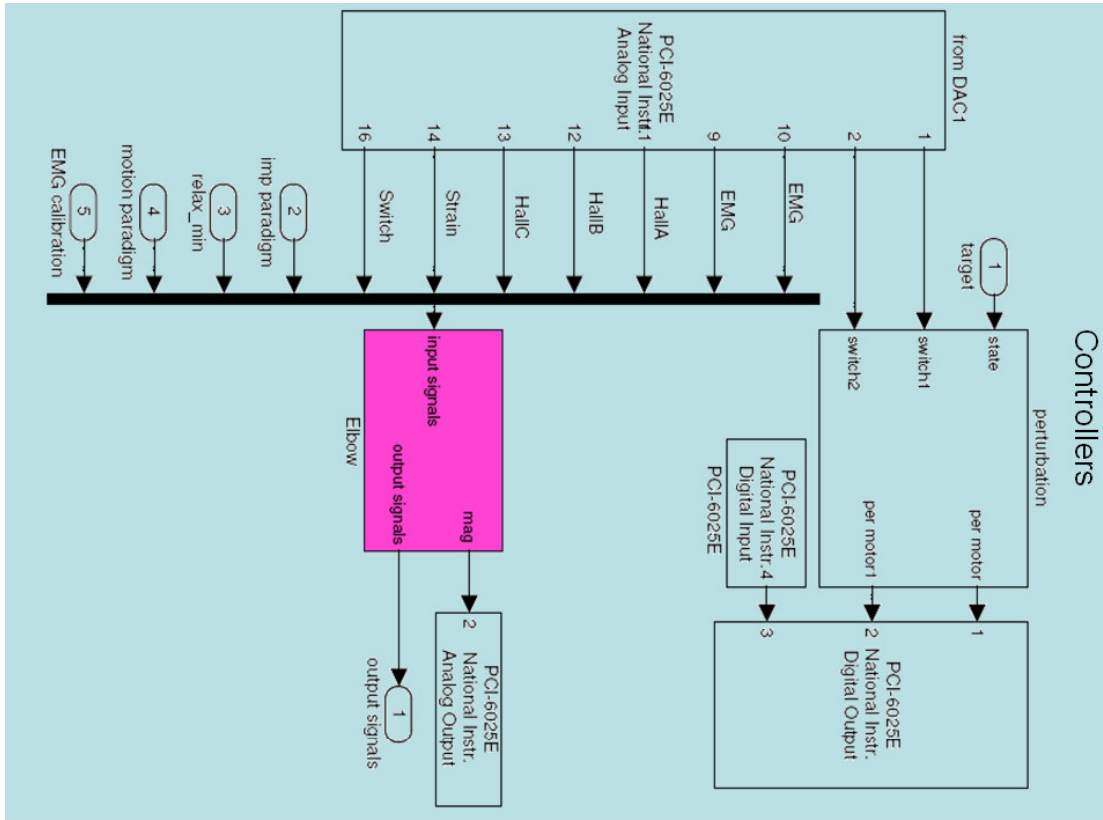


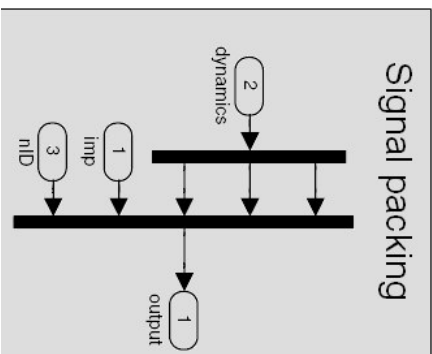
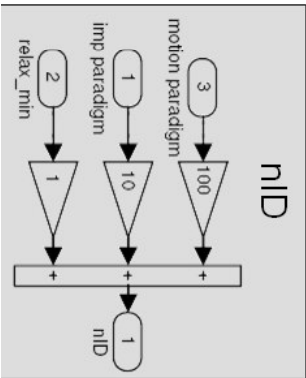
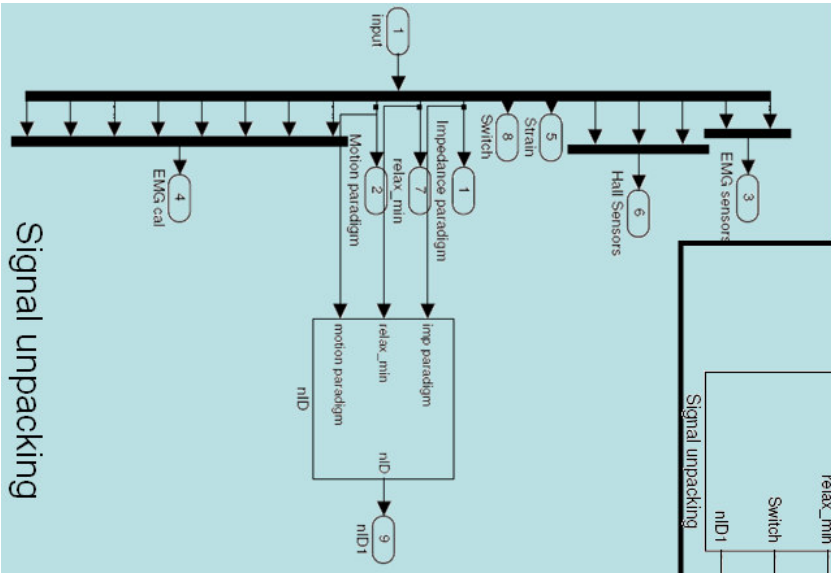
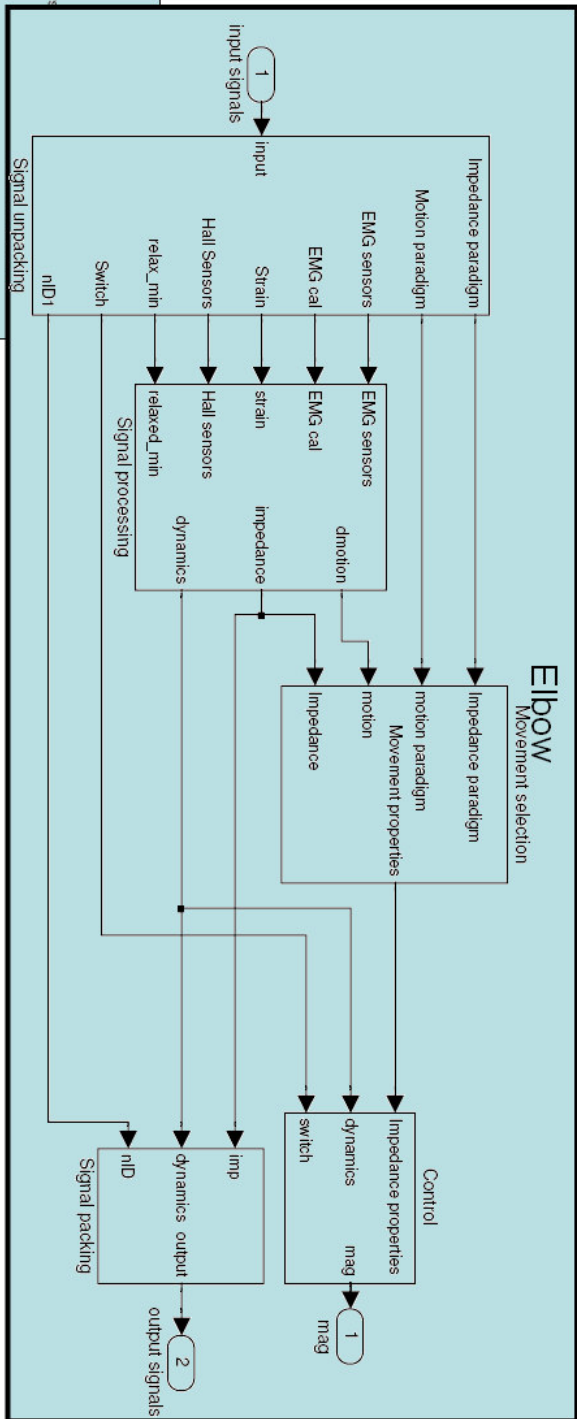


### 12.8 Pilot Matlab Control

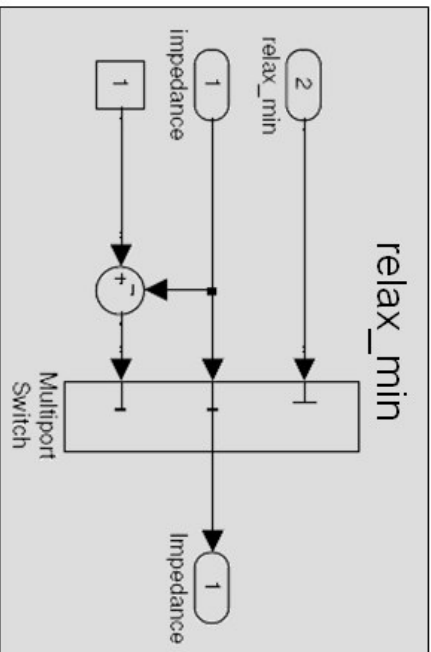
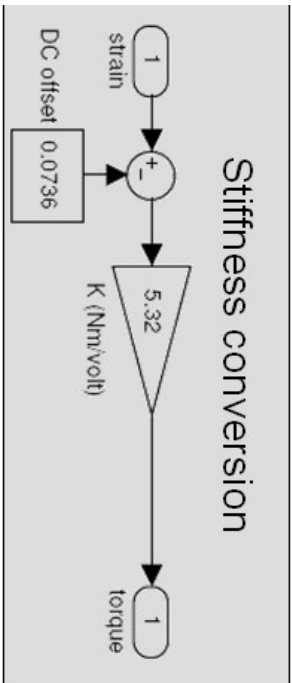
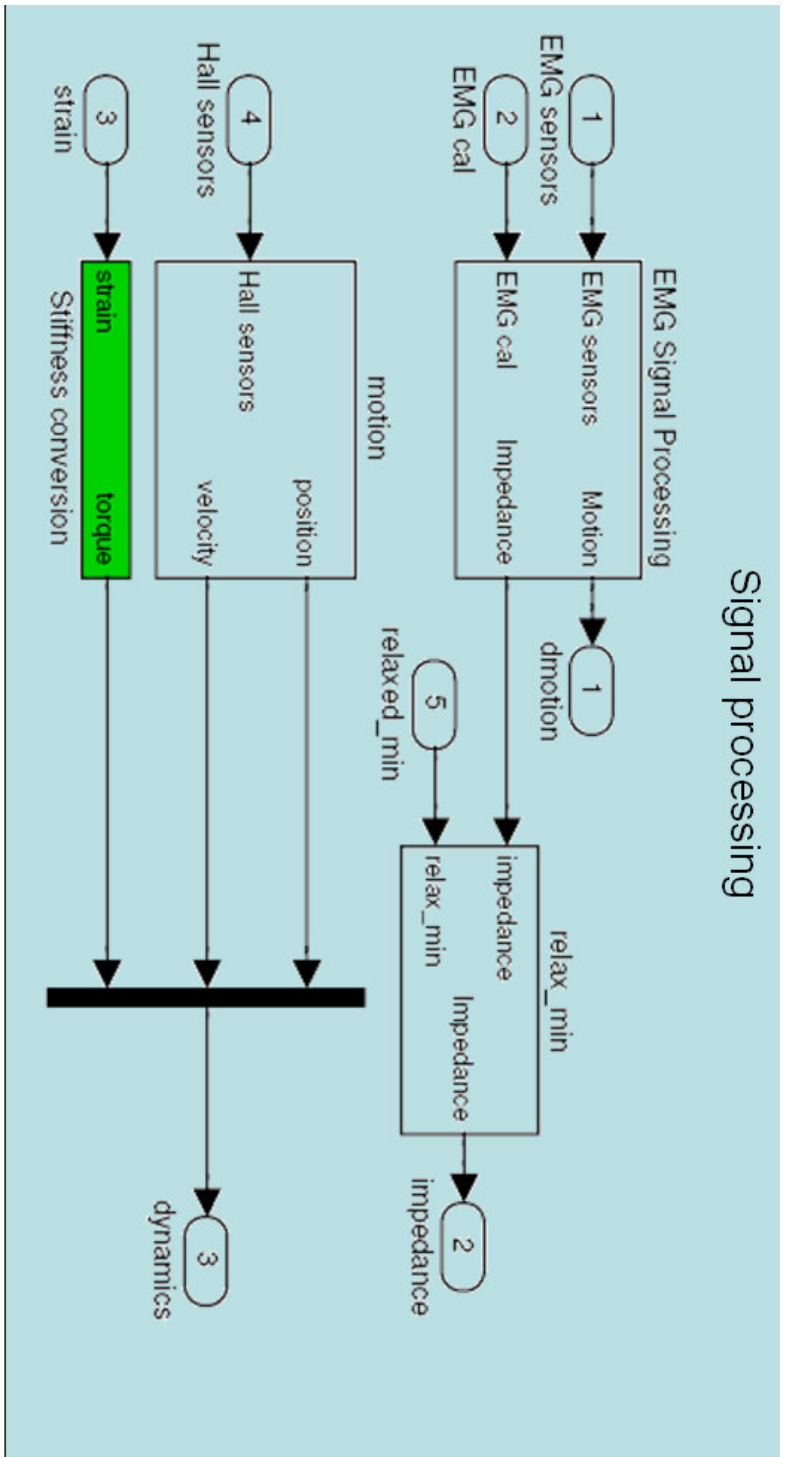


### 12.8.1 Controllers

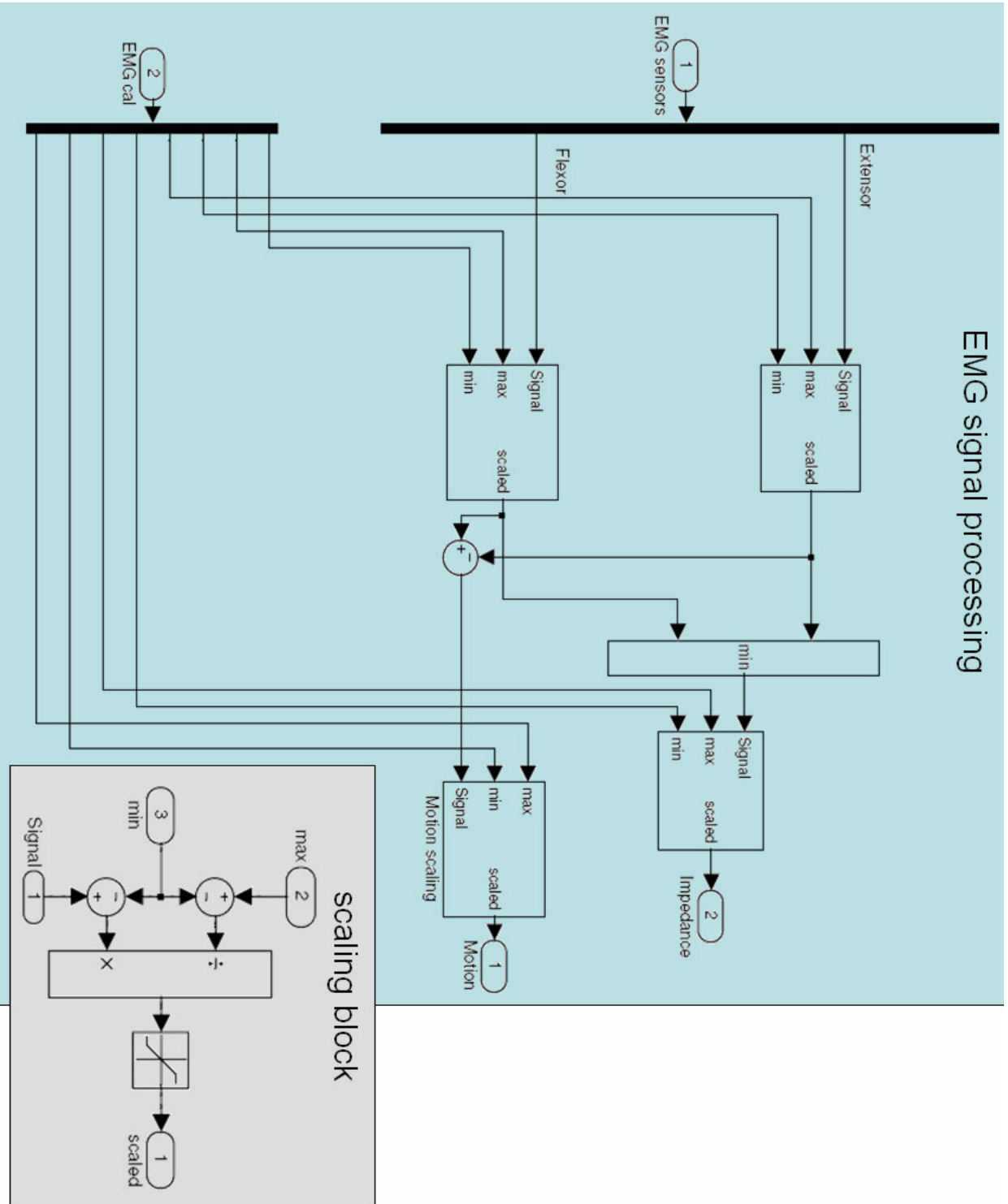


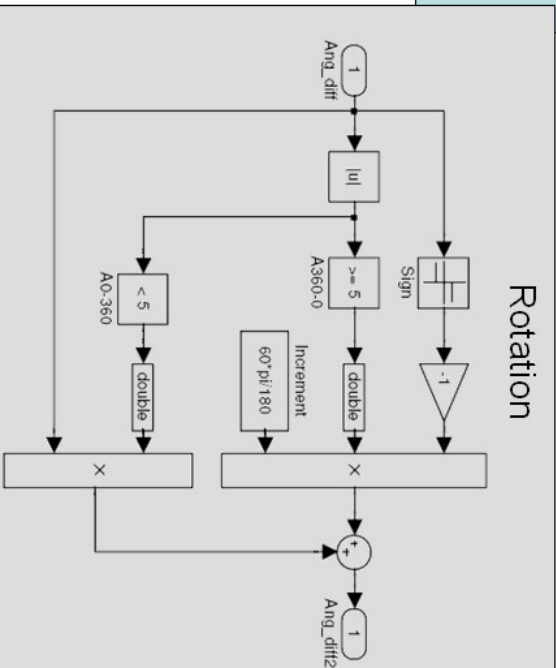
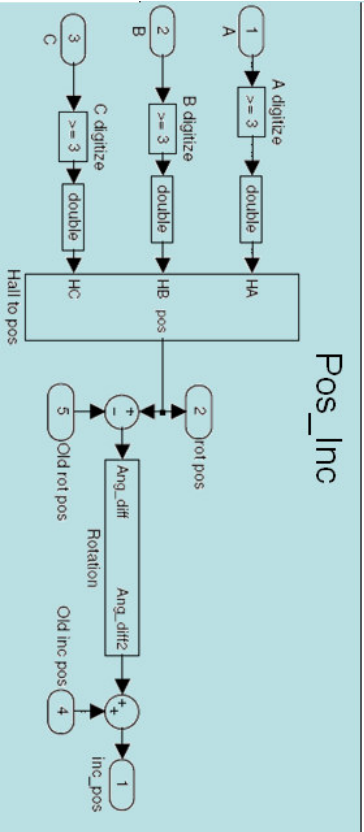
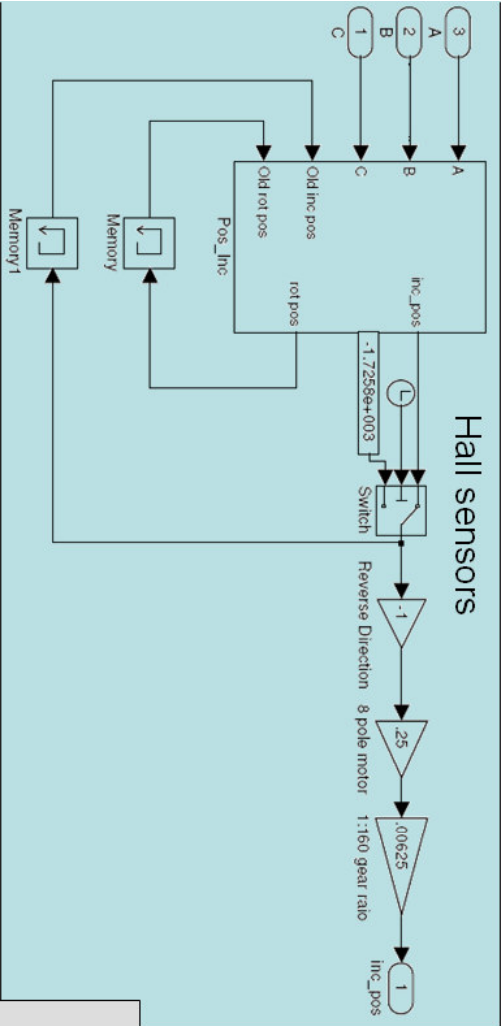
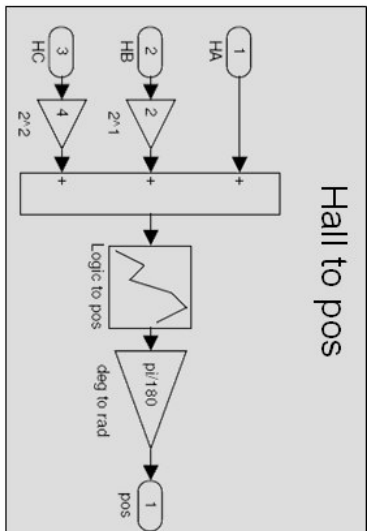
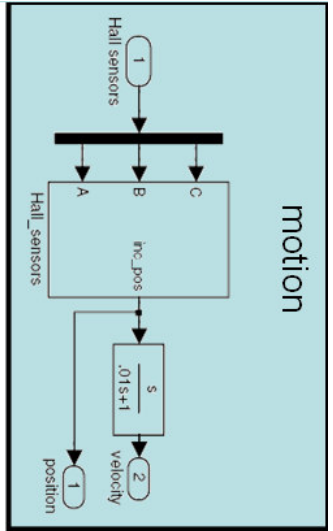


12.8.1.1 Signal Processing

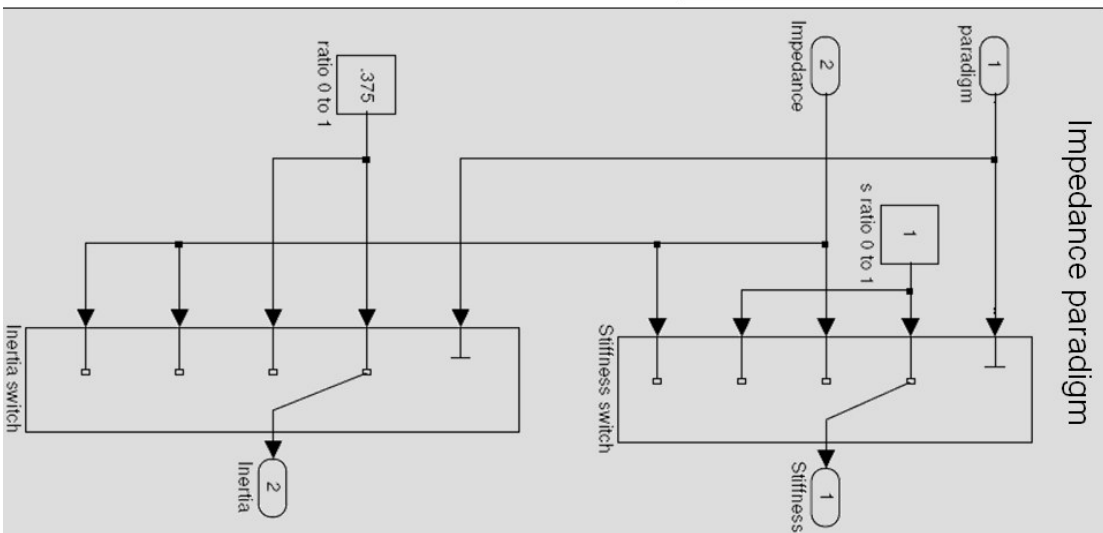
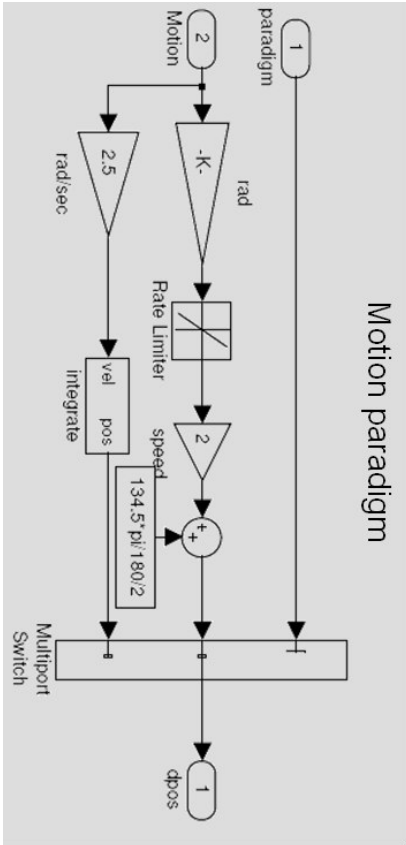
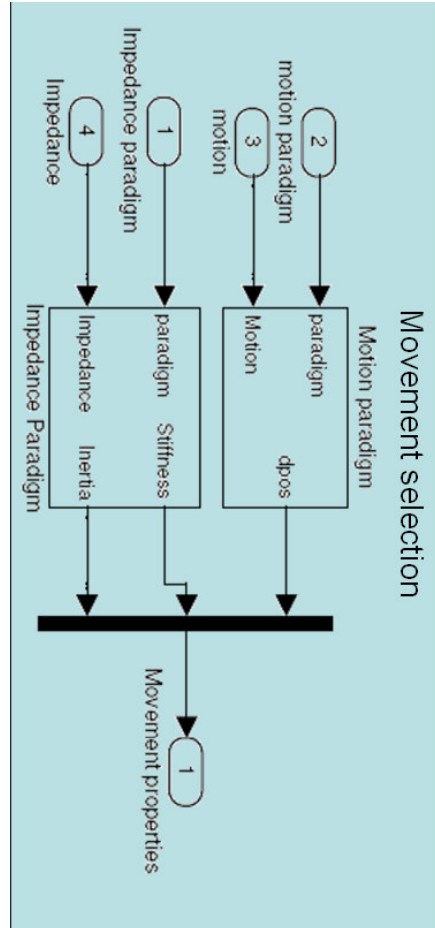


# EMG signal processing

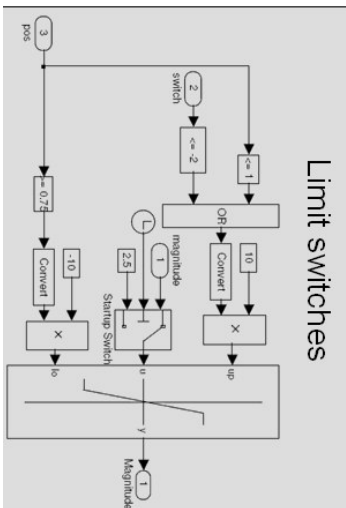
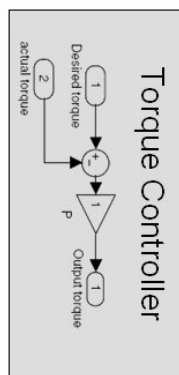
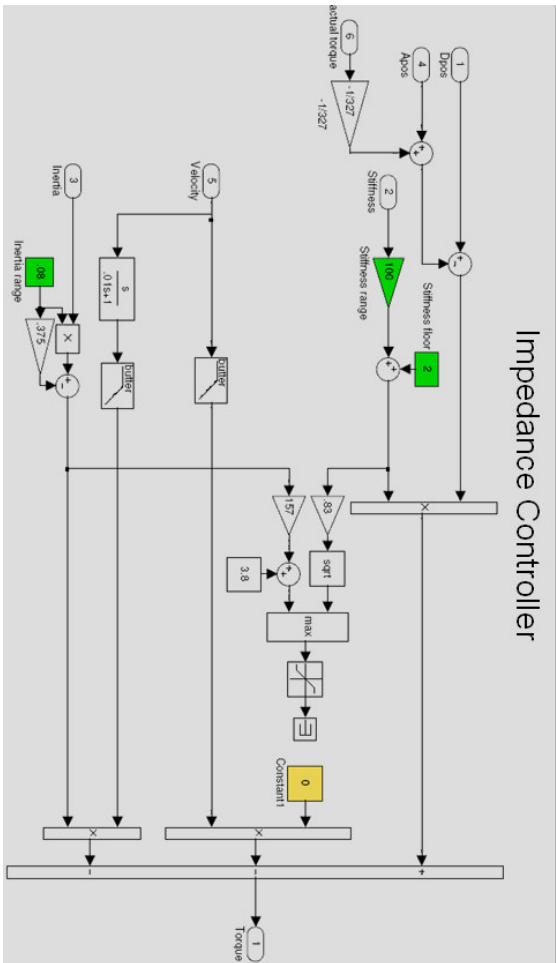
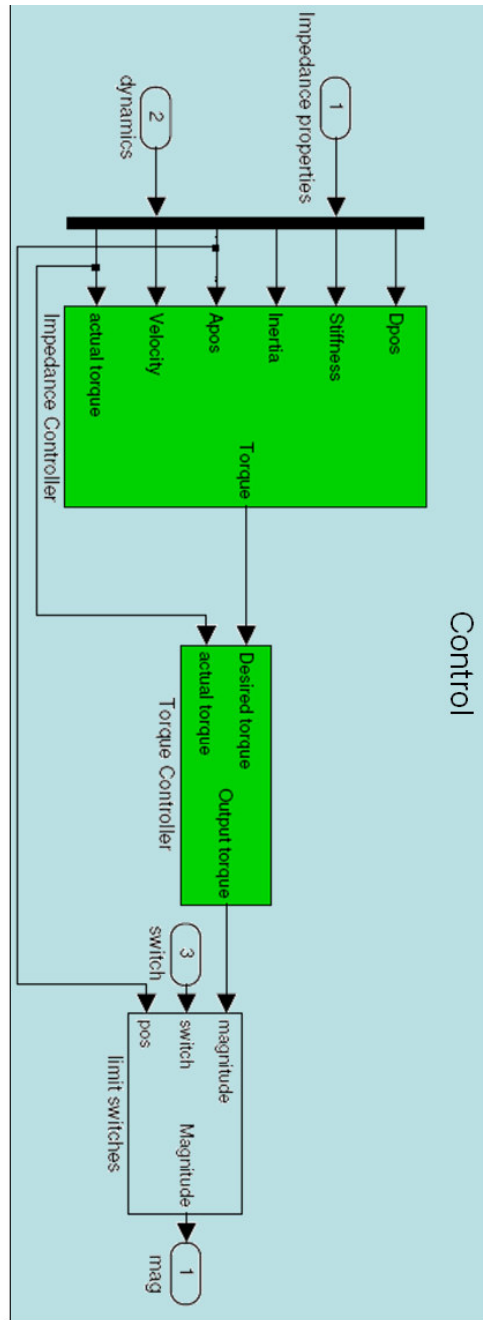




12.8.1.2 Movement selection

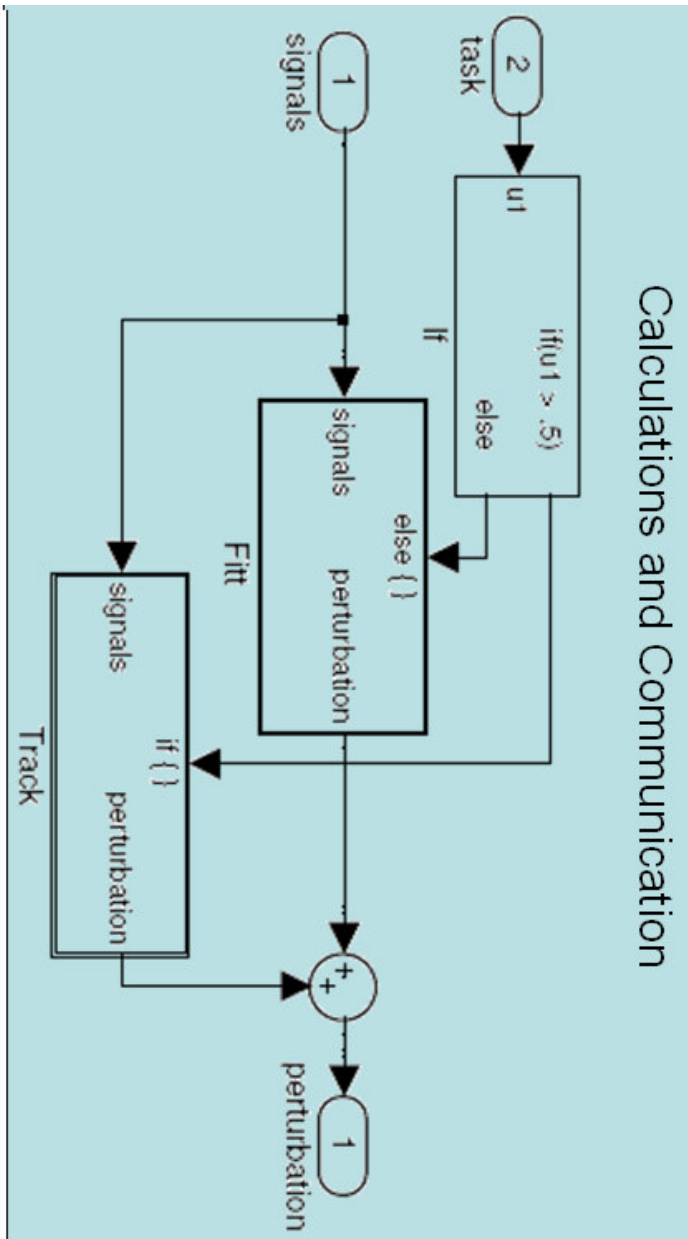


### 12.8.1.3 Control

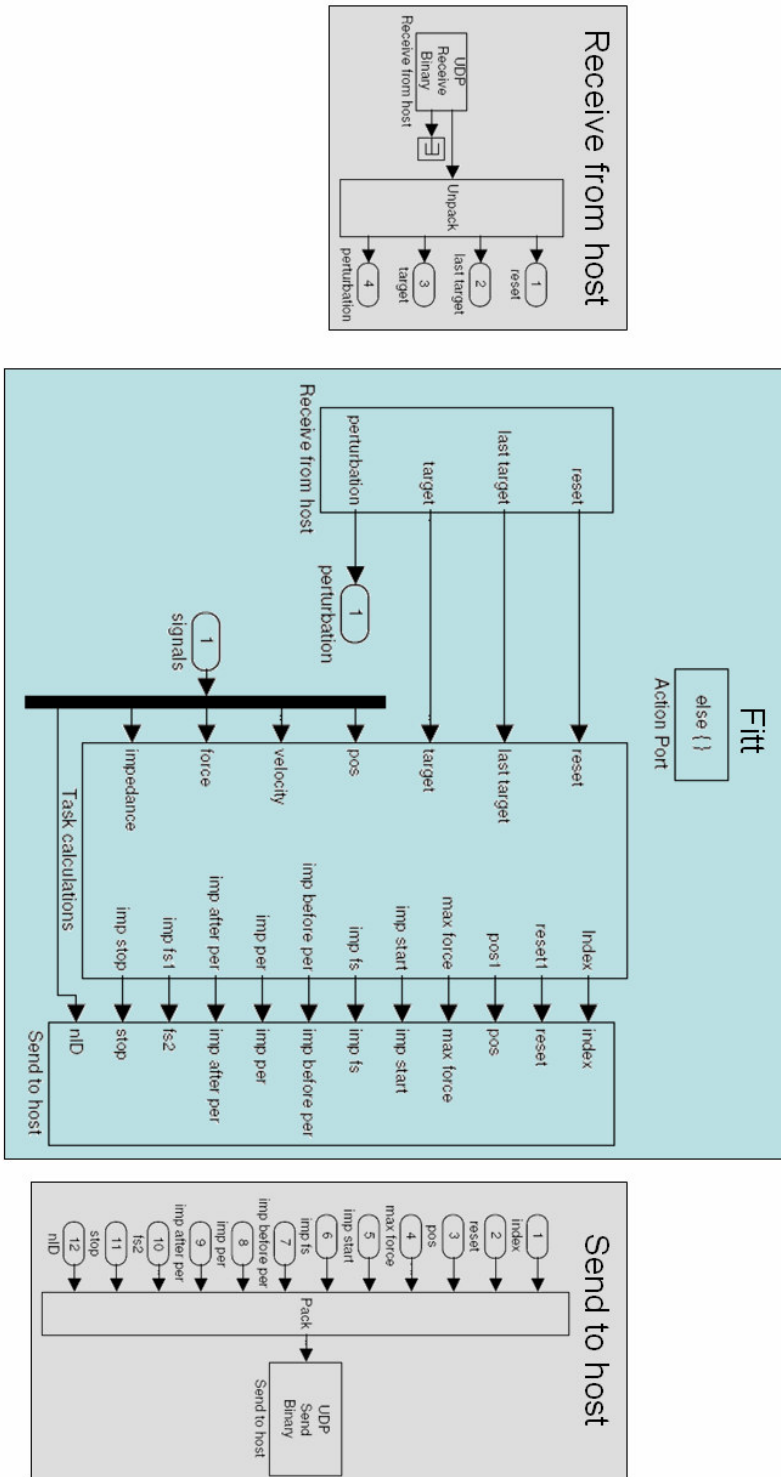


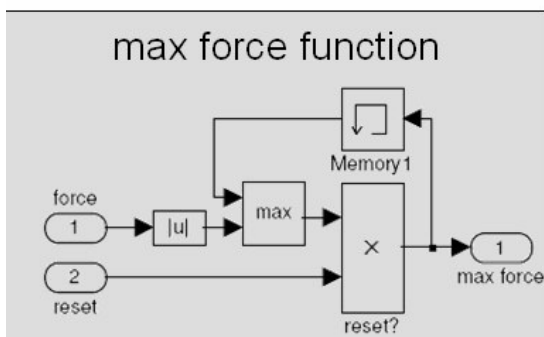
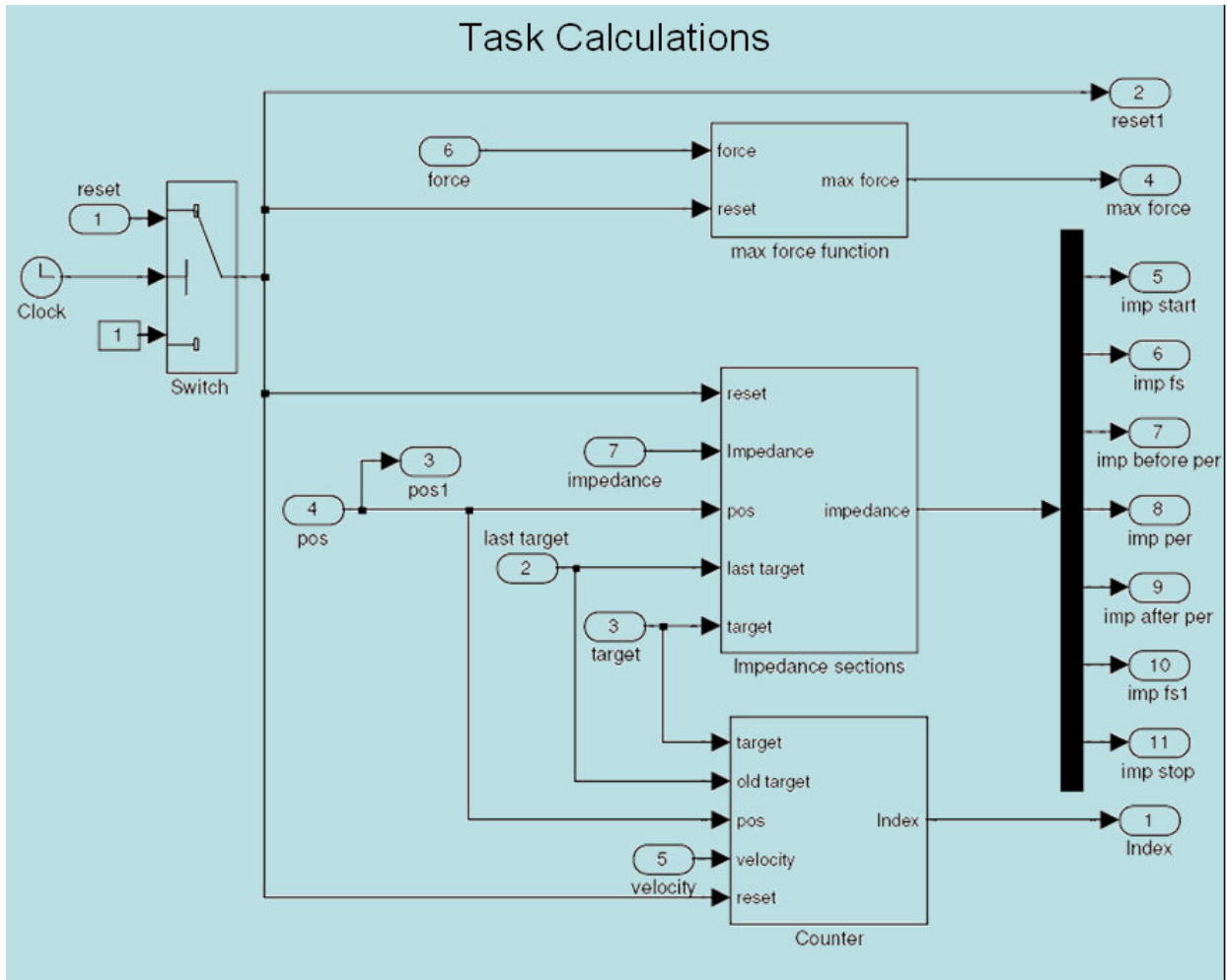


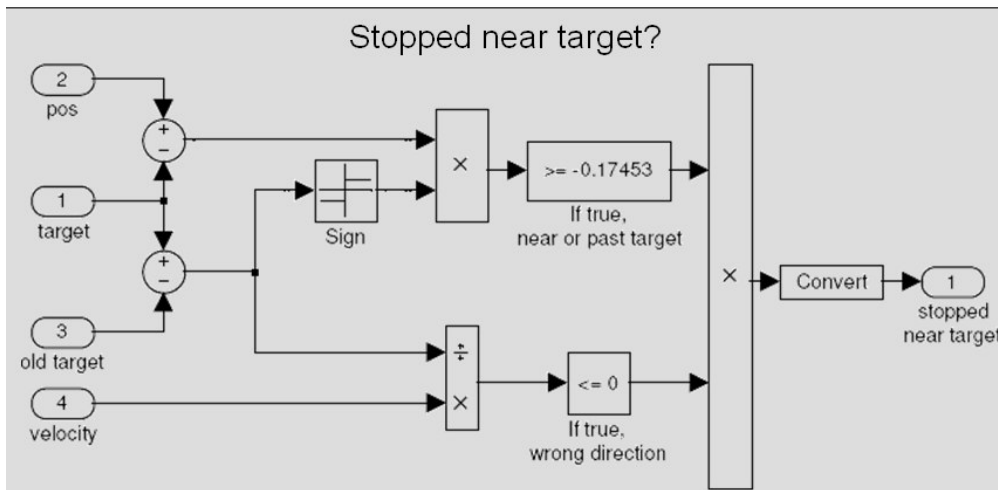
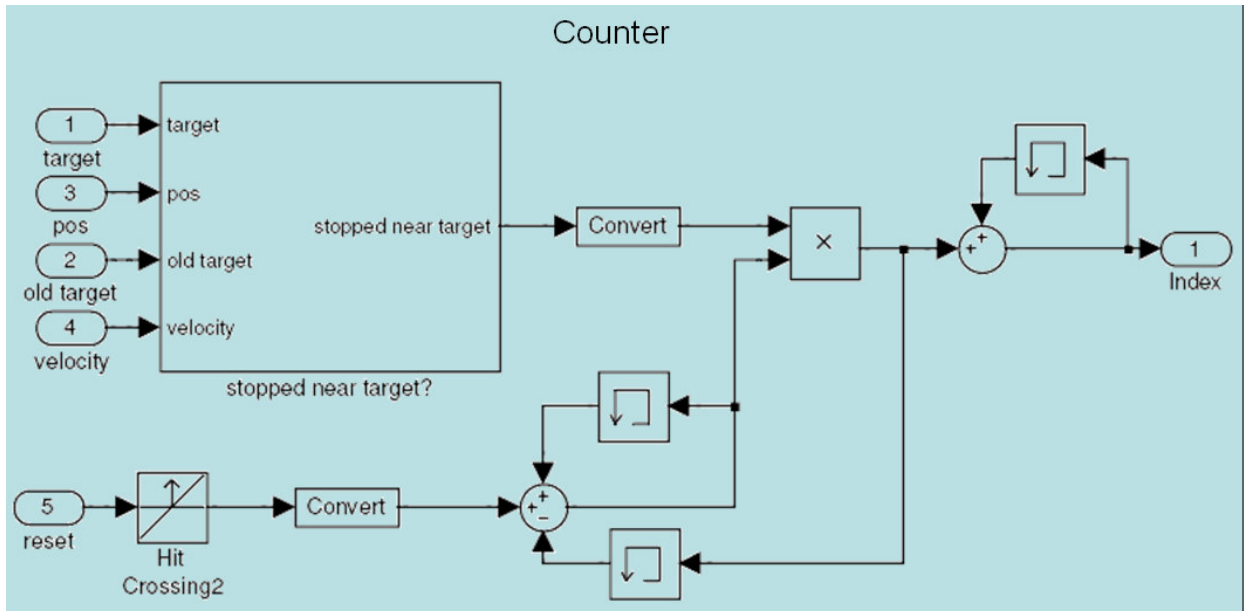
## 12.8.2 Processing

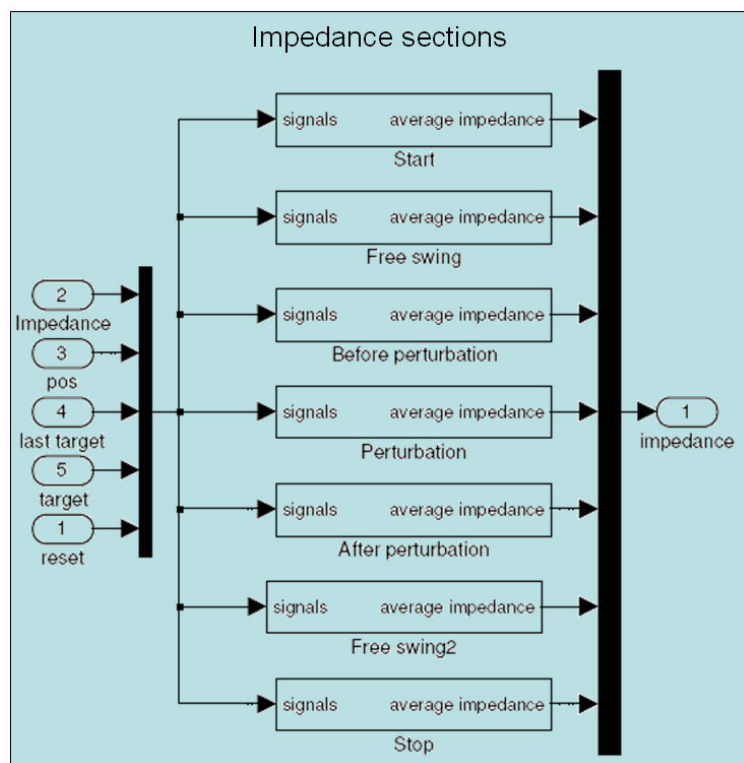


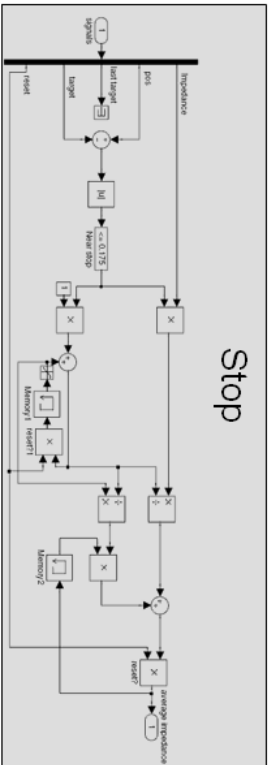
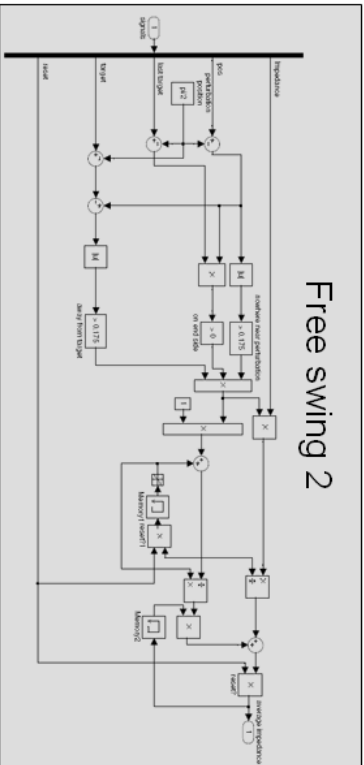
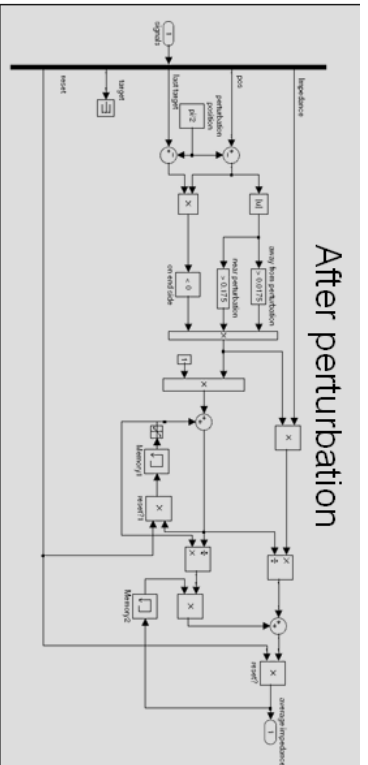
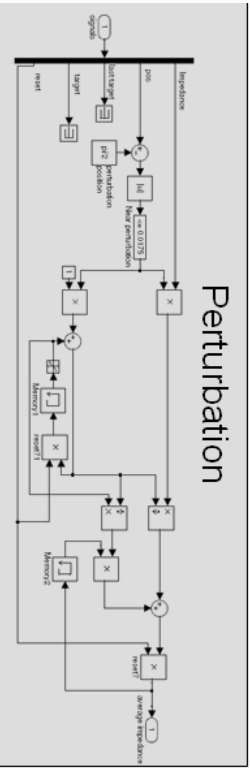
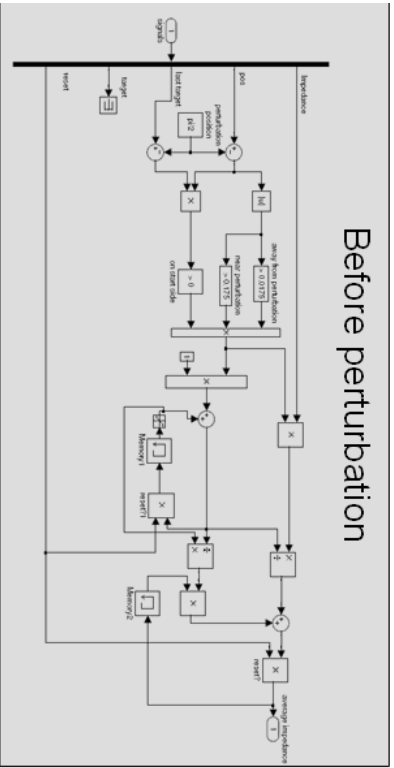
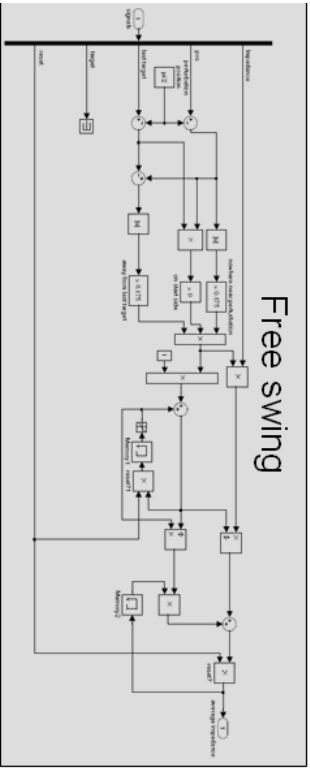
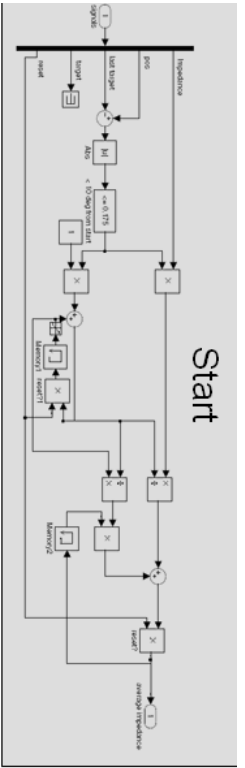
### 12.8.2.1 Fitt



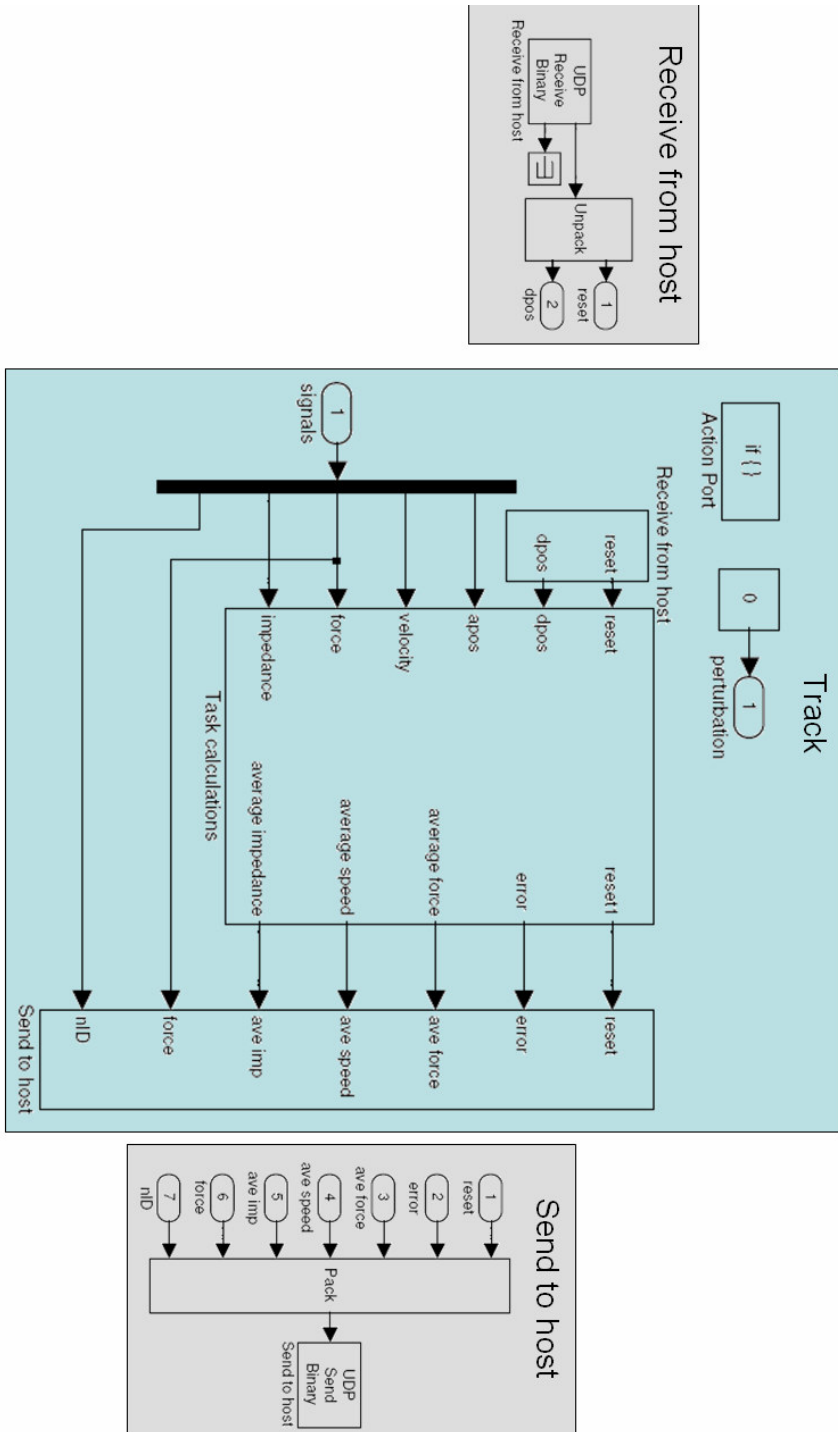


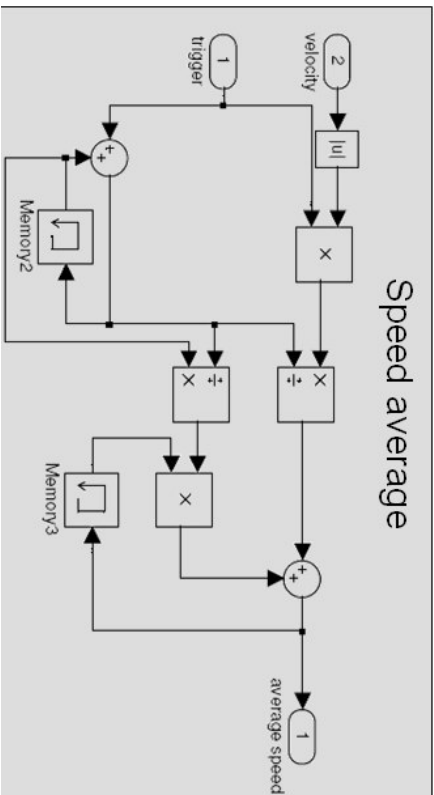
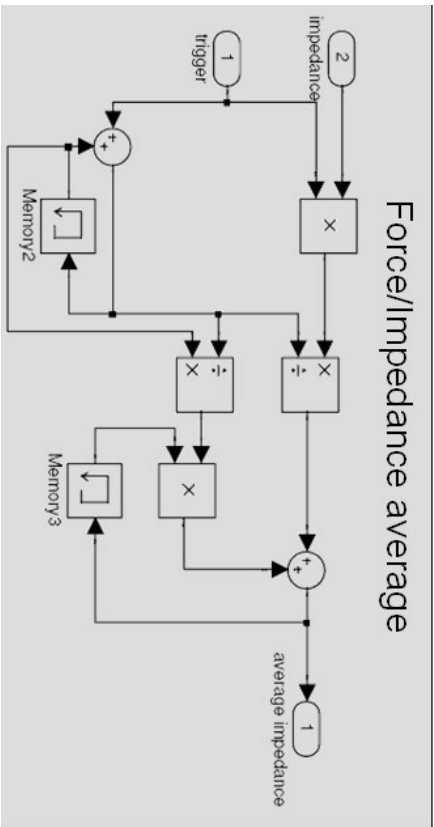
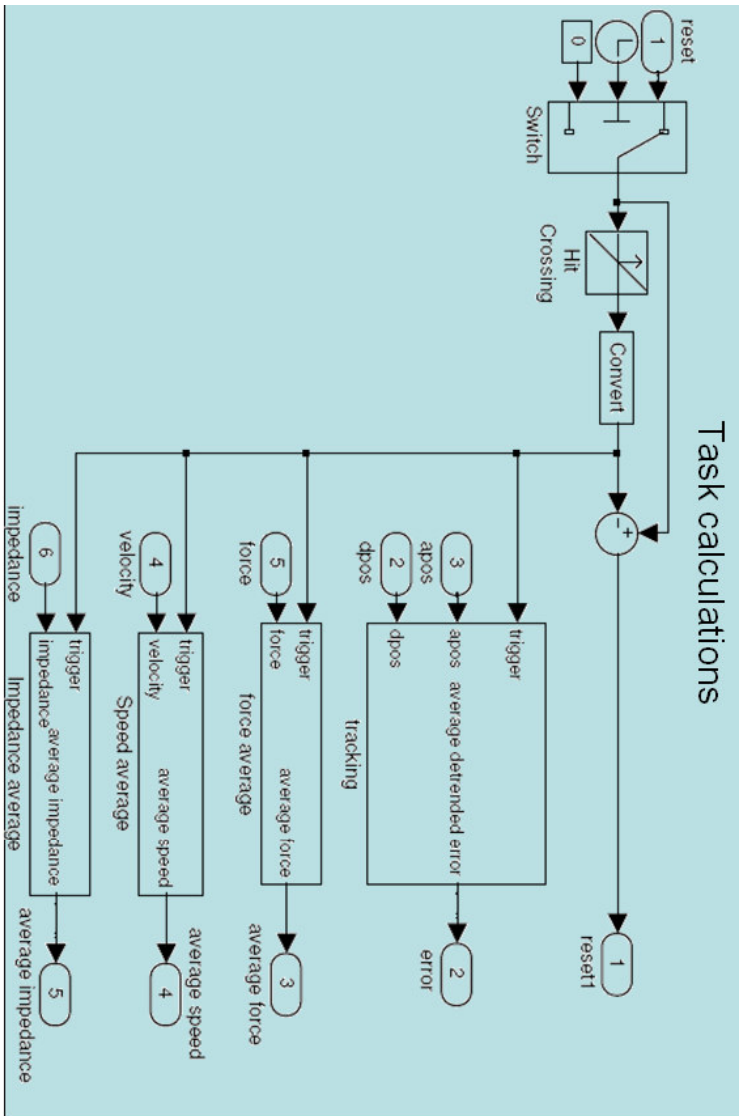




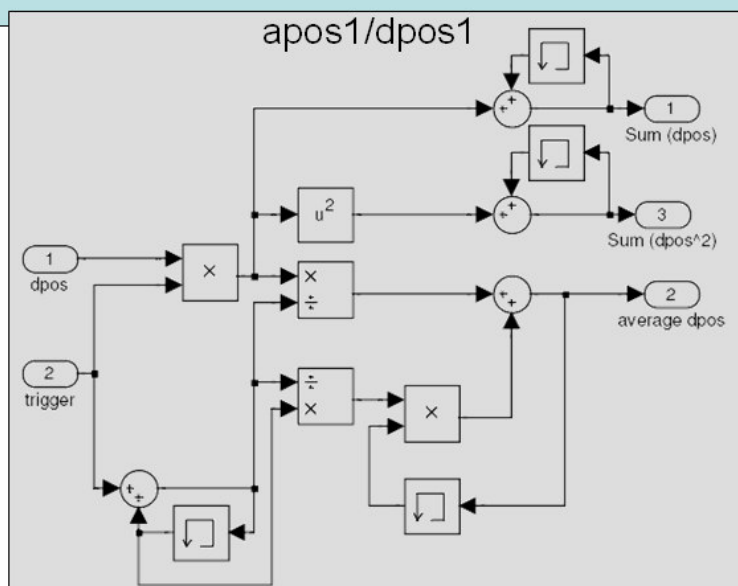
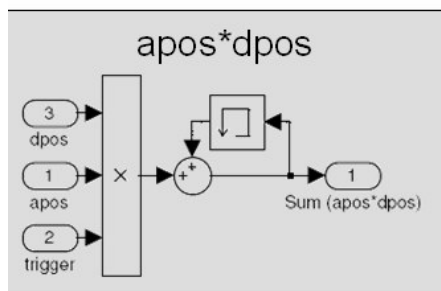
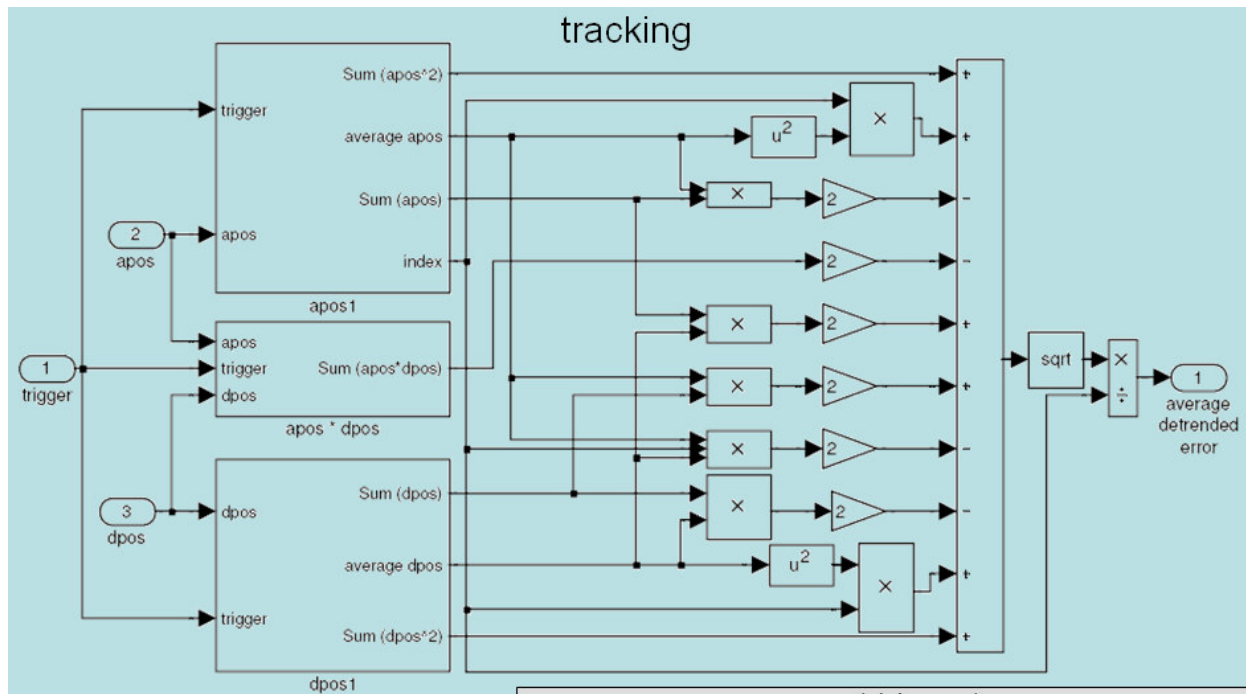


### 12.8.2.2 Tracking

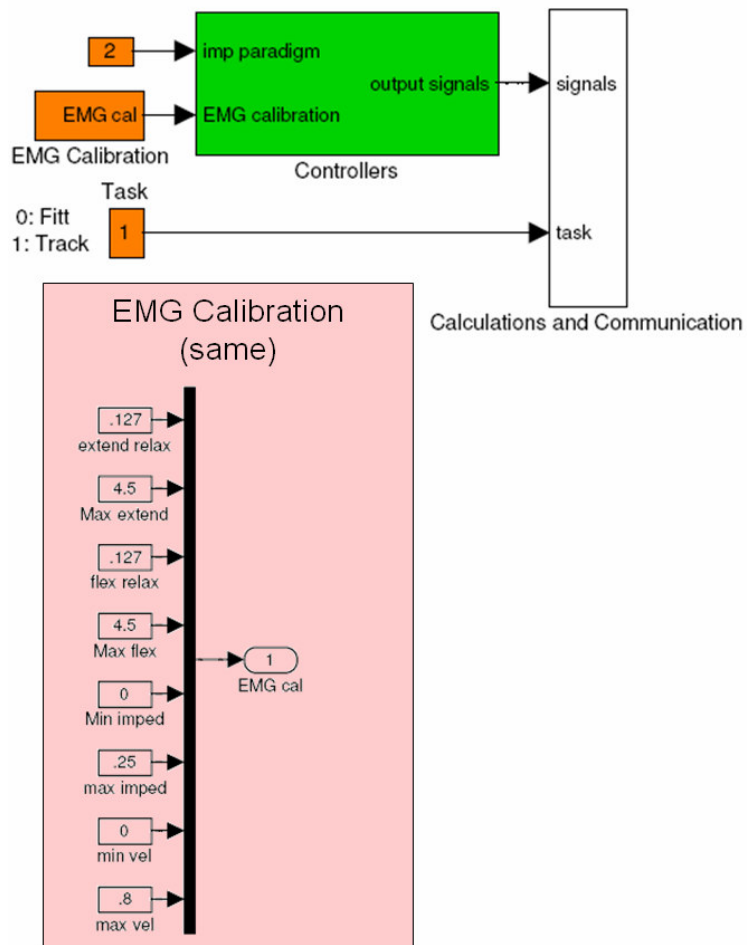




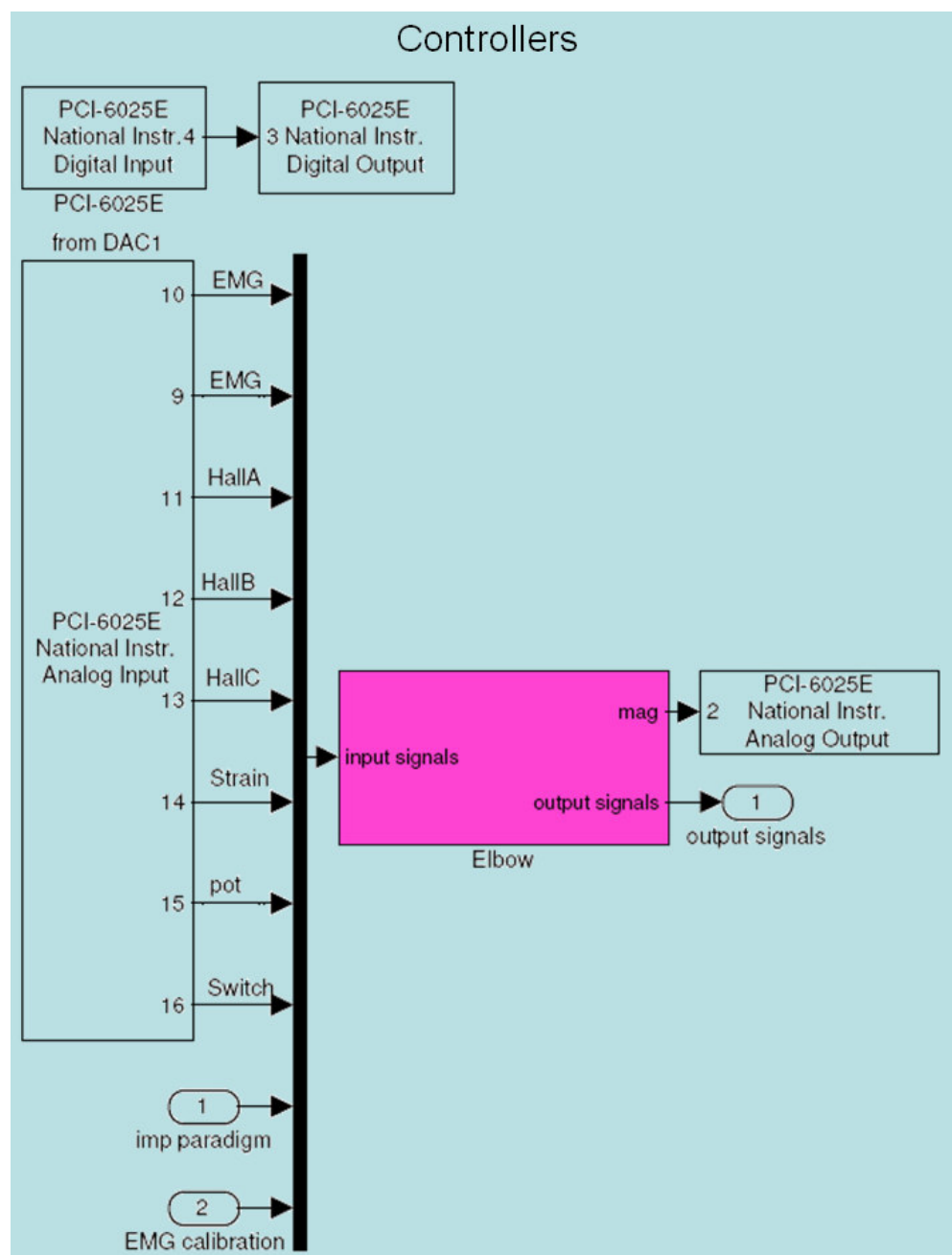


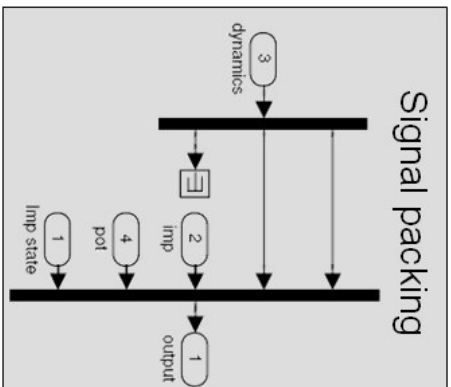
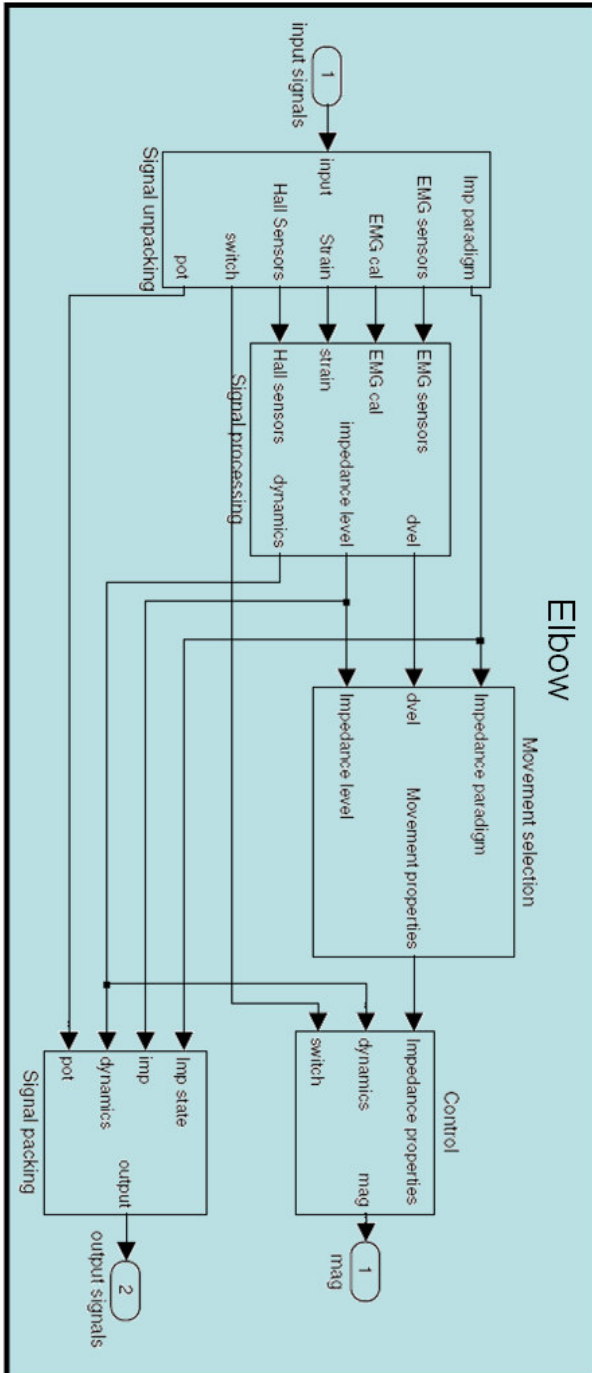
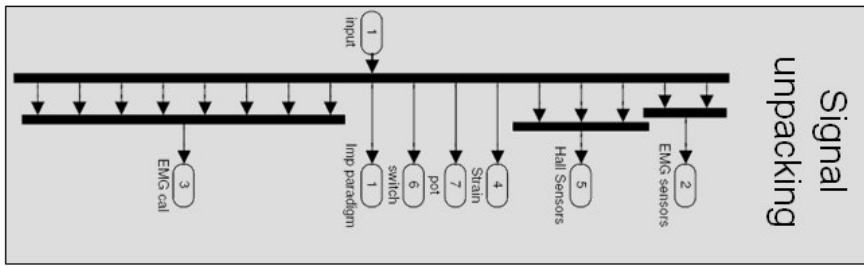


## 12.9 Remaining Subject Matlab Control

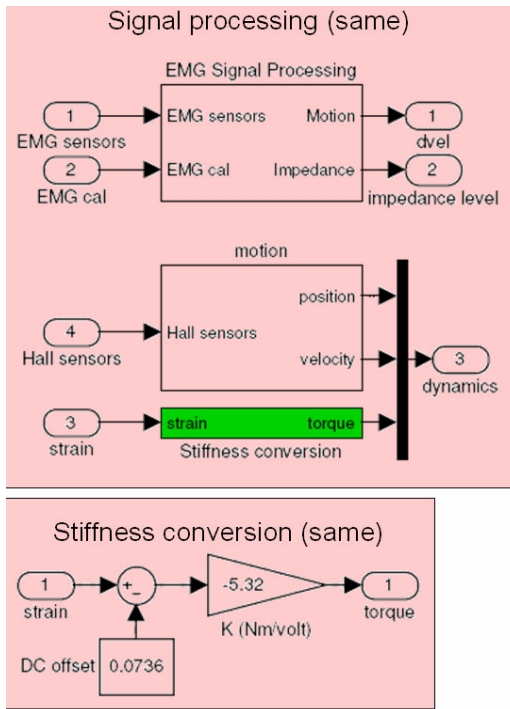


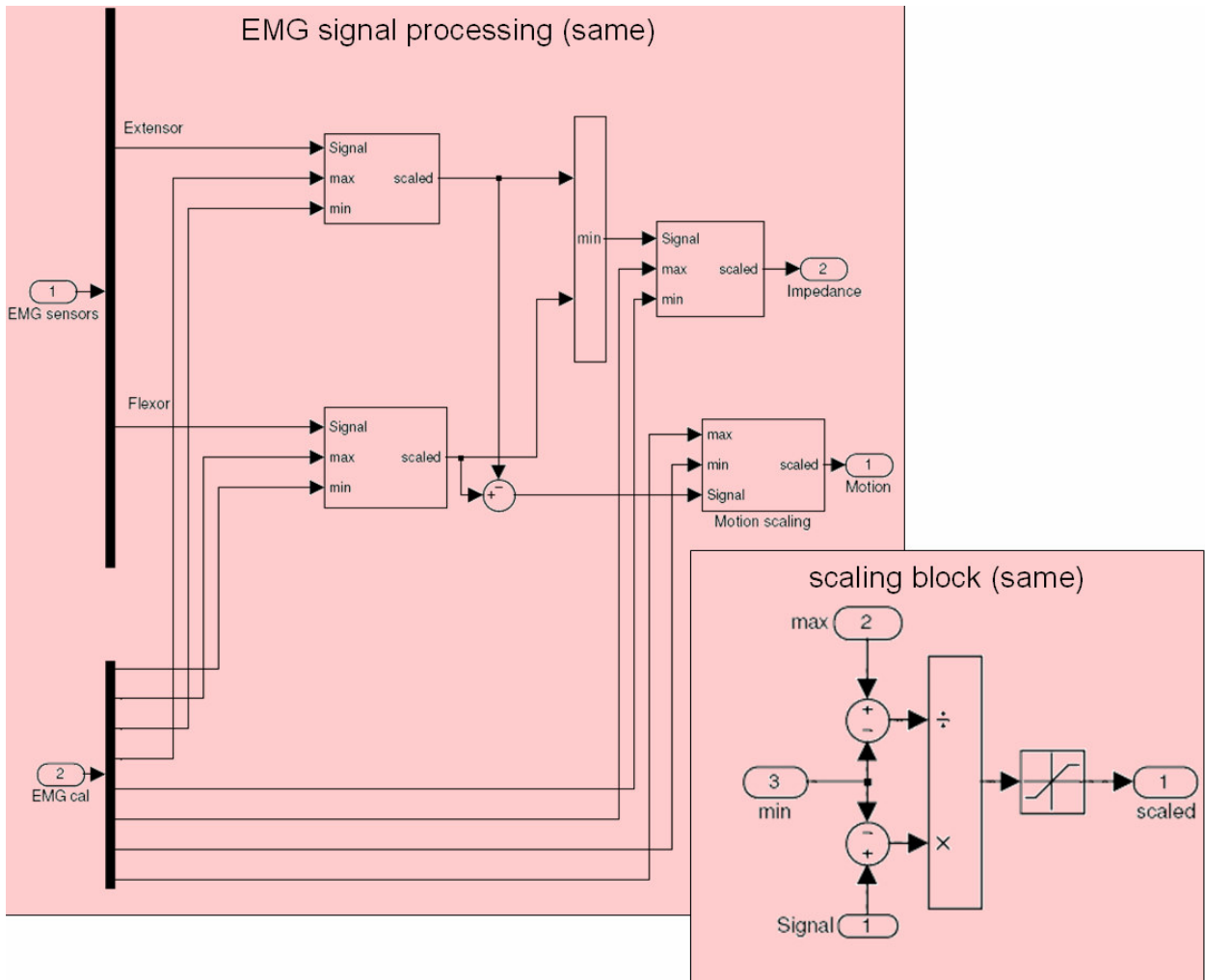
## 12.9.1 Controllers

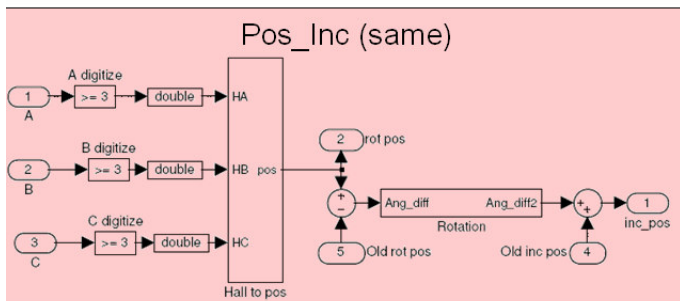
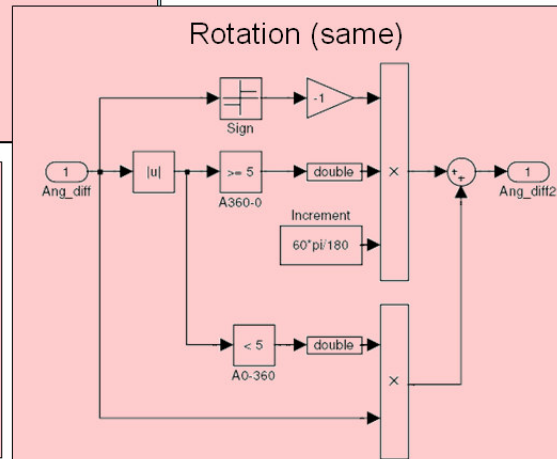
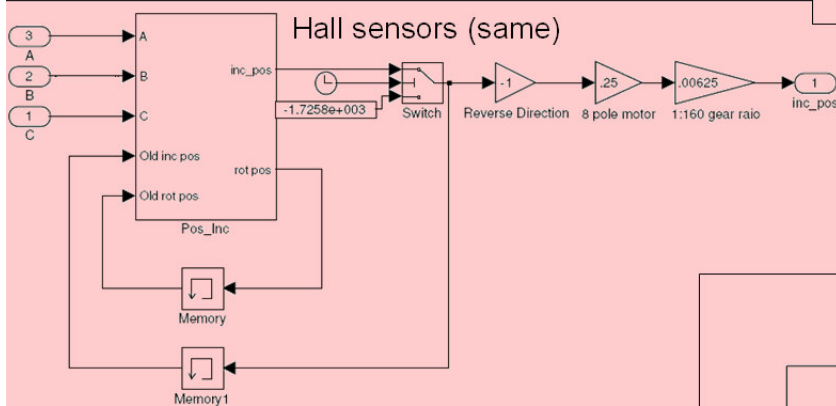
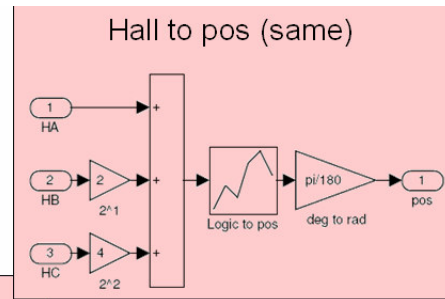
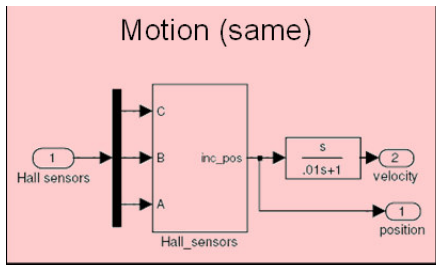




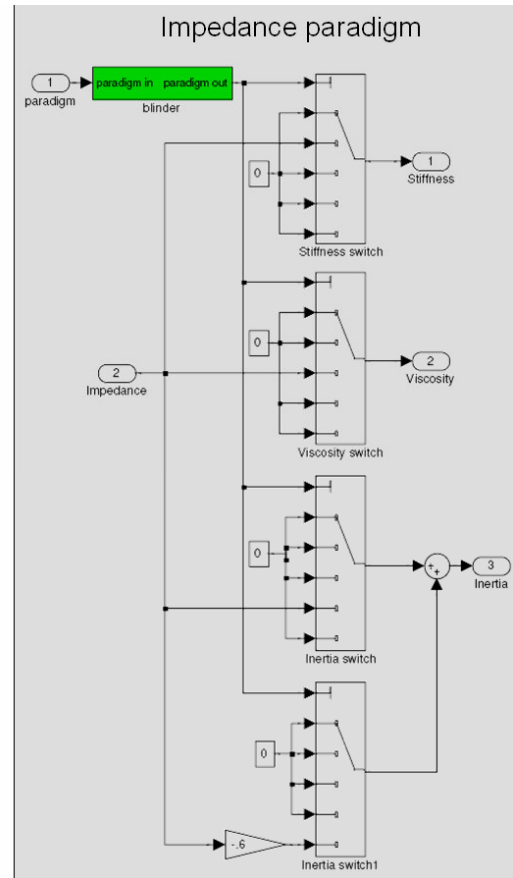
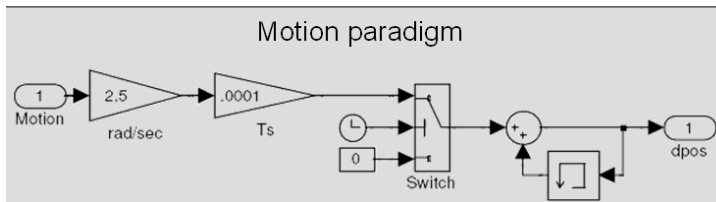
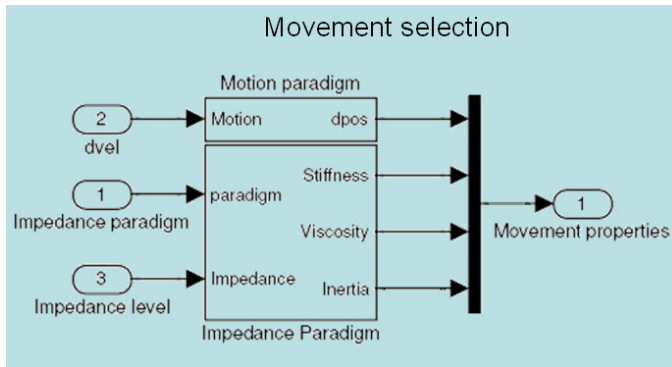
### 12.9.1.1 Signal Processing





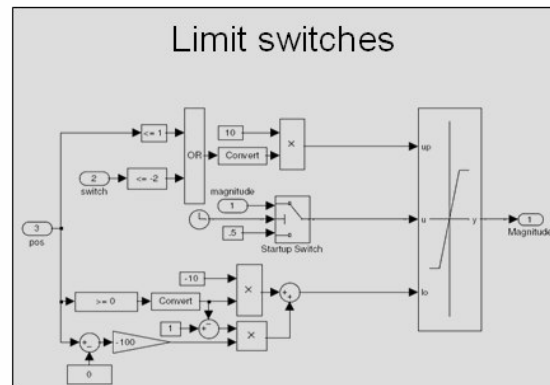
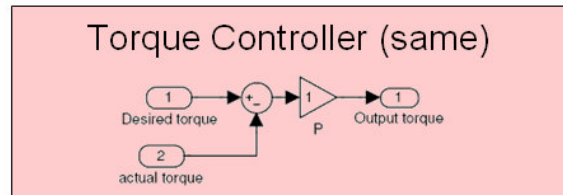
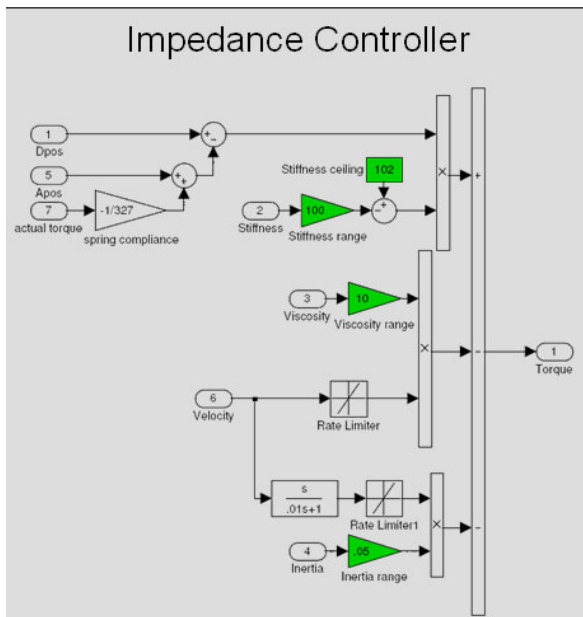
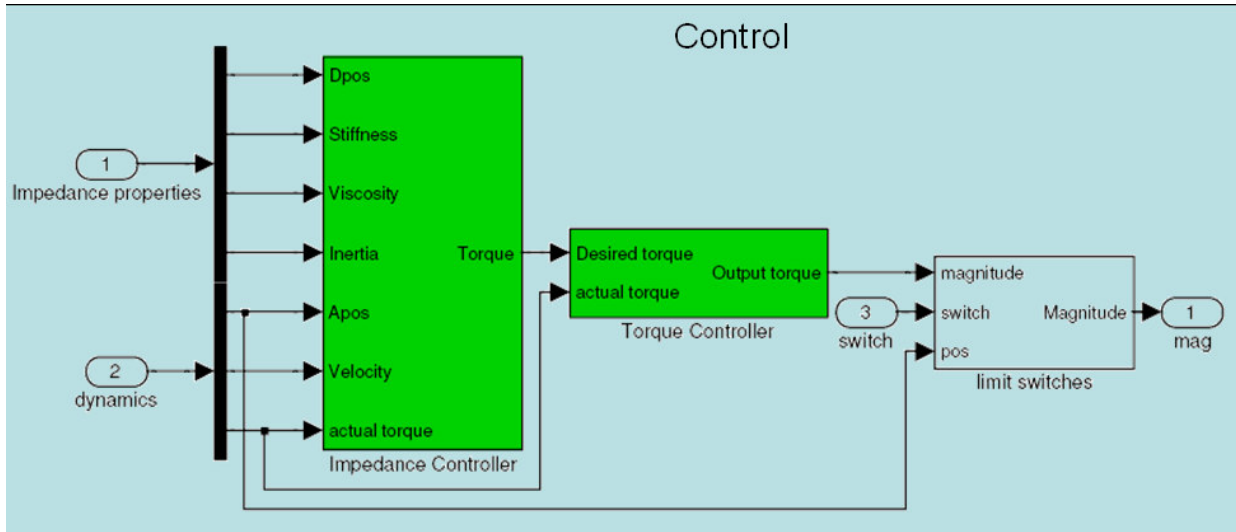


### 12.9.1.2 Movement selection

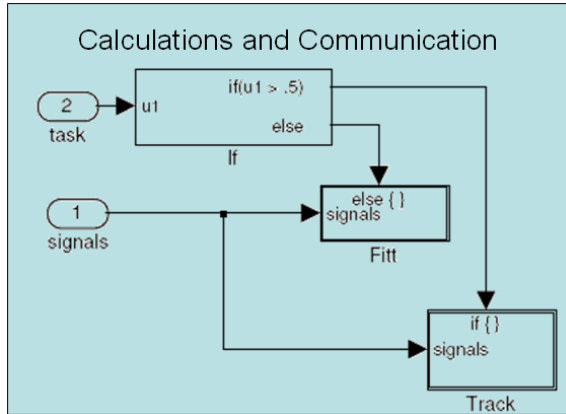




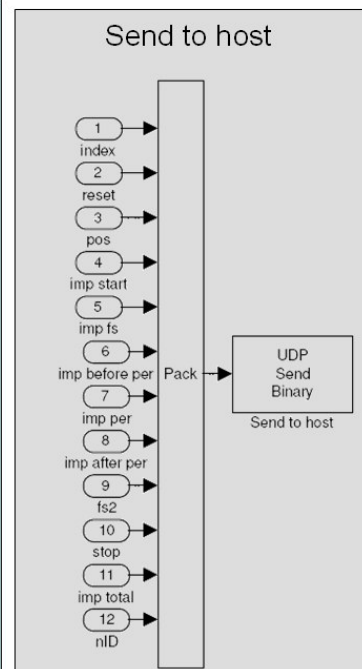
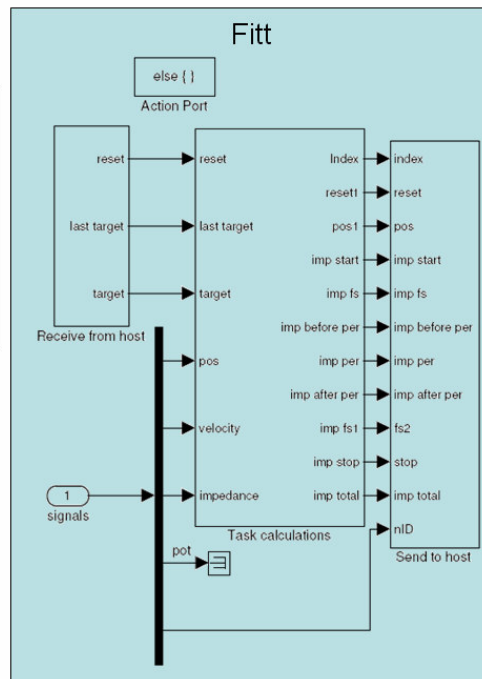
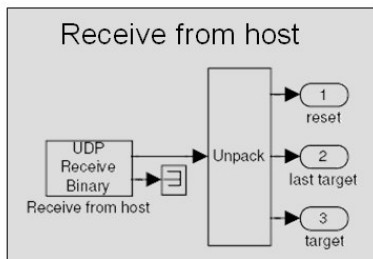
### 12.9.1.3 Control

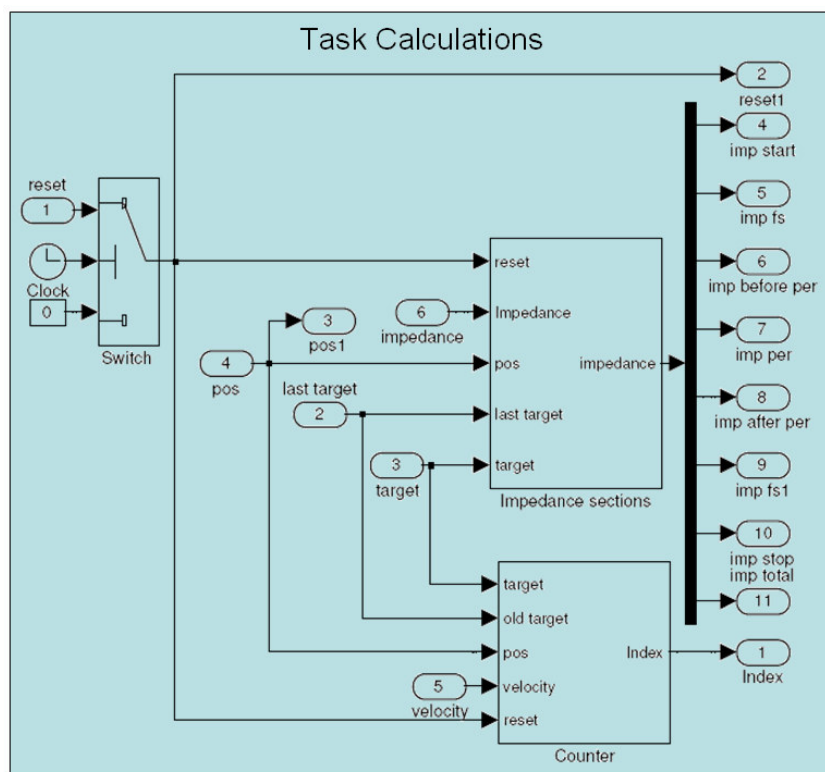


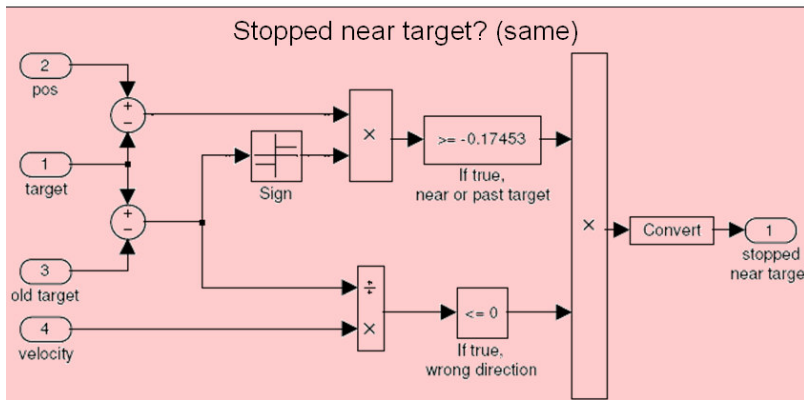
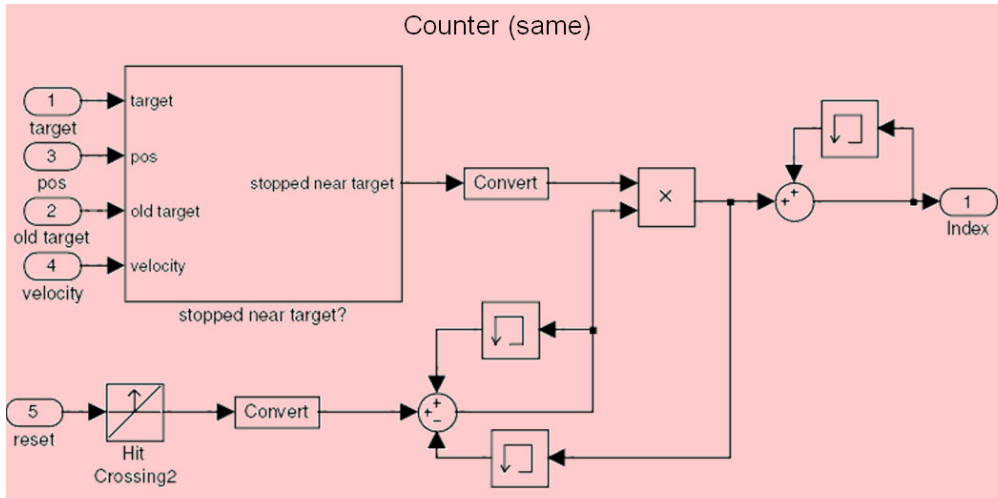
## 12.9.2 Processing

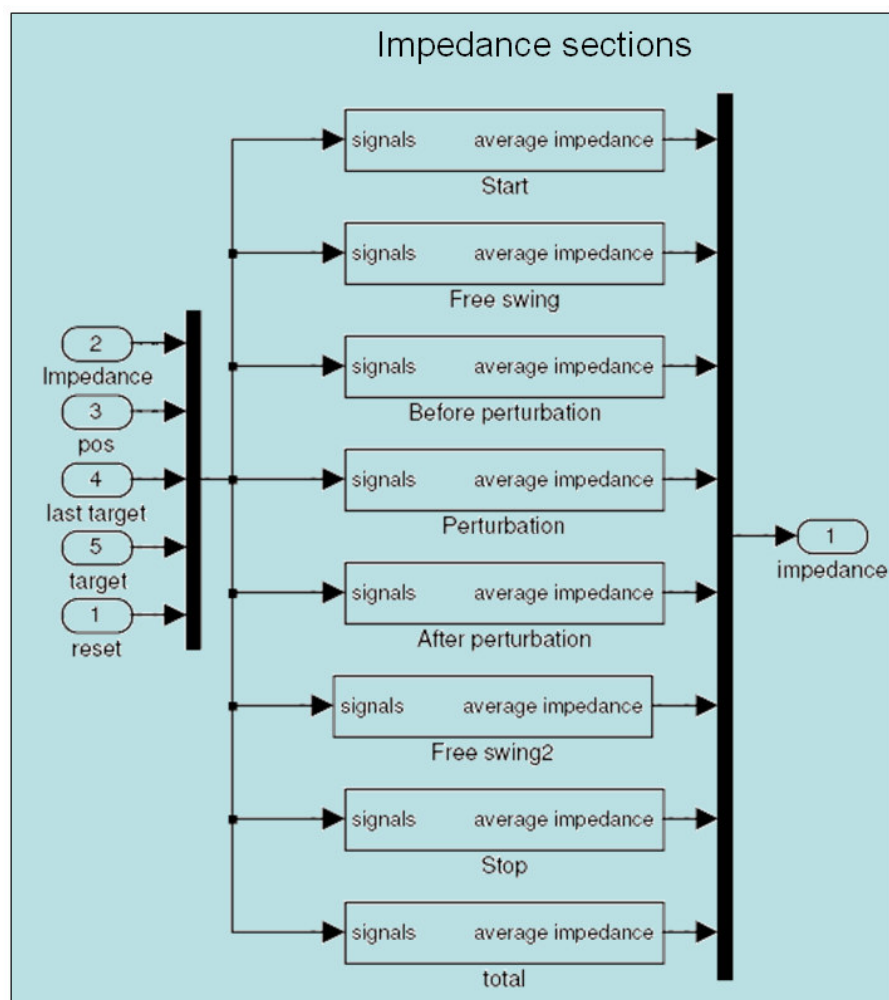


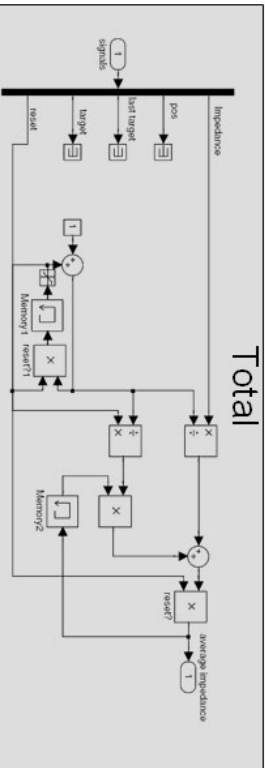
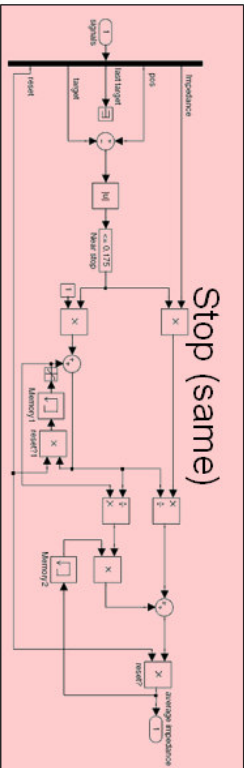
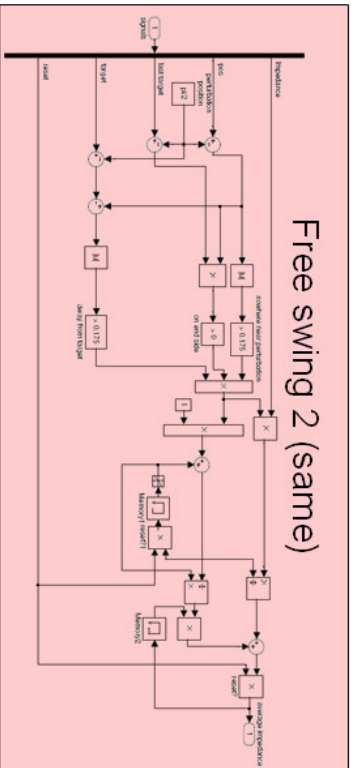
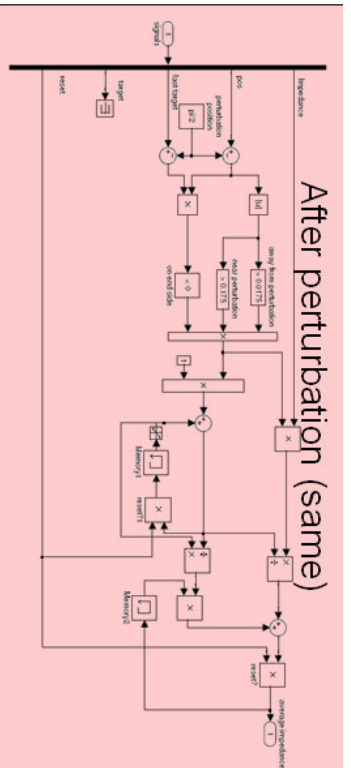
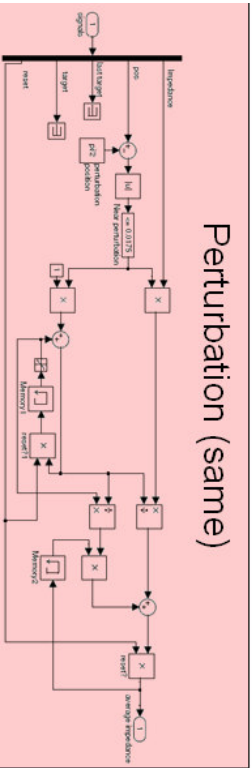
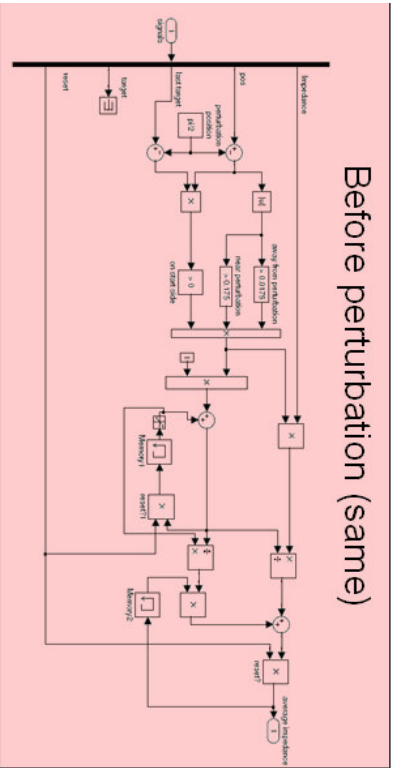
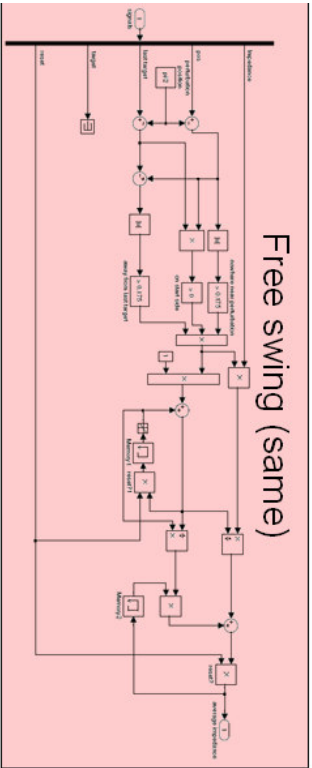
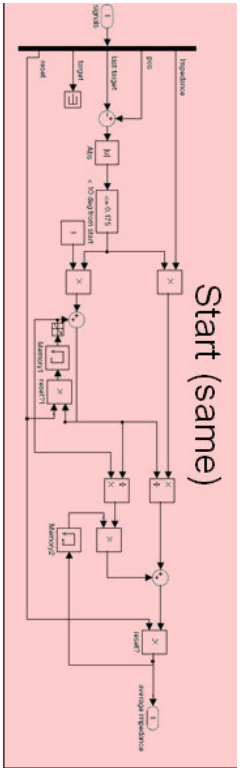
### 12.9.2.1 Fitts



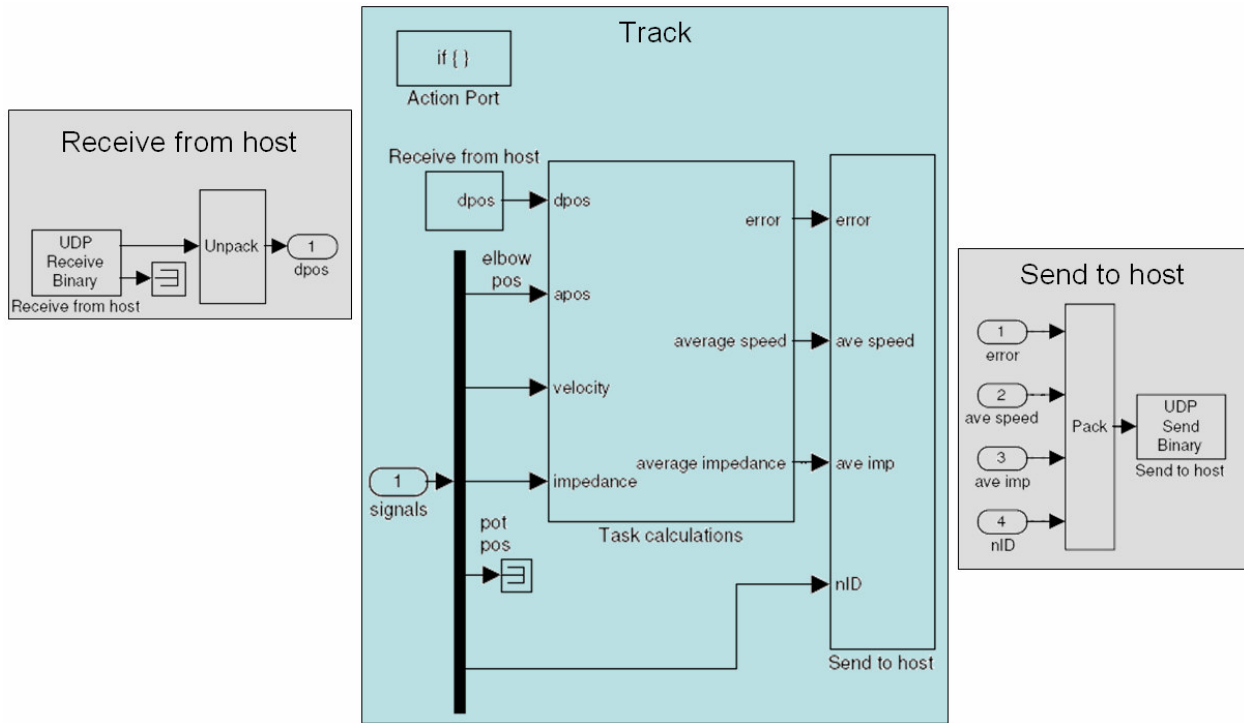


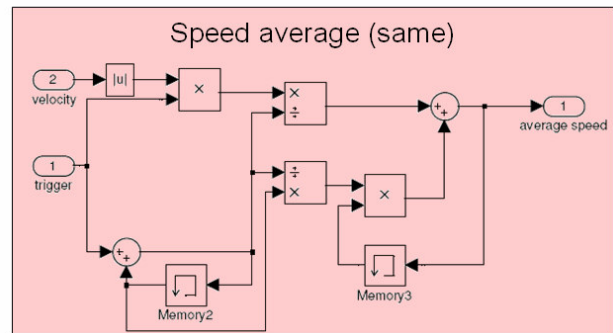
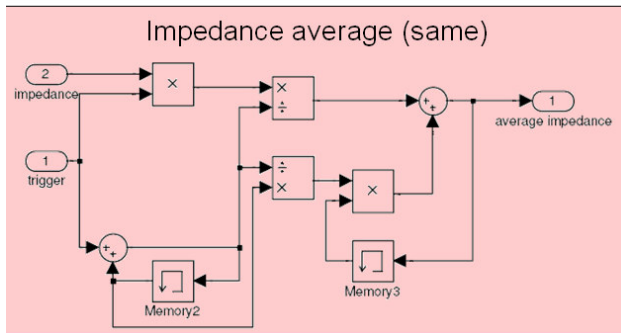
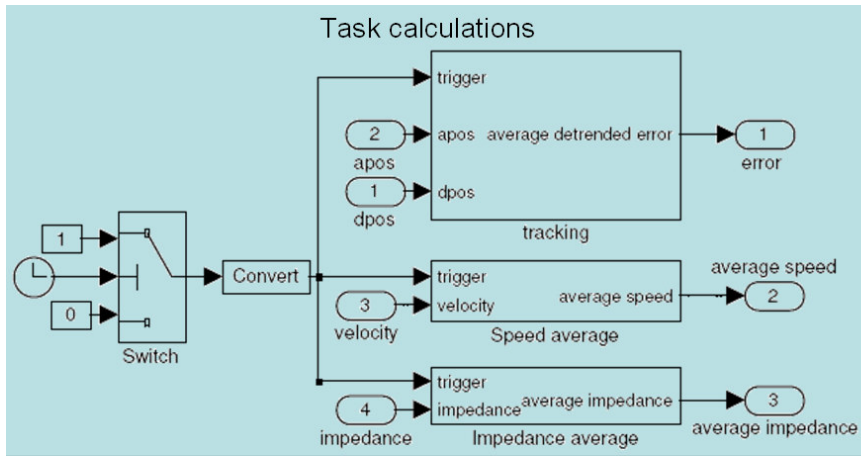




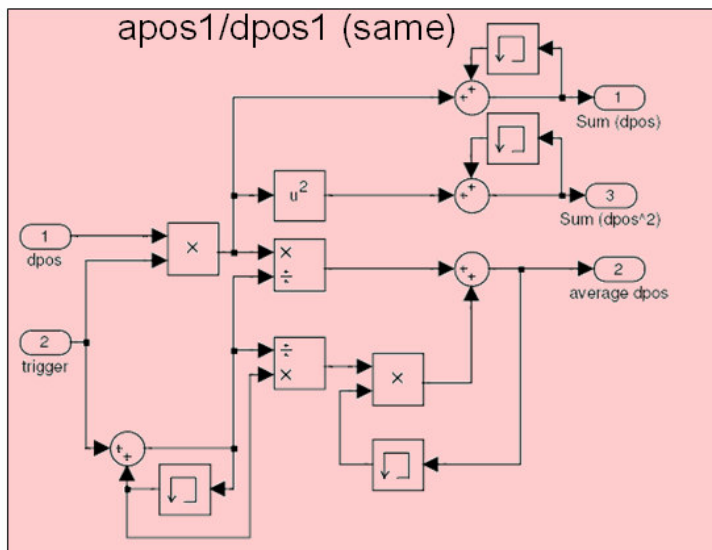
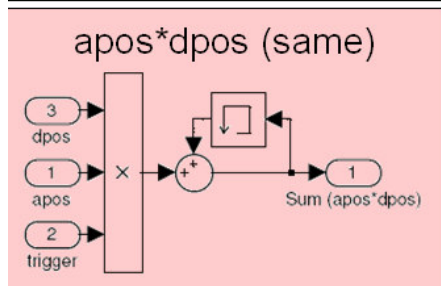
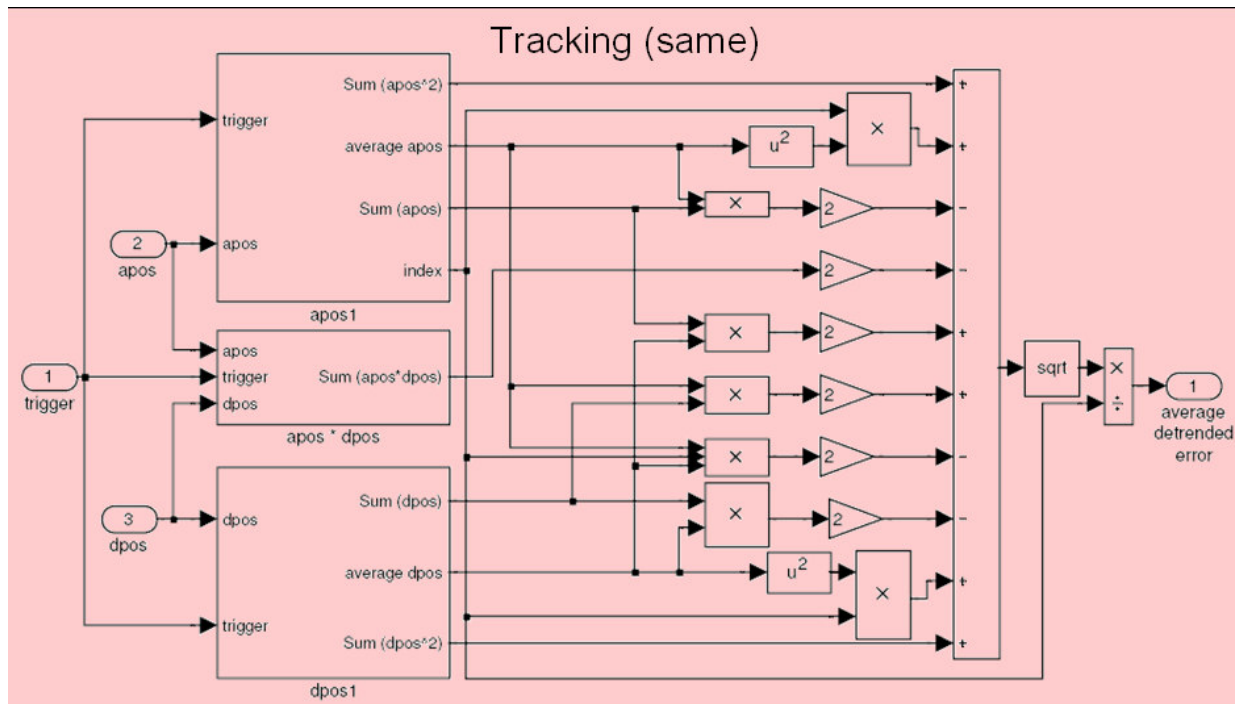


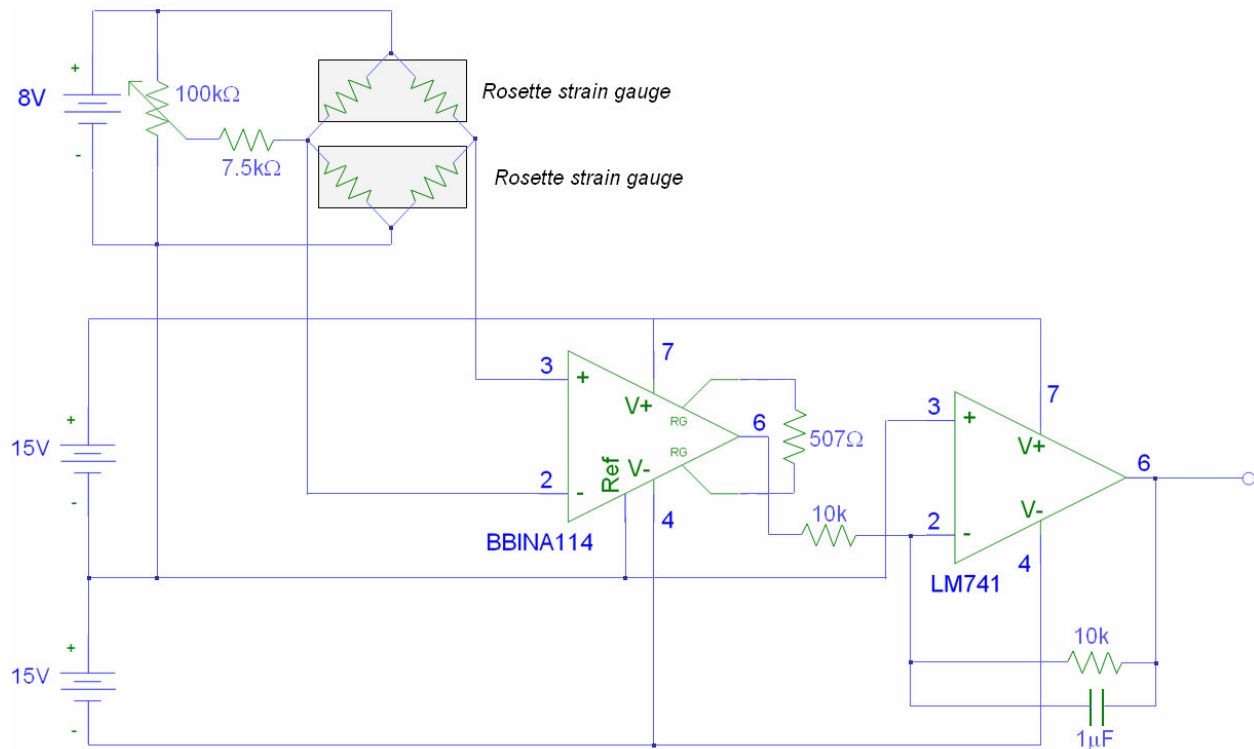
### 12.9.2.2 Track











## 12.10 Matlab Code

### 12.10.1 Calibration.m

```
function K=Calibration(Kold)
% Function K = Calibration Kold
% This function corrects projects misalignment and calibrates scale
% It creates an appropriate Homogeneous transform matrix
% XY origin positioning is performed first
% Rotation is performed next: the x axis should be horizontal.
% The Y axis is sheared
% X and Y scaling are performed
%
% This function calls script setscreen

global figure_handle;
global hline vline;      % horizontal & vertical crosshair lines
global x y;
global phi;              % Rotation angle
global sh;               % Y shear
```

```

global Sx Sy;           % X and Y scaling
global res;            % Resolution of adjustments
global sec;           % The current adjustment section
global flag;          % Flag to determine if the current adjustment is
done
global length;        % length of pointer

% -----
figure_handle = figure('KeyPressFcn',@printfig); % Set figure up to
accept keyboard input

setscreen; % Script to size
screen
% -----
% Initialize variables
x = 0;
y = 0;
phi = 0; % Rotation angle
sh = 0; % Y shear
Sx = 1; % X scaling
Sy = 1; % Y scaling
res = 4; % Set resolution of adjustments
flag = 0; % Flag to determine if the current adjustment is
done
length = 53.4; % Length of pointer
% -----
% Create crosshair
hline = line([-length,length],[y,y]);
vline = line([x,x],[-length,length]);
set(hline,'erasemode','normal','Color','w','LineWidth',1);
set(vline,'erasemode','normal','Color','w','LineWidth',1);
% -----
% Section 1: Adjust origin
sec = 1;
tit = title('Adjust origin x & y coordinates (4 6 8 2, 7 inc res, 1 dec
res, 5 enter)','Color','w','Rotation',90,'HorizontalAlignment','right')
while(flag==0)
    K = transform(Kold,x,y,phi,sh,Sx,Sy);
    redraw(K);
end
flag = 0;
% -----
% Section 2: Rotate Z axis
sec = 2;
set(tit,'string','Rotate Y axis (4 6) (Level vertical)')
while(flag==0)
    K = transform(Kold,x,y,phi,sh,Sx,Sy);
    redraw(K);
end
flag = 0;
% -----

```

```

% Section 3: Skew Y axis
sec = 3;
set(tit, 'string', 'Skew X axis to horizontal (4 6)')
while(flag==0)
    K = transform(Kold, x, y, phi, sh, Sx, Sy);
    redraw(K);
end
flag = 0;

% -----
% Section 4: Scale X axis
sec = 4;
set(tit, 'string', 'Scale Y axis(8 2)')
while(flag==0)
    K = transform(Kold, x, y, phi, sh, Sx, Sy);
    redraw(K);
end
flag = 0;

% -----
% Section 5: Scale Y axis
sec = 5;
set(tit, 'string', 'Scale X axis (8 2)')
while(flag==0)
    K = transform(Kold, x, y, phi, sh, Sx, Sy);
    redraw(K);
end
close all;
%end-----

function printfig(src, evnt)
% This function figures out which button you pushed
global figure_handle;
global x y;
global phi;           % Rotation angle
global sh;           % Y shear
global Sx Sy;       % X and Y scaling
global res;         % Resolution of adjustments
global sec;         % The current adjustment section
global flag;       % Flag to determine if the current adjustment is
done

vert = 0;           % Vertical adustment (keyboard 8 or 2)
hor = 0;           % Horizontal adjustment (keyboard 4 or 6)
cc = get(figure_handle, 'CurrentCharacter');
switch (cc)
    case('8')       % Up
        vert = 2^res;
    case('2')       % Down
        vert = - 2^res;
    case('4')       % Left
        hor = -2^res;
    case('6')       % Right

```

```

        hor = 2^res;
    case('7')           % Coarser resolution
        res = res + 1;
    case('1')           % Finer resolution
        res = res - 1;
    case('5')           % End section adjustment
        flag = 1;
end
% -----
% Match motion to corresponding translation/rotation
switch(sec)
    case(1)             % Translate origin
        x = x - vert;
        y = y + hor;
    case(2)             % Rotate
        phi = phi - hor/10;
    case(3)             % Shear Y
        sh = sh + hor;
    case(4)             % Scale X
        Sx = Sx + vert;
    case(5)             % Scale Y
        Sy = Sy + vert;
end
%end-----

function redraw (K)
% This function moves the crosshair to the new position & orientation
global hline vline length;

% Transform lines
h1 = K*[[ -length length]
         [ 0 0 ]
         [ 1 1 ]];

v1 = K*[[ 0 0 ]
         [-length length]
         [ 1 1 ]];

% Move lines
set(hline, 'xdata', [h1(1,1),h1(1,2)], 'ydata', [h1(2,1),h1(2,2)]);
set(vline, 'xdata', [v1(1,1),v1(1,2)], 'ydata', [v1(2,1),v1(2,2)]);
drawnow;
%end-----

function K = transform(Kold,x,y,phi,sh,Sx,Sy)
% This function creates the Homogeneous transformation matrix

% X & Y Translation
Txy = [[1 0 x]
        [0 1 y]
        [0 0 1]];

```

```

% Rotation
Rz = [[cos(phi) -sin(phi) 0]
      [sin(phi)  cos(phi) 0]
      [0         0        1]];

% Y shearing
Hshy = [[1 sh 0]
        [0 1 0]
        [0 0 1]];

% X scaling
Hsx = [[Sx 0 0]
       [0 1 0]
       [0 0 1]];

% Y scaling
Hsy = [[1 0 0]
       [0 Sy 0]
       [0 0 1]];

% Homogeneous transformation matrix
K = Kold*Txy*Rz*Hshy*Hsx*Hsy;

%end-----

```

## 12.10.2 Fmain.m

```

function fmain(K,tg,ml)
% function fmain(K,tg)
% This function Initiates a Fitts Law task
% It starts the execution of the host program (Fitt_host)
% and the precompiled and loaded target program (Fitt_target)
% K is the homogeneous transformation matrix of the projector to the screen
% tg is the address of the XPC target
% ml is the mental load: 0 = none, 1 = yes.
% This function calls scriptssetscreen, target, mlt and Econ
% This function creates global variables used by function Fitt
% K may be found by running function Calibration

global K2;           % Homogeneous transformation matrix
global tg2;         % XPC Target address
global i;           % Target index number
global Num;         % Number of Targets
global fhold;       % Flush out old averages
global figure_handle; % Figure handle
global target_handle; % Target handle
global mlt_handle;  % Mental Loading task word handle
global force_below; % Handle of Force below threshold

```

```

global force_above;      % Handle of Force above force threshold
global corner;          % Corner of Force bar
global fbc;             % Coordinates for force below
global fac;             % Coordinates for force above
global ml;              % Use a mental task (1) or not (0)
global choice;         % Mental load word & color
global time            % Time of last mental task loading
global stime;          % time simulation started;
global tflag           % Has the sound started yet?
global shape;         % The pixels in each target
global bs1;           % Sound to play when index is reached;
global results;       % Results is a structure including:
                        %   apos      Actual position
                        %   time      Time of target aquisition
                        %   diameter  Diameter of target
                        %   force     Max force
                        %   imp       A substructure containing various
impedance states      %   perturbation  Is the perturbation out (1)
or not (0)
    ml=ml1;
    K2 = K;
    tg2= tg;
    load bs;
    bs1 = bs;
force index is reached;
    Num = 52;
    Length = 53.4;
    results(1).pos = 30*pi/180;
target pos
    results(1).diameter = 1;
diameter
    shape(1).pixels = target(K,results(1).pos,1,Length);% Generate target
pixels

% Set display options -----
    figure_handle = figure(1);
    target_handle =
plot(shape(1).pixels(:,1),shape(1).pixels(:,2),'.','MarkerSize',20,'Color','w
','EraseMode','background');
    setscreen;
    mlt_handle = text(0,0,' ');
set(mlt_handle,'FontSize',20,'FontWeight','bold','HorizontalAlignment','Left'
,'Rotation',90);

% Generate desired targets -----
    D = .5;
    theta = 30;
for (i=2:Num)
    % Initialize a target that can't happen to prime the while loop

```

```

        dir = round(rand)*2-1;                                % Either 1 or - 1
        while ((30>(results(i-1).pos*180/pi + dir*theta)) |(125<(results(i-
1).pos*180/pi + dir*theta))) % Make sure target is in 180 deg workspace
            dir = round(rand)*2-1;                            % Either 1 or
- 1
        end

        results(i).pos = results(i-1).pos + dir*theta*pi/180;    % Store
target position
        results(i).diameter = D;                                % Store
diameter of target
        shape(i).pixels = target(K,results(i).pos,D,Length);    % Generate
target pixels

        results(i+1).time = 0;                                  % Record time
        results(i).apos = 0;
        results(i).Istart = 0;
        results(i).IFS1 = 0;
        results(i).IBP = 0;
        results(i).IP = 0;
        results(i).IAP = 0;
        results(i).IFS2 = 0;
        results(i).Istop = 0;
        results(i).Itotal = 0;
    end
    i = 2;                                                       % target to
start with
    tflag=1;
    time = now;
    stime= now;                                                 % Time
simulation started
    choice = 0;                                                 % Mental load
display to start with

% Run Simulink -----
    Fitt_host;                                                 % Load host
    +tg;                                                         % Start
target. Make sure Target is NOT connected.
    set_param('Fitt_host','SimulationCommand','start');       % Start host

```

### 12.10.3 Fitt.m

```

function [sys,x0,str,ts] = Fitt(t,x,u,flag)
% function [sys,x0,str,ts] = Fitt(t,x,u,flag)
% This function is called by model Fitt_host
% It records the status of the variables
% It displays the target, mental loading task, and force bar
%
% This function uses global variables created by function fmain
% and calls script mlt and function nid

```



```

%
% u(1) = Index
% u(2) = Reset
% u(3) = actual position
% u(4) = Impedance, start section
% u(5) = Impedance, Free swing section
% u(6) = Impedance, Before Perturbation section
% u(7) = Impedance, Perturbation section
% u(8) = Impedance, After Perturbation section
% u(9) = Impedance, Free swing 2
% u(10) = Impedance, Stop section
% u(11) = Impedance, Entire movement
% u(12) = nID (name ID)
%
%
% sys(1) = Reset
% sys(2) = last target
% sys(3) = Target

global K2; % Homogeneous matrix
global tg2; % target
global i % Target index number
global Num % Number of targets
global fhold; % Flush out old averages
global figure_handle; % Handle of figure
global target_handle; % Handle of the target
global mlt_handle; % Handle of the mental loading task
global force_above; % Handle of force below
global force_below; % Handle of force above
global corner; % Corner of Force bar
global fbc; % Coordinates for force below
global fac; % Coordinates for force above
global ml; % Use a mental task (1) or not (0)
global choice; % Mental load word & color
global time % Time of last mental task loading
global stime; % time simulation started;
global tflag % Has the sound started yet?
global shape; % The pixels in each target
global bs1; % Sound to play when index is reached.
global flag_sound; % Play the sound?
global results; % Results is a structure including:
% apos Actual position
% time Time of task initiation
% diameter Diameter of target
% imp A substructure containing various
impedance states

switch flag,
case 0, % Initialization %
[sys,x0,str,ts]=mdlInitializeSizes;
case 2, % Update - this is where the heart of the program is
sys = mdlUpdate(t,x,u);

```

```

case 3, % Output
    sys = mdlOutputs(t,x,u);
case 1,4,9, 'Stop', % Terminate
    name=nid(u(12));
    name=['results\F',name];
    if(ml==0)
        name=[name, 'N'];
    else
        name=[name, 'M'];
    end
    if(exist([name, '.mat'])==2)
        disp(['@@@@@@@@ WARNING! ',name, ' already exists. File has been
renamed ',name, '2 @@@@@@@@@@']);
        name=[name, '2'];
    end
    save(name, 'results');
    -tg2;
    close(figure_handle);
otherwise
    error(['unhandled flag = ',num2str(flag)]);
end
%end Fitt-----

```

```
function sys = mdlUpdate(t,x,u) % Update the system
```

```

global K2; % Homogeneous matrix
global tg2;
global i % Target index number
global Num % Number of targets
global fhold; % Flush out old averages
global figure_handle; % Handle of figure
global target_handle; % Handle of the target
global mlt_handle; % Handle of the mental loading task
global mlt_handle; % Handle of the mental loading task
global force_above; % Handle of force below
global force_below; % Handle of force above
global corner; % Corner of Force bar
global fbc; % Coordinates for force below
global fac; % Coordinates for force above
global ml; % Use a mental task (1) or not (0)
global choice; % Mental load word & color
global time % Time of last mental task loading
global stime; % time simulation started;
global tflag % Has the sound started yet?
global shape; % The pixels in each target
global bs1; % Sound to play when index is reached.
global results; % Results is a structure including:
% apos Actual position
% time Time of target aquisition
% diameter Diameter of target
% force Max force

```

```

                                %   imp           A substructure containing various
impedance states
    sys = [];
    Length = 53.4;                % Radius of pointer

% Beep if it's time to begin tracking
    if((now-stime>5e-5)&&tflag)
        sound(bs1,10000);
        tflag=0;
    end
% Display targets -----
    if(u(1)~=i & u(1)>=2) % Time for a new target
        results(i+1).time = now;                % Record time
        results(i).apos = u(3);
        results(i).Istart = u(4);
        results(i).IFS1 = u(5);
        results(i).IBP = u(6);
        results(i).IP = u(7);
        results(i).IAP = u(8);
        results(i).IFS2 = u(9);
        results(i).Istop = u(10);
        results(i).Itotal = u(11);

        if(u(1) > Num) % Done with the experiment
            set_param('Fitt_host','SimulationCommand','stop');
        else
            flag_sound=0;
            fhold = 0;                % Flush out
target PC averages & maxes for trial
            i = u(1);                % Update the
index
            results(i).time = now;                % Record time

set(target_handle,'xdata',shape(i).pixels(:,1),'ydata',shape(i).pixels(:,2));
% Draw the new target
    if (ml)                % If a mental
load word should be displayed

        xt = (Length+2)*sin(pi/2-results(i).pos);    % Figure out
where to place word
        if(abs(results(i).pos-pi/2)>10*pi/180)
            yt = (Length+2)*cos(pi/2-results(i).pos);
        else
            yt = -12+(Length)*cos(pi/2-results(i).pos);
        end
        q = K2*[xt; yt; 1];
        xt = q(1);
        yt = q(2);
        mlt;                % Pick a word
        drawnow;

```

```

                                time = now;                                % Start mental
loading clock
                                end
                                end
                                end

                                if(u(2)==0)                                % target PC
averages & maxes have been flushed
                                fhold = 1;
                                end

% mental loading -----
%   if(ml&&(u(1)<=Num))                                % If a mental load
is displayed

%   if(now - time > 2e-5)                                % Time to update
word (2.5 sec)
%   xt = (Length+2)*sin(pi/2-results(i).pos);          % Figure out where
to place word
%   if(abs(results(i).pos-pi/2)>10*pi/180)
%   yt = (Length+2)*cos(pi/2-results(i).pos);
%   else
%   yt = -12+(Length)*cos(pi/2-results(i).pos);
%   end
%   q = K2*[xt; yt; 1];
%   xt = q(1);
%   yt = q(2);
%   mlt;                                % Pick a word
%   drawnow;
%   time = now;
%   end
%   end

%end mdlUpdate -----

function sys = mdlOutputs(t,x,u)
    global i;
    global results;
    global fhold;
    x(3) = results(i).pos;
    x(2) = results(i-1).pos;
    if(fhold==0)                                % Flush out thresholds
        x(1) = 0;
    else
        x(1) = 1;
    end
    sys = x;
%end mdlOutputs-----

function [sys,x0,str,ts]=mdlInitializeSizes

```



```

    load dp3;                                % Load pre-generated desired position directory.
This is created by model targ_gen
    dpo=dp3;                                % Make dp a global variable
    K2 = K;                                  % Make K a global variable
    tg2 = tg;                                % make tg a global variable

    load bs;
    bs1 = bs;                                % Sound to play when
force index is reached;

    Length = 53.4;                            % Radius of pointer
    shape = target(K,1,1,Length);             % Generate target pixels
% Set display options -----
    figure_handle = figure(1);
    target_handle =
plot(shape(:,1),shape(:,2),'.','MarkerSize',20,'Color','w','EraseMode','backg
round');
    setscreen;                                % Set up the screen
    % Create force bar

    tflag=1;
% Run Simulink -----
    traj_host;                                % Load host
    stime = now;                               % Start clock
    +tg;                                       % Start
target. Make sure Target is NOT connected.
    set_param('traj_host','SimulationCommand','start'); % Start host

```

### 12.10.5 Track.m

```

function [sys,x0,str,ts] = track(t,x,u,flag)
% function [sys,x0,str,ts] = track(t,x,u,flag)
% This function is called by model track_host
% It records the status of the variables
% It displays the target and force bar
%
% This function uses global variables created by function tmain
% and calls function nid
%
% u(1) = error
% u(2) = average speed
% u(3) = average impedance
% u(4) = nid (Name ID)
%
% sys(1) = dpos

global K2;                                % Homogeneous matrix
global tg2;                                % target
global Length;                             % length of pointer;
global figure_handle;                       % Figure handle

```

```

global target_handle; % Target handle
global stime; % Start the stopwatch
global tflag; % Has the sound started yet?
global bs1; % Sound to play when index is reached.
global dpo; % Pre-generated desired position trajectory
global p; % Interpolated position for current time
global tresults; % Results is a structure including:
                    %   error   Difference between desired and actual
position
                    %   forcei  force index of exceeded threshold
                    %   speed   average speed
                    %   imp     average impedance

switch flag,
case 0, % Initialization %
    [sys,x0,str,ts]=mdlInitializeSizes;
case 2, % Update - this is where the heart of the program is
    sys = mdlUpdate(t,x,u);
case 3, % Output
    sys = mdlOutputs(t,x,u);
case 1,4,9,'Stop', % Terminate
    if(~isempty(u(1)))
        tresults.error = u(1);
    end
    if(~isempty(u(2)))
        tresults.speed = u(2);
    end
    if(~isempty(u(3)))
        tresults.imp = u(3);
    end
    name=nid(u(4));
    name=['results\T',name];
    if(exist([name, '.mat'])==2)
        disp(['@@@@@@@@ WARNING! ',name,' already exists. File has
been renamed ',name,'2 @@@@@@@@@@']);
        name=[name,'2'];
    end
    save(name,'tresults');
    -tg2;
    close(figure_handle);
otherwise
    error(['unhandled flag = ',num2str(flag)]);
end
%end Fitt-----

function sys = mdlUpdate(t,x,u) % Update the system
%   u(1) = reset
%   u(2) = error
%   u(3) = average speed
%   u(4) = average impedance
%   u(5) = nid (Name ID)

```

```

global K2;           % Homogeneous matrix
global tg2;         % target
global Length;     % length of pointer;
global target_handle; % Target handle
global stime;       % Start the stopwatch
global tflag        % Has the sound started yet?
global bs1;         % Sound to play when index is reached.
global dpo;         % Pre-generated desired position trajectory
global p;           % Interpolated position for current time
global tresults;    % Results is a structure including:
                    %   error   Difference between desired and actual
                    %   position
                    %   forcei  force index of exceeded threshold
                    %   speed   average speed
                    %   imp     average impedance

% Update results -----
if(~isempty(u(1)))
    tresults.error = u(1);
end
if(~isempty(u(2)))
    tresults.speed = u(2);
end
if(~isempty(u(3)))
    tresults.imp = u(3);
end
% Beep if it's time to begin tracking
if((now-stime>5e-5)&&tflag)
    sound(bs1,10000);
    tflag=0;
end
% Update target -----
elap=now-stime;
if(elap>7e-4)
    set_param('traj_host','SimulationCommand','stop');
else
    p= dpo(round((elap)*1.6667e+6));
    shape = target(K2,p,1,Length);           % Generate target pixels

    set(target_handle,'xdata',shape(:,1),'ydata',shape(:,2)); % Draw
the new target
    drawnow
end
sys = [];

%end mdlUpdate -----

function sys = mdlOutputs(t,x,u)
%   sys(1) = dpos

```



```

    global p; % Interpolated position for
current time
    x(1) = p;
    sys = x;
%end mdlOutputs-----

function [sys,x0,str,ts]=mdlInitializeSizes
    global p;
    sizes = simsizes;
    sizes.NumContStates = 0;
    sizes.NumDiscStates = 1;
    sizes.NumOutputs = 1;
    sizes.NumInputs = -1; % Inherited number of inputs
    sizes.DirFeedthrough = 0;
    sizes.NumSampleTimes = 1;
    p = 0;
    sys = simsizes(sizes);
    x0 = 0;
    str = [];
    ts = [-1 0]; % Inherited sample time
    figure(1)
    results(1).time = now;
% end mdlInitializeSizes

```

## 12.10.6 Setscreen.m

```

% Script setscreen
% This script formats figure figure_handle in terms of:
% size, scaling, color, and refresh rate
%
% This script is called by functions Calibrate, fmain, and tmain
% This script assumes the computer is using 2 monitors.

    v = get(0, 'MonitorPosition'); % Get the combined size of the 2 monitors
    set(figure_handle, 'position', [v(2,1) v(1,4)-v(2,4) v(2,3)-v(2,1)+1
v(2,4)], 'menubar', 'none', 'numbertitle', 'off', 'name', 'Experiment B
screen', 'Renderer', 'OpenGL');
    set(figure_handle, 'color', [0 0 0]); % [1 1 1] is white, [0 0 0] is black

    ar = 60; % Set X/Y +/- scale

    % Set axis
    r = (v(2,3)-v(2,1))/(v(2,4)-v(2,2));
    axislimits = [-ar ar -10 ar+15];
    axis(axislimits);

    axis equal; % Make circles look like circles, not
ellipses
    axis manual; % Make axes permanent
    axis off; % Don't display axes
    q=gca;

```

```

    set(q, 'OuterPosition', [-.2 -.2 1.4 1.4]);           % Get rid of the figure
borders
    % Speed up animation
    set(figure_handle, 'BackingStore', 'off', 'Interruptible', 'off')
    axes_handle=gca;
    set(axes_handle, 'DrawMode', 'fast');

```

### 12.10.7 nid.m

```

function name = nid(paradigm)
% function name = nid(paradigm)
% This function determines what to name the results file
% It is called by Fitt and track
switch(paradigm)
    case(1)
        name='A';
    case(2)
        name='B';
    case(3)
        name='C';
    case(4)
        name='D';
    case(5)
        name='E'
end

```

### 12.10.8 mlt.m

```

% Script mlt creates a mental loading task
% It is called by functions fmain and Fitt
ochoice = choice;
while(ochoice == choice)
    choice = 1+round(11*rand);
end
switch (choice)
    case(1)
        set(mlt_handle, 'Color', 'b', 'String', 'RED', 'position', [xt yt]);
    case(2)
        set(mlt_handle, 'Color', 'b', 'String', 'GREEN', 'position', [xt yt]);
    case(3)
        set(mlt_handle, 'Color', 'b', 'String', 'WHITE', 'position', [xt yt]);
    case(4)
        set(mlt_handle, 'Color', 'r', 'String', 'BLUE', 'position', [xt yt]);
    case(5)
        set(mlt_handle, 'Color', 'r', 'String', 'GREEN', 'position', [xt yt]);
    case(6)
        set(mlt_handle, 'Color', 'r', 'String', 'WHITE', 'position', [xt yt]);
    case(7)
        set(mlt_handle, 'Color', 'g', 'String', 'BLUE', 'position', [xt yt]);
    case(8)
        set(mlt_handle, 'Color', 'g', 'String', 'RED', 'position', [xt yt]);
    case(9)

```

```

set(mlt_handle, 'Color', 'g', 'String', 'WHITE', 'position', [xt yt]);
case(10)
set(mlt_handle, 'Color', [1 1 1], 'String', 'RED', 'position', [xt yt]);
case(11)
set(mlt_handle, 'Color', [1 1 1], 'String', 'BLUE', 'position', [xt yt]);
case(12)
set(mlt_handle, 'Color', [1 1 1], 'String', 'GREEN', 'position', [xt yt]);
end

```

## 12.11 Data sheets

Emoteq Corporation: Division of Allied Motion Technologies (12 /16/2004

HT02500-X0X      NUPRL

SIZE CONSTANTS **			
Parameter	Symbol	Unit	VALUE
Maximum Rated Torque	Tr	Nm	2.711
Maximum Continuous Stall Torque @Temperature Rise 75°C	Tc	Nm	0.176
Motor Constant	Km	Nm/sqrt.w	0.044
Electrical Time Constant	Te	msec	0.387
Mechanical Time Constant	Tm	msec	4.519
Angular Acceleration (theoretical)		rad/sec <sup>2</sup>	109000
Thermal Resistance *	TPR	°C/watts	3.64
Maximum Cogging Torque	Tf	Nm	0.014
Viscous Damping (Infinite Source Impedance)	Fi	Nm/rpm	3.15E-06
Hysteresis Drag Torque	Th	Nm	2.76E-03
Rotor Inertia Frameless	Jm	kg.m <sup>2</sup>	8.72E-06
Motor Weight Frameless	Wt	kg	0.176
No. of Poles		P	8
* TPR Assumes motor mounted to aluminium heat sink 3.5, 3.5, .250 in @ Ambient Temperature , 25°C ches (Still air)			

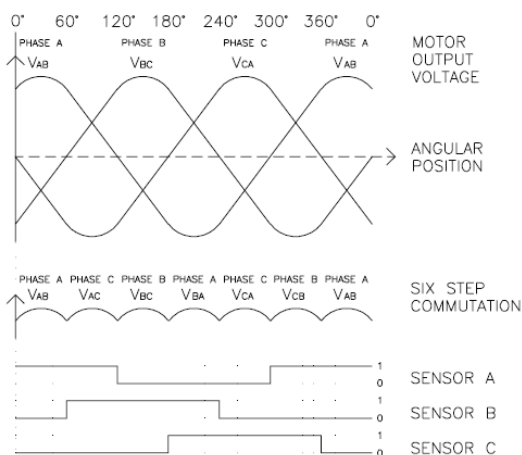
WINDING CONSTANTS *			
Parameter	Symbol	Unit	VALUE
Design Voltage	Vp	volt	12
Peak Torque, +/-25%	Tp	Nm	1.11
Peak Current, +/-15%	Ip	ampere	53.258
Torque Sensitivity +/-10%	Kt	Nm/Amp	0.021
No Load Speed	Snl	rad/sec	545.865
Voltage Constant +/-10%	Kb	v/rad/sec	0.021
Terminal Resistance +/-12%	Rm	ohms	0.225
Terminal Inductance +/-30%	Lm	mH	0.087
* Performance @ 25.000°C			
RMS TORQUE PERFORMANCE			
Design Voltage	Vp	volt	12
Continuous Power Output @	Power	watt	4.114
Temperature Rise: 30°C	Torque	Nm	8.57E-03
COOLING :			
{Still air}	Speed	rpm	4583
Ambient temperature 25°C	Iphase	amperes	1.27
	I(dc-link)	amperes	1.036
	Efficiency	%	33.092

### Motor Connections and Commutation Logic

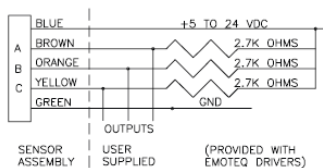
UNHOUSED MECHANICAL		
Stator Stack OD		63.500 mm
Stator Stack Length (UNmachined)		6.985 mm
Stator Stack Length (Machined)		6.350 mm
No.Of Stator Laminations		11
Lamination Thickness		0.635 mm
Lamination Material	M19 24	gage
Stator ID		38.833 mm
No. Of Phases		3
Phase Connection		WYE
Parallel path		1
Turns/Coil		5
Wire gage (AWG)		26
No.Of Wires In Hand		4
Copper Weight		0.045 kg
Length Over Coil (Maximum)		24.892 mm
End Turns OD (Maximum)		57.912 mm
End Turns ID (Maximum)		36.322 mm
Lead Wire Gage		18 AWG
Lead Wire Length		304.800 mm
ROTOR OD		33.020 mm
HUB OD ACROSS FLAT		28.498 mm
Rotor ID		12.700 mm
Rotor Axial Length "B"		10.922 mm
Magnet Type	34K	
Magnet Length		10.160 mm
Magnet Width		9.929 mm
Magnet Thickness		2.261 mm
Magnet Weight		1.520E-03 kg
No. Of Poles		8

MOTOR EXCITATION SEQUENCE AND SENSOR OUTPUT LOGIC FOR CW ROTATION VIEWING LEADWIRE END.

EXCITATION	STEP	1	2	3	4	5	6	1
(RED) A		+	+	-	-	+	+	
(WHT) B		-	-	+	+	-	-	
(BLK) C		-	-	+	+	-	-	
(BRN) A		1	1	0	0	1	1	
(ORG) B		0	1	1	1	0	0	
(YEL) C		0	0	1	1	1	1	



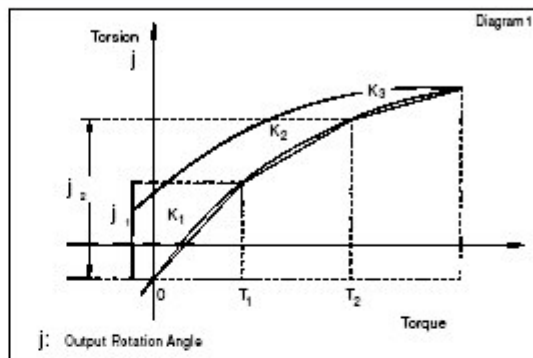
HALL EFFECT CONNECTION DIAGRAM



## High Performance Gearing and Motion Control CSD Series Ultra Flat Component Sets

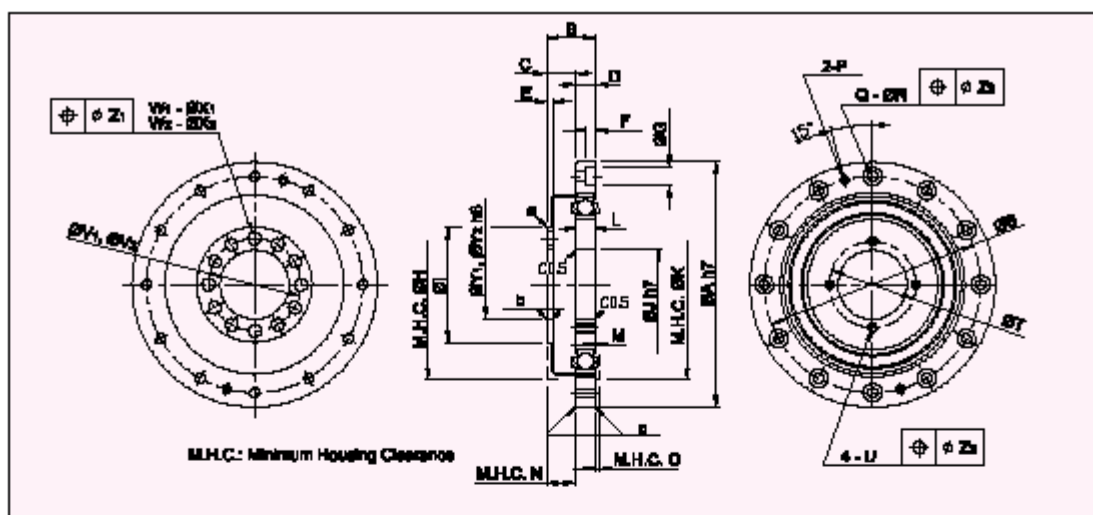
Compact      Lightweight      Zero Backlash      High Accuracy

The axial length of the CSD Series has been reduced by 50% versus the CSF series. This design is made possible by HD Systems patented "S" tooth profile, as well as manufacturing expertise. The CSD series is ideal for many applications including robotics, aerospace, and factory automation. The design of the CSD component set allows the surrounding enclosure to be made very compact for additional size and weight savings.



Item	Unit	CSD-20			CSD-25			CSD-32			CSD-40			CSD-50		
		50	100	160	50	100	160	50	100	160	50	100	160	50	100	160
Gear Ratio		50	100	160	50	100	160	50	100	160	50	100	160	50	100	160
Rated Input Speed	rpm	2000			2000			2000			2000			2000		
Rated Torque	Nm	17	28	28	27	47	47	53	96	96	96	185	206	172	329	370
Limit for Repeated Peak Torque	Nm	39	57	64	68	110	123	151	233	261	281	398	453	500	686	823
Limit for Average Torque	Nm	24	34	34	38	75	75	75	151	151	137	260	316	247	466	590
Limit for Momentary Peak Torque (Standard Flexspline)	Nm	69	78*	76*	127	152*	152*	268	359*	359*	480	696*	696*	1000	1440	1560*
Limit for Momentary Peak Torque (Big Bore Flexspline)	Nm	64*	64*	64*	127	135*	135*	268	331*	331*	480	578*	578*	1000	1320*	1320*
Max. Input Speed	Grease	6500			5600			4800			4000			3500		
	Oil	10000			7500			7000			5600			4500		
Limit for Average Input Speed	Grease	3500			3500			3500			3000			2500		
	Oil	6500			5600			4600			3600			3000		
Moment of Inertia	J	$\times 10^{-4} \text{kg-m}^2$			0.090			0.282			1.09			2.85		
		$\times 10^{-4} \text{kg-m-s}^2$			0.092			0.288			1.12			2.91		
Life W/G LB-10	hr	7000			7000			7000			7000			7000		
Torsional Stiffness (See Diagram 1 for Definition)	T1	Nm			7.0			14			29			54		
	K1	$\times 10^4 \text{Nm/rad}$			1.1			1.3			2.0			2.7		
	T2	Nm			25			48			108			196		
	K2	$\times 10^4 \text{Nm/rad}$			1.3			1.7			2.7			3.7		
K3	$\times 10^4 \text{Nm/rad}$			2.0			2.5			3.7			4.7			
Hysteresis Loss	$\times 10^{-4} \text{rad}$	5.8			5.8			5.8			5.8			5.8		
Starting Torque (Max.)	Ncm	7.3	4.3	3.4	13.7	7.9	6.4	28.4	17.6	13.7	50.0	29.4	23.5	94.1	55.9	44.1
No-Load Backdriving Torque (Max.)	Nm	4.4	5.2	6.6	8.3	9.6	12.3	17.1	21.2	28.4	30.0	35.3	45.2	56.5	67.1	84.7
Ratcheting Torque (Min.)	Nm	157	185	157	315	357	315	686	754	686	1300	1500	1300	2600	2980	2530
Positioning Accuracy (Max.)	$\times 10^{-4} \text{rad}$	2.9			2.9			2.9			2.9			2.9		
	arc-min	1.0			1.0			1.0			1.0			1.0		
Lubrication	Grease	Harmonic Grease 4B No.2			Harmonic Grease 4B No.2			Harmonic Grease 4B No.2			Harmonic Grease 4B No.2			Harmonic Grease 4B No.2		
	Oil	Industrial Gear Oil #2 (Brianna Pressure Agent ISOVG68)			Industrial Gear Oil #2 (Brianna Pressure Agent ISOVG68)			Industrial Gear Oil #2 (Brianna Pressure Agent ISOVG68)			Industrial Gear Oil #2 (Brianna Pressure Agent ISOVG68)			Industrial Gear Oil #2 (Brianna Pressure Agent ISOVG68)		
Weight	Kg	0.13			0.24			0.51			0.92			1.9		

\* The Momentary Peak Torque is limited by the tightening torque of the Flexspline Mounting Bolts. For notes on design and assembly please refer to the CSF catalog.



SIZE	A	B	C	D	E	F	G	H	I	J	K	L	M	N	O	P	Q	R
CSD-20	70	14	8	6	2	3.2	6.5	59	32	20	59	5.2	0.3	8	1.5	M3	12	3.4
CSD-25	85	17	10	7	2	3.2	6.5	66	40	24	66	6.2	0.4	10	1.5	M3	12	3.4
CSD-32	110	22	13	9	2.5	4.4	8	86	52	32	86	8.6	0.5	13	2	M4	12	4.5
CSD-40	135	27	16	11	3	5.4	9.5	106	64	40	106	10.3	0.6	16	2.5	M5	12	5.5
CSD-50	170	33	19.5	13.5	3.5	6.5	11	139	80	50	139	12.7	0.8	19.5	3.5	M6	12	6.6

SIZE	Standard Flexspline								Big Bore Flexspline								
	S	T	U	V1	W1	X1	Y1	V2	W2	X2	Y2	Z1	Z2	Z3	a	b	c
CSD-20	62	26	M3	24	9	4.5	16	26	12	3.4	20	0.25	0.2	0.2	C0.3	C0.3	C0.4
CSD-25	75	30	M3	30	9	5.5	20	32	12	4.5	24	0.25	0.2	0.2	C0.3	C0.3	C0.4
CSD-32	100	40	M4	41	11	6.6	30	42	14	5.5	32	0.3	0.25	0.25	C0.3	C0.3	C0.4
CSD-40	120	50	M5	48	10	9	32	52	14	6.6	40	0.5	0.25	0.25	C0.5	C0.5	C0.4
CSD-50	150	60	M6	62	11	11	44	65	14	9	50	0.5	0.3	0.3	C0.5	C0.5	C0.4

ORDERING CODE

Model	Size	Gear Ratio					Flexspline Configuration	*Option
CSD	20	50	100	160	2A-GR	Standard Flexspline: No Designation is Necessary	Our Application Engineers Can Assist With Any Special Configurations And Their Ordering Code	
	25	50	100	160				
	32	50	100	160				
	40	50	100	160				
	50	50	100	160				

CSD - 25 - 160 - 2A-GR - Blank (Standard Flexspline) - SP\*

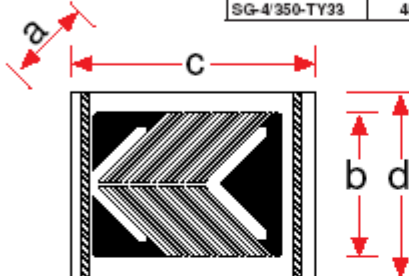
CSD - 25 - 160 - 2A-GR - BB (Big Bore Flexspline) - SP\*

All products are warranted to be free from design or manufacturing defects for a period of one year from the date of shipment. Such items will be repaired or replaced at the discretion of the HD Systems. The seller makes no warranty, expressed or implied, concerning the material to be furnished other than it shall be of the quality and specifications stated. The seller's liability for any breach is limited to the purchase price of the product. All efforts have been made to assure that the information in this catalog is complete and accurate. However, HD Systems is not liable for any errors, omissions or inaccuracies in the reported data. HD Systems reserves the right to change the product specifications, for any reason, without prior notice.

## ROSETTE STRAIN GAGES

**To Order (Specify Model Number)**

TYPE SERIES	MODEL NO.	PRICE PER PKG OF 5	FOIL MATERIAL	TEMP. COEF.*	$\Omega$	DIMENSIONS [MM]				MAX EXC	TERM PADS
						GRID	CARRIER				
Diagrams Shown Larger Than Actual Size	SG-4/1000-TY37K	\$49	Karma	SS	350	3.8	3.2	9.5	6.9	10	TP-2
	SG-4/350-TY37	45	Constantan	SS	350	3.8	3.2	9.5	6.9	10	TP-2
	SG-4/350-TY31	45	Constantan	CS	350	3.8	3.2	9.5	6.9	10	TP-2
	SG-4/350-TY33	45	Constantan	ALUM	350	3.8	3.2	9.5	6.9	10	TP-2



**TY SERIES TORQUE GAGES**

- ✓ Encapsulated Gages with Three Solder Pads (Accessory Terminal Pads Are Used for Strain Relief and Connecting Different Gage Wires)

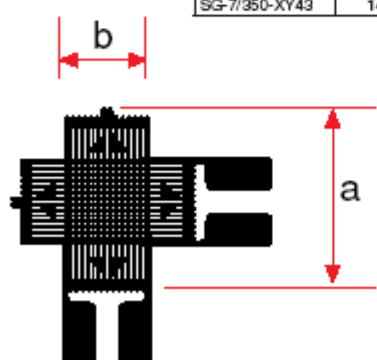
Ordering Example: SG-4/1000-TY37K is a package of five torque gages with two Karma grids, encapsulated with three solder pads, \$49.  
 \*SS\* is a temperature coefficient matched to stainless steel. (TY37)  
 \*CS\* is a temperature coefficient matched to carbon steel. (TY31)  
 \*ALUM\* is a temperature coefficient matched to aluminum. (TY33)

Dimensions

For Accessory Terminal Pads, see page E-25.

**To Order (Specify Model Number)**

TYPE SERIES	MODEL NO.	PRICE PER PKG OF 5	FOIL MATERIAL	TEMP. COEF.*	$\Omega$	DIMENSIONS [MM]				MAX EXC	TERM PADS
						GRID	CARRIER				
Diagram Shown Larger Than Actual Size	SG-3/350-XY47K	\$115	Karma	SS	350	3.0	2.8	8.0	8.0	10	TP-2
	SG-7/350-XY47K	149	Karma	SS	350	7.0	3.5	13.0	13.0	15	TP-3
	SG-3/350-XY47	109	Constantan	SS	350	3.0	2.8	8.0	8.0	10	TP-2
	SG-7/350-XY47	145	Constantan	SS	350	6.8	2.8	13.0	13.0	15	TP-3
	SG-3/350-XY41	105	Constantan	CS	350	3.0	2.8	8.0	8.0	10	TP-2
	SG-7/350-XY41	149	Constantan	CS	350	7.0	3.5	13.0	13.0	15	TP-3
	SG-3/350-XY43	105	Constantan	ALUM	350	3.0	2.8	8.0	8.0	10	TP-2
	SG-7/350-XY43	149	Constantan	ALUM	350	6.8	2.8	13.0	13.0	15	TP-3



**XY SERIES BIAxIAL GAGES FOR AXIAL STRAIN**

- ✓ Encapsulated Gages with Solder Pads (Accessory Terminal Pads Are Used for Strain Relief and Connecting Different Gage Wires)

Ordering Example: SG-3/350-XY47K is a package of five biaxial gages with two Karma grids, encapsulated with solder pads, \$115.  
 \*SS\* is a temperature coefficient matched to stainless steel. (XY47)  
 \*CS\* is a temperature coefficient matched to carbon steel. (XY41)  
 \*ALUM\* is a temperature coefficient matched to aluminum. (XY43)

Dimensions

For Accessory Terminal Pads, see page E-25.





INA114

## Precision INSTRUMENTATION AMPLIFIER

### FEATURES

- LOW OFFSET VOLTAGE: 50 $\mu$ V max
- LOW DRIFT: 0.25 $\mu$ V/ $^{\circ}$ C max
- LOW INPUT BIAS CURRENT: 2nA max
- HIGH COMMON-MODE REJECTION: 115dB min
- INPUT OVER-VOLTAGE PROTECTION:  $\pm$ 40V
- WIDE SUPPLY RANGE:  $\pm$ 2.25 to  $\pm$ 18V
- LOW QUIESCENT CURRENT: 3mA max
- 8-PIN PLASTIC AND SOL-16

### APPLICATIONS

- BRIDGE AMPLIFIER
- THERMOCOUPLE AMPLIFIER
- RTD SENSOR AMPLIFIER
- MEDICAL INSTRUMENTATION
- DATA ACQUISITION

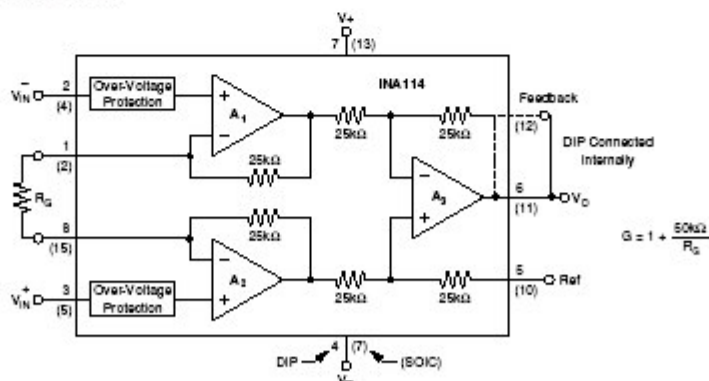
### DESCRIPTION

The INA114 is a low cost, general purpose instrumentation amplifier offering excellent accuracy. Its versatile 3-op amp design and small size make it ideal for a wide range of applications.

A single external resistor sets any gain from 1 to 10,000. Internal input protection can withstand up to  $\pm$ 40V without damage.

The INA114 is laser trimmed for very low offset voltage (50 $\mu$ V), drift (0.25 $\mu$ V/ $^{\circ}$ C) and high common-mode rejection (115dB at G = 1000). It operates with power supplies as low as  $\pm$ 2.25V, allowing use in battery operated and single 5V supply systems. Quiescent current is 3mA maximum.

The INA114 is available in 8-pin plastic and SOL-16 surface-mount packages. Both are specified for the  $-40^{\circ}$ C to  $+85^{\circ}$ C temperature range.



International Alorton Industrial Park • Milling Address: PO Box 11400, Tucson, AZ 85734 • Street Address: 4730 S. Tucson Blvd., Tucson, AZ 85706 • Tel: (520) 746-1111 • Telex: 918-653-1111  
 Inquiries: <http://www.burr-brown.com> • FAX Line: (908) 542-4133 (US/Canada Only) • Cable: BURROCEP • Telex: 098-6401 • FAX: (520) 680-1510 • Immediate Product Info: (908) 542-4132

## SPECIFICATIONS

### ELECTRICAL

At  $T_A = +25^\circ\text{C}$ ,  $V_S = \pm 15\text{V}$ ,  $R_L = 2\text{k}\Omega$ , unless otherwise noted.

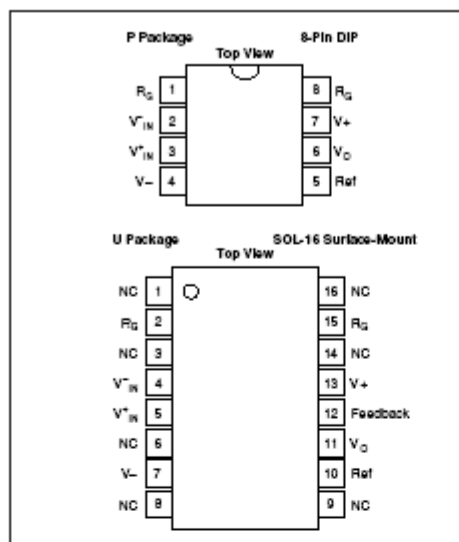
PARAMETER	CONDITIONS	INA114BP, BU			INA114AP, AU			UNITS	
		MIN	TYP	MAX	MIN	TYP	MAX		
INPUT Offset Voltage, RTI Initial vs Temperature vs Power Supply Long-Term Stability Impedance, Differential Common-Mode Input Common-Mode Range Safe Input Voltage Common-Mode Rejection	$T_A = +25^\circ\text{C}$ $T_A = T_{\text{MIN}}$ to $T_{\text{MAX}}$ $V_S = \pm 2.25\text{V}$ to $\pm 15\text{V}$		$\pm 10 + 20/\text{G}$ $\pm 0.1 + 0.5/\text{G}$	$\pm 50 + 100/\text{G}$ $\pm 0.25 + 5/\text{G}$ $3 + 10/\text{G}$		$\pm 25 + 30/\text{G}$ $\pm 0.25 + 5/\text{G}$	$\pm 125 + 500/\text{G}$ $\pm 1 + 10/\text{G}$	$\mu\text{V}$ $\mu\text{V}/^\circ\text{C}$	
				$0.5 + 2/\text{G}$ $\pm 0.2 + 0.5/\text{G}$		*	*	$\mu\text{V/V}$ $\mu\text{V/mo}$	
				$10^{13} \parallel 6$ $10^{13} \parallel 6$		*	*	$\Omega \parallel \text{pF}$ $\Omega \parallel \text{pF}$	
				$\pm 11$	$\pm 13.5$	*	*	*	V V
			$V_{\text{CM}} = \pm 10\text{V}$ , $\Delta R_{\text{D}} = 1\text{k}\Omega$ $\text{G} = 1$ $\text{G} = 10$ $\text{G} = 100$ $\text{G} = 1000$	80 96 110 115	95 115 120 120	$\pm 40$	75 90 106 106	90 105 110 110	dB dB dB dB
BIAS CURRENT vs Temperature			$\pm 0.5$ $\pm 8$	$\pm 2$		*	$\pm 5$	nA $\text{pA}/^\circ\text{C}$	
OFFSET CURRENT vs Temperature			$\pm 0.5$ $\pm 8$	$\pm 2$		*	$\pm 5$	nA $\text{pA}/^\circ\text{C}$	
NOISE VOLTAGE, RTI $f = 10\text{Hz}$ $f = 100\text{Hz}$ $f = 1\text{kHz}$ $f_p = 0.1\text{Hz}$ to $10\text{Hz}$ Noise Current $f = 10\text{Hz}$ $f = 1\text{kHz}$ $f_p = 0.1\text{Hz}$ to $10\text{Hz}$	$\text{G} = 1000$ , $R_{\text{D}} = 0\Omega$		15 11 11 0.4			*	*	$\text{mV}/\sqrt{\text{Hz}}$ $\text{mV}/\sqrt{\text{Hz}}$ $\text{mV}/\sqrt{\text{Hz}}$ $\mu\text{V}/\text{p-p}$	
				0.4 0.2 18			*	*	$\text{pA}/\sqrt{\text{Hz}}$ $\text{pA}/\sqrt{\text{Hz}}$ $\text{pA}/\text{p-p}$
				1	$1 + (50\text{k}\Omega/R_{\text{D}})$	10000	*	*	V/V V/V
			$\text{G} = 1$ $\text{G} = 10$ $\text{G} = 100$ $\text{G} = 1000$		$\pm 0.01$ $\pm 0.02$ $\pm 0.05$ $\pm 0.5$	$\pm 0.05$ $\pm 0.4$ $\pm 0.5$ $\pm 1$	*	*	% % % %
			$\text{G} = 1$ $\text{G} = 10$ $\text{G} = 100$ $\text{G} = 1000$		$\pm 2$ $\pm 25$ $\pm 0.0001$ $\pm 0.0005$ $\pm 0.0005$ $\pm 0.002$	$\pm 10$ $\pm 100$ $\pm 0.001$ $\pm 0.002$ $\pm 0.002$ $\pm 0.01$	*	*	ppm/ $^\circ\text{C}$ ppm/ $^\circ\text{C}$ % of FSR % of FSR % of FSR % of FSR
OUTPUT Voltage Load Capacitance Stability Short Circuit Current	$I_{\text{O}} = 5\text{mA}$ , $T_{\text{MIN}}$ to $T_{\text{MAX}}$ $V_S = \pm 11.4\text{V}$ , $R_L = 2\text{k}\Omega$ $V_S = \pm 2.25\text{V}$ , $R_L = 2\text{k}\Omega$		$\pm 13.5$ $\pm 10$ $\pm 1$	$\pm 13.7$ $\pm 10.5$ $\pm 1.5$ 1000 $\pm 20$ – $15$		*	*	V V V pF mA	
							*	*	
FREQUENCY RESPONSE Bandwidth, $-3\text{dB}$ Slow Rate Setting Time, 0.01% Overload Recovery	$V_{\text{O}} = \pm 10\text{V}$ , $\text{G} = 10$ $\text{G} = 1$ $\text{G} = 10$ $\text{G} = 100$ $\text{G} = 1000$ 50% Overdrive		1 100 10 1			*	*	MHz kHz kHz kHz	
			0.3	0.6 18 20 120 1100		*	*	*	$\mu\text{s}$ $\mu\text{s}$ $\mu\text{s}$ $\mu\text{s}$ $\mu\text{s}$
				20			*	*	$\mu\text{s}$
							*	*	$\mu\text{s}$
							*	*	$\mu\text{s}$
POWER SUPPLY Voltage Range Current	$V_{\text{IN}} = 0\text{V}$	$\pm 2.25$	$\pm 15$ $\pm 2.2$	$\pm 18$ $\pm 3$	*	*	*	V mA	
TEMPERATURE RANGE Specification Operating $\theta_{\text{JA}}$			$-40$ $-40$	85 125	*	*	*	$^\circ\text{C}$ $^\circ\text{C}$ $^\circ\text{C/W}$	
				80		*	*		

\* Specification same as INA114BP, BU.

NOTE: (1) Temperature coefficient of the "50k $\Omega$ " term in the gain equation.

The information provided herein is believed to be reliable; however, BURR-BROWN assumes no responsibility for inaccuracies or omissions. BURR-BROWN assumes no responsibility for the use of this information, and all use of such information shall be entirely at the user's own risk. Prices and specifications are subject to change without notice. No patent rights or licenses to any of the circuits described herein are implied or granted to any third party. BURR-BROWN does not authorize or warrant any BURR-BROWN product for use in life support devices and/or systems.

## PIN CONFIGURATIONS

ABSOLUTE MAXIMUM RATINGS<sup>(1)</sup>

Supply Voltage .....	$\pm 18V$
Input Voltage Range .....	$\pm 40V$
Output Short-Circuit (to ground) .....	Continuous
Operating Temperature .....	$-40^{\circ}C$ to $+125^{\circ}C$
Storage Temperature .....	$-40^{\circ}C$ to $+125^{\circ}C$
Junction Temperature .....	$+150^{\circ}C$
Lead Temperature (soldering, 10s) .....	$+300^{\circ}C$

NOTE: (1) Stresses above these ratings may cause permanent damage.


**ELECTROSTATIC DISCHARGE SENSITIVITY**

This integrated circuit can be damaged by ESD. Burr-Brown recommends that all integrated circuits be handled with appropriate precautions. Failure to observe proper handling and installation procedures can cause damage.

ESD damage can range from subtle performance degradation to complete device failure. Precision integrated circuits may be more susceptible to damage because very small parametric changes could cause the device not to meet its published specifications.

## PACKAGE/ORDERING INFORMATION

PRODUCT	PACKAGE	PACKAGE DRAWING NUMBER <sup>(1)</sup>	TEMPERATURE RANGE
INA114AP	8-Pin Plastic DIP	005	$-40^{\circ}C$ to $+85^{\circ}C$
INA114BP	8-Pin Plastic DIP	005	$-40^{\circ}C$ to $+85^{\circ}C$
INA114AU	SOL-16 Surface-Mount	211	$-40^{\circ}C$ to $+85^{\circ}C$
INA114BU	SOL-16 Surface-Mount	211	$-40^{\circ}C$ to $+85^{\circ}C$

NOTE: (1) For detailed drawing and dimension table, please see end of data sheet, or Appendix C of Burr-Brown IC Data Book.

## APPLICATION INFORMATION

Figure 1 shows the basic connections required for operation of the INA114. Applications with noisy or high impedance power supplies may require decoupling capacitors close to the device pins as shown.

The output is referred to the output reference (Ref) terminal which is normally grounded. This must be a low-impedance connection to assure good common-mode rejection. A resistance of  $5\Omega$  in series with the Ref pin will cause a typical device to degrade to approximately 80dB CMR ( $G = 1$ ).

### SETTING THE GAIN

Gain of the INA114 is set by connecting a single external resistor,  $R_G$ :

$$G = 1 + \frac{50\text{ k}\Omega}{R_G} \quad (1)$$

Commonly used gains and resistor values are shown in Figure 1.

The  $50\text{k}\Omega$  term in equation (1) comes from the sum of the two internal feedback resistors. These are on-chip metal film resistors which are laser trimmed to accurate absolute val-

ues. The accuracy and temperature coefficient of these resistors are included in the gain accuracy and drift specifications of the INA114.

The stability and temperature drift of the external gain setting resistor,  $R_G$ , also affects gain.  $R_G$ 's contribution to gain accuracy and drift can be directly inferred from the gain equation (1). Low resistor values required for high gain can make wiring resistance important. Sockets add to the wiring resistance which will contribute additional gain error (possibly an unstable gain error) in gains of approximately 100 or greater.

### NOISE PERFORMANCE

The INA114 provides very low noise in most applications. For differential source impedances less than  $1\text{k}\Omega$ , the INA103 may provide lower noise. For source impedances greater than  $50\text{k}\Omega$ , the INA111 FET-input instrumentation amplifier may provide lower noise.

Low frequency noise of the INA114 is approximately  $0.4\mu\text{V p-p}$  measured from 0.1 to 10Hz. This is approximately one-tenth the noise of "low noise" chopper-stabilized amplifiers.

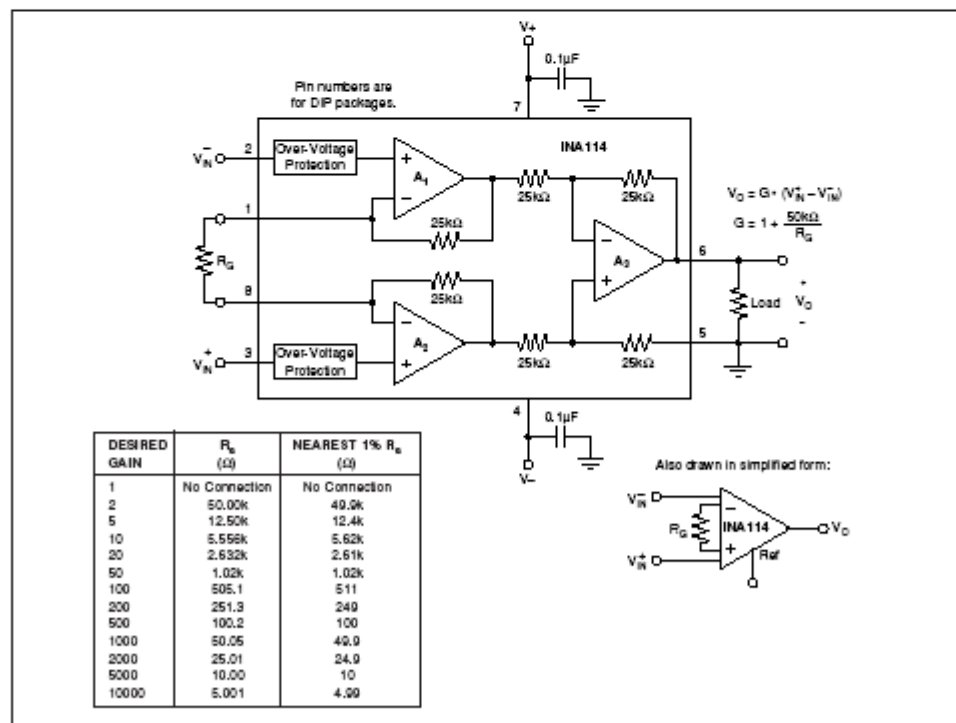


FIGURE 1. Basic Connections.



## Servo Amplifier

### 4-Quadrant PWM

For combination with:  
Brushless DC-Servomotors

### Series BLD 7010

	BLD 7010-SC4P	
Power supply	11 + 70	V DC
Switching frequency	48	kHz
Continuous output current @ TA = 22°C	10	A
Peak current limit	20	A
Analog input command <sup>1)</sup> – Voltage range	± 10	V DC
Logic input: – Encoder – Encoder frequency – Enable	TTL 100 8 - 30	kHz V DC
Output voltage for external use: – Positive (max. 20 mA) – Negative (max. 100 mA) – Negative (max. 20 mA)	+15 +5 –15	V DC V DC V DC
Maximum controllable speed with Hall Sensor <sup>2)</sup>	5 000 / 40 000	rpm
Minimum controllable speed with Hall Sensor <sup>3)</sup>	250 / 2 000	rpm
Maximum controllable speed with Encoder (with 1 000 lines per revolution) <sup>4)</sup>	1 250 / 10 000	rpm
Minimum controllable speed with Encoder <sup>4)</sup>	5 / 40	rpm
External inductance <sup>5)</sup>	100 + 300	µH
Temperature range: – Operating temperature – Storage temperature	–10 ... + 45 –40 ... + 80	°C °C
Dimension and Weight: – Dimensions (L x W x H) – Weight	180 x 100 x 40 650	mm g

<sup>1)</sup> Analog input command may be set by an external potentiometer or an external voltage.

<sup>2)</sup> The maximum controllable speed depends on the power supply, the motor type, the load and the feedback.

<sup>3)</sup> The minimum controllable speed depends on the motor type, the load and the feedback.

<sup>4)</sup> The appropriate value depends on the operating cycle and working conditions. An external inductance from 100 to 300 µH can be used to reduce the temperature of the motor series 4490 ... B.

Note: The Servo Amplifier is supplied with an operating instruction manual for installation and start-up.

#### General description

The Servo Amplifier BLD 7010 is a powerful 4-quadrant PWM Controller with electronic commutation for our three-phase brushless DC-Servomotors with Hall sensors.

#### Operating modes:

- Torque / current control
- Speed control by Encoder
- Speed control by Hall sensors

The required operation mode is selected by setting jumpers.

The Servo Amplifier is protected against over current, overheat and short-circuit of the motor connections against each other and to the power supply.

Advanced technology design with power MOSFET assure high efficiency of up to 95%.

The robust controller design and screw terminals assure simple and easy installation and safe operation.

The solid aluminium case offers several mounting possibilities to allow easy system integration.

#### Features:

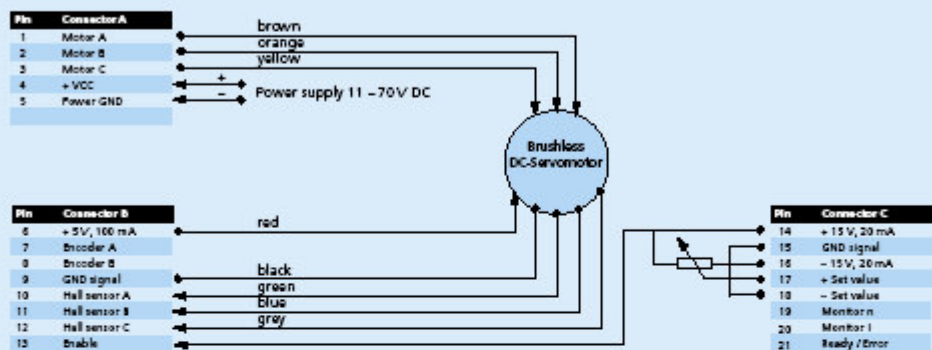
- Operation from a single supply source
- 4-Quadrant PWM
- Efficiency 95%
- Excellent linearity
- User friendly
- Torque / current control
- Speed control
- Bandwidth of current control 2,5 kHz

#### Ordering Information

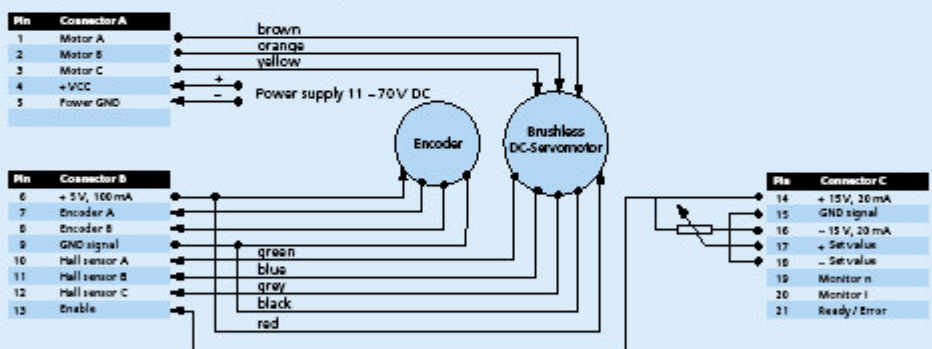
Servo Amplifier	Brushless DC-Servomotors	Encoder
BLD 7010-SC4P	4400 H 024 B	
BLD 7010-SC4P	4400 H 036 B	
BLD 7010-SC4P	4400 H 040 B	
BLD 7010-SC4P	4400 H 024 B - K 1500	40827 - 1000/3
BLD 7010-SC4P	4400 H 036 B - K 1500	40827 - 1000/3
BLD 7010-SC4P	4400 H 040 B - K 1500	40827 - 1000/3

Specifications subject to change without notice

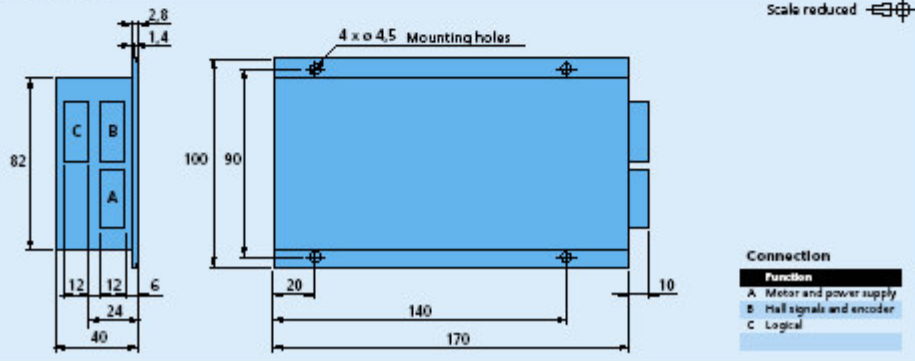
**Block diagram of the Servo Amplifier BLD 7010 for speed control with Hall sensor feedback**



**Block diagram of the Servo Amplifier BLD 7010 for speed control with Encoder feedback**



**Dimensional drawing**



Specifications subject to change without notice

## Vita

### Jonathon W. Sensinger

Born in Syracuse, New York, USA

#### EDUCATION:

University of Illinois at Chicago  
*Bachelor of Science in the field of Bioengineering*  
 GPA: 4.96/5.00, May 2002

Northwestern University  
*Masters of Science in the field of Biomedical Engineering*  
 GPA: 3.8/4.0, June 2005

Northwestern University  
*Doctor of Philosophy in the field of Biomedical Engineering*  
 June 2007

#### EXPERIENCE:

**Prosthetics Research Laboratory:** Northwestern University, Evanston, 2003 - 2006

- Research Assistant in the Mechatronic upper limb division
- Designed and tested non-backdrivable Series Elastic Actuators (SEA) for use in a prosthesis. Design was awarded a provisional patent.
- Created closed-form equations to characterize the unique torsional member used in rotary SEA.
- Created torque reduction technique to implement Harmonic Drive torque sensing.
- Formed and moderated weekly research meeting

**Neural Engineering Center for Artificial Limbs:** Rehabilitation Institute of Chicago, Chicago, 2005

- present

2007 – present: Research Engineer.

2005-2006 – no formal affiliation

- Applied SEA concepts to a prototype plunger mechanism in conjunction with NECAL, led by Dr. Todd Kuiken
- Obtained provisional patent for design (Prosthetic Haptic Interface for Reinnervated Skin. Application No.60/707,481; August 11, 2005
- Performed experiments to evaluate ability of subjects with targeted sensory reinnervation to discriminate pressure.

**EXCEL:** Northwestern University, 2005

- Designed and taught Linear Algebra and Matlab course for 16 freshmen. Designed syllabus and assignments, instructed students, and graded results.
- Created four real-world application projects including a Wheatstone bridge, chemical distillation, Biomechanical shape-roll over shape, and acoustic instrument modeling project. For each project students had to obtain their own parameters through research, create appropriate Matlab code, and present comprehensive reports.
- Challenged and inspired students to think outside the box through introducing new thought paradigms on all quizzes and exams, thus forcing students to apply existing principles to completely new problems.
- Inspired student to create “I love Matlab” tee-shirt.

**Biomechanics Research Lab:** University of Illinois at Chicago, 1999 - 2002

- Design of an orthotic glove for patients with minimal muscle function in the hands. Innovative use of Nitinol wire as an actuator in design to minimize weight and volume while increasing ergonomics of use and cosmetic appeal. Design received interest by Dean of Research and received identification disclosure number CV44. The invention has been demonstrated to Johnson and Johnson, who is interested in further development of the project.
- Biomechanical study of the Finger Joint system during surgical repair. Created a biomechanical model of the index and little finger during A2 and A4 pulley proximal and distal partial resection, to assess the proper procedure for surgical venting. Created new algorithms to accurately filter and process the data in an accurate and concise manner. Results presented at the Orthopedic Research Society 2002 conference and the Surgery of the Hand 2002 conference, and will be submitted to the Journal of Hand Surgery for publication. Interest in this technique led DePuy to fund a secondary study, using the technique to diagnose their MCP joint prosthesis.

**Research and Design Engineer :** CNY Prosthetics, May 2002 – September 2002

Designed and fabricated prototypes for:

- lockable wrist unit with large torque capabilities and fine resolution



- movable umbrella pin for transfemoral sockets
- Cord Knee with ankle linkage

Technical briefings:

- Development of a Recessed Fulcrum Prosthetic Socket
- Transtibial synostosis utilizing a VASS system
- Narrow Medial-Lateral Socket Justification

**Research and Design Engineer Intern:** CNY Prosthetics, May 2001 – July 2001

Researched optimization of current terminal devices in regards to material properties and geometry. Created innovative prototypes in most of the areas of prosthetics. Examples include a specialized hand for use with karate weapons, a kinematically linked joint system, and a knee prosthesis design to allow user feedback quicker and more reliable than the Seattle Knee. Worked closely with CEO John Tyo and patients to produce realistic and usable designs using novel materials and techniques.

## **BIBLIOGRAPHY:**

### **Papers**

Sensinger, J.W., & Weir, R.F.*ff.* (2007). User-Modulated Impedance Control of a Prosthetic Elbow in Unconstrained, Perturbed Motion. *IEEE Transactions on Biomedical Engineering, TBME-00028-2007, accepted for publication*

Sensinger, J.W., & Weir, R.F.*ff.* (2007). Modeling and Measurement of Rotational Stiffness in Trans-humeral Socket-residual limb interface. *IEEE Transactions on Biomedical Engineering, TBME-00053-2007, submitted for publication*

Sensinger, J.W., & Weir, R.F.*ff.* (2006). 2D Projection of a Multivariate Root Locus. *IEEE/ASME Transactions on Mechatronics, MT06-100, submitted for publication*

Sensinger, J.W., & Weir, R.F.*ff.* (2006). Improved Torque Fidelity in Harmonic Drive Sensors through the Union of Two Existing Strategies. *IEEE/ASME Transactions on Mechatronics, 11 (4), 457-461.*

### **Conferences**

Sensinger, J.W., & Weir, R.F.*ff.* (2007). Inherently Compensating Body Powered Elbow. *12th World Congress of the International Society of Prosthetics and Orthotics (Vancouver).*

Sensinger, J.W., & Weir, R.F.ff. (2007). User-Modulated Impedance Control of a Prosthesis. *12th World Congress of the International Society of Prosthetics and Orthotics* (Vancouver).

Sensinger, J.W., & Weir, R.F.ff. (2007). Trans-humeral socket residual-limb interface stiffness. *12th World Congress of the International Society of Prosthetics and Orthotics* (Vancouver).

Sensinger, J.W., Lock, B.A., Weir, R.F.ff., & Kuiken, T.A. (2007). Targeted Sensory Reinervation Subject Force Perception. *12th World Congress of the International Society of Prosthetics and Orthotics* (Vancouver).

Sensinger, J.W., & Weir, R.F.ff. (2006). Impedance Control Using a Compact Series Elastic Actuator. *IEEE/ASME International Conference on Mechatronic and Embedded Systems and Applications* (Beijing, China).

Sensinger, J.W., & Weir, R.F.ff. (2006). Improvements to Series Elastic Actuators. *IEEE/ASME International Conference on Mechatronic and Embedded Systems and Applications* (pp. 160-166). Beijing, China.

Sensinger, J.W., & Weir, R.F.ff. (2006). Non-backdrivable Impedance Control. *Robotics: Science and Systems; Robotic Systems for Rehabilitation, Exoskeleton, and Prosthetics Workshop* (Philadelphia, PA).

Sensinger, J.W., & Weir, R.F.ff. (2006). User-modulated Impedance Control. *Biomedical Engineering Society Annual Meeting* (pp. 167-172). Chicago, IL.

Sensinger, J.W., Lock, B.A., Weir, R.F.ff., & Kuiken, T. (2006). Physiological differences in targeted hyper-reinervation subject's force perception. *Biomedical Engineering Society Annual Meeting* (Chicago).

Sensinger, J.W., & Weir, R.F.ff. (2006). Biomimetic Control of Traditional Prostheses. *American Academy of Orthotists and Prosthetists Scientific Symposium* (Chicago).

Kuiken, T.A., Sensinger, J.W., & Weir, R.F.ff. (2006). Phantom Limb Sensory Feedback through nerve transfer surgery. *American Academy of Orthotists and Prosthetists Scientific Symposium* (Chicago).

Sensinger, J.W., & Weir, R.F.ff. (2005). Design and Analysis of Non-backdrivable Series Elastic Actuators. *IEEE 9th International Conference on Rehabilitation Robotics* (Chicago).

Sensinger, J.W., & Weir, R.F.ff. (2005). Non-Backdrivable Series Elastic Actuator For Use In A Prosthetic Elbow. *Myoelectric Controls Symposium* (New Brunswick).

Kuiken, T.A., Sensinger, J.W., & Weir, R.F.ff. (2005). Phantom Limb Sensory Feedback through nerve transfer surgery. *Myoelectric Controls Symposium* (New Brunswick).

Gonzalez, M.H., Sensinger, J.W., Chow, J.C., & Amirouche, F. (2003). Effect of Partial Resection of A2 and A4 Pulleys on Finger Joint Torques and Radii. *American Society for Surgery of the Hand Annual Meeting* (Chicago).

## Periodicals

Sensinger, J.W. (2005). May the Force Be with You: Physiologically appropriate prostheses. *Capabilities*, 13 (2), 2-5.

Sensinger, J.W. (2005). Series Elastic Actuators: Providing Safe Power in Electric Prostheses. *Capabilities*, 14 (1), 8-9.

## Theses

Sensinger, J.W. (2005). Design & Analysis of a Non-backdrivable Series Elastic Actuator for use in prostheses. *MSC Thesis, Biomedical Engineering* (p. 135). Evanston: Northwestern University.

Sensinger, J.W. (2007). User-Modulated Impedance Control Using Two-Site Proportional Myoelectric Signals. Ph.D. Thesis, Biomedical Engineering (p. 307). Evanston: Northwestern University.

---

<sup>i</sup> Hosmer Dorrance Corporation, Campbell, CA

<sup>ii</sup> Liberating Technologies, Inc., Holliston, MA

<sup>iii</sup> Motion Control, Inc., Salt Lake City, UT

<sup>iv</sup> Pro/Mechanica© is a trademark of Parametric Technology Corporation, Needham, MA

<sup>v</sup> Omega, Stamford, Connecticut

<sup>vi</sup> Matlab is a product of Mathworks, Natick, Massachusetts

<sup>vii</sup> MicroMo Electronics, Clearwater, Florida

<sup>viii</sup> McMaster-Carr, Atlanta, Georgia

<sup>ix</sup> Load Cell Central, Monroeton, Pennsylvania

<sup>x</sup> ETI, Carlsbad, California

<sup>xi</sup> Emoteq, Inc. a division of Hathaway, Tulsa Oklahoma

<sup>xii</sup> Harmonic Drive LLC., Hauppauge, New York

<sup>xiii</sup> Faullhauber, Clearwater, Florida

<sup>xiv</sup> Otto Bock, Minneapolis, Minnesota